STUDIES OF CARBONATE ROCK DEFORMATION
MOINE THRUST ZONE, N. W. SCOTLAND

A thesis submitted for the degree of Doctor of Philosophy (University of London).

by

Michael Ikpi Oden, M.Sc., D.I.C.

Department of Geology,
Royal School of Mines,
Imperial College of Science & Technology,
London, S.W.7.

February, 1985

ABSTRACT

This thesis is concerned with an analysis of deformation of and associated metamorphic effects in, The Durness Formation in the Moine Thrust Zone of North West Scotland. The Durness Formation, also referred to as the Durness Carbonates, forms the topmost lithologic formation of the Cambrian-Ordovician succession of North West Scotland. As a result of the Caledonian deformation the entire succession was involved in a series of thrusting episodes which culminated in the emplacement of the Moine nappe over the carbonates in many places.

Field research was carried out to study the macroscopic structures and metamorphism resulting from the deformation and rock samples from various stages of deformation were collected. By means of x-ray diffraction and backscattered electron microscopy these samples were analysed for stable phases. Mineral microchemistry, particularly of calcite, mica and chlorite was studied by means of electron probe microanalysers with and without backscattered viewing facilities. Detailed study of the samples in thin and ultrathin - thin sections was carried out by optical and scanning electron microscopy to provide a general and dynamic view of the deformation, to measure grain size and also to analyse the crystallographic fabric of deformed minerals.

By means of calcite/dolomite geothermometry temperatures in the Durness Carbonates below the Moines were estimated as 295.0 $\pm$ 55°c at Knockan and approximately 390.0 $\pm$ 41°c at Eriboll. The difference in temperature was confirmed by differences in crystallinity index of mica minerals, deformation microstructure and stable phase assemblage between the two areas. A new relationship is proposed between chlorite microchemistry and temperature while that between dolomite c-axis crystallographic preferred orientation and temperature is not that obvious.

Fluid pressure estimates ranged between 143 and 186 MPa while confining pressures had similar ranges viz: from 133 to 176 MPa between Knockan and Eriboll respectively. Deviatoric stresses associated with the last phase of carbonate deformation were estimated by means of calcite/dolomite grain sizes, yielding values of approximately 44 to 76 MPa in the whole area.

C-axis crystallographic fabrics showed a transition from complex orthorhombic patterns in Assynt towards more foliation-normal patterns at Eriboll. These highly symmetric dolomite fabrics are not only characteristic of plane strain deformation paths but also different from calcite fabrics in the same rocks.

It is proposed that thermal energy for the metamorphism of the carbonate rocks below the Moine Thrust could have resulted from (1) the emplacement of a hotter suite of Moine rocks over the carbonates (2) retrogressive chemical reactions in the Moine rocks (3) heat produced from deformation of minerals within the Moines and (4) warm siliceous fluids accompanying Moine thrusting.

CONTENTS

ACKNOWLEDGEMENTS

I wish to thank Dr. S. White for the patient guidance, stimulating discussion and encouragement he rendered throughout the long period of preparation of this thesis and also for introducing me to the Moine Thrust Zone of N.W. Scotland.

Special thanks also go to Dr. J. Cosgrove, P. Suddaby and P. Grant for their continuous interest and encouragement. A. Cash of photography section, M. Gill of sedimentology laboratory, D. Giddens of electron microscopy laboratory, late R. Curtis of XRD laboratory and A. Jones of rock cutting section rendered immeasurable help throughout the research period and I am very grateful to them all. My research colleagues, M . R. Drury, D. Evans, P.G. Bretan, H. Obee, and J.P. Latham are remembered for their continuous concern and helpful discussion.

Many thanks are also due to E. Eyong, A. Bassey and Lawrence Oden as well as Miss M. Masene and J. Sagonda for the strength and encouragement they offered at various stages of the work. I am also indebted to Chief E. Okoi-Obuli and Miss D. David for their kind gestures.

Finally I thank my parents Mr. Okereke Ikpi and Mma Abam Ofem for their relentless efforts and encouragement and Mrs. S. Sheindemi and Miss J. Sheek for typing the thesis. The research was financed by the University of Calabar - Nigeria, under the Staff Development Scheme.

CHAPTER ONE

INTRODUCTION

1.1 AIMS AND SCOPE OF THE THESIS

This thesis is a report of the deformation of a carbonate (mainly dolomitic) rock type in a natural setting - the Moine Thrust Zone. The original aim of the research was to elucidate the role of pressure solution as a deformation mechanism in this rock type. This aim was later expanded when its limitations were realised, leading to the establishment of a scheme based on the following aims:

(i) To analyse the deformation of the Durness Formation from the Caledonian foreland to the Moine thrust plane.

(ii) To illustrate the change in microchemistry and microstructure especially between Eriboll and Assynt and how these could be used to determine parameters associated with the carbonate material deformation.

(iii) To show how changes in deformation mechanisms relate to the physical/chemical characteristics of the environment of which the carbonate rocks are a part.

The main areas covered by the thesis include estimates of temperature associated with the deformation/metamorphism of the carbonate rocks and models to explain the sources of energy, estimates of tectonic stresses, fluid pressures and confining pressures associates with the last phase of deformation and a detailed study of the microstructure of the carbonate rocks. Other aspects also covered in the thesis are the variation of microchemistry of clinochlore - the main neomineral phyllosilicate in the carbonate rocks and an analysis of the preferred orientation of dolomite and calcite crystallites along the Moine thrust zone.

Due mainly to the vastness of the area covered by the field research in order to do justice to the outlined aims, the great detail to which most of it has been mapped by earlier workers, the report hereby presented does not include original maps of the author. All maps used for presentation of sample locations have been referenced.

1.2 METHODS

The research consisted of two unequal parts: the fieldwork and the laboratory study, the latter of which took the greater part of the time and effort. The main aim of the fieldwork was to provide samples for laboratory study, although it became inevitable to study the macroscopic structures in the field. Rock samples of Durness Carbonates were collected as well as those of contiguous rock types - Moine Schists/ mylonites, Serpulite Grit, Fucoid Beds and some quartzites.

Thin sections and ultrathin-thin sections were prepared of these samples for optical microscopical studies, electron microscopy and electron probe microanalysis. Bulk rock phase analysis was achieved by a combination of x-ray diffraction, optical microscopy and backscattered electron microscopy, while specific mineral microchemistry was studied by means of electron probe microanalysers with and without backscattered imaging. Crystallographic preferred orientation was studied by means of universal stage attached to an optical microscope. In all cases analytical facilities were chosen on their ability to provide very accurate analytical data.

1.3 STRUCTURE OF THESIS

The outline of the thesis is as presented in the table of contents. The introductory Chapter One is followed by a review of deformation and metamorphism of carbonate rocks and minerals, in particular calcite and dolomite. Chapter Three starts with a review of literature on the Moine Thrust Zone and ends with a report of fieldwork carried out and presentation of sample locations. In Chapter Four the analysis of temperatures associated with carbonate deformation and metamorphism is presented and models are suggested to explain the observed thermal anomaly, while Chapter Five presents the variation of the microchemistry of chlorite with respect to the observed temperature differences. Chapter Five ends with an analysis of fluid pressures and confining pressures likely to have obtained in the last phase of carbonate deformation. The evolution of deformation microstructure in the Durness carbonates is traced in Chapter Six, thereby providing the background to the estimation of tectonic stresses associated with Moine thrusting and the analysis of the fabric of the deformed rocks.

Finally the general conclusions, inferences arising and suggestions for further research are presented in Chapter Seven.

CHAPTER TWO

REVIEW OF ASPECTS OF THE DEFORMATION AND METAMORPHISM OF CARBONATE ROCKS

2.1 INTRODUCTION

The Durness Formation is a dolomitic rock with local changes to calcite marble and calcareous dolostones. In this chapter the deformation and metamorphism of calcite and dolomite are reviewed to the extent that they are likely to throw light on or be the basis on which work in later chapters develops. The bulk of the literature on deformation and metamorphism of carbonate rocks is too great to contain in a single chapter, hence only those aspects which are closely related to the present study are chosen for inclusion here. Deformation mechanisms of dolomite and calcite are presented in separate sections, while their metamorphism is, of necessity, treated together.

2.2 DEFORMATION OF CALCITE - THE PLASTIC FIELD

2.2.1 Introduction

Calcite, the most abundant carbonate mineral (Lipmann, 1973), is the trigonal ($\bar{3}$m) polymorph of calcium carbonate ($CaCO_3$), with a rhombohedral symmetry and space group $R\bar{3}C$ (see Fig. 2.1). The low rhombohedral symmetry, together with the ease of calcite deformation, have greatly enabled rock mechanicists to study and separate effects of glide activity on individual planes on the overall texture in trigonal calcite. The deformation mechanisms of calcite are now discussed, starting from the most common, but first an illustration of the type of indices adopted and the

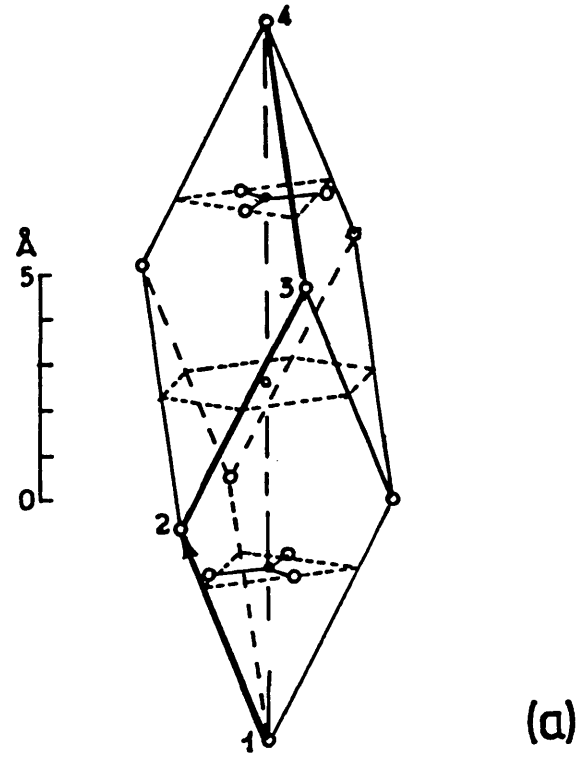

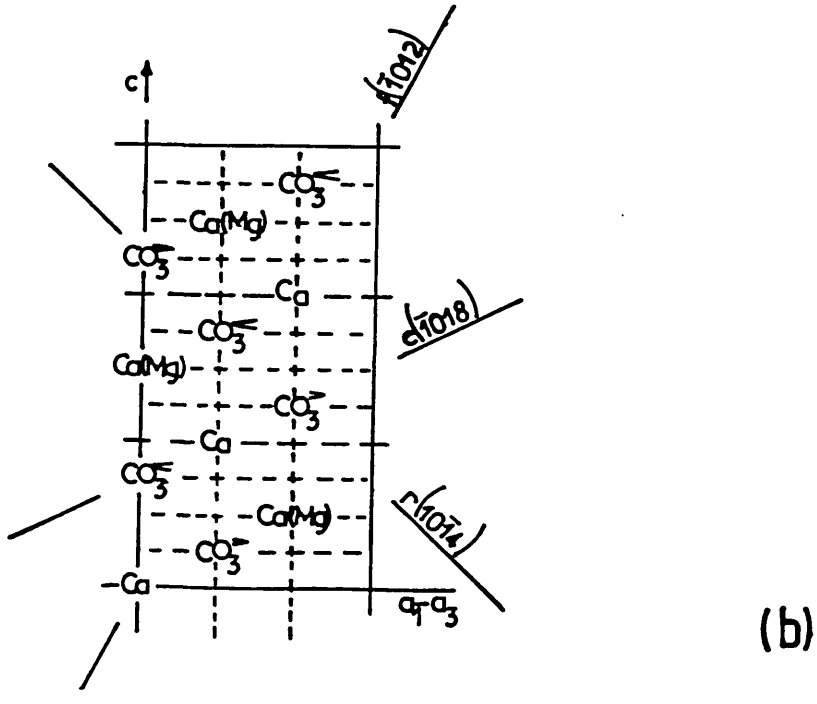

Fig. 2.1

(a) A primitive rhombohedral unit cell of calcite or dolomite. This one contains one formula $CaMg(CO_3)_2$. The two CO_3^{2-} planes are opposed in orientation, while calcium positions are marked 1,2,3,4 (after Lippmann 1973).

(b) The calcite and dolomite structures as seen in a section normal to an a-axis. In the case of calcite all cation sites are occupied by calcium and in the case of dolomite alternate basal plane cation sites are occupied by magnesium, as shown in parenthesis.

Fig. 2.2

Stereographic projection showing principal glide planes and directions in calcite and dolomite. For calcite, all possible non-equivalent orientations can be represented by the unit triangle (60° sector), while for dolomite a 120° sector is needed (after Paterson 1979).

Fig. 2.3 Definition of the twinning shear

(a) A mechanical twin develops in a crystal under the influence of a shear stress. The plane of drawing is perpendicular to the twin plane. γ is the angle of shear.

(b) A large number of thin, lamellar-shaped twins (black) in a crystallite produce an approximately homogeneous shear. The amount of shear is determined by the twinning shear-tanγ , and the volume fraction of the twins (black after Wagner et al. 1982).

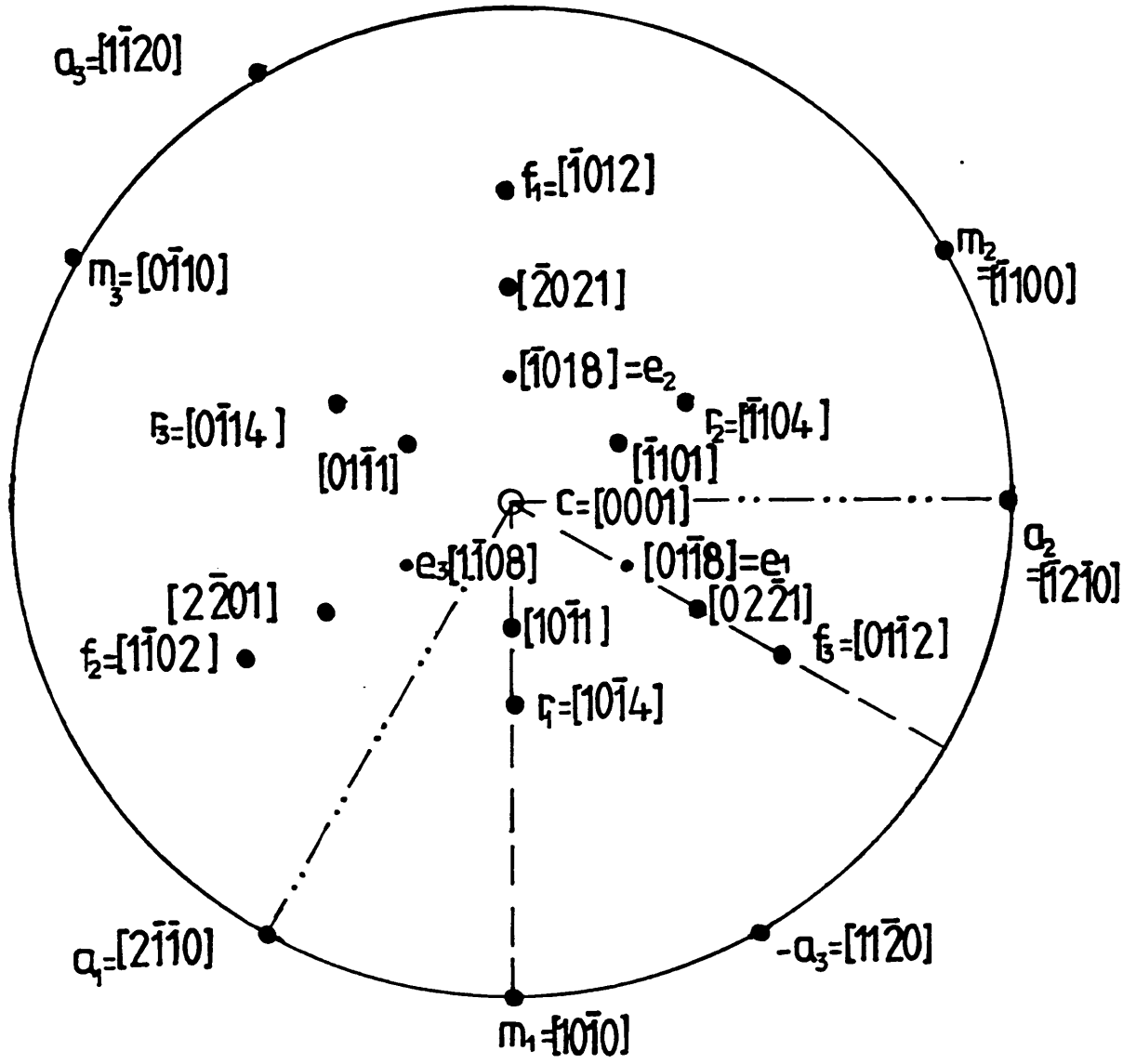

Fig. 2.2

Fig. 2.3 (a)

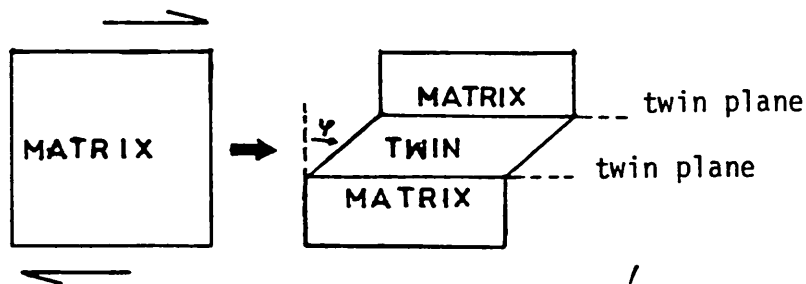

(b)

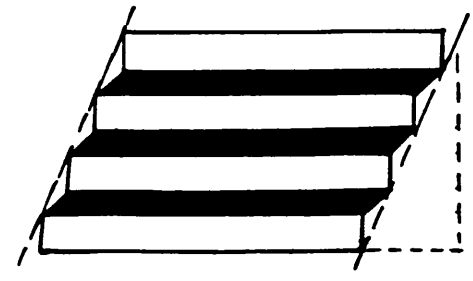

crystal planes referred to in the rest of the thesis.

2.2.2 Important Glide Planes in Carbonate Minerals

The important planes in calcite and dolomite to which deformation is referred are listed in Table 2.1. The two commonly used unit cells are: the rhombohedral unit cell based on $2(CaCO_3)$, and the hexagonal unit cell, $6(CaCO_3)$. In this report Miller-Bravais indices referred to the more commonly used morphological unit cell of $2(CaCO_3)$ are adopted, and where reference is made using the Miller-Bravais structural unit cell, the letter designation of the particular plane is also attached to reduce the risk of confusion (see also Figure 2.2).

Table 2.1 Designation of the important planes in carbonate minerals in Miller-Bravais Hexagonal and Rhombohedral indices (after Paterson, 1976)

Plane	Miller-Bravais Hexagonal Indices		Rhombohedral Indices	
	Structural	Morphological	Structural	Morphological
c	0001	0001	111	111
m	$10\bar{1}0$	$10\bar{1}0$	$2\bar{1}\bar{1}$	$2\bar{1}\bar{1}$
M	$10\bar{1}1$	$40\bar{4}1$	100	$3\bar{1}\bar{1}$
f	$01\bar{1}2$	$02\bar{2}1$	110	$11\bar{1}$
r	$10\bar{1}4$	$10\bar{1}1$	211	100
a	$2\bar{1}\bar{1}0$	$2\bar{1}\bar{1}0$	$1\bar{1}0$	$1\bar{1}0$
e	$01\bar{1}8$	$01\bar{1}2$	332	110

2.2.3 Twinning

Twinning in calcite has been widely studied, due mostly to its abundance. The most common twinning systems in calcite are shown in Table 2.2. A complete description of a "twinning

	Number of Cryst-allographically equivalent systems	Symbol	Critical Shear Stresses MPa for Single Crystals at 400°c	at 600°c	Reference
Twinning Systems					
$(\bar{1}018)\ \langle 40\bar{4}1\rangle$	3	e^+	10	10	Heard et al. (1965) Turner et al. (1954) Friedman (1967)
$(10\bar{1}1)\ \langle 1\bar{1}02\rangle$	3	r^+			Paterson & Turner (1970)
$(02\bar{2}1)\ \langle 01\bar{1}4\rangle$	3	f^-			Paterson & Turner (1970)
Slip Systems					
$(10\bar{1}4)\ \langle\bar{2}021\rangle$	3	r^+	40	16	Spiers & Wenk (1980) Griggs et al (1960)
$(10\bar{1}4)\ \langle 20\bar{2}1\rangle$	3	r^-	25	10	Heard et al. (1965) Turner et al (1954)
$(10\bar{1}2)\ \langle 20\bar{2}1\rangle$ $(10\bar{1}2)\ \langle 20\bar{2}1\rangle$	6	f^+	70	18	Spiers & Wenk (1980)
$(\bar{1}012)\ \langle\bar{2}20\bar{1}\rangle$ $(\bar{1}012)\ \langle 0\bar{2}2\bar{1}\rangle$	6	f^-	40	10	Heard et al (1965)
$(\bar{1}2\bar{1}0)\ \langle 1\bar{1}02\rangle$	3	a			Borg & Handin (1967) Friedman (1967)
$(10\bar{1}0)\ \langle\bar{1}2\bar{1}0\rangle$	3	m			Thomas & Renshaw (1967
$(0001)\ \langle\bar{1}2\bar{1}0\rangle$	3	c			Turner & Orozco (1976)

TABLE 2.2 The different glide systems in calcite and some of the known critical shear stresses. Slip and twinning senses are specified (+) or (-) according to the convention of Turner et al. (1954)

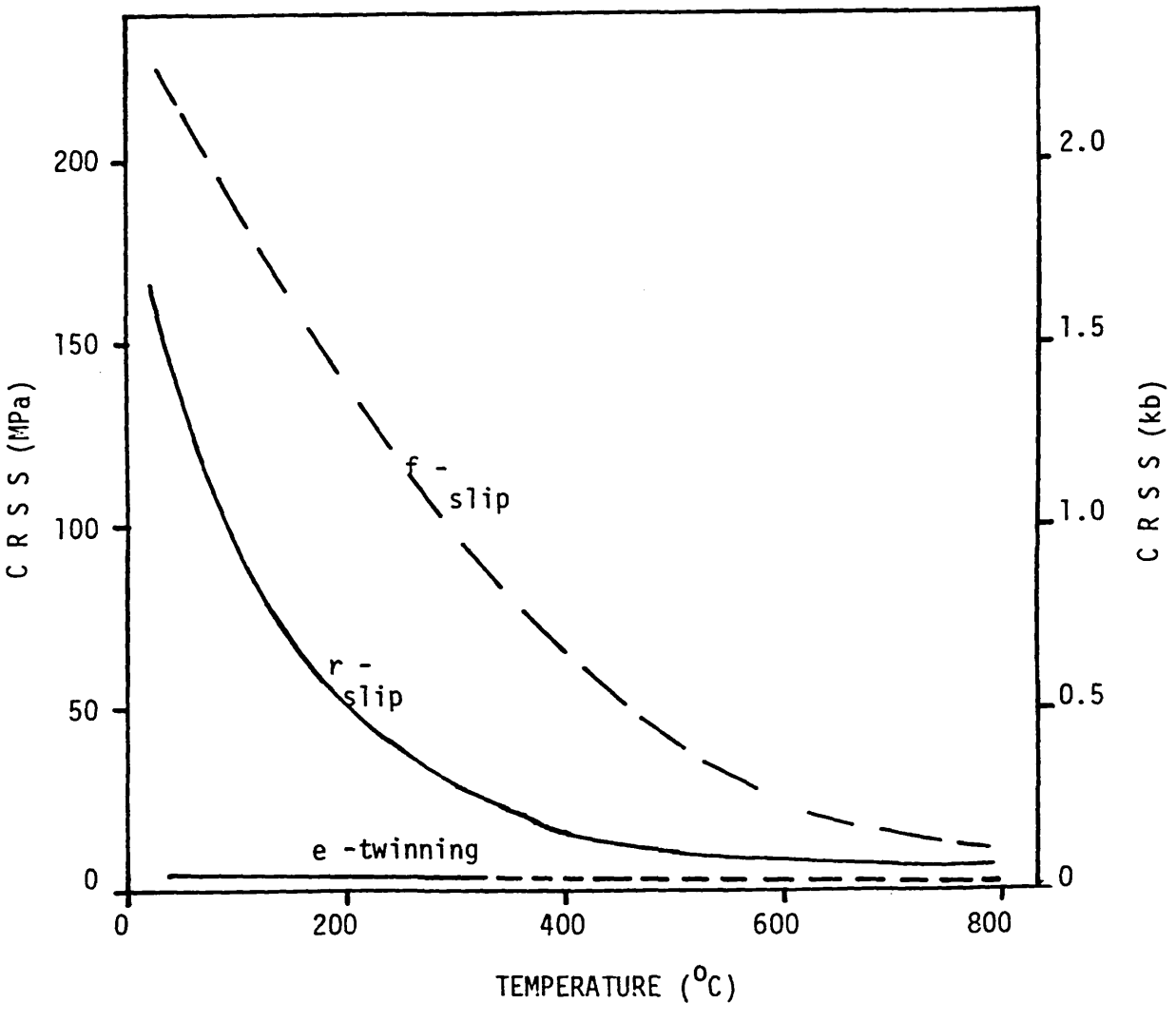

Fig 2.4

Variation of critical resolved shear stress data at yield for e-twinning, r(-), and f(-) slip in calcite. All data was obtained at $\dot{e} = 10^{-3}$ to 10^{-4} s^{-1}, under a confining pressure of 500 MPa (after Turner et al. 1954; Griggs et al. 1960; Braillon et al. 1972; Spiers 1982).

system" in a similar manner as a slip system requires the knowledge of the twin plane, the twinning direction and, in addition, the twinning shear $\gamma = \tan\psi$ (Wagner et al, 1982, and also fig. 2.3). Although twinning on $\underline{e}(\bar{1}018)$, $\underline{r}$ $(10\bar{1}1)$ and $\underline{f}$ $(02\bar{2}1)$ are now known, the commonest and earliest known system is the $\underline{e}$ (Table 2.2). It starts from room temperature, becoming less important at around 700 to 800°C (Turner et al, 1954; Griggs et al, 1960; Spiers, 1981; see also fig. 2.4). Although the critical resolved shear stress (CRSS) for $\underline{e}$-twinning remains almost constant within this range of temperatures, those for the other competing systems, namely $\underline{f}$- and $\underline{r}$-slip decrease so rapidly that at the higher temperatures CRSS values for the three systems are almost equal.

The twinning field in calcite depends on the grain size, the stress, the strain rate as well as the temperature. Spiers (1981) showed that for a given grain size the temperature marking the transition from $\underline{e}$-twinning to non-twinning, that is, the temperature at which a twinning polycrystal gets rid of its twins, decreases as the strain rate decreases. Also, the larger the grain size, the lower is the transition temperature at a particular strain rate, or at a particular twinning temperature. The larger the grain size, the greater the strain rate required to cross the texture transition boundary into slip. This behaviour is illustrated for Solnhofen limestone as well as Carrara marble in Figure 2.5. The way the grain size, strain rate and stress are related is shown in Figure 2.6, where Spiers (1981) showed experimentally that the stress to initiate $\underline{e}$-twins at a particular strain rate is higher for fine grained limestones than for

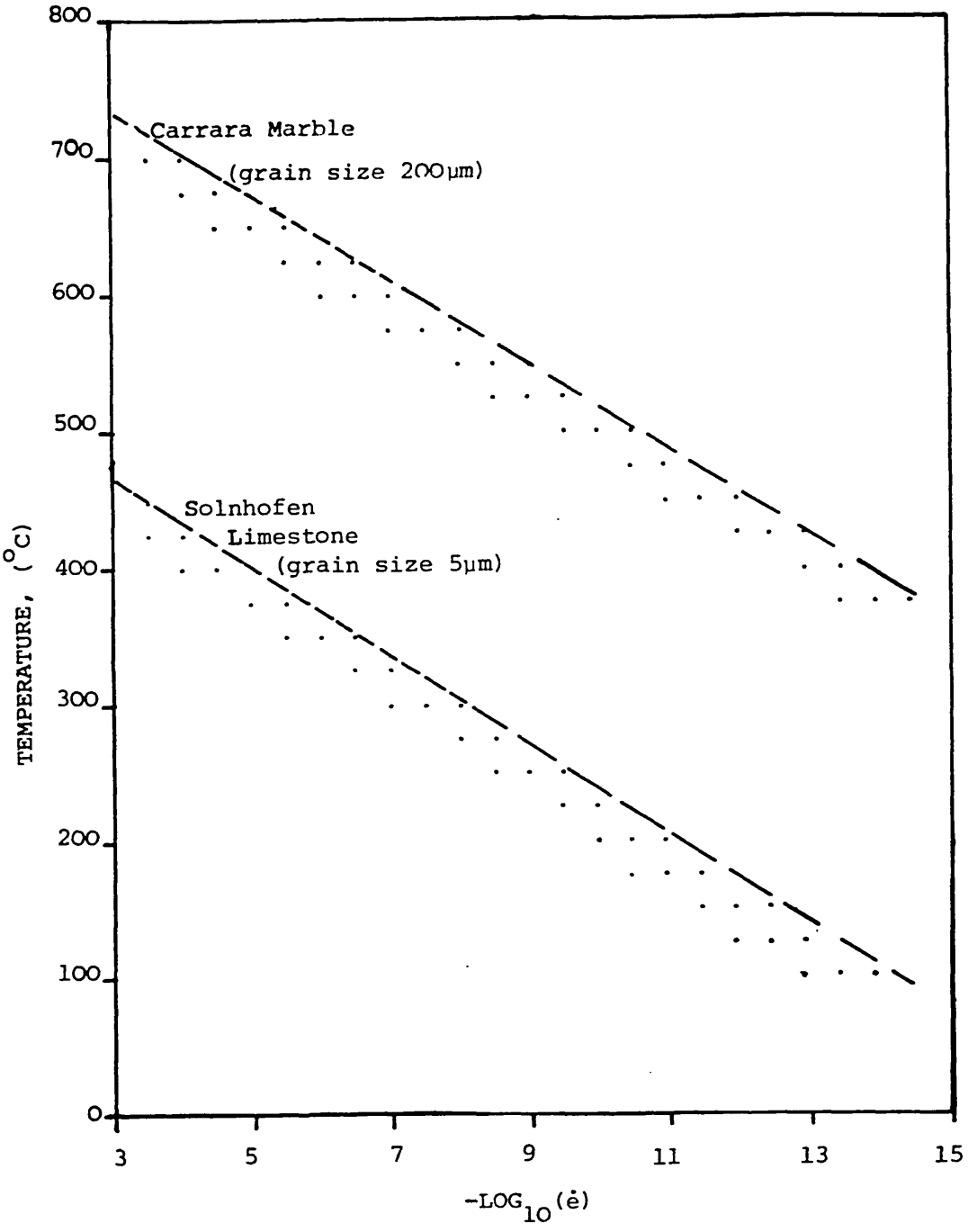

Fig 2.5

The twinning field boundaries for Carrara marble and Solnhofen limestone (after Spiers 1981). The twinning field side of each boundary is indicated by stippling. Both dashed boundaries after - Log_{10} (ė) of about 7 are obtained by extra polation.

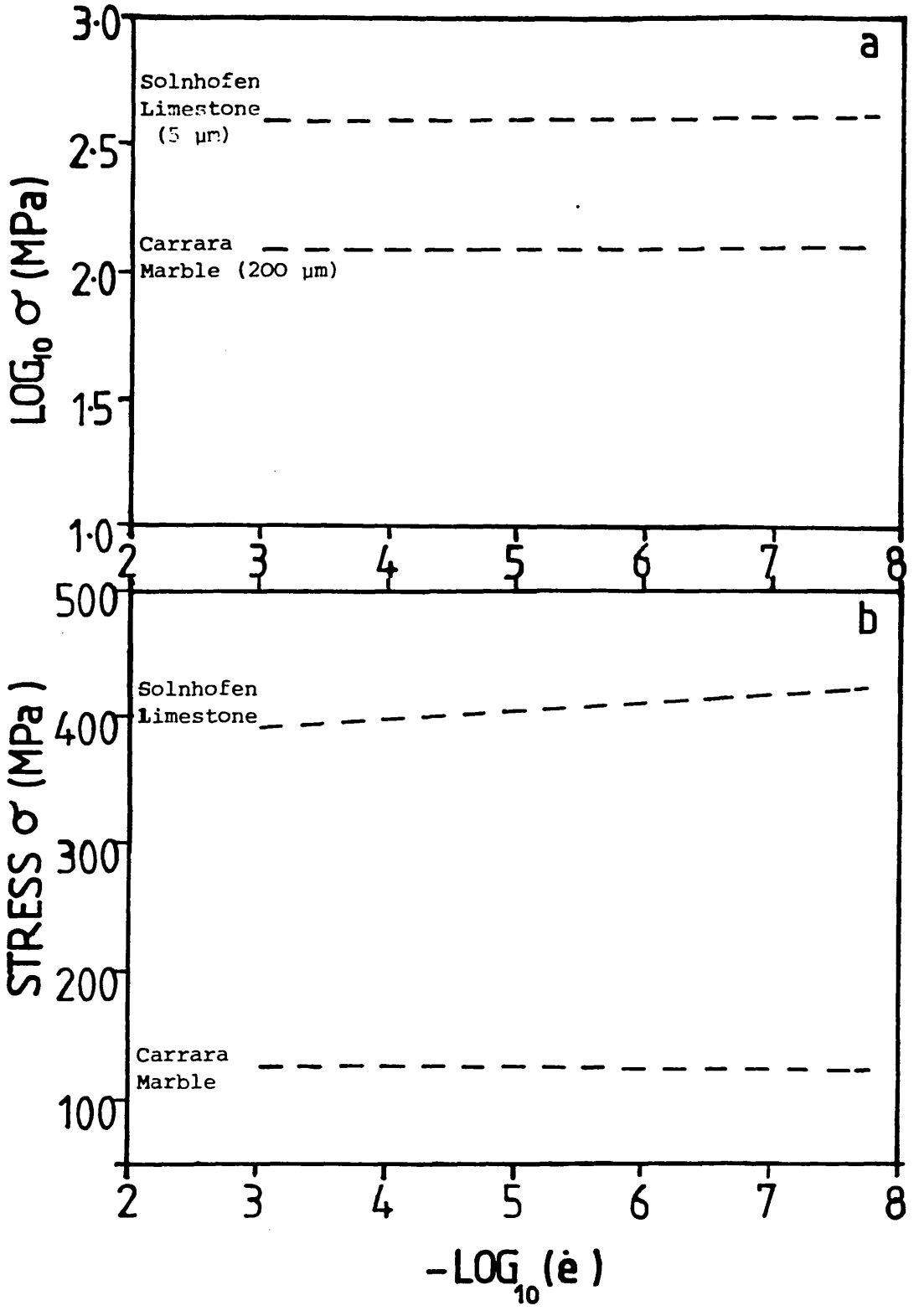

Fig 2.6 (a and b)

The twinning field boundaries (dotted line) for Carrara Marble and Solnhofen limestone plotted in $\sigma/\dot{e}$ space (after Spiers 1982). σ denotes the differential flow stress at 10% strain; $\dot{e}$ denotes the strain rate.

coarse marble. This stress is almost independent of strain rate and, as shown in figure 2.4, the temperature also.

Within the twinning field (0-400°C), Friedman and Higgs (1981) showed that only a very modest increase in grain aspect ratios (long axis ÷ short axis) is possible, even in simple shear (fig. 2.7). This is very little compared to the extensive increase in grain aspect ratios at higher temperatures where competition among various glide systems is very keen. Twinning porphyroclasts develop thin profuse twin lamellae at lower temperatures. As the temperature increases, the lamellae broaden and twinning tends to completion in particular grains (Wenk et al, 1973; Friedman and Higgs, 1981; Spiers, 1981). A critical shear stress for twinning is, according to Spiers and Wenk (1980), Wagner et al. (1982) a very tentative parameter because the stress to nucleate a twin is much higher than that to propagate it, but the use of CRSS generally as a means of predicting the possible combination of glide systems at particular temperatures cannot be doubted.

2.2.4 Lattice Preferred Orientation (Fabric or Texture)

The crystallographic preferred orientation (CPO) of calcite can be divided into three broad fields in temperature space:

2.2.4.1 At Low Homologous Temperatures ($0.03\,T_m$ to $0.43\,T_m$)

Between 25°C - 400°C, the C-axis (0001) orients in a point maximum or small circle girdle of 10-26° radius about the principal compression axis (Turner et al, 1956; Rutter and Rusbridge, 1977; Friedman and Higgs, 1981; Wenk et al, 1973; Kern, 1979; Wagner et al, 1982). This is in response to the rotation of the $\underline{e}(01\bar{1}8)$ twin plane, which tends to

Fig 2.7

Change in aspect ratios of porphyroclasts of sheared calcite with increasing temperature. S.M. is starting material, and values along the curve are corresponding shear strain (after Higgs and Handin, 1981).

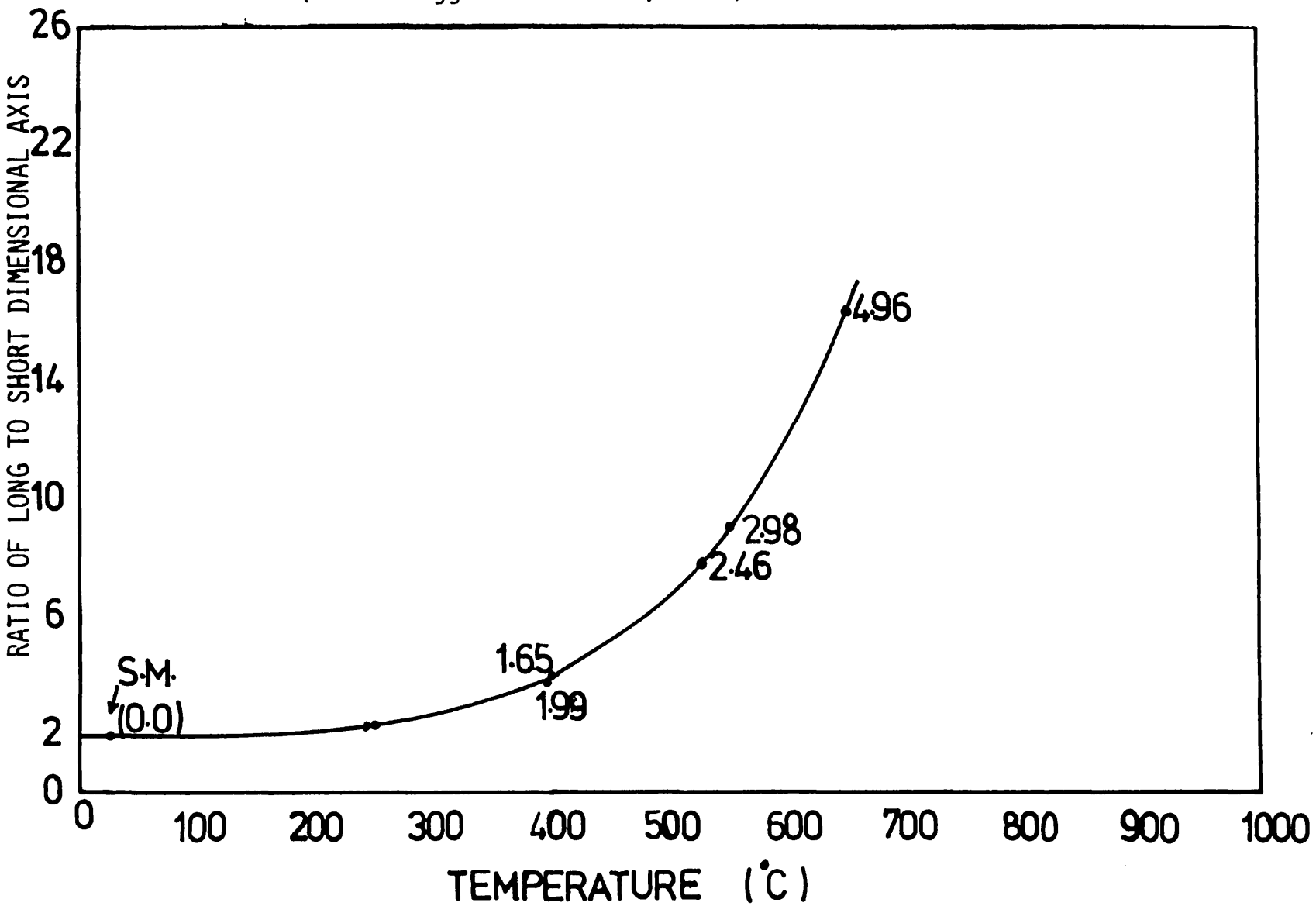

align the normals to e parallel to the maximum stress axis, reducing S_o - the resolved shear stress coefficient to zero (Friedman and Higgs, 1981, also Fig. 2.8). There is no report of recrystallization in this temperature range.

2.2.4.2 At intermediate temperatures (0.43 T_m to 0.75 T_m)

Between 400°C and 700°C CRSS values for r(10$\bar{1}$4) - the main slip system, f(10$\bar{1}$2), ($\bar{1}$012) and possibly other slip systems are so close to e($\bar{1}$018) - (see Fig. 2.4) that for practical purposes Von Mises criterion could be assumed attained. Hence, apart from the deformation becoming more homogeneous at that temperature range (Friedman and Higgs, 1981; Spiers, 1981; Wagner et al, 1982), it is not possible to separate the texture into components or domains in which only one glide system could be inferred. The long axes and the axial ratios of calcite porphyroclasts are dramatically increased (Friedman and Higgs, 1981; see also Fig. 2.7), usually forming a foliation normal to the axis of principal finite shortening ξ_1. In pure shear experiments ξ_1 is parallel to the principal compressive stress axis σ_1, while in simple and pure shear experiments ξ_1 increasingly rotates towards the shear zone normal, deviating from σ_1 as strain is increased (Kern and Wenk, 1983). In simple shear experiments, Friedman and Higgs (1981) noticed that at 650°C grain shape fabric defined a foliation plane inclined at 11° to the shear zone boundary.

Studies of the dislocation structure at this temperature range by Transmission Electron Microscopy illustrate that in each grain many different systems of dislocations are active, cross slip is common and at the higher temperature climb of dislocations also occurs (Goetze and Kohlstedt 1977; Barber and Wenk, 1979a; 1979b).

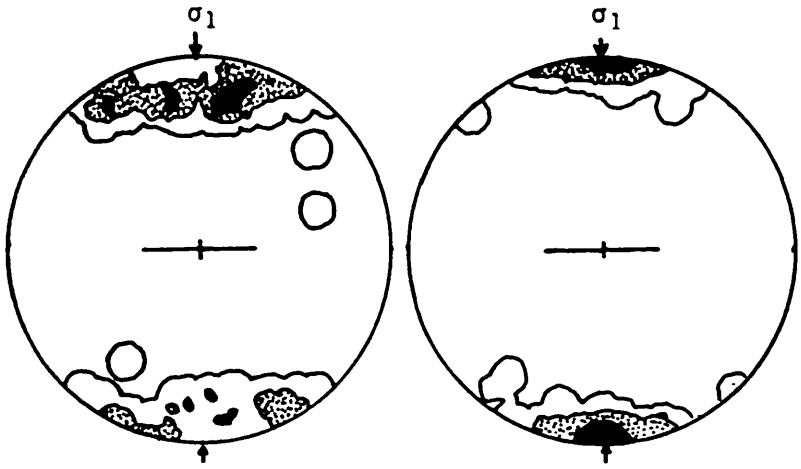

C-axes preferred orientation.

Poles to e-twin planes.

Fig. 2.8 (a) (b)

Yule marble deformed at 400°c (Turner and Weiss, 1963)

(a) C-axis crystallographic preferred orientation

(b) Poles to e-twin planes.
σ_1 marks the direction of principal compresssion.

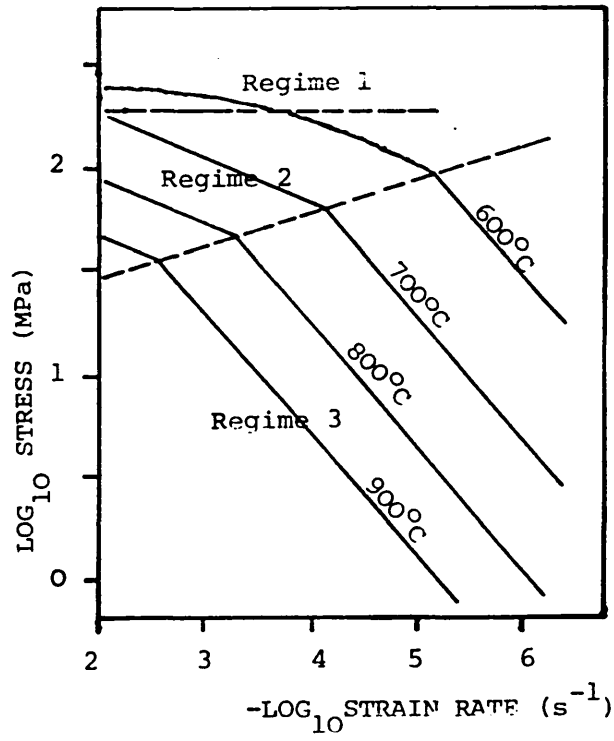

Fig. 2.9

Flow regimes for Solnhofen limestone (after Schmid et al. 1977)

The suppression of e-twinning in the intermediate temperature range is shown by Spiers (1981) to be associated with an e $\longrightarrow$ e/ah texture transition. Friedman and Higgs (1981) noticed an incipient recrystallization of elongated porphyroclasts at about 550°C and shear strains of nearly 3. This becomes more pervasive at 600°C, with most of the fine-grained neoblasts being strain-free.

2.2.4.3 At high temperatures (> 0.75 T_m)

At temperatures above 700°C, recrystallization is dominant, producing mosaics of coarse-grained twin-free neoblasts, which subsequently twin (Friedman and Higgs, 1981). The crystallographic preferred orientation of the strain-free neoblasts may either be random (Friedman and Higgs, 1981) or be controlled by grain growth of crystals which are in a favourable orientation in the stress field (Wenk et al, 1973). Unlike the diffusionless process of twinning, the rate of grain boundary diffusion at these high temperatures is very high (Wenk et al, 1973), hence Friedman and Higgs (1981) noticed that the resulting crystallographic orientations are not those expected from dislocation glide alone. The latter found that the C-axis fabrics for the syntectonically recrystallized grains geometrically tracked neither the incremental stress nor the finite strain axes in simple shear experiments on calcite.

2.2.5 Rheological Behaviour of Calcite

The rheological behaviour of Solnhofen limestone, Carrara and Yule marbles, which are similar (Rutter, 1974), show a work-hardening flow in stress/strain space, with strength virtually independent of strain rate at temperatures from 20°-400°C. These characteristics are unaffected by pore

REGIME 1	REGIME 2	REGIME 3
$\dot{e}=A.\exp(-\Delta H/RT)\exp(C\sigma)$ ---- 2.1	$\dot{e}=A.\exp(-\Delta H/RT)\sigma^n$ --- 2.2	$\dot{e}=A.\exp(-\Delta H/RT)\sigma^n$ --- 2.3
$\log_{10}A = -0.2$	$\log_{10}A = -1.3$	$\log_{10}A = 2.7$
$\Delta H = 47.1$	$\Delta H = 71.1$	$\Delta H = 50.9$
$C = 2.7$	$n = 4.7$	$n = 1.7$
Rutter (1974)	Schmid et al.(1977)	Schmid et al.(1977)
Exponential law Regime	Power-law Regime with high n-values	Schmid et al.(1980) Superplastic Regime/Power-Law Regime with low n-values.

TABLE 2.3 Flow Law Data for Regimes 1-3 in Solnhofen Limestone and Carrara Marble

Units: ΔH (Kcal mol^{-1}), $C(kb^{-1})$, σ(bars), A (sec^{-1} bar^{-n}), (for equations 2.1, 2.2 and 2.3 only).

water in this temperature range in Carrara marble, although Solnhofen limestone is weakened by pore water in this range. This water weakening is thought to be much less significant at higher temperatures. Also, cataclasis is reduced by increasing effective confining pressure and/or temperature.

Above 400°C, particularly between 600°C and 900°C, the Creep behaviour of these rock types is found to fall into three different flow regimes (Fig. 2.9 and Table 2.3). Above 400°C recovery processes begin to gain importance and a transition to thermally activated, steady-state flow occurs where the flow stress reaches a practically constant (steady state) level after a few percent strain (Schmid, 1977), even when the fastest strain rates are used. The flow regimes have

been delineated as:

Regime 1: where the stress dependence of strain rate is best described by an exponential flow law. This regime occurs at flow stresses above 190 MPa, at temperatures of 400°C-600°C, and at laboratory strain rates, a relatively low strain rate sensitivity of the flow stress has been observed (Rutter, 1974; Schmid, 1976; Schmid et al, 1977; 1980), and the flow law is expressed by equation 2.1 above.

Regime 2: In Carrara marble this regime ranges from 20 to 100 MPa, while in stronger and finer Solnhofen limestone the lower stress limit is 40 MPa at 900°C or 100 MPa at 600°C (Schmid et al, 1977). Also, the upper stress boundary for Solnhofen limestone is almost independent of temperature at 190 MPa. For weaker and coarse-grained Yule marble, on the other hand, the upper stress level for regime 2 is 140 MPa, while the stress at the regime 2/regime 3 boundary is as yet unknown (Heard and Raleigh, 1972; Rutter, 1974; Schmid et al, 1980).

The rheology of the rocks can best be described mathematically using a power law equation (equation 2.2), like that of Weertman (1975). The value of n - the stress exponent - ranges from 4.37 to 4.7 for Solnhofen limestone, 7.6 for Carrara marble, and 7.7 for Yule marble.

This regime shows scarcity of twinning, a strong subgrain microstructure and a core and mantle structure in the individual grains. The mantles contain subgrains whose rotation is large enough to form recrystallized grains, while the cores may contain all stages of strain - undulatory extinction, deformation bands and subgrains.

Regime 3: Most of regime 3 is characterized by low stress

and occurs below 20 MPa, although the maximum stress boundary (i.e. regime 3/regime 2 boundary, see Fig. 2.9) could be up to 100 MPa at lower temperatures. It is described by a power law relationship between strain rate and stress, of the form shown in equation 2.3. The stress exponent n ranges from 1.7 for Solnhofen limestone to 4.2 for Carrara marble and could be more for Yule marble (Schmid et al, 1977; 1980). Deformation in this regime has a lower activation energy (ΔH = 51 k cal/mole), and exhibits the characteristics of superplastic flow.

In this regime too, extensive recrystallization takes place with grain growth to an equilibrium size (Schmid et al, 1980) proportional to the flow stress (between 10-100 MPa), as predicted by Twiss (1977).

2.3 DEFORMATION OF DOLOMITE - THE PLASTIC FIELD

2.3.1 Introduction

Like calcite, dolomite ($CaMg[CO_3]_2$) belongs to the rhombohedral group of carbonates. Ideally it has an ordered trigonal structure, of space group ($R\bar{3}$) with planes containing atoms of only Ca, or only Mg, alternating and being interleaved with the planes containing the carbonate groups (Fig. 2.1b). All these planes are perpendicular to the 3-fold axis (the c-axis). All the anions (CO_3^{-2}) of a given plane have the same orientation, but are rotated 60° w.r.t. the anions in the two adjacent planes (Gunderson and Wenk, 1981). Thus, the unit cells contain the same number of atoms in both calcite and dolomite and all repeat distances, and hence potential Burgers vectors, are the same in both minerals (Paterson, 1979).

Apart from the anion rotational disorder mentioned

above, heating dolomites to 1100°C (Reeder, 1980) could also disorder them. Translation of Ca into Mg positions results, by the same vector that translates a CO_3^{-2} group in one orientation into one which is 60° rotated. This type of disorder or the beginning of it was shown by Barber et al (1981) to cause difficulties on the path of moving dislocations. A third type of disorder in dolomite is substitutional, and it accompanies the first phase of dolomite crystallization (Gunderson and Wenk, 1981).

Other differences between calcite and dolomite are the greater ductility of calcite compared to dolomite, the relative ease of slip compared to twinning in dolomite as against twinning before slip in calcite. These are dealt with more exhaustively below.

2.3.2 Twinning in Dolomite

A well established rule in metallurgy is that twinning is a low temperature phenomenon. As temperature increases slip is favoured at the expense of twinning, resulting ultimately in complete cessation of twinning. While calcite adopts this behaviour, as shown in section 2.2.2, dolomite does not.

Dolomite twins on $\underline{f}(02\bar{2}1)$ in the $<10\bar{1}1>$ direction with a -ve sense (Higgs and Handin, 1959; Fairbairn and Hawkes, 1941; Turner et al, 1954b; Barber and Wenk, 1979; Barber et al, 1981). Although Higgs and Handin (1959) suggest that twinning can be activated only within a very limited temperature range - 400-500°C - Barber et al (1981) suggested lowering the onset temperature to at least 300°C, as did Handin and Fairbairn (1953, 1955). As shown in figure 2.10c, although there is a possibility of dolomite twinning starting earlier than 400°C, the critical resolved shear stress (CRSS) becomes too high

	Number of Cryst allographically equivalent systems	Symbol	Critical Shear Stresses MPa for Single Crystals at 400°c	at 600°c	Reference
Twinning System					
$(02\bar{2}1)\ \langle 10\bar{1}1\rangle$	3	f^-	127	-	Higgs and Handin (1959) Barber et al. (1981)
Slip Systems					
$(0001)\ \langle 11\bar{2}0\rangle$	3	$c^{\pm}$	94	118	Higgs and Handin (1959) Barber et al. (1981)
$(\bar{1}012)\ \langle 20\bar{2}1\rangle$	3	f	129	110	Barber et al. (1981) Barber (1977)
$(10\bar{1}4)\ \langle 11\bar{2}0\rangle$	3	r			Barber et al. (1981)
Kinking					
$t = \langle 11\bar{2}0\rangle$					Johnsen (1902) Weiss & Turner (1972)
$t = \langle 10\bar{1}0\rangle$					Weiss & Turner (1972)

TABLE 2.4 Glide systems of dolomite with known values of CRSS. The $+^{ve}$ and $-^{ve}$ signs refer to the direction sense of twin or translation gliding.

Fig. 2.10

Variation of critical resolved shear stress with temperature for dolomite.

(a) Resolved shear stress for c-slip

(b) Resolved shear stress for f-slip

(c) Resolved shear stress for f-twinning (after Higgs and Handin, 1959; Barber et al. 1981).

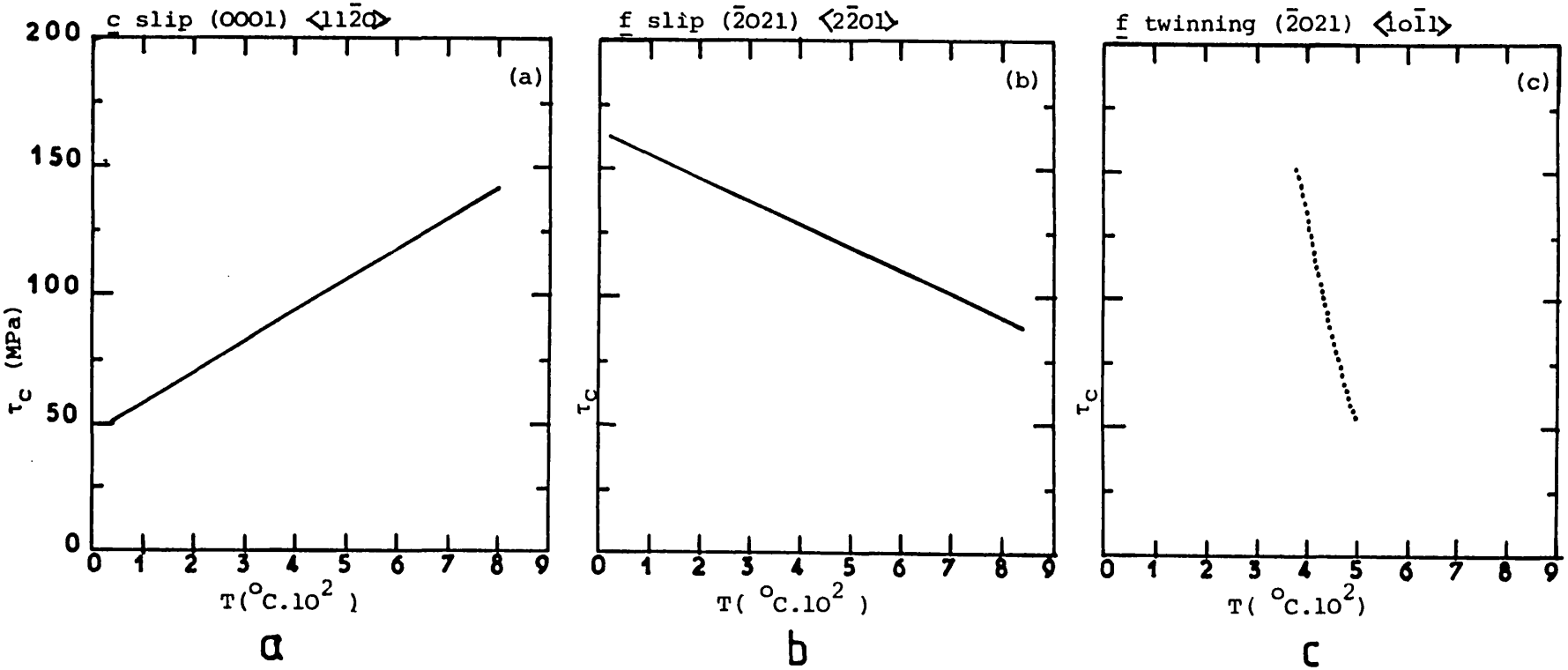

(> 150 MPa) at those low temperatures. Slip dislocations have been imaged on c and f planes above 300°C, showing that while twinning is prevalent, some slip still occurs. As noticed by Barber and Wenk (1979), dolomite twinning does not nucleate dislocations in the surrounding matrix like calcite, and dislocation densities generated at twin intersections in dolomite are seldom as high as those in calcite at similar strains.

2.3.3 Low Temperature Plastic Deformation of Dolomite

Between room temperature and approximately 400°C the only known easy glide mechanism is slip on the basal plane (0001). This system oparates with equal facility in both +a and -a directions, with a CRSS value as low as 50 MPa at room temperature (Higgs and Handin, 1959; Barber et al, 1981; see also fig. 2.10a). The CRSS for basal slip in dolomite increases with temperature, possibly up to 900°C. This was first noticed by Higgs and Handin (1959) and later confirmed by Barber et al.(1981), showing that basal slip is not likely to make large contributions to preferred orientation of dolomite grains at high temperatures. At about 400°C Higgs and Handin (1959) showed that the CRSS for basal translation and f-twinning is the same, and their individual contributions to lattice preferred orientation in dolomite would, therefore, be impossible to differentiate.

Turner et al.(1954b) had earlier noticed that basal slip in dolomite left no trace of visible (0001) lamellae in thin sections, but caused internal rotation of pre-existing $(02\bar{2}1)$ lamellae to an anomalous new orientation they designated L_9. The angle between L_9 and the basal plane was also found to be less than the angle between new $(02\bar{2}1)$ and (0001).

Basal glide was also shown by Weiss and Turner (1972)

to produce two sets of kink bands : t = $\langle 11\bar{2}0 \rangle$ noticed earlier by Johnsen (1902); and t = $\langle 10\bar{1}0 \rangle$ first observed by Weiss and Turner.

Although at room temperature, CRSS for basal glide in dolomite and r-slip in calcite are of the same order of magnitude, the CRSS for the former increases with temperature, while for r-slip it decreases with increase in temperature. The reason for the increase in dolomite has not yet been ascertained without doubt, although Higgs and Handin (1959) thought it might relate to the Mg ion. Barber et al's (1981) explanation for the anomaly may be nearer the true picture and is discussed below. Only layers parallel to the basal plane c contain ions of the same species (Fig. 2.1b), and hence basal gliding means gliding on the "smoothest" plane (Higgs and Handin, 1959). For unit Burgers vector ($1/3\ [2\bar{1}\bar{1}0] = 1/3$ a, Barber et al, 1981) of displacement CO_3^{2-}, Ca^{2+} or Mg^{2+} ions are very likely to go into their species positions, without one species being placed in another's position. However, as temperature increases, thermal vibration of lattice sites increases, the CO_3^{2-} ion expands in size and rotates. All three factors will add to the repulsion between passing anion groups (Barber et al, 1981) and thus obstruct dislocation movement. In addition to this the dolomite lattice loses CO_2 at higher temperatures, resulting in substitution of the CO_3^{2-} group by O^{2-}. Although the rhombohedral carbonate lattice is still preserved, the structure contains considerable CO_3^{2-} vacancies. Such vacancies can pin down dislocations, inhibiting their mobility and making (0001) less easy as a glide plane as temperature increases.

Cataclasis is another important deformation mechanism

at low temperatures and high stresses in carbonate minerals (Rutter, 1974; Barber et al, 1981). In dolomite this produces r-cleavage (Christie, 1963), or shear fracturing (Higgs and Handin, 1959; Handin and Fairbairn, 1953, 1955; Barber et al, 1981). Barber et al.(1981) insist that shear fracturing is a significant deformation mechanism in support of earlier observations. Handin and Fairbairn (1953, 1955) showed that all tests performed between room temperature and 300°C ended in fracture along surfaces inclined at about 60° to the least principal stress axis. Higgs and Handin (1959) on the other hand observed that even within the twinning field macroscopic shearing could take up a large percentage of the total strain imposed on their specimens.

2.3.4 Between 400-600°C

Although Higgs and Handin (1959) would ascribe all strain in plastically deformed dolomite above 400°C to f-twinning alone, later observations on naturally and experimentally deformed dolomite do not seem to bear this out. Wenk and Shore (1975) showed that within this temperature range the inverse pole figure from experimentally deformed dolomite is complex though consistent. Two maxima are formed, one at a negative rhomb near e (30° from c) and the other at a high angle positive rhomb near f' (70-80° from c). C-axes are aligned on a small circle girdle 35° to σ_1 (possibly due to the effect of e) and on a great circle at right angles to σ_1 (Fig. 2.11c). White and White (1980), on the other hand, observed that the dominant mechanism of deformation in a natural dolostone tectonite of maximum estimated temperature of 600°C was basal (0001) slip. They also inferred some r and f-slip activity but of lower effect compared to c-slip. At this temperature they also observed subgrains and recrystallised

grains, but no twinning, which they attributed to an inadequate resolved shear stress to initiate twinning.

Barber et al's (1981) experimental work on dolomite showed that basal slip goes on past 400°C and up to 800°C at least. 400-600°C is also the temperature range within which the CRSS for f-slip falls below that of c-slip, and introduces f-slip as a serious competitor to basal slip and f-twinning. Exactly where f-twinning stops in dolomite is not known. Although it is the dominant glide mechanism between 400 and at least 500°C Higgs and Handin (1959), Barber et al.(1981) have observed f-twinning on a smaller scale between 600° to 800°C. They also confirmed White and White's (1980) observation of activity on r-$(10\bar{1}4)$ at 600°C in an a = $\langle 11\bar{2}0\rangle$ direction.

2.3.5 High Temperature Deformation of Dolomite

At temperatures between 600°C and 1000°C f = $(\bar{1}012)$ and possibly r= $(10\bar{1}4)$ slip gradually take over from c = (0001) slip. The CRSS for f-slip decreases with increasing temperature, becoming lower than that for c-slip from 600°C onwards (Barber et al, 1981; see also Fig. 2.10b). The latter also found that although resolved shear stresses on two f-systems are always equal, slip always occurs only on one and the same f-system. r-slip was observed to be frequently accompanied by cleavage on planes parallel to the slip (Barber et al, 1981) but is mainly a high temperature slip system, the behaviour of which in CRSS-Temperature space is as yet unknown.

Within this temperature range also extensive cross slip of f-dislocations onto the c-plane have been found to accompany climb of dislocations (Barber, 1977; Barber et al, 1981). Grain boundary diffusion and recovery (above 700°C - Wenk and Shore, 1975) and grain boundary sliding (about 600°C - White and White, 1980) may be accompanied by recrystallization

(Neumann, 1969). Neumann's experimental evidence at 1000°C was later confirmed by Wenk and Shore (1975), who showed that at this temperature, and possibly starting from 600°C, the c-axes of recrystallized dolomite grains tend to align parallel or at very small angles to σ_1 (see Fig. 2.11c). She also found that host grain control in dolomite c-axis fabric is weaker 30°-60°, compared to calcite, 25°-35°. The recrystallization mechanism suggested by Neumann's laboratory tests was nucleation of strain free grains rather than sub-grain nucleation and rotation, or bulge nucleation characteristic of annealing recrystallization.

2.3.6 Crystallographic Preferred Orientation in Polycrystalline Dolomite

Since 1930, when Sander published the first fabric diagram of deformed dolomite (Fig. 2.11a), the wealth of knowledge on dolomite fabric has grown steadily, although at far less a pace than other common minerals, in particular quartz and calcite. The nearly foliation-normal double maxima of c-axes recorded by Sander (1930) were later reproduced by Fairbairn and Hawkes (1941) from Clair River dolomite marble and Hasmark dolomite marble. This prompted the conclusion from the latter that for dolomite only those grains with vertical axes approximately paralllel to the stress would deform by basal translation and twinning. For a maximum principal stress orientation parallel to C_v = [0001], the resolved shear stress on the basal plane would be zero, making basal translation impossible. This same orientation would put a maximum resolved shear stress on $(02\bar{2}1)$, the pole of which is 62½° to C_v (Christie, 1958), and thereby result in twinning only. Christie (1958) on the other hand showed

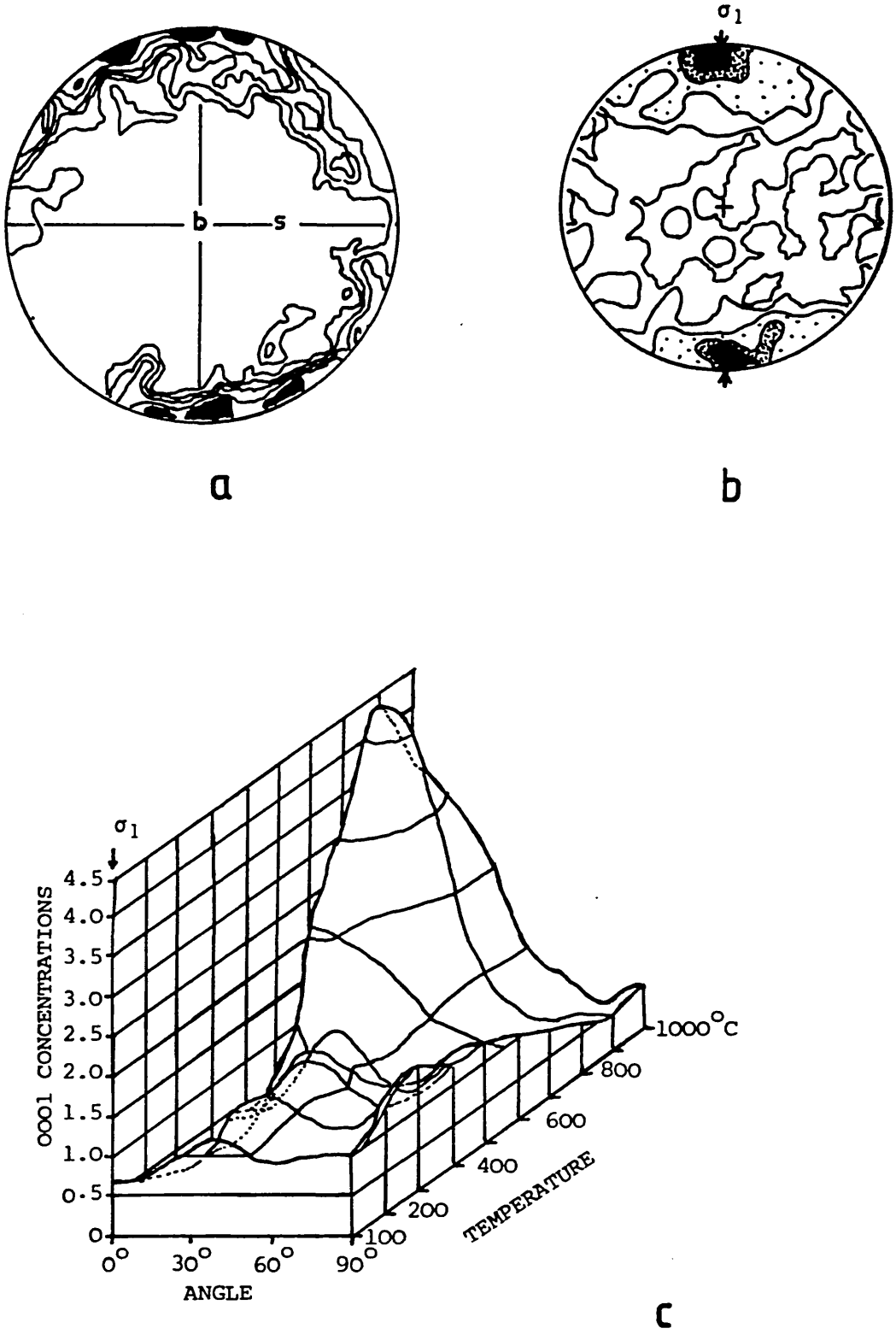

Fig. 2.11

C-axis crystallographic preferred orientation of dolomite (a and b) after Sander (1970) and Neumann (1969) respectively.

(c) block diagram with normalized c-axis profiles from parallel to normal to the compression axis as a function of temperature. All experiments were deformed at $\dot{e} = 10^{-6}$ sec $^{-1}$ and 10 kb confining pressure. Overall shortening varied between 15 and 40% (after Wenk and Shore, 1975). b and s refer to lineation and foliation respectively, while σ_1 is the maximum compressive stress.

that compression of a randomly oriented dolomite polycrystal would produce c-axes close to the axis of maximum compression if basal translation was effective, whereas twingliding on $(02\bar{2}1)$ would produce the opposite effect - a rotation of c-axes from the axis of compression. Such a rigid framework is only useful where the operating glide system and the contributions from other competing systems are known.

The fabric of Crevola dolomite marble also showed a strong preferred orientation of the c-axes normal to the foliation plane (Trommsdorf and Wenk, 1965). All the grains analysed contained one or more sets of visible $\underline{f}=(02\bar{2}1)$ twin lamellae.

C-axis fabric analysis from experimentally deformed dolomite polycrystals was started by Turner et al. (1954b), who showed that shortening a cylinder of dolomite rock by 9.4% led to only slight changes in the pattern of preferred orientation at 380°C. Later Wenk and Shore (1975) showed that between 300°C and 700°C c-axes of deformed dolomite tend to align in a small circle girdle of about 35° to σ_1 or in a great circle at right angles to σ_1 (Fig. 2.11c). At higher temperatures (700-1000°C) where grain boundary diffusion and recovery (Wenk and Shore, 1975) are likely to be accompanied by recrystallization (Neumann, 1969), c-axes tend to align parallel to the axis of compression, with a weak host grain control (Fig. 2.11b). This latter dolomite fabric resembles calcite fabrics produced at low temperatures so much that Neumann (1969) suggested that slip and twinning mechanisms may not be the real causes of crystallographic preferred orientation in both minerals.

Laboratory simulation of natural tectonite fabrics in carbonate rocks is likely to yield more information when:

(i) the range of values of CRSS at which a particular glide system contributes to the overall fabric is known;

(ii) experimental strain rates are lower than those presently used;

(iii) the nature of tectonic deformation conditions is more closely approximated, for example by the inclusion of water in laboratory rock deformation, and

(iv) more information is made available about dolomite, magnesite and calcite glide systems.

2.4 DEFORMATION OF CALCITE AND DOLOMITE BY SOLUTION PROCESS

The stress, strain or temperature-induced dissolution of common carbonate minerals has not received as much attention as their behaviour in the plastic field. A lot more investigation has been directed at the free dissolution kinetics in pure and carbonated water than what is usually referred to as pressure solution behaviour of calcite and dolomite. Here, too, as in the plastic field, more information is available for calcite than dolomite.

2.4.1 Dissolution of Calcite

The effect of temperature on the solubility of calcite has been studied by a few geologists, and among those who studied this behaviour in CO_2-free water, Morey's (1962) experiments produced some of the most interesting results. As shown in figure 2.12a, the solubility of calcite in CO_2-free water remains constant at about 20 ppm from room temperature to about 150°C. This study was done at atmospheric pressure using crushed fine-grained calcite powder. Above 200°C the solubility decreases almost linearly

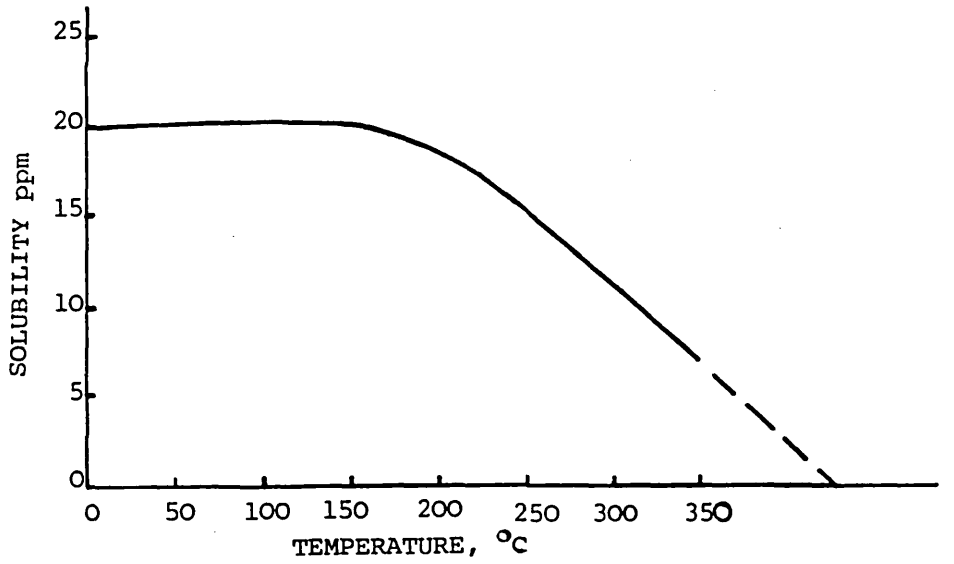

a

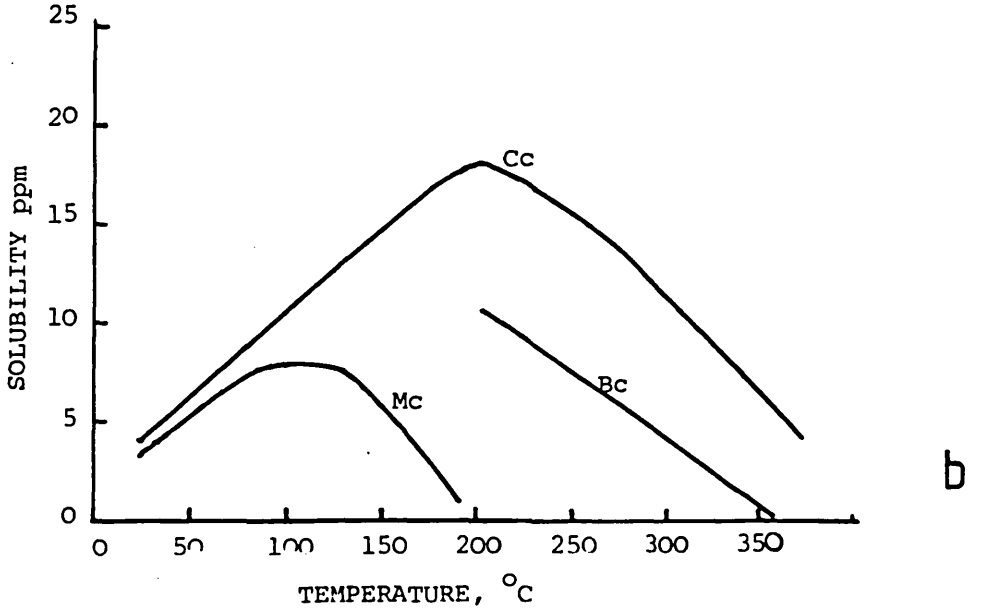

b

Fig. 2.12

(a) The solubility of $CaCO_3$ in CO_2-free water. The solubility remains practically constant up to about 150°c, after which it falls off rapidly - to about zero at the critical temperature of water.

(b) The incongruent dissolution of dolomite in CO_2 - free water as a function of temperature Cc = $CaCO_3$, Mc = $MgCO_3$, Bc = $Mg(OH)_2$ (after Morey, 1962).

till 350°C, tending to zero at the critical temperature of water (374.11°C). Segnit et al. (1962) showed that at any CO_2 pressure (between 0.2-6.0 MPa) the solubility of calcite decreases as the temperature increases. At all temperatures investigated, the solubility increased fairly rapidly with increase in CO_2 pressure. This behaviour shows that in natural environments where calcite is undergoing metamorphism, increase in temperature will result in decrease in calcite content in fluids and an equal increase in calcite precipitation and cementation.

The pressure-induced dissolution of calcite has been studied by Rutter (1976), Baker et al. (1979, 1980) and Girou et al. (1982). Based on the assumption that textures characteristic of diffusive mass transfer by pressure solution are found commonly in rocks deformed at temperatures up to about 400°C, Rutter (1976) constructed a deformation mechanism map for calcite incorporating a pressure solution field. Figure 2.13 shows a solid boundary between pressure solution at low temperatures (0-450°C) and Coble creep (450-600°C) in calcite rock of grain diameter 100μm and activation volume V = 37 cm^3. There is no geological evidence so far that the boundaries between Nabarro-Herring Creep and Coble Creep or Coble Creep and Pressure Solution Creep are really solid, not transitional boundaries.

Baker et al (1980) showed that increasing the effective stress increased the amount of dissolution, and hence the amount of crystallization, while the addition of clay, basaltic glass and silica minerals only retarded the rate of recrystallization of the carbonate. Girou et al. (1982) found by applying axial loads of 0-240 MPa parallel to the a_3 axes of calcite rhombs that solubility was mainly controlled

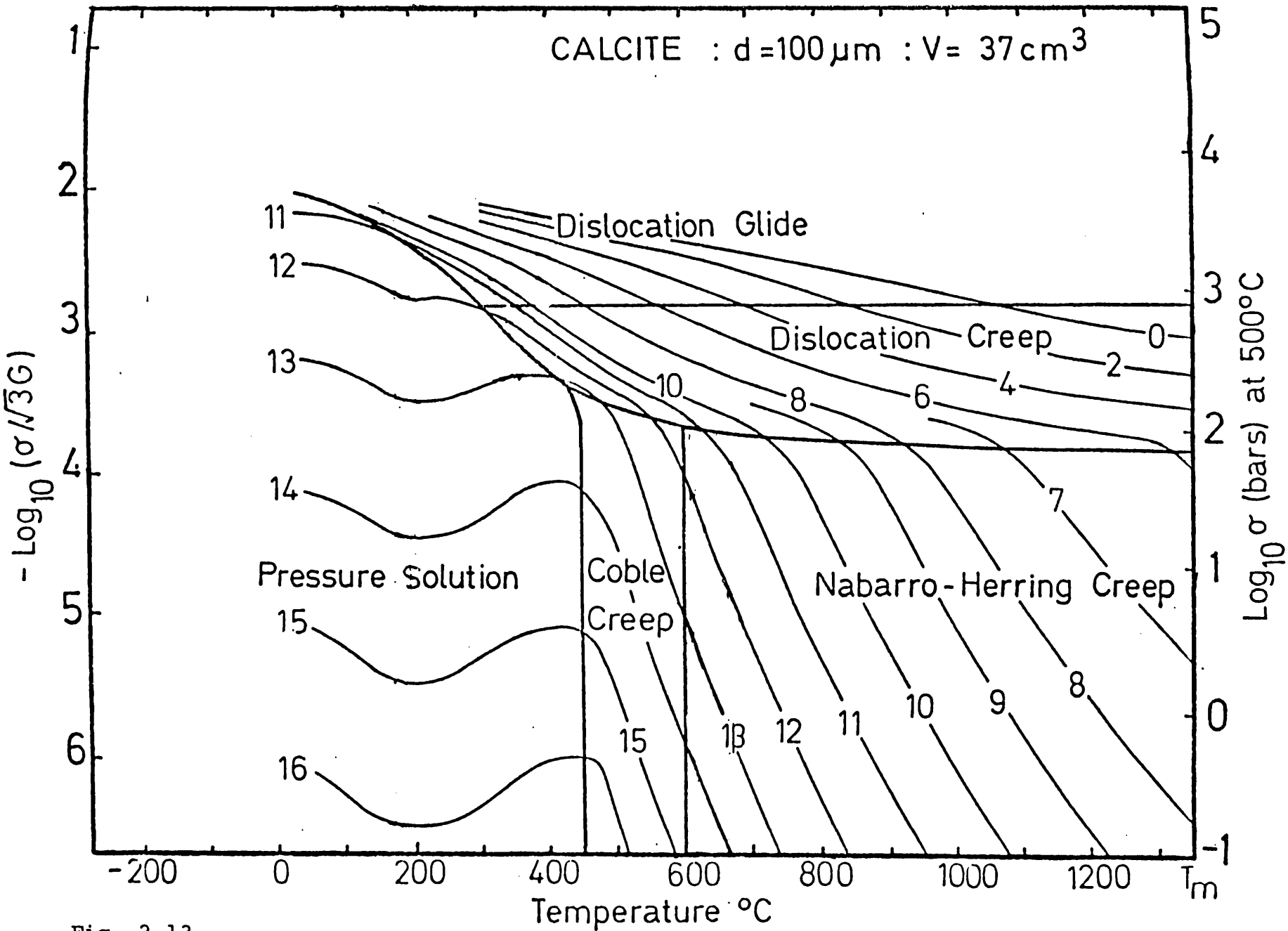

Fig. 2.13

Deformation mechanism map for calcite - including a pressure solution field (after Rutter 1976). d and V are the material grain size and molar volume respectively while σ and the numbers on the curves are the differential stress and the strain rates res ectivel .

by stress-dependent mechanical activation, while chemical effects like chemical activity and the effects of internal energy, entropy and solid molar volume under stress (Paterson, 1973) on solubility seemed negligible.

2.4.2 Dissolution of Dolomite

The dissolution behaviour of dolomite is not only less well known, but as Morey (1962) showed, is more complicated than that of calcite. As figure 2.12b shows, the dissolution of dolomite [$CaMg(CO_3)_2$] in CO_2-free water is incongruent. At all temperatures between 0 and 350°C, more calcite is dissolved than magnesite, and at about 200°C the solubility of magnesite is about zero while that of calcite reaches a maximum. Busenberg and Plummer (1982) confirmed the non-stoichiometric dissolution of dolomite, showing also that the dissolution of dolomite decreases with increasing pH and that at a constant pH the dissolution increases as the partial pressure of carbon dioxide (PCO_2) increases. At temperatures above 200°C the dissolution of dolomite is actually the separate dissolution of calcite and brucite, if the water is CO_2-free. To prevent the formation of brucite [$Mg(OH)_2$], Rosenberg and Holland (1964) passed carbon dioxide into the solution at 6.0 MPa. They showed that the stability field of dolomite lies entirely in the Ca-rich portion of the system between 275° and 420°C, and that the lowest temperature at which dolomite dissolved congruently was still unknown.

The pressure-induced dissolution of dolomite is a relatively neglected area, possibly because the role of pressure solution in rock deformation is not very easy to model, and as a result the importance of the interaction between crystal plasticity and pressure solution, particularly

in the greeschist facies has been relatively neglected.

2.5 STABILITY AND METAMORPHISM OF CARBONATE ROCKS

The dissociation of common carbonate rocks like calcite, dolomite and magnesite has been extensively studied, not only as an aid in determining metamorphic conditions in the field, but also for its industrial applications. Their stability fields can be defined with respect to temperature, fluid pressure, the amount of strain energy stored in them, the whole rock composition of which they are a part and probably the composition of the respective mineral in question.

2.5.1 The Relative Stabilities of Pure and Strain-free Calcite and Dolomite

With dolomite as starting material, thermal dissociation is not very significant below 600°C. Above 600°C an increasing amount of CO_2 pressure is necessary to stabilize dolomite with respect to calcite, periclase and CO_2. This behaviour is shown by Harker and Tuttle (1955), Graf and Goldsmith (1955), Goldsmith (1980). Figure 2.14 is a univariant pressure (CO_2)-temperature curve for the dissociation of dolomite. The dissociation equation proposed by Harker and Tuttle (1955) was later revised by Goldsmith (1980) on the evidence that the calcite produced by the process is never pure $CaCO_3$, but, depending on the temperature and CO_2 pressure, contains more or less $MgCO_3$ in solid solution: the equation for high temperature dissociation is:

$$\underset{\text{Ca - dolomite}}{Ca_1Mg_x(CO_3)_{(1+x)}} \rightleftharpoons \underset{\text{Mg - calcite}}{Ca_1Mg_{(x-y)}(CO_3)_{(1+x-y)}} + yMgO + \underset{\text{periclase}}{yCO_2} \quad \ldots 2.4$$

At low temperatures and pressures the solid solution in

Fig 2.14

Univariant pressure (CO_2) - temperature curve for the dissociation of dolomite according to the equation: $CaMg(CO_3)_2 = CaCO_3 + MgO + CO_2$ (after Harker and Tuttle, 1955). do = dolomite, cp = calcite and periclase.

Fig 2.15

Pressure (CO_2) - temperature curves for the dissociation of calcite, dolomite and magnesite. The triangular diagrams show the phases which would be stable in the divariant regions defined by the P - T curves ignoring any solid solution there may be among the phases.
F = CO_2, C = calcite, D = Dolomite, M = Magnesite, L = Lime and P = Periclase (after Harker and Tuttle, 1955).

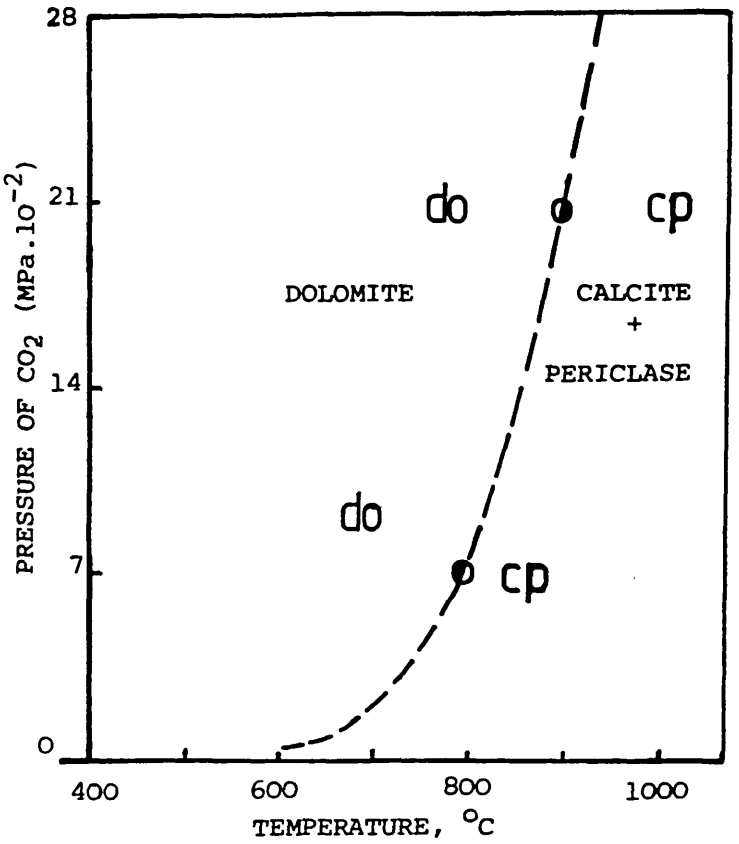

Fig. 2.14

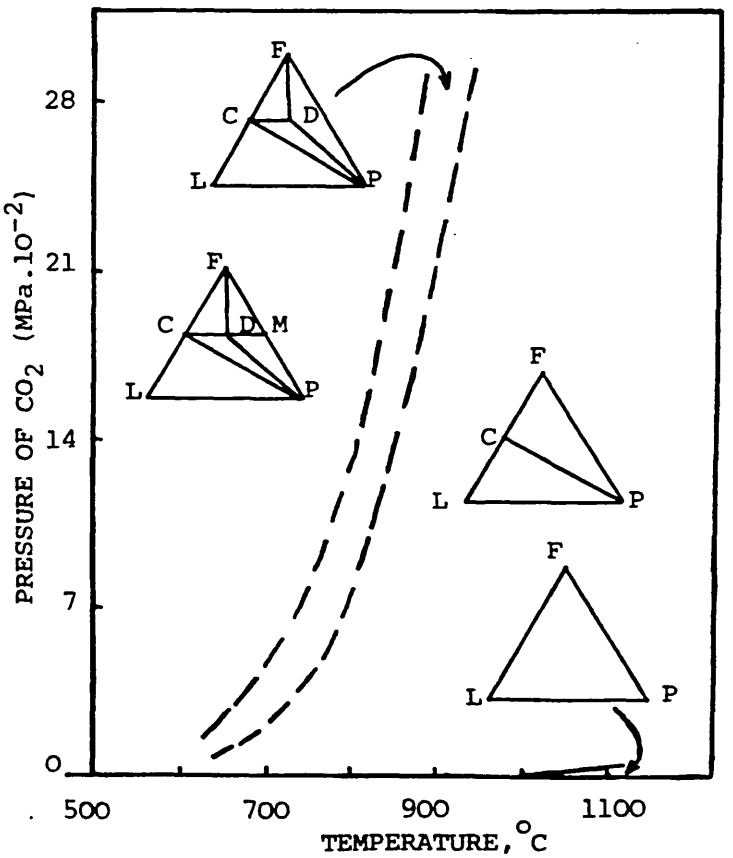

Fig. 2.15

dolomite is so little that $x \approx 1$, and the equation becomes:

$$Ca_1Mg_1(CO_3)_2 \rightleftharpoons Ca_1Mg_{(1-x)}(CO_3)_{(2-x)} + xMgO + xCO_2$$

dolomite Mg-calcite periclase

. . .2.5

as expressed by Graf and Goldsmith (1955). Stability studies have shown that dolomite is still stable at 1600°C, provided pressures of up to 2000 MPa are applied (Goldsmith, 1980), which physical conditions may be attained in the upper mantle.

Calcite is a lot more stable than dolomite, as shown by Figure 2.15, and both are more stable than magnesite. By deforming single crystals of $CaCO_3$ at 700°C and subsequently allowing decomposition to continue at very low rates, Thomas and Renshaw (1967) noticed that there was preferential decomposition at dislocations gliding on $(40\bar{4}1)$, $(10\bar{1}0)$ and less in $(02\bar{2}1)$ planes. Decomposition was also favoured along twin boundaries, necessitating the tentative suggestion that the intrinsic energy of a dislocation contributes to the energy of activation of decomposition. Pure calcite dissociates to lime at very high temperatures and extremely low CO_2-pressures (fig. 2.15).

As mentioned earlier, decomposing dolomite produces an impure calcite which contains variable amounts of $MgCO_3$ in solid solution. The amount of $MgCO_3$ contained in solid solution with such calcite has been shown by Goldsmith and Newton (1969) to be a function of both temperature and total pressure. Hence they proposed a geothermometer based on the relationship of temperature and moles of $MgCO_3$ in calcite required to equilibrate with dolomite (fig. 2.16). The usability of the geothermometer is due mainly to the fact that an increase in total pressure of 1000 MPa caused only a 1.2 mole percent $MgCO_3$

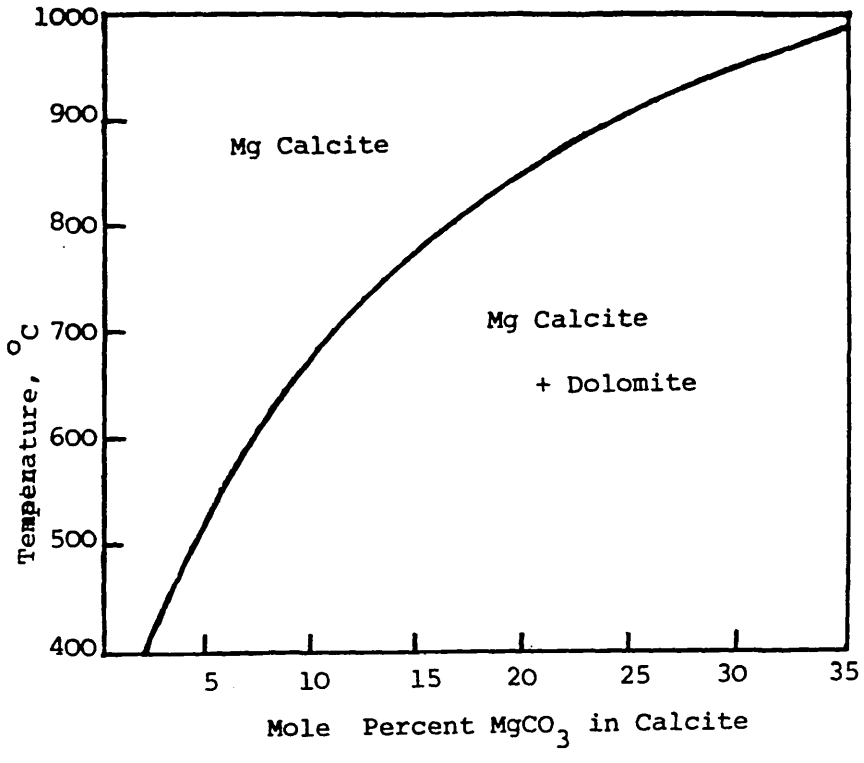

Fig. 2.16

The polybaric calcite - dolomite solvus, showing the unique relationship between temperature and moles of $MgCO_3$ in calcite in an equilibrium composition of dolomite and calcite (Goldsmith and Newton, 1969).

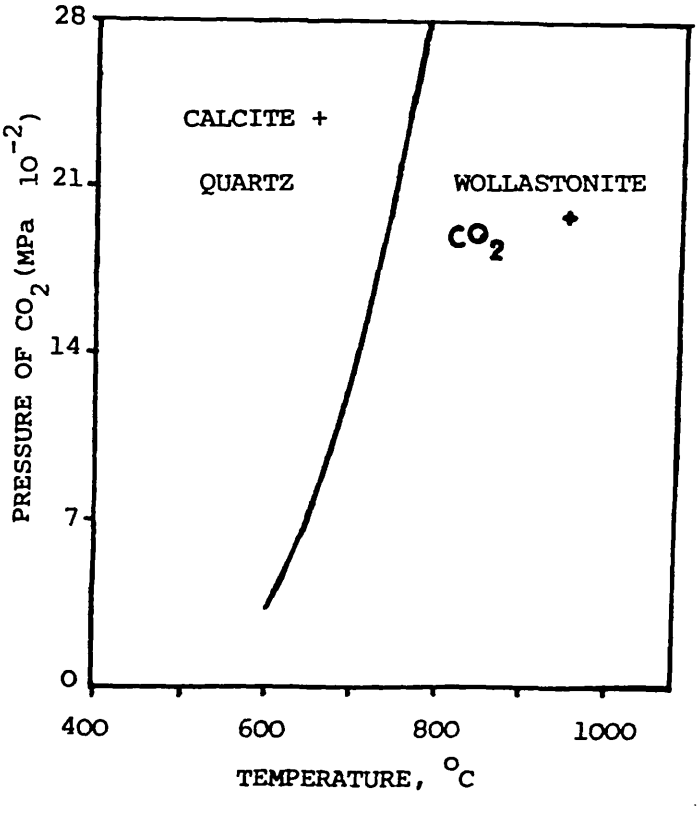

Fig. 2.17

The experimentally determined univariant Pco_2 - T curve for the reaction $CaCO_3 + SiO_2 = CaSiO_3 + CO_2$ (after Harker and Tuttle, 1956).

increase, making the polybaric solvus of Figure 2.16 essentially the same in configuration at 100 or 200 MPa total pressure. More discussion and application of the geothermometer is presented in Chapter 4 (section 4.3).

2.5.2 Metamorphism of Impure Carbonate Rocks

Very often dolomite or calcite occurs in the field in association with quartz and/or phyllosilicate minerals, or the latter materials and their elements may be provided by metasomatic introduction. A reaction of the type:

$$CaCO_3 + SiO_2 \rightleftharpoons CaSiO_3 + CO_2 \quad \ldots . 2.6$$

calcite quartz wollastonite

is possible, as shown by Goldschmidt (1912), Danielsson (1950), Harker and Tuttle (1956). Figure 2.17 shows the experimentally derived univariant PCO_2-T curve for the above reaction, by means of which Harker and Tuttle estimated that at atmospheric pressure the reaction would take place at about 400°C. Generally where CO_2 has the means of fast escape, as in shallow intrusions or where volatile components can dilute it, the equilibrium in the above reaction is towards the right and the stability of wollastonite is greater with respect to calcite and quartz. The reaction may then proceed at lower temperatures.

The metamorphism of aluminium-free siliceous dolomites has been extensively studied by Metz and Winkler (1963), (1964); Metz (1966,1967); Metz, Puhan and Winkler (1968); Metz and Trommsdorff (1968) and Metz and Puhan (1970); who showed that progressive metamorphism of a carbonate rock represented by some point in the calcite-dolomite-quartz triangle leads to a series of step reactions, each involving the partial elimination of CO_2. Such a series, according to Turner (1968), leads to progressive increase in the entropy of the system.

At least fifteen such reactions are known or can be imagined, corresponding to the fifteen curves in Figure 2.18. These reactions mark the first appearance (each in rocks of appropriate limited composition) of talc, tremolite, forsterite, diopside, periclase, wollastonite and monticellite, and are listed as follows:

(1) 3 dolomite + 4 quartz + 1 $H_2O \rightleftharpoons$ 1 talc + 3 calcite + $3CO_2$

(2) 5 talc + 6 calcite + 4 quartz $\rightleftharpoons$ 3 tremolite + $6CO_2$ + $2H_2O$

(3) 2 talc + 3 calcite $\rightleftharpoons$ 1 tremolite + 1 dolomite + 1 CO_2 + 1 H_2O

(4) 4 dolomite + 8 quartz + 1 $H_2O \rightleftharpoons$ 1 tremolite + 3 calcite + $7CO_2$

(5) 2 dolomite + 1 talc + 4 quartz $\rightleftharpoons$ 1 tremolite + $4CO_2$

(6) 1 tremolite + 3 calcite + 2 quartz $\rightleftharpoons$ 5 diopside + $3CO_2$ + $1H_2O$

(7) 1 tremolite + 3 calcite $\rightleftharpoons$ 1 dolomite + 4 diopside + $1CO_2$ + $1H_2O$

(8) 1 dolomite + 2 quartz $\rightleftharpoons$ 1 diopside + $2CO_2$

(9) 1 talc + 5 dolomite $\rightleftharpoons$ 4 forsterite + 5 calcite + $5CO_2$ + $1H_2O$

(10) 11 talc + 10 calcite $\rightleftharpoons$ 5 tremolite + 4 forsterite + $10CO_2$ + $6H_2O$

(11) 1 tremolite + 11 dolomite $\rightleftharpoons$ 8 forsterite + 13 calcite + $9CO_2$ + $1H_2O$

(12) 13 talc + 10 dolomite $\rightleftharpoons$ 5 tremolite + 12 forsterite + $20CO_2$ + $8H_2O$

(13) 3 tremolite + 5 calcite $\rightleftharpoons$ 11 diopside + 2 forsterite + $5CO_2$ + $3H_2O$

(14) 1 diopside + 3 dolomite $\rightleftharpoons$ 2 forsterite + 4 calcite + $2CO_2$

Fig. 2.18

Isobaric Temperature - Mole fraction Xco_2 diagram for the reactions 1 to 15. Xco_2 is the mole fraction of CO_2 in fluid phase, which consists of CO_2 and H_2O. Total fluid pressure P_f = 1000 bars. I, II, III and IV are isobaric invariant points. The numbers of the curves refer to reactions 1 - 15 of section 2.5. Continuous lines refer to experimentally determined equilibria; broken lines represent schematic equilibrium boundaries from calculations (Metz and Trommsdorff, 1968).

Fig. 2.19

The equilibrium: 3 Dolomite + 4 Quartz + 1 $H_2O \rightleftharpoons$ 1 Talc + 3 Calcite + 3 CO_2, in T, X_{CO_2} and total fluid pressure space. Each curve shows the behaviour of the same equilibrium reaction at a different total pressure (of H_2O + CO_2, after Metz and Puhan, 1970).

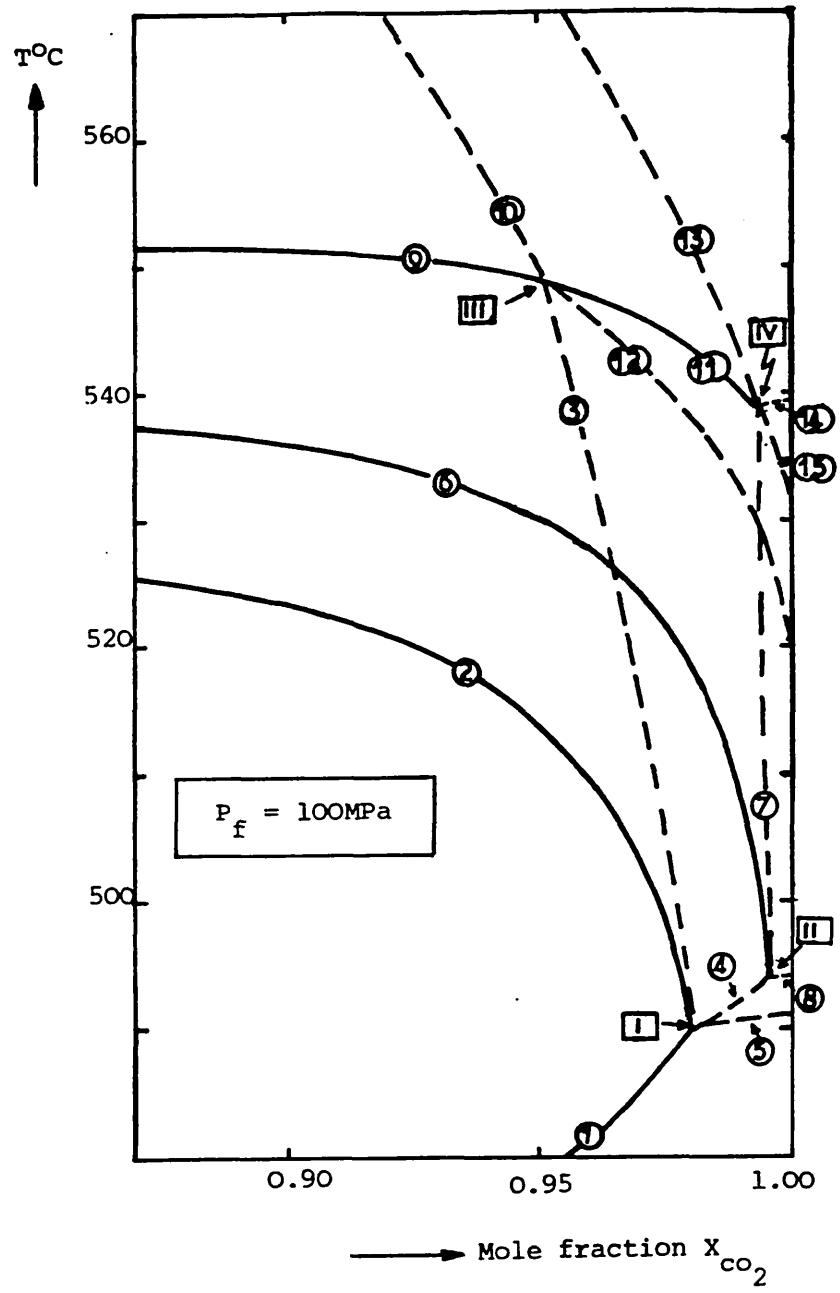

Fig. 2.18

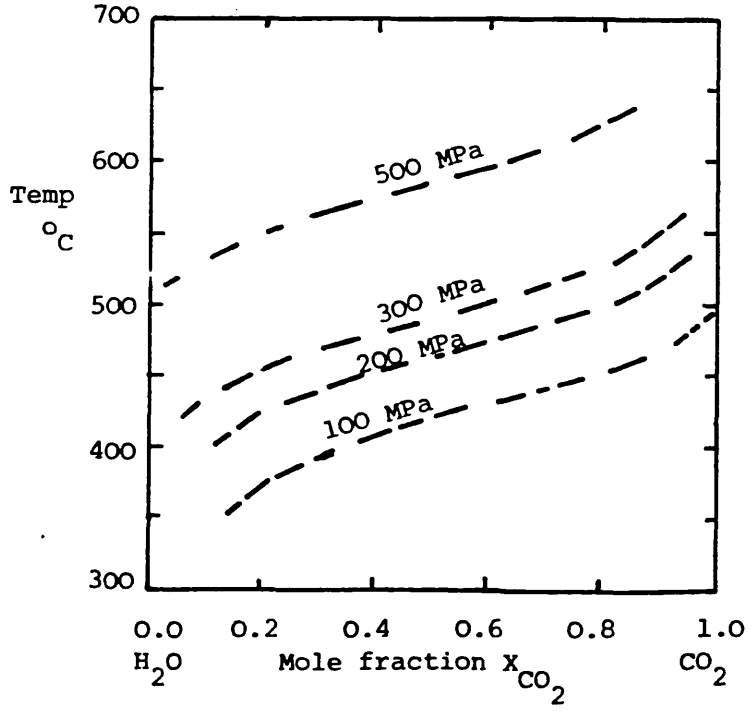

Fig. 2.19

(15) 4 tremolite + 5 dolomite $\rightleftharpoons$ 13 diopside + 6 forsterite + $10CO_2 + 4H_2O$

(Metz and Trommsdorff, 1968) . . . 2.7

In an isobaric T/X_{CO_2}-diagram like Figure 2.18, these reactions have univariant equilibrium curves which intersect at four isobaric invariant points I - IV . As Winkler (1979) shows, a continuous increase in the partial pressure of CO_2 subsequent to the formation of talc will drive reaction 1 - (Fig. 2.18) - to the first invariant point I , where the equilibrium assemblages of reactions 1 and 2 are capable of coexistence. This invariant point refers to the paragenesis: Tremolite + talc + calcite + dolomite + quartz. The invariant points are fixed in $T\text{-}X_{CO_2}$ space only if the total fluid pressure is known, and can then be used with great accuracy for temperature estimates, but as Puhan and Metz (1978) and Winkler (1979) point out, in three-dimensional $P\text{-}T\text{-}X_{CO_2}$ space I - IV themselves generate curves which are not exactly parallel to the P_f axis, making their use greatly limited.

Reaction (1) has been extensively studied further by Metz and Puhan (1970), who showed, as in Figure 2.19, that increasing the fluid pressure from 100 MPa to 500 MPa increases the reaction temperature by about 175°C at any value of X_{CO_2}. Also, each isobaric curve tends to approach its highest temperature at the point where the partial pressure of CO_2 tends to unity.

2.5.2.1 Influence of Al_2O_3

The presence of aluminium oxide during the metamorphism of siliceous dolomites results in the formation of a chlorite species rich in magnesium-clinochlore (Fawcett and Yoder,

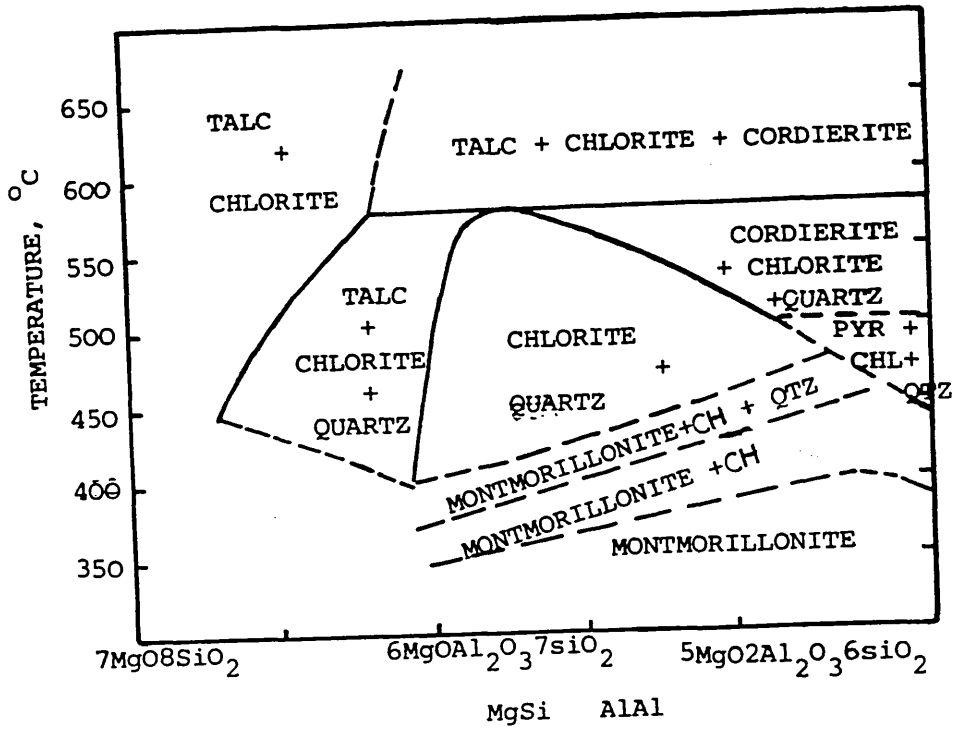

Fig. 2.20

Temperature-composition field at 200 MPa P_{H_2O}, showing the stability of chlorite and other possible phases with change in Mg, Si and Al. The stability fields were determined experimentally by Fawcett and Yoder (1966). CH = Chlorite.

1966; Turner, 1968; Winkler, 1979). In the absence of quartz this chlorite will persist to high temperatures, giving rise to the paragenesis:

forsterite + calcite + dolomite + clinochlore, in medium and even high-grade amphibolite facies. The presence of quartz results in the formation of talc and/or cordierite as shown in Figure 2.20, in coexistence with chlorite.

Phase relations of the magnesian chlorites presented in all experimental studies prior to 1966 tended to portray that chlorites and quartz do not co-exist in the temperature range 130° to 800°C, and water pressures up to 200 MPa. But Fawcett and Yoder (1966) showed both from field and experimental data that the most common occurrence of chlorite in nature (low-grade regional metamorphic rocks) is in the presence of excess quartz.

CHAPTER THREE

This chapter focuses on the geology of the Moines and Moine Thrust Zone, especially the Assynt and Eriboll areas. Most attention has been given to the tectonic-metamorphic setting, as this forms a background to the rest of the thesis. The last part of the chapter is a report of the field work carried out in 1981 and 1982 in the same areas. All field data is presented mainly as a supplement to the general geology already known. The main purpose of the fieldwork was to accurately locate specimens used in laboratory studies.

3.1 GEOLOGICAL SETTING

3.1.1 Introduction

The Moine thrust belt of North West Scotland has a known stretch of about 200km from Point of Sleat-Skye to Eriboll, and a possible offshore continuation to about 460km both north and south (Elliott and Johnson, 1980). The thrust plane has a north-north east strike, (Fig.3.1), an east south-east dip of 8°-12° on land (Elliott and Johnson, 1980) but levelling off at about 18km depth (Brewer and Smythe, 1984). Its significance has been in dispute since the last century, just as the tectonic-metamorphic history of the entire Moine rocks has been. Some of the points of controversy concern not only what has happened to the Moine rocks in the thrust zone, but also at what time of the tectonic-metamorphic history some of the better known structures in the Moine rocks developed. Courtesy of a wide embayment in the Assynt region between Cromalt Hills in Wester Ross and Lock Glendhu in Sutherland - often called the "Assynt Bulge" - the Moine thrust as well as

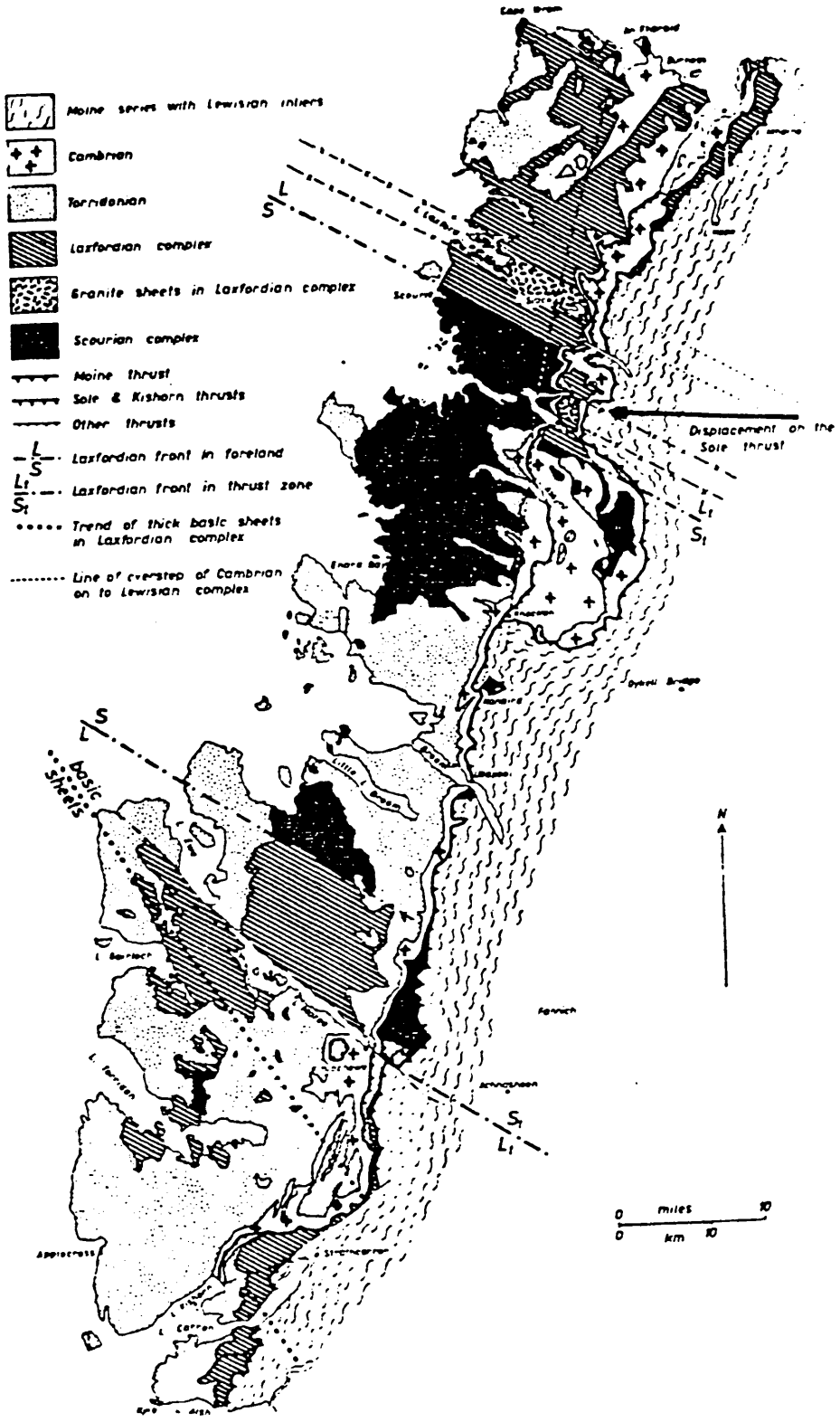

Fig. 3.I.

The Moine Thrust Zone and foreland showing the major rock types,with undifferentiated Cambrian (after Ramsey 1969)

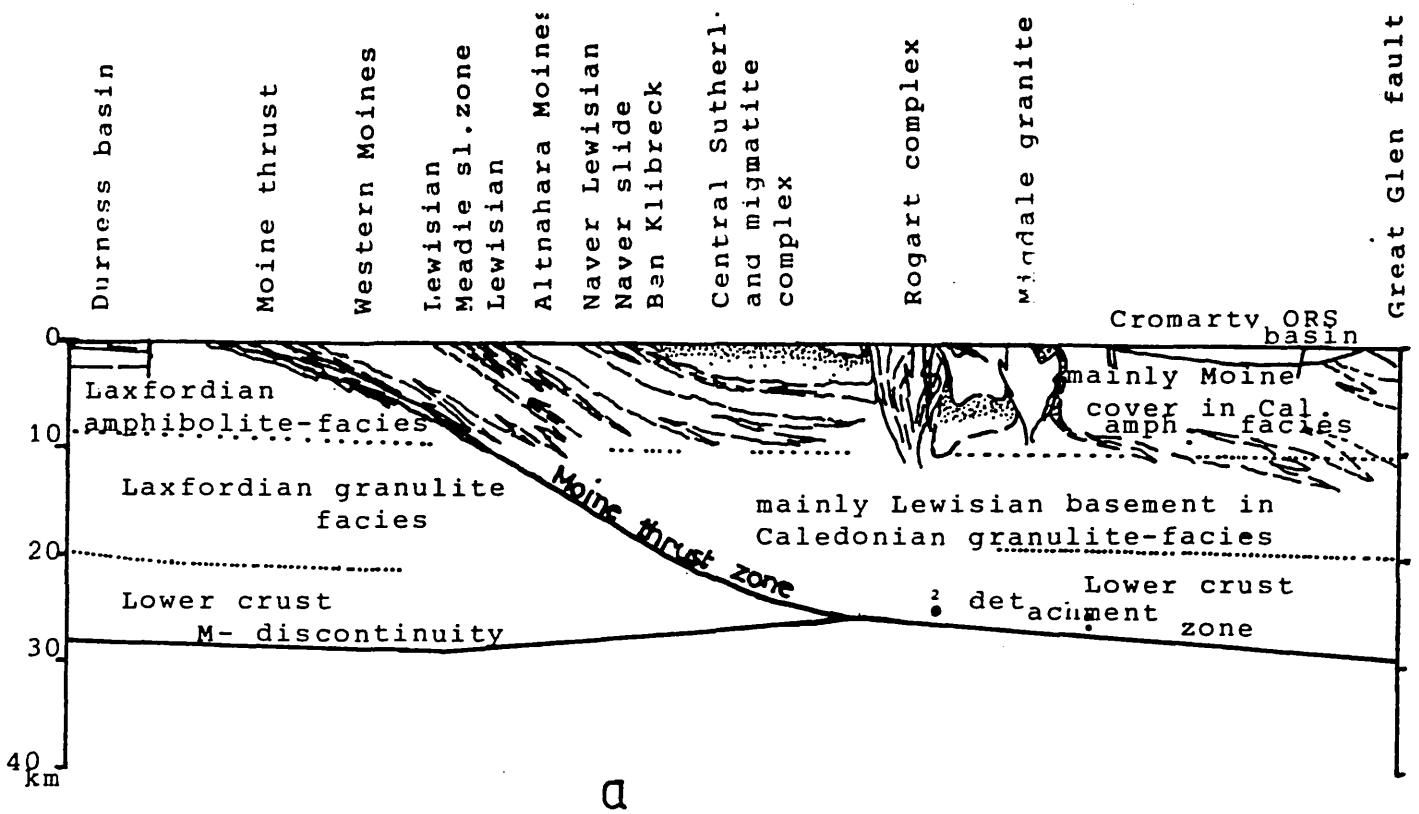

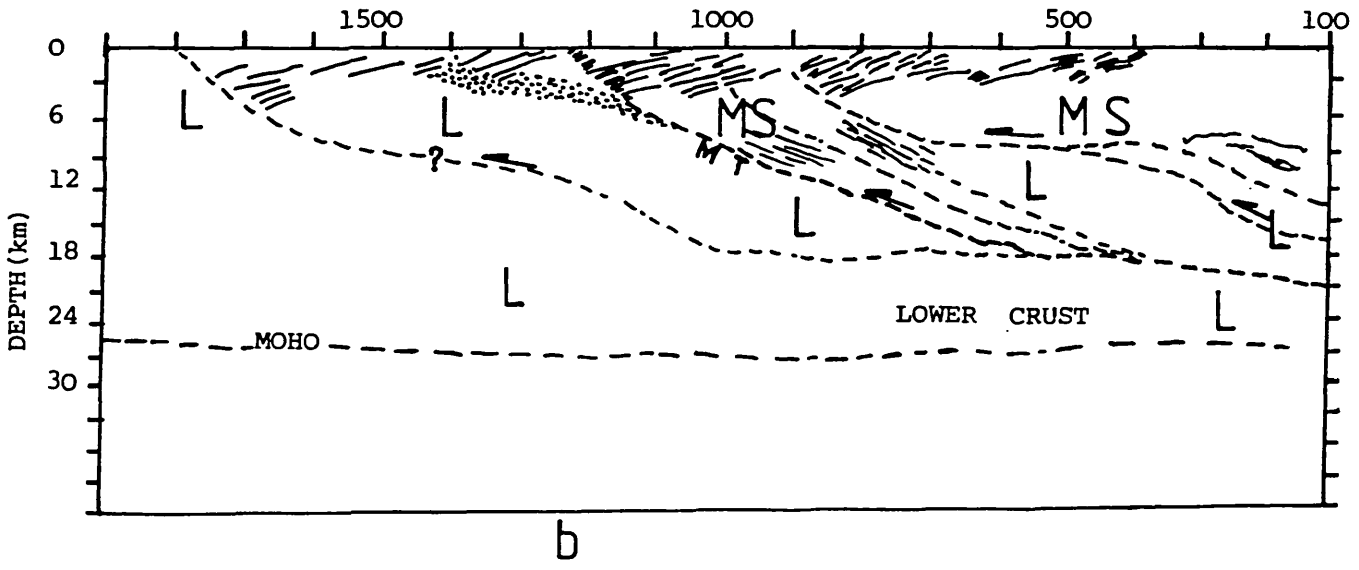

Fig. 3.2 The two models of the deep structure of the Moine Thrust Zone: (a) by Soper and Barber (1982) and (b) by Brewer and Smythe (1984). L = Lewisian gneiss, MS = Moine Schists, MT = Moine Thrust.

lower major and minor thrusts can be seen in the Moine thrust zone. In this "bulge" or "culmination" several slices of varying lithologic combinations and thicknesses are carried on thrusts of varying dips and ages, albeit all Caledonian, from the Sole thrust bordering the foreland to the Moine thrust in the east.

Recently acquired geophical evidence showed the existence of intraforeland thrusts (Outer Isles and Flannan thrusts) which, because of their similarity in dip and strike to the demonstrably Caledonian thrusts, have been ascribed to the Caledonian deformation (Brewer and Smythe, 1984). This recognition throws a question on the definition of the Moine thrust as the Caledonian Orogenic Front. The deep seismic study also showed that although the Moine thrust is no where as deep as the Moho-Discontinuity, its lateral extent at depth is much wider than the area exposed in the Assynt window (see Fig. 3.2).

3.1.2 Stratigraphy

The stratigraphy of the Caledonian Foreland is as shown in Table 3.1, with the oldest geologic unit being the Lewisian gneiss. This is a metamorphic complex composed mainly of orthogneiss (Swett, 1969) but also including Schists recognisable as altered sedimentary rocks. First described in detail by Peach et al. (1907), these gneisses are crosscut by a suite of NW trending metamorphosed dolerite dikes in some places or granites and pegmatites in others.

Variably deformed bodies of Lewisian gneiss occur as inliers in the Moine psammite between the Moine thrust and the Great Glen fault (Johnson et al., 1979; Brewer

TABLE 3.1

STRATIGRAPHY IN THE MOINE THRUST ZONE

STRATIGRAPHIC UNIT		THICKNESS	AGE	CHARACTERISTICS
DURNESS FORMATION				
	DURINE MEMBER	283.3m	CAMBRO-ORDOVICIAN	Conodont Fauna
	CROISPHUILL) BALNAKIEL) SANGAMORE) SAILMHOR)	800.0		Ceratopea, Petigurus, Gastropods and Cephalopods
	EILEAN DUBH) GRUDAIDH)	100.0		Oncolithic flora Salterella, planolites
AN T'SRON FORMATION	SERPULITE GRIT	10		Olenellus, Salterella, skolithos
	FUCOID BEDS	17		Trilobites, olenelus, planolites, etc.
ERIBOLL SANDSTONE	PIPE ROCK	93.3		Skolithos, Monocraterion
	BASAL QUARTZITE	77.0		White colour, cross-bedding
—— —— —— —— —— —— ——				-Unconformity
TORRIDONIAN	TORRIDON GROUP	7km	800Ma	
	STOER GROUP	2.3km	995Ma	

Grenville age deformation and metamorphism of the Moines = 1100Ma.

Moine Sediments - age unknown (1250 - 1100 Ma approximately).

—— —— —— —— —— —— —— Unconformity

LEWISIAN BASEMENT GNEISS

1800-1650 Laxfordian deformation and metamorphism

2200-2600 Scourie dykes intrusion.

2600-2900 Scourian deformation and metamorphism

(Gobbett and Wilson, 1960; Higgins, 1967; Swett, 1967; Cowie et al. 1972; Brasier, 1977; Coward and McClay, 1979).

et al., 1979; Johnstone et al., 1979 and Piasecki and van Breemen, 1979). This correlates with Brewer and Smythes (1984) deep seismic finding that Lewisian gneisses form the base of the Moine thrust at depth (18km), to show that those Lewisian inliers must have been carried up by the Moine rocks as the latter were gliding along the low level Lewisian decollement.

The Torridonian: This is a thick sequence of red arkosic sand stone which rests unconformably on the Lewisian gneisses of the foreland. Detailed geological studies, paleomagnetic studies and radio-metric dating reveal the presence within these sand-stones of a 25° angular unconformity, a 50° change in paleomagnetic pole position and an age difference of about 180m.y. between the Stoer Group at the base, and the top Torridon group, (Coward and McClay, 1979). The former is 2.3km thick where it is best preserved and has a maximum thickness of 7km. Preceding the deposition of the Cambro-Ordovician sequence, the Torridonian was gently folded about a north-south axis.

The Early Cambrian Sediments: These sediments were deposited unconformably on a planar surface following the erosion of the Torridonian Sandstone. In places they rest directly on the Lewisian, defining a double unconformity. The base of the Cambrian sediments is a quartz-rich, feldspathic to orthoquartzitic, current-bedded member (the Basal Quartzite) sometimes with a conglomerate at the base. Its whitish colour is very characteristic.

Conformably above the Basal Quartzite lies the Pipe Rock a well-bedded, orthoquartzitic sandstone with vertical, bedding-normal, cylindrical bioturbation structures. These vertical burrows belong to the genus Skolithus (Hallam and Swett, 1961), and their presence here with Monocraterion, as well as Olenellus in the Fucoid Beds above have been used as criteria for according a Cambrian age to this sequence. Diagenesis of the Eriboll Sandstone produced extensive porosity reduction and some redeposition (Swett, 1969).

Conformably above the quartzite lie the Fucoid Beds. These have been misnamed because of the erroneous interpretation of planolites trace fossils as fucoids. The Fucoid Beds are a dolomitic siltstone, containing arenaceous and argillaceous units. The presence of the trilobite Olenellus here is characteristic, and the earliest shelly fossil in the Cambrian-Ordovician sequence is found here.

The Fucoid Beds are followed by about 10m of principally orthoquartzitic sandstone - the Serpulite Grit in which some

units contain carbonate cement. It takes its name from small conical fossil shells - serpulites, now called Salterella, (Coward and McClay, 1979). There are some vertical worm burrows also just like the lower two units. It preserves a characteristic close association between the presence of large amounts of quartz and carbonate cement, and the lack of quartz deformation. This, according to Swett (1969), suggests an early cementation which reduced the susceptibility of the sandstones to deformation and solution.

The Middle Cambrian - Ordovician Sediments:

The Durness Formation:

This has been variously referred to as the Durness carbonate, the Durness Calcaceous Series, the Durness group etc., but according to the American Code of Stratigraphic Nomenclature (1961), Durness Formation would be a more appropriate name. It is a Cambrain to Lower Ordovician deposit of dolostone, limestone, marble and chert, which closely resembles the Cambrian-Lower Ordovician Series of East Greenland and the Oslobreen Series of North Spitsbergen, (Gobbett and Wilson, 1960; Swett 1981). It lies conformably on the Serpulite Grit, attains a maximum thickness of about 1,290 meters at its type locality - Durness, (Gobbett and Wilson, 1960) and has been subdivided into seven members, formerly known as Groups by Peach et al. (1907) - Table 3.1.

Apart from a chertified oncolite association (Brasier 1977), the Eilean Dubh Member has no proven middle Cambrian fossil record, though the Lower Cambrian Grudaidh member contains

Salterella fossils, like the Ant-Sron units below. From the Sailmhor up to the top of the Croisphuill a Canadian fauna is predominant, while by correlation with the Swedish Ordovician faunas, Higgins (1967), shows that the middle part of the 283m thick Durine member is of late Arenig or early Llanvirn age by virtue of thirteen identifiable conodont species found in it.

Palmer et al.(1980) reported the first known break in deposition in the Durness Carbonates - between the Sailmhor and the Sangomore members. This is a minor hiatus, and not an angular unconformity, showing that unlike the Oslobreen Carbonates, the Durness carbonates in the field have no angular unconformities within, although erosion surfaces, minor non-sequences, diagenetic mottling and post-Cambrian intrusive sills are abundant (Gobbett and Wilson, 1960; Swett, 1966a; Coward and McClay, 1979).

The traditional nomenclature "Durness Limestone" is the principal reason forthe earlier misconception that most of the Durness carbonate is limestone. The sequence includes calcareous dolostones, illitic dolostones, dolomitic limestones and pure limestones, as major lithologic types. The contacts between these lithologic types range from gradational to sharp. Swett (1966a) has noticed a characteristic network of interpenetrating, dolomitic and calcitic patches, streaks and bands which he ascribed to diagenetic mottling. The dolomitic portions, he noticed, are more coarsely crystalline and darker than the calcitic portions. The relative grain sizes of calcite and dolomite may be

influenced by the environment of derivation of the samples. The mottling is interpreted as probably the result of an early diagenetic unmixing, as original magnesian limestones which possessed limited permeability with respect to dolomitising Mg-ions, tried to establish chemical stability. Swett (1965b) proposes a diagenetic sequence of five events thus: (i) recrystallization, (ii) dolomitization, (iii) silicification, (iv) calcitization, and (v) redolomitization. These are explained below.

(i) Recrystallization - during which most of the original oolitic texture was destroyed. This is acutally crystallization.

(ii) Dolomitization - which seemed to proceed randomly from centres of indeterminate origin, probably aided by Mg-ions released from the breakdown of earlier-formed minerals.

Swett (1965b) supposed these Mg-ions to have come from the breakdown of illite, which is very unlikely in view of the chemical composition of illite in the Durness Carbonates.

The problem of the genesis of dolomite has intrigued earth scientists for some time, thereby giving rise to a vast number of publications. The concensus of opinion resulting both from laboratory and field investigations points to the following reaction:

$$2CaCO_3(solid) + Mg^{2+} \rightleftarrows CaMg(CO_3)_2(solid) + Ca^{2+} \quad .....3.1$$

(Lipmann, 1973; Deffeyes et al. 1965; Katz and Mathews, 1977; Carpenter, 1980). Katz and Mathews (1977) reported the hydrothermal dolomitization of calcite between 252° and 295°C, proposing a four-stage process thus:

(1) dissolution of reactants,

(2) precipitation from the solution of an intermediate Magnesian Calcite phase,

(3) dissolution of the intermediate(s), and

(4) final precipitation of dolomite.

Gaines (1979) confirmed the solution - reprecipitation model, by experimental studies, proposing with Fischbeck (1979) the term "protodolomite" for the product of stage (2) above. The two remaining problems then seemed to be the source of the Mg^{2+} ions and why dolomite is so rare in Recent and Pleistocene sediments in proportion to the total amount of carbonate sediment of that age, and also in comparison with the abundance of dolomite in ancient sedimentary rocks. Johnson and Pyktowiczs (1978) and Carpenter (1980) show that cations in sea water are paired with chloride to a greater extent than with sulphate and bicarbonate, and that approximately fifty per cent of calcium and magnesium in sea water is paired with chloride. Also reasearch in modern sea-marginal pools of the Red Sea shows that dolomite formsonly where gypsum and/or anhydrite is likewise present, (Friedman, 1979). Hence the magnesium ions for forming dolomite are likely to come from sea water as magnesium chloride. Also Deffeyes etal. (1965) showed that dolomitization of sediments by marine evaporite waters on Bonaire in the Caribbean Islands took place in Recent and Plio-Pleistocene times. Carbon-14 dates on dolomite found in most of the Recent supratidal sediments in Bonaire showed that the time since dolomitization has been less than 2,200 years.

In the Durness carbonates, the interpenetration of dolomite grains across diagenetic stylolites and other solution surfaces could be an indication that much of the process of dolomitization was over before diagenesis set in.

(iii) The third diagenetic event of Swett (1965b) is Silicification - when decomposing illite is likely to have provided silica for the formation of chert, or as Beach (1977) suggested, the breakdown of detrital feldspar produces illite and quartz. This is likely to have made some contribution to silicification in the carbonates if the original amount of feldspar present was high enough.

(iv) Calcitization i.e. dedolomitisation - either of hydrothermal origin or of some diagenetic processes.

(v) Redolomitisation: during which some of the calcite was converted into dolomite.

Although the oolitic texture of the rock particularly in the foreland area is held in certain instances to have exerted a control over the patterns of diagenesis, no undisputable evidence was presented to support the five-stage sequence.

The Cambro-Ordovician sequence from the Basal quartzite and Pipe rock overlain by siltstone and capped by carbonate rocks is consistent with a gradual marine transgression, but does not necessarily indicate a continuous increase in the water depth.

The Moine Schists:

These are a sequence of metamorphosed sandstones and shales which overlie the Moine thrust. Moine rocks proper are bounded to the NW by the Moine thrust and to the SE by the Great Glen fault (Harris et al. 1978; McClay and Coward, 1979), although the psammitic granulites of the Central Highlands east of the Great Glen fault (Fig.3.3) are either an extension of the Moines across the fault (Christie, 1963; Piasecki and van Breemen, 1979) or equivalents of the Moines (Harris et al. 1978; McClay and Coward, 1979).

West of the Great Glen fault the Moine rocks can be subdivided into the Morar, Glenfinnan and Loch Eil divisions (Fig.3.3b). The boundary between the Morar and Glenfinnan divisions may be tectonic (Johnstone et al. 1979), while the Loch Eil division lies over the Glenfinnan and both possibly extend into the Grampian Highlands. The Moines in places lie unconformably upon a Lewisian gneiss basement while in others are interleaved with wedges and slices of basement (Peach et al. 1907; Johnstone et al. 1979). They are overlain by Old Red Sandstone and intruded by granites and pegmatites. The Ardgour granite has yielded Rb-Sr-isochron ages of 1000 Ma (Brook et al. 1976), while the Carn Chuinneag Granite of Ross-shire showed a 560±10Ma age (Long, 1964). Pegmatites intruded in Moine rocks have been dated (Rb-Sr from muscovite) at 730 - 780 Ma (van Breemen, 1974; Powell et al. 1983). These results reflect a fairly complex past for the Moine rocks, which has been partly interpreted by Johnstone et al. (1979) and Coward (1983) to mean that at least some part of the Moines underwent deformation and

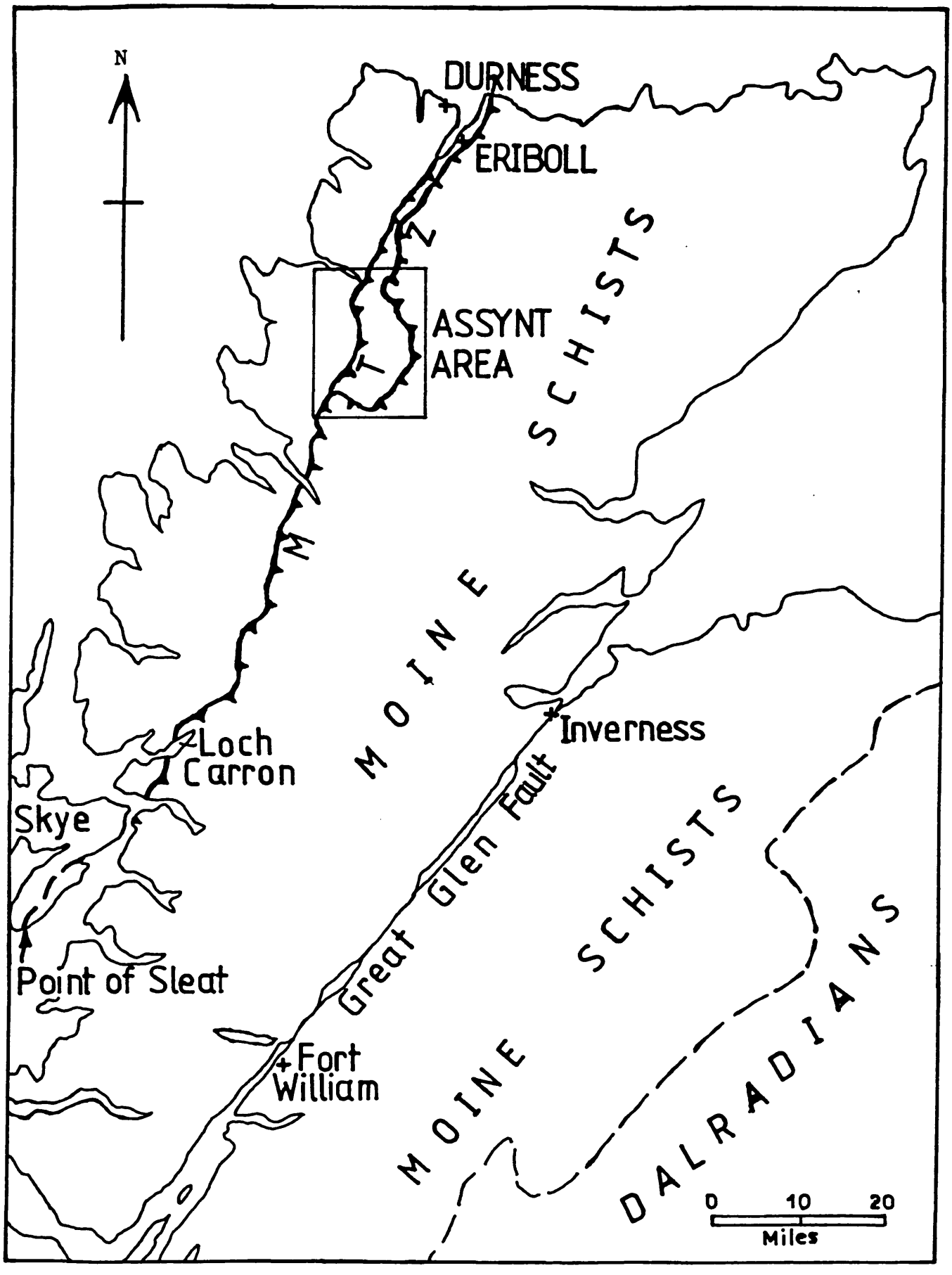

Fig. 3.3a Geology and major structures of the Northwest Highlands of Scotland(after Christie 1963).The Moine Thrust Zone(MTZ) shows the two areas where field study was carried out : Eriboll and Assynt.

metamorphism during Grenville times (~ 1000Ma). This may have been followed by a Morarian Orogeny (~780Ma) marking the emplacement of the pegmatites, and both changed the Moines into a crystalline suite that took active part in deformation during Caledonian times (470 - 420Ma).

3.1.3 The Moine-Torridonian Relationship

There is considerable controversy concerning the age of sedimentation of the Moine Series, its tectono-metamorphic history and, its relationship to the Lewisian-Torridonian succession on both sides of the Caledonian front.

The Moine rocks are often thought to be bounded on the South East by the Great Glen Fault (Harris et al. 1978), and on the north west by the Moine thrust, though the metamorphic Caledonides of which the Moines are a part extend much further south and east than the Great Glen Fault (Watson, 1975, also see Fig.3.3a). They comprise of meta morphosed sandstones and shales of uncertain age.

Using Rb-Sr whole rock isochron data from the Moines, Brook et al. (1976) inferred an age of 1,050 ± 46Ma, as the age of the earliest metamorphism of Moine sediments, or 1250 to 1050 Ma as the ages for sedimentation of the Moines. Harris et al's (1978) accepted radiometric ages range from 1100 to 320 Ma. If the age of sedimentation of the Stoer Group of the Torridonian can be considered as 995 ± 24Ma (Moorbath, 1969), it is likely that Moine sedimentation was earlier than that of the Torridonian.

Basement gneisses below the Moines have been correlated with Lewisian gneisses in the foreland (Johnson, 1975;

Watson, 1975; Soper and Barber, 1982; Brewer and Smythe, 1984). Hence the present line of the Moine thrust could not be regarded as a suture between two Grenville-age plates (Brook et al. 1976), but the possibility remains that the Stoer Group could have been molasse derived from the Moines. Soper and Barber (1979) proposed that the Moine and Torridonian clastic sequences were associated in part as stratigraphic equivalents, but it may be that they are erosional products the latter derived from the former.

A gneissic basement is known to underlie the Moines in the Moine nappe, and this has been interpreted by Coward (1980) and McClay and Coward (1981) as a lower gneissic crust that became uplifted possibly during the Grenville Orogeny. This view seems to have the support of Johnson (1975).

3.2 METAMORPHISM

3.2.1 In The Thrust Zone:

The processes and effects associated with the Moine Thrust Zone have suffered from mistaken identity since the early days of its discovery, and not the least of these is the metamorphism of both the Moine and Cambrian rocks close to the Moine thrust. At best the metamorphism of the Moine sequence can be regarded as polyphase,(Powell, 1974; Harris et al. 1978; Mendum, 1979), with a grade generally increasing from chlorite or chlorite/biotite in the west to a belt of migmatitic gneisses in the east (Kennedy, 1949, Harris et al. 1978). In detail the pattern of metamorphism is complex, but evidence suggests that there probably were up to two overlapping major episodes of metamorphism (Long &

Lambert, 1963; Powell, 1974; van Breeman et al., 1974).

Rb-Sr isotope dilution analyses on muscovites and U-Pb zircon and monazite analyses demonstrate two distinct episodes of pegmatite emplacement in the Moines: A 730 ± 20 Ma Precambrian group (van Breeman et al., 1974) confirming Giletti et al's (1961), Long and Lambert's (1963) and Brook et al's (1976) ages in excess of 700 Ma, and a Caledonian group between 560-320 Ma. The precise constitution and nature of these two groups and the extent to which these dates actually track the regional and dislocation metamorphisms of the Moine rocks are points of debate (van Breeman et al., 1974, Powell 1974).

This level of general consensus was born out of several years of disagreement by workers in the Moine thrust zone. For instance the regional metamorphism of the Moine schists was, for a long time, tied to the processes associated with Moine thrusting (e.g. Lapworth, 1884; Geikie,1889; Christie , 1963; Soper and Wilkinson, 1975). In 1888 Geikie, wrote: "It is obvious that the facts now brought forward furnish a large amount of evidence in support of the theory that regional metamorphism is due to the dynamical and chemical effects of mechanical movement acting alike on crystalline and clastic rocks." From then on metamorphism and deformation in the Moine rocks were related and also coupled with both processes in the nappes below the Moines, a view which survived till recently.

Horne, in disagreeing with Peach (Peach & Horne, 1930), was probably the first to recognise that in the vicinity of the

thrusts, the old crystalline structure of the schists (due presumably to an earlier metamorphism) had been broken down by later movements. This view was stressed more strongly by Read (1934) who observed that "the dislocation metamorphism is undoubtedly superposed upon the general Moine metamorphism - - - - - - I am of the opinion that the general metamorphism and the dislocation metamorphism are two separate events in the histroy of the Moine series - - - The dislocation metamorphism arises from the post-Cambrian movements that are of late Caledonian age", (1934, pp307-8). Phillips (1937) using petrographic evidence showed that the Moine Schists were brought to their present state of regional metamorphism by a deformation acting along approximately South West and North East lines, prior to the dislocation phase of the Caledonian movements. This conclusion is supported by Phillips (1949, 1951), McIntyre (1950, 1951) and Wilson (1953).

Within and below the Moine nappes, Lewisian to Torridonian and Cambrian rocks have been involved in the Caledonian metamorphism (Christie 1963; Barber 1965; Powell 1974; Soper and Wilkinson 1975). The Lewisian and Torridonian of Coulin Forest (Johnson, 1957) and the Lewisian of Eriboll (Soper & Wilkinson, 1975) have been shown to develop strong schistosity and even mylonitization, while parts of the Cambrian succession particularly the Eriboll Quartzite (Christie, 1963; Soper & Wilkinson, 1975; Evans and White, 1984) and the Durness Carbonate (Soper & Wilkinson, 1975) have been metamorphosed close to shear-planes. Neomineral assemblages in these rocks are consistent

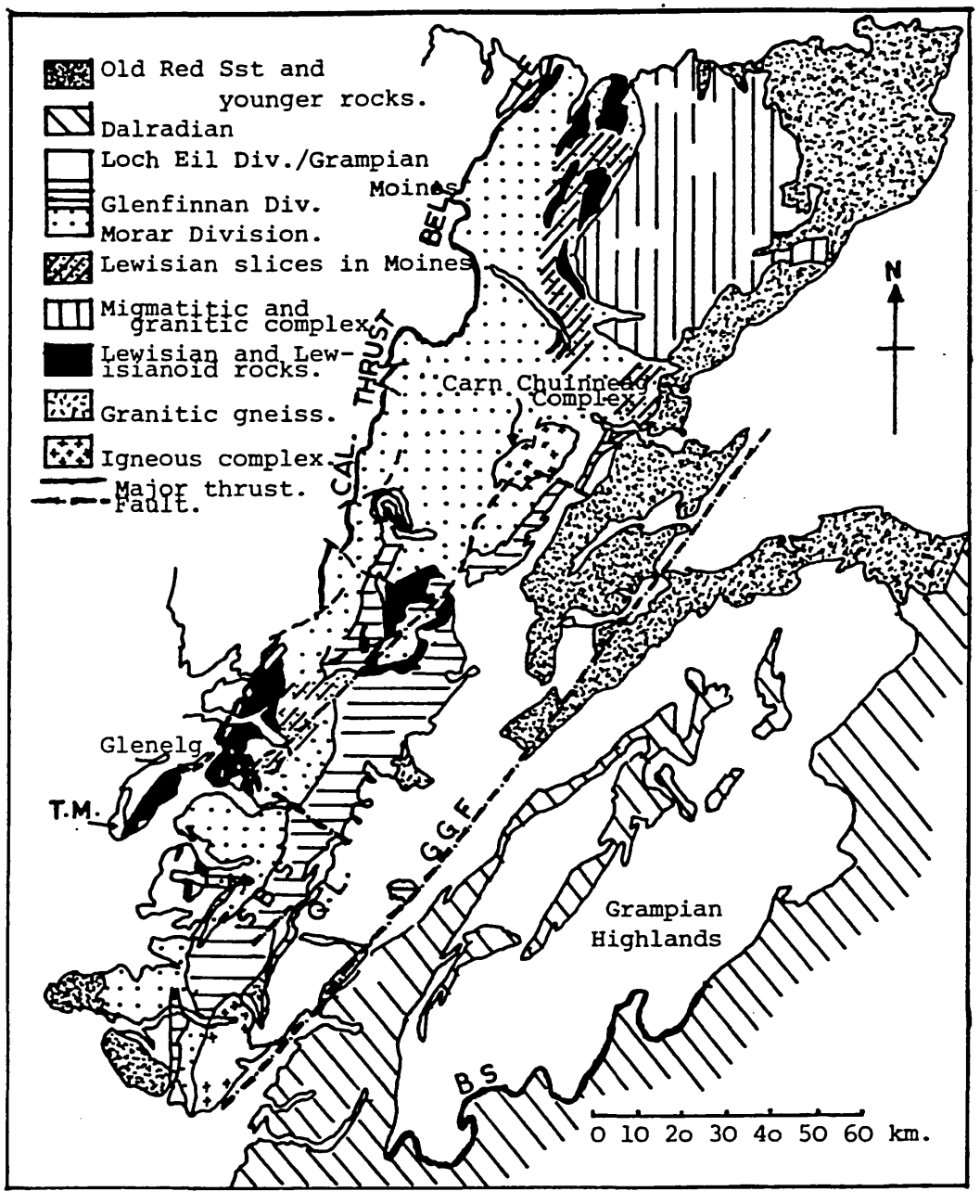

Fig.3.3b. Distribution of the Moine rocks(after Johnstone,1975,1979; and Piasecki,1979).
BS--Boundary Slide. SBS--Sgurr Beag Slide.

LE--Loch Eriboll. LM--Loch Morar.QL--Quoich Line.

TM--Tarskavaig Moines.

with low grade greenschist facies of metamorphism as observed by Johnson (1960), Barber (1965); Soper & Brown (1971), Soper & Wilkinson (1875), and Evans and White (1984). A disporportionately large percentage of literature on the Moine Thrust Zone centres on the Moine nappe . Literature on the metamorphism and deformation of the Cambrian succession is relatively little.

3.2.2 Metamorphism of Moine Rocks outside the Thrust Zone

The Moine rocks can now be considered in two major areas: the Western Moine Region between the Moine thrust and the Great Glen fault, and the Grampian Moines bounded on the west by the Great Glen fault and on the east and south by the Dalradian rocks (Fig 3.3b). The Western Moines consist of three lithologically and structurally distinct assemblages - the Morar, Glenfinnan and Loch Eil Divisions, in younging order (Johnstone, 1975; Johnstone et al. 1979; Piasecki and van Breeman, 1979; Piasecki, 1980), while the Grampian Highland Moines have been subdivided into the Central Highland Division, almost completely surrounded by a more extensive Grampian Group (Piasecki and van Breeman, 1979; Piasecki, 1980). The Central Highland Division is a more gneissose and migmatitic basement, while the Grampian Group is a cover of non-migmatitic, less metamorphosed, flaggy, pelitic schists with sedimentary structures. Johnson et al., (1979) refer to these Western and Grampian major divisions as the northern and southern parts respectively of an orthotectonic zone. Their model of the Moines also denies the Great Glen fault the status of a major tectonic boundary. This is in opposition to Coward's (1983) views of

regarding the Great Glen fault as a major structural break, and separating the northern from the southern Moines on the grounds of differences in rock-type, structures and age of deformation.

At least three distinct periods of metamorphism have been inferred for the Moines, but whether these periods are properly represented all over the Moines or not is as yet unanswered.

The primary metamorphic event in the Western Moines has been recognised as that which caused the major distribution pattern of Rb-Sr throughout the Moine pelites at around 1004±28 Ma (Greenville), (Brook et al. 1976; 1977; Brewer et al. 1979). There is no evidence of Grenville metamorphism West of the Moine thrust (McClay and Coward, 1981) or east of the Great Glen fault (McClay and Coward 1981; Coward 1983). This is understandable if the Grampian Moines are accepted as a cover sequence on the basement of Western Moines.

Using deformed pegmatites, a second more pervasive age of metamorphim with deformation has been shown to lie between 780-700 Ma (Morarian). This bracket includes ages determined all over the northern Highlands by Gilletti et al. (1961), Long and Lambert (1963), van Breeman et al (1974, 1978), and Powell et al (1983), and in the Grampian Moines (Piasecki and van Breeman, 1979b; Piaseccki, 1980). The spatial distribution of isotopic ages in Morarian pegmatites so far reported is shown by Powell et al; (1983) to represent a progressive decrease in maximum apparent ages from West to East.

The third main metamorphic period in the Moines often produces ages that fall in the >400<500 Ma bracket. This range also includes the Caledonian tectono-thermal period, during which radiometric clocks were reset partly duri ng retrogressive metamorphism with liberal fluid activity (Brewer et al. 1979; Piasecki and van Breeman, 1979b), Pankhurst's (1970, 1974) reported age of 485 Ma for the main metamorphism of the NE Dalradian (Fig.3.3b) would mean that this last metamorphic episode was far more pervasive than the previous ones. Caledonian thermal activity was still on in the Glenfinan Division of the Western Moines up to 413±17 Ma (Brewer et al. 1979), and the pattern of cooling ages was shown by the latter to follow the sequential uplift of the Moines along discrete thrust or slide zones.

These periods of metamorphism and intervening periods of apparent quiescence have produced rocks which range in grade from greenchist/lower amphibolite facies, to upper amphibolite gneisses, with or without anatexis.

3.3 DEFORMATION IN THE MOINE THRUST ZONE

3.3.1 Introduction

The Moine thrust belt is a narrow zone of thrust faults and nappes, more than 250km long and up to 18km wide (Harris et al, 1978), dividing the Moine Mainland block from the so-called Caledonian foreland (Fig.3.1). Recent geophysical evidence shows that although the Moine thrust zone is by no means the greatest thrust zone in the area from the Outer Hebrides to the Great Glen Fault (see Fig.3.2b),

it is the one known to preserve the characteristics of classic thrusting - emplacement of older rocks over young ones. The Moine thrust carries Moine and Lewisian rocks with small units of Torridonian and Cambro-Ordovician rocks in a WNW direction, over the foreland. The thicknesses and complexities of Moine and lower nappes have only recently been proved to vary within the thrust zone, although several field studies have long since indicated the variation in structural pattern and the presence of east-dipping imbricate sequences within the thrust-bound nappes (Coward et al. 1980; Elliott & Johnson, 1980, McClay and Coward, 1981).

3.3.2 Dating of the Moine Tectonic event:

Up to 1975 it was not particularly easy to accord any other age to Moine thrusting and even mylonitization than a post-Cambrian or Middle-Ordovician age. This was due to the realization that postulated earliest deformation features in the thrust zone also affected the Eriboll Quartzite and the Durness Carbonates (Christie, 1963; Higgins 1967; Soper, 1971; Soper & Wilkinson, 1975). Hence Soper & Wilkinson, (1975) concluded unequivocally that "the whole tectonic-metamorphic sequence in the thrust belt is thus of lower Palæozoic age".

Recent isotopic studies favour the separation of not only metamorphic, but also tectonic events into an earlier Precambrian phase: 1050-730 Ma, and a later or Caledonian phase: 560-320 Ma (van Breeman et al. 1974; Brook et al. 1976; Brewer et al. 1979). The validity of a Precambrian orogenic event in the Moines is gaining rapid acceptance (Powell, 1974 Harris et al. 1978; Piasecki and van Breeman, 1980; Watson & Dunning, 1979; Piasecki, 1980). Watson

and Dunning, (1979) observed a coincidence between metamorphic zoning attributable to Precambrian and to Caledonian events particularly in Inverness-shire. Such coincidences, they propose, suggest a continuity in thermal and probably orogenic conditions at depth which may best fit the alternative view that the initial metamorphism (and orogeny) of the old Moines was an early event in a Caledonian cycle.

3.3.3 The nature of the Deformation in the Moine Thrust Zone:

By means of common structural parameters, the last three decades have seen the establishment of a fairly rigid framework of deformation (and metamorphism) in the Moine thrust zone. Although the timing of the general metamorphism of the Moine schist tends to influence the timing of the tectonic events - compare, for example, Barber (1965), Soper (1973), with Brown (1971) and Powell (1974) - there generally was agreement among past workers about the four-phase nature of the deformation.

A summary of the deformation phases is tabulated by Powell (1974), ever since which some new additions have been made, (e.g. Soper & Wilkinson, 1975; Mendum, 1979). Briefly the phases of deformation involve:

D1 - the development of a primary mylonitic foliation (S_1), and isoclinal major and minor folds (F1). The folds are generally intrafolial in nature, plunging about 20° to the SE. The Moine mylonites, according to Johnson (1965), were not formed at the level at which they are now exposed; they have been carried forward by movement on the Moine and lower thrusts. Hence tying the age of generation of Moine mylonites

to that for the generation of similar structures in the Cambro-Ordovician sequence (see Barber, 1965, Soper, 1973, Soper & Wilkinson, 1975), may be questionable in view of the difference in their respective crustal levels.

D2 - A penetrative linear fabric L2 is the most widely developed D_2 element. It has a mean plunge of 13° to 112° both above and below the Moine thrust and also in Moine Schists, except, where later folding has reoriented the earlier-formed lineations. L_2 is congruous with an E.S.E - plunging fold phase-F_2, is a direction of maximum mineral elongation and has been identified as a stretching lineation. The superimposition of F_2 on S_1 has produced axial planar cleavage S_2, and based on the symmetry, geometry and trend of the axes of these F_2 folds, Christie (1963, 1965) insists that a strike-slip displacement with movement towards the SSW is an inescapable conclusion. D2 according to Soper and Barber (1979) marks the emplacement of the intermediate-napp es like the **Arnaboll, Benmore and Kishorn,** as well as the development of underlying duplex structures. This view is against the "piggy-back" mode of transport supposed to take place in areas of crustal duplex (see Elliott and Johnson, 1980).

D3 - involved open folding of the intermediate thrust planes, coaxially with D_1 (Ramsay, 1963; Powell, 1974, Soper and Barber, 1979), and has been correlated with Christie's(1963) Phase II deformation by Johnson & Shepherd (1970). F_3 is a set of minor folds which crenulate S_1 and L_2 . They are asymmetric, overturned towards the WNW and their axial planes dip at about 42° to 108° (Soper & Wilkinson, 1975). F3 shows

more scatter than F1 and F2, with a nearly horizontal microfold lineation which fans the angle between NW and N. D3 produced S3 - a crenulation cleavage.

D4 - is thought to involve the development of brittle conjugate structures like paired monoclinal folds with broken limbs, conjugate kink-bands, box folds and breccia bands. Movements on the Moine thrust have also been related to this phase of deformation (Barber, 1965; Soper, 1973; Soper & Barber, 1979), in support of their anti-"piggy-back" view.

Although Christie (1963; 1965) insists that the ESE folds in primary mylonitic rocks and Moine Schists are similar in orientation, style and internal fabric, showing that the deformation and recrystallization responsible for both was contemporaneous; Johnson (1957) shows that the Moine Schists are characterized by a different structural pattern and microfabric from the Moine mylonites. This latter view is also supported by Evans & White (1984), who are convinced that structures within and outside the Moine mylonite zone should not be correlated. Also recent geophysical evidence (fig.3.2) shows that at its present outcrop the Moine thrust plane could be up to sixty kilometers wide from west to east. This may mean that the Moine nappe has been transported continuously or possibly episodically towards the WNW, with some help from the lower thrust planes, and that the relationships between the observed small structures above and below the thrust plane and the thrust movements may be very complex. Hence a D1- D4 framework may be too restrictive as a means of studying the past history of the Moine thrust zone.

There is much evidence to suggest that general tectonic transport in the Moine thrust zone is towards the WNW, approximately N290° (Coward, 1980; Coward et al., 1980; McClay and Coward, 1981). This includes the attitude of sheared pipes in deformed Pipe Rock (McLeish, 1971), the orientation of the ESE lineations and some microfolds with axes normal to this direction - F3, the general attitude of imbricate and major thrusts (Coward, 1980; Coward et al. 1980) and recently, the assymetry of quartz C-axis fabric of Moine tectonites (Evans and White, 1984).

3.4 FIELDWORK

3.4.1 Aim of the Fieldwork:

The main aim of the fieldwork was to accurately locate and collect rock specimens. This was done with particular attention to the Durness Formation of the Moine thrust zone. Although contiguous rock types were also sampled, these were only used to confirm or contrast with microprocesses and microstructures observed or inferred in the carbonates. To realise this aim it was inevitable to obtain as general an overview of the Moine thrust zone as possible, and this was achieved in three field trips to North West Scotland. In the field a detailed study of the structures and macroscopic processes relatable to history of the Durness Formation from late diagenesis to deformation was carried out. The relevant data is presented in the subsections below.

The field study was centred in two main areas of the Moine thrust zone: The Assynt area, and Eriboll Area (Fig.3.3a). In both places sampling spanned across from the foreland to

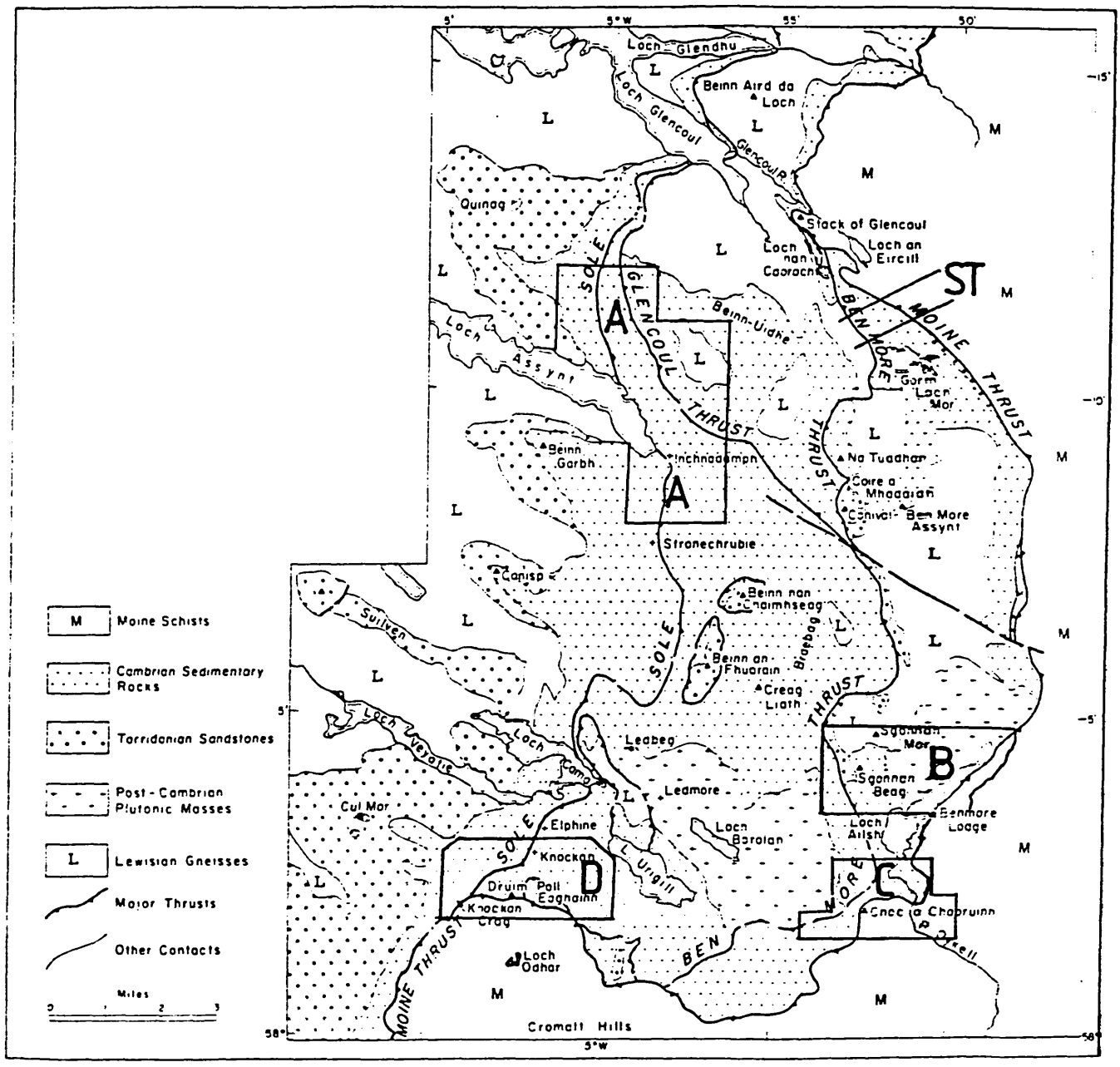

Fig. 3.4

Geology and Structure in Assynt(after Christie,1963).

Sub-areas of detailed study are labelled in.

the highstrain zone close to the Moine thrust. Figure 3.4 shows the Assynt Area, and the various subareas where detailed work relating to the above aim was carried out. The following is a description of each area in terms of geology, structure and specific samples collected, with a final section devoted to correlation and synthesis of the separate observations towards a regional framework. Grid references of all sample locations are given in Appendix 2

3.4.2 Sub-Area - A (Fig. 3.5)

This is the area around Inchnadamph. Sampling and study covered the lower parts of the Glencoul nappe near the Glencoul thrust, sole nappe and the foreland, though more attention was paid to the area between the Glencoul thrust and the Sole thrust (the Sole nappe). This latter area was studied more closely because of the presence within it of deformed carbonates. The Glencoul nappe is bounded below by the Glencoul thrust, while the lower nappe rests on the Sole thrust. The Sole nappe preserves a wide range of structural features, from imbricate thrusts and minor fractures to micro- and intermediate folds. Fold axes plunge mainly to the north, east and a few scatters in the SE direction Fig.3.11c). A lot of these minor folds were measured at the SE end of Loch Assynt in Serpulite Grit, Fucoid Beds and Durness Carbonates. They are mostly assymetric, overturned west and southwest, as observed by Christie (1963).

In places the hornblende dioritic sills in the above-three rock types are fractured, displaced and lineated. The plunge of the lineations could not be determined with

Fig. 3.5 Sub-Area-A around Inchnadamph, showing main rock types, some major structures and sample locations.

Adapted from the Geological Survey Map of Assynt District (sheets 107, 108, 101 and 102).

Grid references of all sample locations are given in Appendix 2

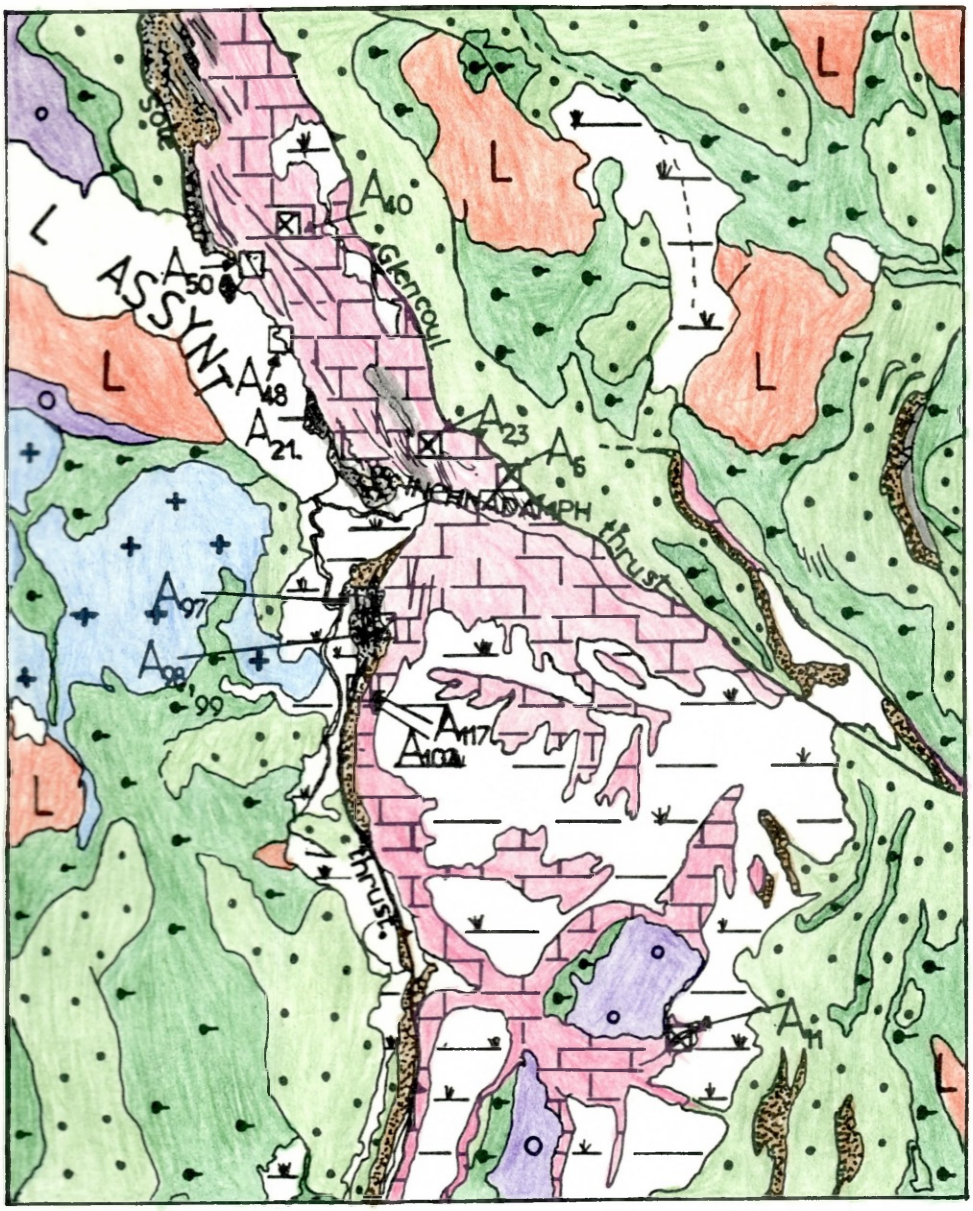

Scale 0 1 2 3 miles

Fig.3.5

- Marble
- Durness Formation
- Serpulite Grit
- Fucoid Beds
- Pipe Rock
- Basal Quartzite
- Intrusive igneous rocks
- Peat and alluvium
- Sample Source
- Torridonian Sandstones
- Moine Schists
- Lewisian Gneiss

Minor faults and imbricate thrusts.

high accuracy since the blocks of lineated sills have been displaced.

Characteristic of imbricate stacking in this area is a progressive change in strike southwards, and a change in dip from top to bottom of each stack. Imbricate thrusts at the northern end of the area are more north-north westerly in strike, while nearer the village, at the eastward veer of the Glencoul thrust they are more northwesterly (see also McClay and Coward, 1981, Fig.4a of page 248). The sequence of stacking in one duplex unit is such that dips at the bottom are usually semihorizontal (Plate 3.1a), changing to more than 45° SE at the top. Close to the Sole Thrust (which is a repeated horizon in this area, see also Elliott and Johnson, 1980), the carbonates are fractured very intensely producing a rock flour in some cases (Plate 3.1c).

Away from the thrusts (Plate 3.1b) the carbonates and Fucoid Beds normally preserve thick clay-filled seams and stylolites. These solution features are found parallel to bedding and usually affected by later stage folding and faulting suggesting they are of diagenetic origin.

The dolomite of the Durness Formation in this area is usually unaltered even if fractured and very close to the major thrusts. Sills intruded into carbonate rocks often cause the development of a limited alteration halo around them, with the development of chlorite being a major aspect of neomineralization in the carbonates. The dominant deformation mechanism in the carbonates of this area is cataclasis, with fracturing ranging in size from within-the-

PLATE 3.1

The low strain area of the Sole nappe, north and south of Inch nadamph.

a. At the base of an imbricate stack the beds are usually semi horizontal, and may experience extensive bedding plane-parallel flattening, producing thin beds with or without cataclasis. The top of the imbricate stack often dips at about 45^{o} south easterly.

b. Away from the major and imbricate thrusts bedding is normally well preserved including diagenetic stylolites and seams (s), parallel to bedding. Note also how the stylolites are warped. Scale 5cm diameter.

c. Cataclasis close to the Sole thrust produced a rock flour out of the Durness carbonates just north of Loch Assynt. Fracturing is very intense and a road-side cliff here is supported by gauze.

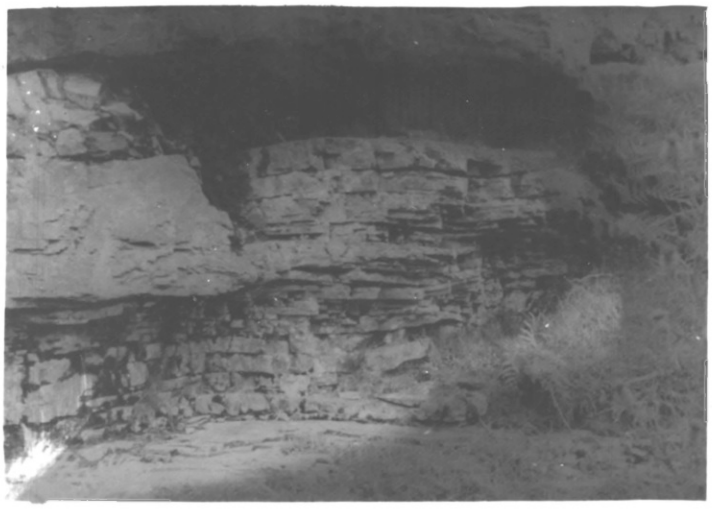

a

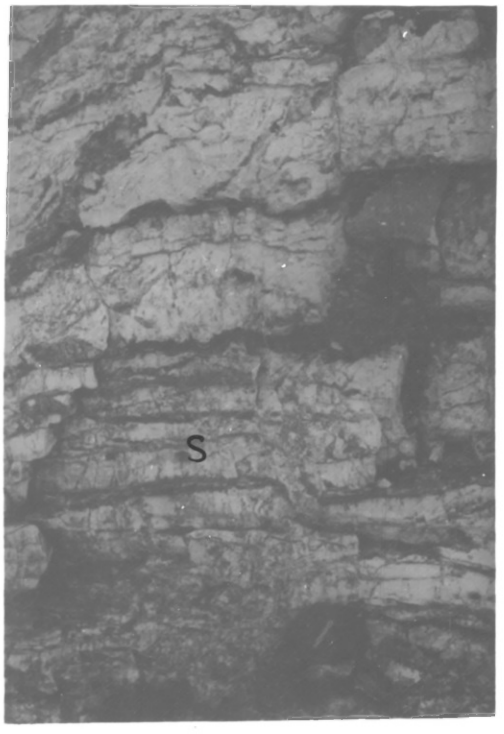

b

c

grain to intermediate imbricate and major thrusts.

Samples Collected in Sub-Area A

The locations of samples collected in Sub-Area A are as shown in Fig.3.5. The samples ranged from highly deformed to underformed carbonates, Serpulite Grit and Fucoid Beds. The aim was to collect samples of varying deformation macrostructure as well as undeformed ones in order to compare or study the evolution of deformation microstructure and mineralogy.

A-6 - Durness carbonate, a dense, dark dolomite sample with a network of fractures, taken immediately below the Glencoul Thrust east of Loch Assynt.

A-11 - (including A11a, A11b, A11c) - undeformed dolomite samples taken close to a hornblende dolerite sill. A_{11} and A_{11b} are dark, dense and coarsely crystalline.

A-21 - Highly fractured Serpulite Grit close to the Sole thrust very near Loch Assynt.

A-23 - dolomite sample from the imbricates north of Inchnadamph village.

A-40 - whitish dolomite with closely spaced stylolites and few vugs, taken from the imbricates.

A-48 - A-50 - Highly deformed, finely laminated Serpulite Grit samples.

A-97 - Serpulite Grit with diagenetic stylolites.

A-98 - Dark dolomite at the base in contact with grit south of Inchnadamph village. It has bedding-parallel diagenetic

stylolites and many vugs.

A-99 - More than 30m above A-98; a whitish-coloured dolomite with no vugs, but containing high angle tectonic seams.

A-102 - very finely laminated Fucoid Beds near the Sole Thrust.

A-117 - Serpulite Grit with many solution seams parallel to bedding and high clay content of seams.

3.4.3 SUB-AREA - B (Fig.3.6)

This is the fairly complex area north-west to north-east of Loch Ailsh. It is affected structurally by the Moine Thrust to the east, the Loch Ailsh Syenite complex and the Assynt Thrust to the west. West of Sgonnan More, i.e. below the Assynt Thrust the Durness carbonates are metamorphosed by late intrusives producing brucite marble. These show nearly vertical solution seams that have been annealed (Plate 3.2a), but no late stage fracturing is obvious either macro or microscopically. The evidence is presented by the Loch Ailsh syenite just north of Loch Ailsh. Here the syenite is fractured, and the spaced fracture planes dip to the east. This fracturing in the syenite affects the Durness carbonates nearer the Loch in the form of east-dipping imbricate thrusts, subparallel to the Moine thrust (see Christie,1963; Milne, 1978; and also Fig.3.6). The metamorphism of the carbonates by the intrusives decreases towards the Moine thrust and generally, apart from a sedimentary bedding, a deformation-induced schistosity is also present in the Serpulite Grit,

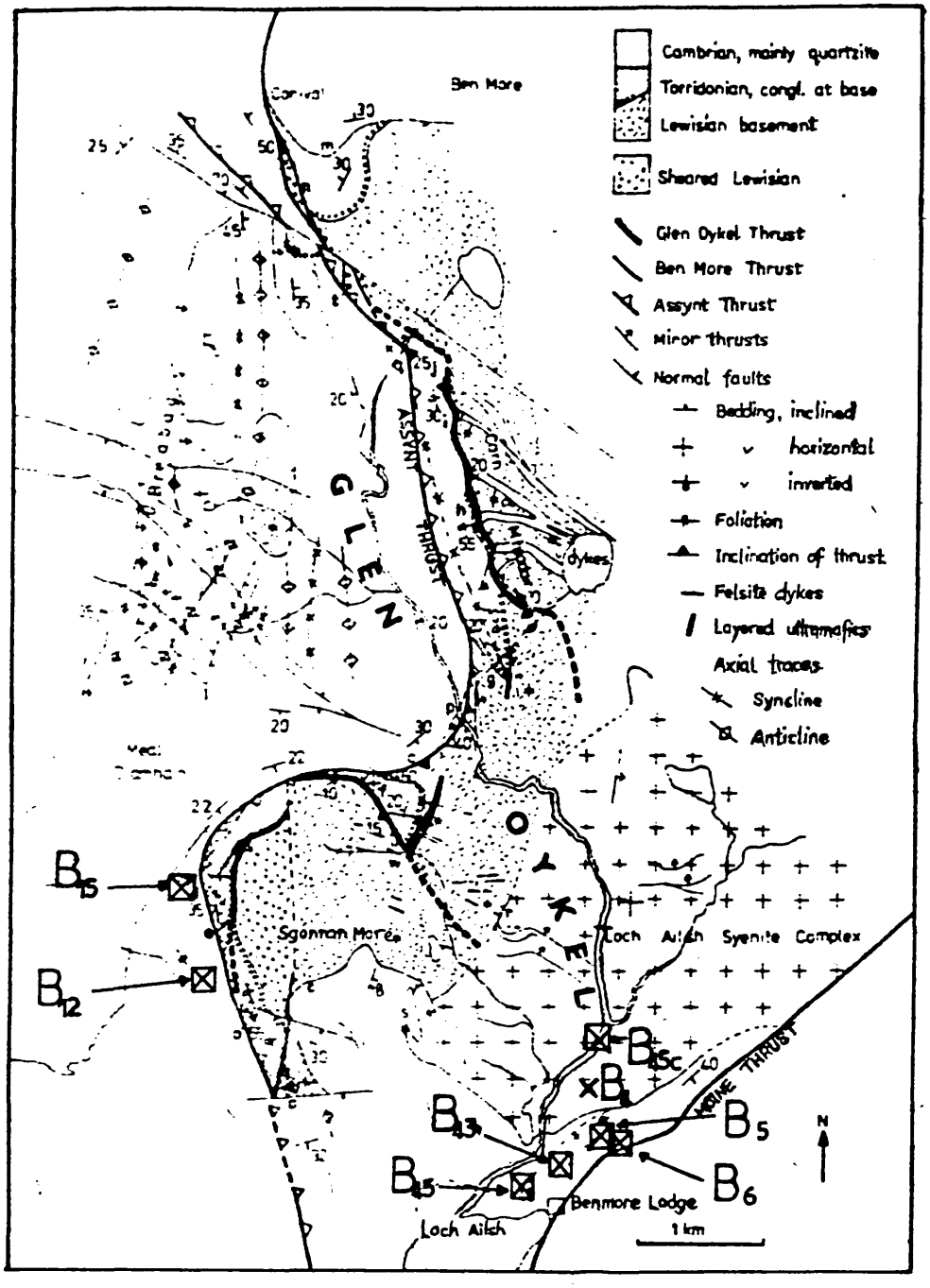

Fig. 3.6

Sub-Area B (after Milne I978)

Grid references of all sample locations are given in Appendix 2

Fucoid Beds and the Durness Carbonates of this area. Lineations plunge shallowly (less than 45° to the ESE, Fig.3.11b), while minor folds have a wider distribution (Fig.3.11c). Some of the latter plunge N-S, but the majority are either ESE- or SE-plunging.

Milne (1978) concluded that some deformation probably occured before and after the intrusion of the Loch Ailsh Syenites. As discussed above, although most of the movement along the Assynt thrust had ceased before the last intrusion, movement along the Moine thrust seems to have continued after the intru sion, hence the late fracturing in the Syenite.

Samples Collected in Sub-Area B:

Of the large number of samples collected in this sub-area, only those shown in Figure 3.6 were used in the analysis that follows in Chapters Four to Seven.

B4 - a coarse grained syenite with large grains of orthoclase and plagioclase feldspars and some biotite. It is intensely cross-cut by fractures, but the dominant ones are a set of fracture cleavage dipping south east. Sample B4 is about 1km west of the Moine thrust.

B5 - B6 - Loch Ailsh Marble samples of strike/dip 34/62°E and 62/30°E respectively. The samples are unlineated and fine grained. B6 was taken immediately below the Moine thrust, while B5 was collected more than 2 metres away.

B12 - B15 - these are the hardest marble samples in the sub-

area, and were collected just below the Assynt thrust west of Sgnonnan More (Fig.3.6). Cleavage dips at very high angles >80° to the east.

B43 - B45 - these are marbles of the Loch Ailsh type, harder than B5 - B6 but not as hard as B12 - B15. They occur within the imbricate sequence north of Loch Ailsh; and between ½ to 1km west of the Moine thrust. B45c - taken at the confluence of River Oykel (Fig.3.6) was found fused with the syenite.

The samples ranged from undeformed ones away from the thrusts to highly deformed and/or neomineralised ones close to the thrusts. The aim was to analyse the evolution of micro structure and neomineralisation from the undeformed to the highly deformed samples.

3.4.4 Sub-Area C, (Fig.3.7)

This is the area south of Loch Ailsh to Cnoc A' Chaoruinn. It is structurally complex, preserving three major thrust planes in very close juxtaposition, together with their imbricate structures. East of River Oykell, the Moine mylonites are involved in imbrication with the carbonates - (C89, C91 and Plate 3.2b & c). Each sequence has flaggy Moine psammites at the top and Moine mylonites at the bottom in a succession interleaved with carbonate rocks. Although lineations are very strong, plunging ESE (see also Plate 3.2d and Fig.3.11b), in both rock types, only the Moine rocks in this area are mylonites. Dips are generally low to the ESE, and occasionally the impression of horizontal (zero dip) foliation is given. Carbonate rocks here are given a

SUB - AREA - C around Cnoc a' Chaoruinn - showing the major thrusts, rock types and sample locations (adopted from Christie 1963).

A Thrust = Assynt Thrust, M Thrust = Moine Thrust.

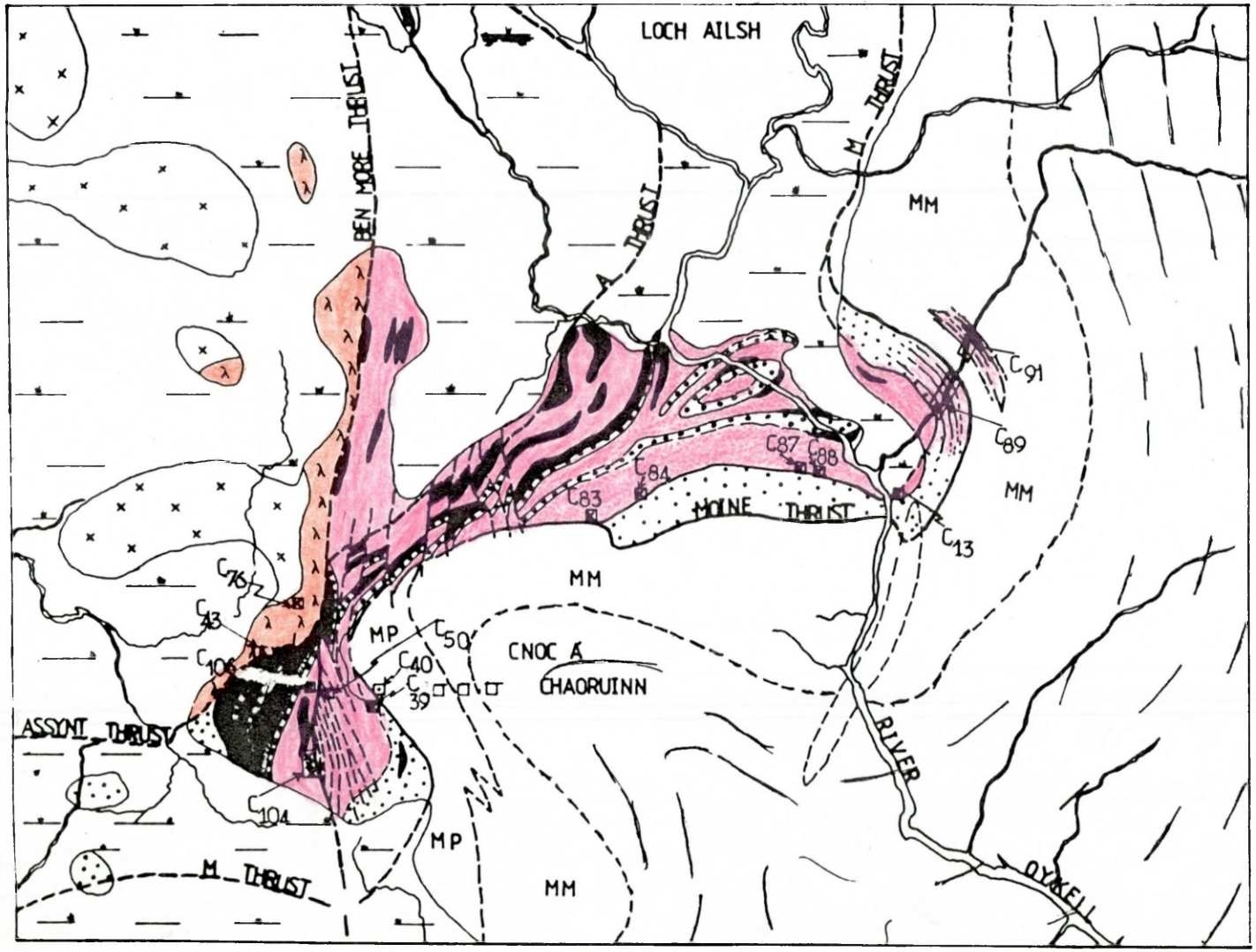

Fig. 3·7

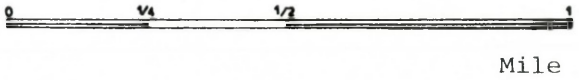

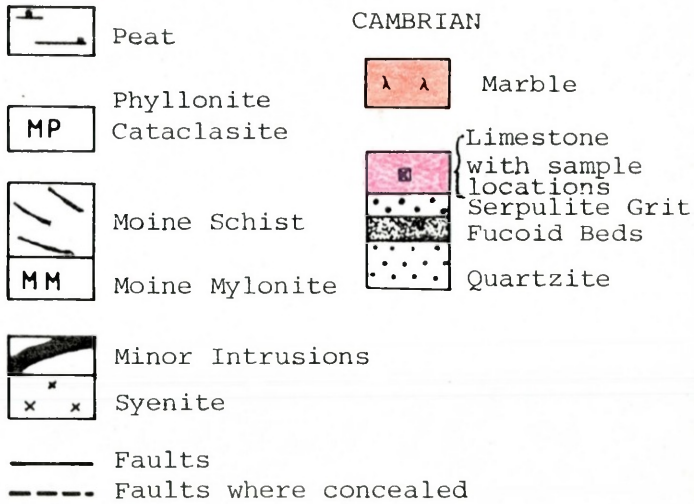

yellowish colour, are very hard and preserve a set of fractures almost normal to the lineations (Plate 3.2d), some of which are filled with calcite veins. Late monoclinal folds with NNE/SSW axes are developed particularly in the carbonates interleaved with the Moines, while the nearly-lineation-normal fractures break up the hinges and limbs of these folds. The gentle limbs of these few monoclines dip East to East-south-east. Southwest of this subarea is the complex zone bounded by the Moine thrust to the East and the Assynt thrust to the West, with the Ben More thrust running through the imbricate sequence (Fig.3.7). This zone lies between the Cnoc A' Chaoruinn hill and the Lairg-Loch Ailsh road junction. Lineations in both the Moine mylonites and Cambro-Ordovician rocks plunge to the ESE (Fig.3.11b). This is as true of the rocks below the Ben More thrust as above the Moine thrust. Poles to foliation on either side of the Moine thrust (Fig.3.11a) plunge generally in the same West to WNW quadrant as poles to foliation close to the Ben More thrust. But the latter are more gently plunging than the former, showing that dips of foliation or schistosity are generally greater close to the Ben More thrust than the Moine thrust in this area. The foliation and diagenetic solution surfaces in highly deformed carbonates here are transposed and caused to interfere. This leaves the impression that both surfaces have been used as movement horizons in the deformation process (see Plate 3.2e). Figure 3.11c shows that folds in Moine rocks of this area (▲) plunge at low angles to the SE mainly, although southerly-, and some easterly- plunging folds

are also present.

Imbricate structures are intensively developed, the ones above the Ben More thrust being often crescentic in shape after the curvature of the Moine thrust (see also Christie 1963). Moine rocks in this area - schists, mylonites and phyllonites - are well described in Christie (1963).

Samples Collected in Sub-Area C:

A large collection of samples from sub-area C eventually reduced to those shown in Figure 3.7. With respect to the major thrusts in the area they are:

C13 - close to the intersection of River Oykell with the Moine thrust. It is a highly deformed dolomite sample collected just below the Moine thrust. It is lineated, with clay seams up to 3cm thick.

C39 - a highly deformed, strongly lineated carbonate sample just below the Moine thrust. It has very closely spaced slip surfaces (Plate 3.2e) which give the appearance of a mylonite.

C40 - A greenish, highly micaceous Moine mylonite (phyllonite) sample collected above the thrust.

C43 - Highly deformed Fucoid Beds with the appearance of a mylonite collected behind the Assynt thrust, on a steeply dipping imbricate face. The lineation plunges steeply (88°) to 125°.

C50 - Dolomite sample collected in the imbricates behind the Ben More thrust. It is hard, crystallized and preserves a stylolite.

PLATE 3.2

Structures in sub-areas B (a), and C (b,c,d and e).

a. High angle ($> 70^{o}$) solution structures (parallel to the pencil) in highly metamorphosed marble west of Sgonnan More (See B12 and B15 of Fig. 3.6). This marble occurs just below the Assynt thrust, and the structures seem to have been annealed during contact metamorphism. Also the marble shows no later structures that may be attributed to post-metamorphic deformation.

b and c North-east of Cnoc a' Chaoruinn along the tributary of River Oykell (see sample locations C89 and C91 on Fig. 3.7), the darker coloured Moine mylonites (M) are interleaved with Durness carbonates (C) (brighter coloured) in imbricate sequences. Note the thinness of the individual units and their low dips.

d. Lineations in the carbonates, as in the Moine rocks of (b and c) above are very strong. Here they are parallel to the long dimension of the clinometer and are intersected almost orthogonally by later fractures. The lineations plunge to the E S E.

e. A highly deformed lens of dolomite shows both foliation and solution planes closely spaced, while adjacent solution planes are transposed to interfere crest-to-trough.

a

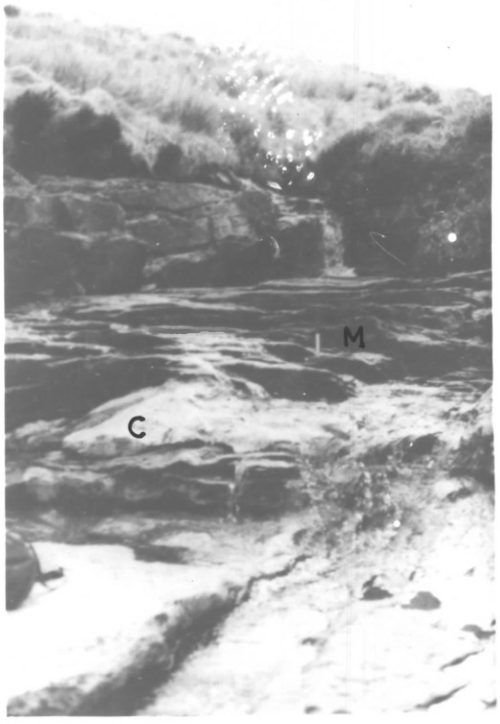

b

d

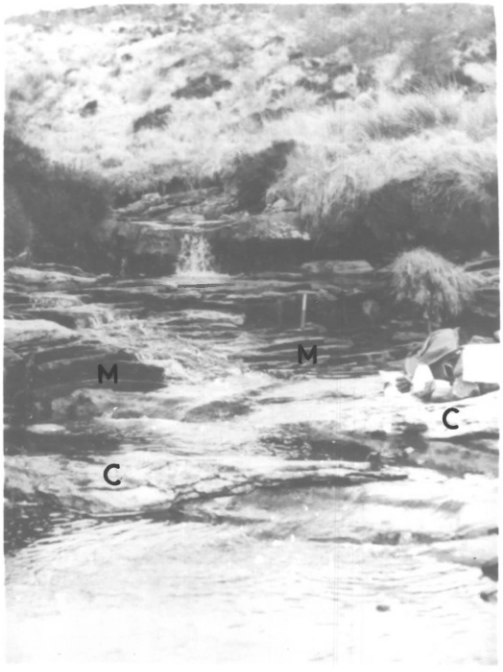

c

e

C76 - very hard and dark marble just west of the junction of the Ben More and Assynt thrusts. It is associated with the syenite intrusives.

C83-C91 - a series of carbonate (dolomite) samples collected just below the Moine thrust all along from north of Cnoc A' Chaoruinn eastwards. C89 and C91 form subseries of Moine/Carbonate imbricates at the NE tributary of River Oykell (Fig.3.7). At C91 for instance Moine and dolomite rocks alternate in very close succession, with low dips and very prominent lineations. These thin alternating slabs were sampled and denoted C91A, C91C, C91E for the schistose mylonites, and C91B, C91D, C91F for the dolomites.

C105-C106 - strongly lineated, highly deformed Fucoid Beds just below the Ben More thrust at the zone of complex deformation. C106 consists of C106A, C106B and C106C all collected in the same area below the thrust.

3.4.5 Sub-Area - D (Fig.3.8)

This is the area around Knockan Information Centre including Knockan Crag and Knockan Village. The Moine Thrust brings highly fractured Moine mylonites over equally fractured whitish Durness Carbonates (Plate 3.3a), and both rest on dark-coloured carbonates of the foreland (Plate 3.3b). Due to the extent of cataclasis in the carbonates, there is a complete absence of diagenetic stylolites within the first one meter below the thrust. Such solution features are very densely packed in the next one to one and a half meters (see Plate 3.3a), where the effect of cataclasis seems to have decreased. No lineations are visible in the carbonates

Fig. 3.8

SUB - AREA - D - around Knockan - showing major rock types, the Moine thrust and sample locations. The map is adapted from the Geological Survey Map of Assynt District (sheets 107, 108, 101 and 102) between latitudes 58^{o} o' and 58^{o} 5'N and longitudes 4^{o} 57' and 5^{o} 9'W. Most of the samples were collected close to the thrust plane, both above and below.

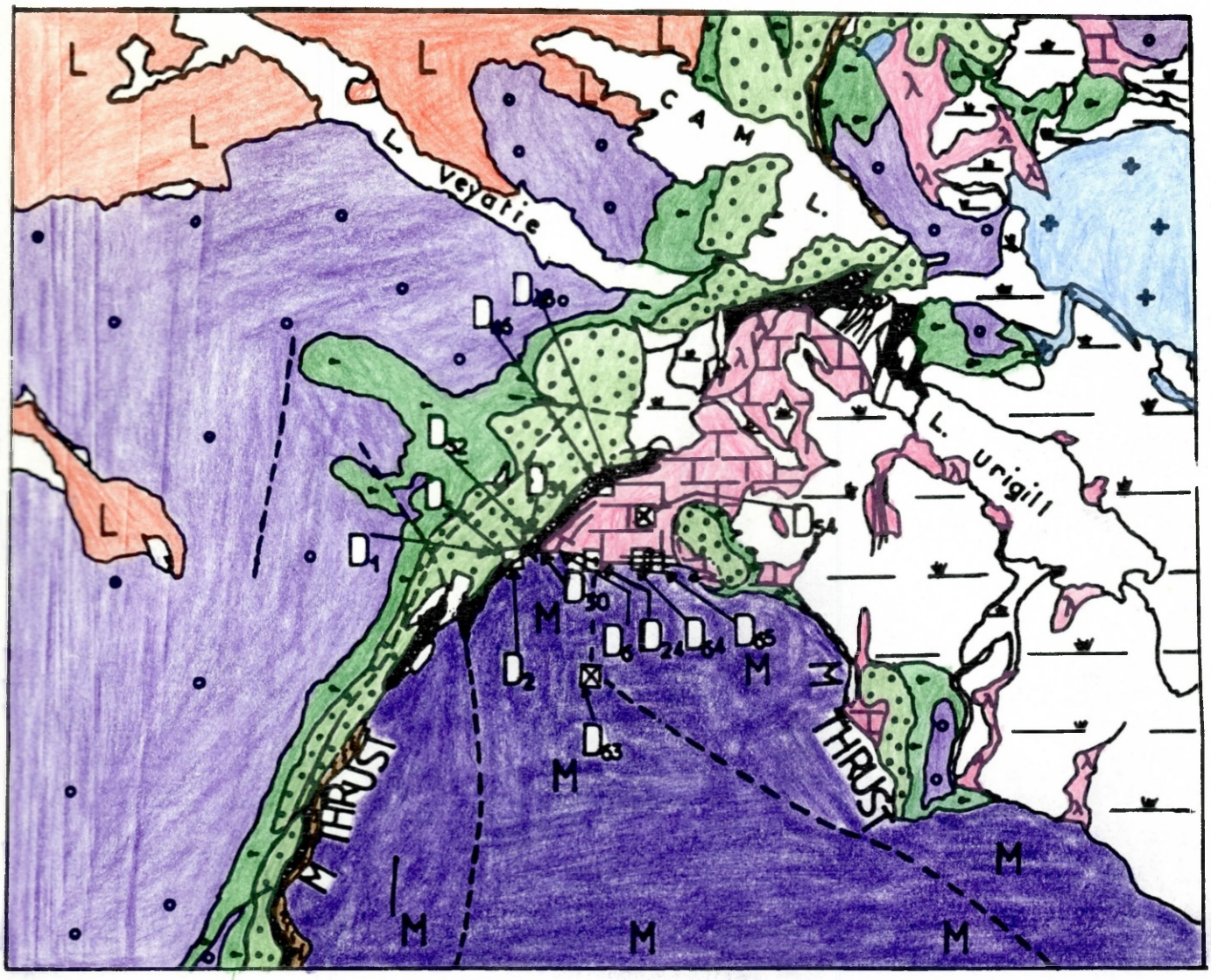

0 1 2 3
miles

Durness Formation

Serpulite Grit

Fucoid Beds

Pipe Rock

Basal Quartzite

Marble

Intrusive igneous rocks

Peat and alluvium

Sample source

Thrusts and faults where concealed.

Torridonian Sandstones

M Moine Schists

L Lewisian Gneiss

here, while about twenty feet above the thrust plane faint ESE lineations can be measured in the Moine schists. Exposure of the Moine/Carbonate contact is quite good for more than 1km eastwards, toward Druim Poll Eoghainn. Lineations in the Moine rocks continue to get stronger eastwards, while minor folds plunging ESE, SE and S (Fig.3.11c) are fairly common in the Moine mylonites and schists. Cataclasis in the calcareous rocks outlasts that in the schists above toward the east. Below the carbonates near the Information Centre, Fucoid Beds have also suffered a lot of deformation, with sedimentary and diagenetic clay-filled and bedding-parallel surfaces being used as movement horizons. These could be accommodation structures related to the Sole thrust (Plate 3.3c).

Away from the thrust, and towards Knockan Village minor thrusts and faults displace the carbonate rocks. Most of these are east-dipping, but some are west-dipping and of extensional nature. Also extensively developed are solution and fracture cleavage of tectonic origin. These are at high angle to bedding (Plate 3.3d), and have their poles plunging variably WNW (Fig.3.11d). The tectonic cleavage planes are taken as XY planes of the strain ellipsoid. The few other poles plunging towards the NNW in Figure 3.11d were measured in sub-area A, near Inchnadamph.

Samples Collected in Sub-Area D:

Due to the generally good exposure of the Moine Thrust

zone in this sub-area, vertical sampling (above and below the Moine thrust) and lateral sampling to follow the thrust eastwards were done without much difficulty. Figure 3.8 is an adaptation of the Geological Survey Map (Sheets 107, 108, 101 and 102) of Assynt District between Latitudes 58°0' and 58°5'N and Longitudes 4°57' and 5°8'W, to show the geology and sample positions for the area around Knockan. Only those samples used in the analysis that follows are marked in Figure 3.8, although a much larger population of samples was collected at the beginning. These are:

D1 - a dolomite sample 1.5m below the Moine thrust. It is whitish, highly fractured and contains diagenetic stylolites.

D2 - Dolomite just below the fault gauge (first 1m).

D3 - Moine cataclasite just above the fault gauge and above D2.

D6 - a finely foliated and weakly lineated Moine mylonite about 10m above the thrust plane.

D24-D23-D60-D61-D62-D63 - this is a series of Moine samples starting at the thrust (D24), through some more Moine mylonites (D23-D60) into the Moine psammites D63. It is used later in Chapter Four to show the effect of retrogressive metamorphism on the Moine Schists.

D31 - Dolomite sample just below the fault gauge.

D31A - Dolomite sample 1m below the thrust.

D31B - Dolomite sample 2m below the thrust.

D31C - Dolomite sample 3m below the thrust.

D31D - Dolomite sample 4-5m below the thrust.

This is a vertical sample profile from the Moine thrust

PLATE 3.3

Sub-Area-D - around Knockan.

a. The first 1m below the Moine thrust here is marked by extensive cataclasis with high fracture density down to grain scale.

Two meters below the thrust (note the position of the clinometer) fracture intensity is lower and bedding-plane parallel solution features persist.

b. About 5m below the thrust plane the highly deformed whitish dolomite rests on the dark-coloured foreland-type carbonate (hammer position). The latter is not so highly deformed, and fracture intensity in it is much lower.

c. Fucoid Beds below the Durness Formation in this area contain bedding-parallel parting planes with thick clay seams. They may have been utilised as intraformational movement (slide) planes to accommodate strain from the Moine thrust above.

d. Cleavage in carbonate rock near Knockan village. The cleavage planes are steeply dipping, with their poles plunging mainly to the west (Fig. 3.11d), opposite to the general plunge of lineations.

a

b

d

c

through the whitish-coloured, highly fractured dolomite rock.

D32 - more than 5m below the thrust here is a dark, foreland type dolomite that rests on the Serpulite Grit (Plate 3.3b).

D46 - Cataclastic dolomite from the hanging wall of a minor thrust near the road at Knockan. The thrust was referred to as one of the pieces of the Sole thrust (Coward, pers. comm). It carries whitish crystallized calcitic dolomite over dark, crystallized but finer-grained dolomite.

D48 - Dolomite with cleavage (Plate 3.3d). The sample was not near any of the major thrusts.

D64-D65 - these are two pairs of Moine mylonite/Dolomite samples taken in pairs as close as possible on either side of the Moine thrust towards Druin Poll Eoghainn. They are the most easterly group of samples collected near the Moine thrust.

3.4.6 Sub-Area ST (Fig.3.9)

The fifth area sampled, though not mapped in detail is that north of Gorm Loch Mor, and south-east of the Stack of Glencoul. Sampling was confined to the Ben More and Moine nappes, with the samples taken from the entire succession from the Pipe Rock Quartzites to the Durness Carbonates, and across into Moine mylonites and Moine Schists. The pipe rock in this area has developed good schistosity with foliation planes dipping east, while Fucoid Beds above it have fairly steep cleavage also dipping eastwards. Similar cleavage planes in the dolomites of the Durness Formation had a strike of about 340°, dipping up to 30° east. The Fucoid

Fig. 3.9 Legend

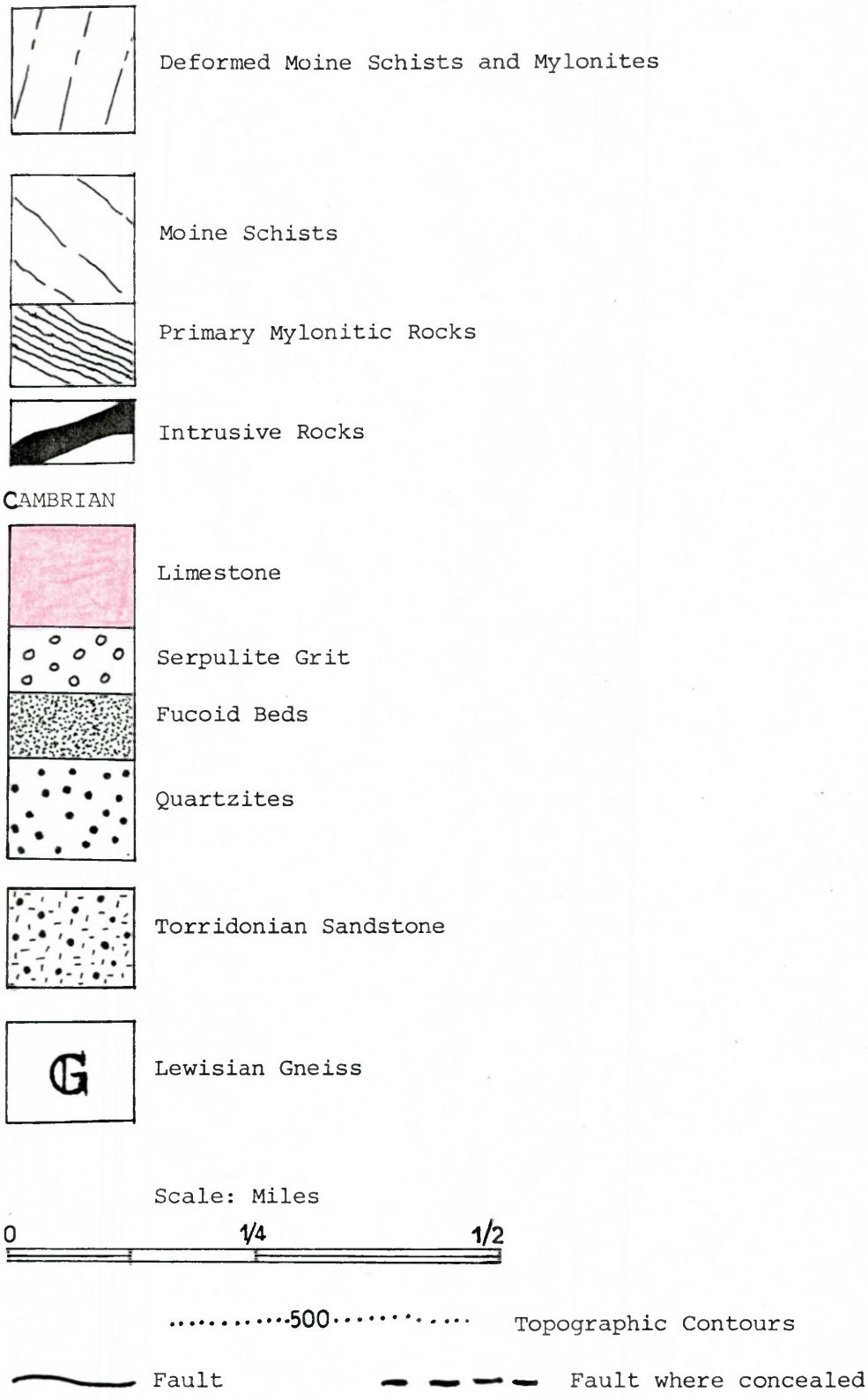

SUB - AREA - ST - south east of the stack of Glencoul, showing sample locations ST_1 - ST_{12}, on a map of the geology and major structures of the area after Christie (1963). The national grid references of all samples from this sub-area are presented in Appendix 2.

APPROX BOUNDARY MOINE SCHIST
MOINE THRUST
BEN MORE THRUST
FIONN ALLT
GORM LOCH MOR
N
1300
1200
1100
1000

Beds, Serpulite Grits and Durness Carbonates here are imbricated and intensely deformed with the dioritic sills in them.

The quartzite shown by Christie (1963, Fig.4) to separate the Ben More nappe from the Moine nappe has more affinity with the Moine Schists than the Basal Quartzite and for that reason the Moine thrust in Figure 3.9 may be moved more westward to coincide with the eastern end of the imbricates.

Samples Collected in Sub-Area ST:

ST-1 and ST-2, finely foliated Pipe Rock between the Ben More thrust and the Moine thrust, but closer to the imbricates.

ST-3 - Fucoid Beds with foliation (cleavage) within the imbricate zone.

ST4 - Highly deformed Hornblende sill within the imbricates.

ST5 - Deformed dolomite with cleavage, in close contact with the sill.

ST7 - highly deformed thinly foliated marble just below the Moine thrust.

ST7A - Moine mylonite lying above ST7, separated by the Moine thrust.

ST8 - ST9 - ST10 - continuation of a series of Moine samples including ST7A- at the thrust, to ST10 in the Moine psammites. ST10 - is more than 15m above the thrust.

ST11 - very finely foliated, mylonitised carbonate rock inter-

bedded with dark, highly deformed hornblende sills. ST11- and ST12- of similar composition and appearance were taken from the imbricates just below the Moine thrust.

3.4.7 Sub-Area - Er (Fig.3.10) Eriboll:

At about the 700ft contour line, bearings [4400, 5640] east of Eriboll house is a tectonic lens of dolomite marble, ascribed to the Balnakiel group of the Durness Formation by Peach et al. (1907). Soper and Wilkinson (1975) noticed that it is interposed within the mylonites of their "zone of complication" (Plate 3.4a). It is bluish to greenish in places due to chloritization, andcan be traced discontinuously southward to very close to Creagan road. Where exposure is good, it could be up to 20m thick, overlies highly deformed Lewisian gneiss and quartzite and is itself overlain by highly deformed Moine/Lewisian mylonites. This tectonic lens is itself made up of smaller lenses that must have been pushed westward on mica/chlorite - filled movement surfaces within it (Plate 3.4,b). The strong cleavage referred to by Soper and Wilkinson (1975), is actually a mylonitic foliation (Plate 3.4c), as confirmed by optical microscopy.

The mylonitic foliation is deformed by folds plunging SE and ESE, and the lineations fan from east to SE, while a third set of minor folds trend north-south. Most of the ESE minor folds are overturned to the north.

Samples collected in this sub-area:

Most of the samples were collected from the tectonic lens of marble referred to as "Eriboll Marble" in Figure 3.10. Other

Fig. 3.10

SUB- AREA - Er. (Eriboll) (after McClay and Coward, 1981) showing locations of Eriboll marble, samples from the Oystershell Rock carbonate band (OY_1 - OY_4), and the samples from the Cambrian - Ordovician succession around Kempie Bay (K_1 - K_5). The rest of the symbols are explained in the Legend.

MOINE THRUST ZONE, LOCH ERIBOLL, NW SCOTLAND.

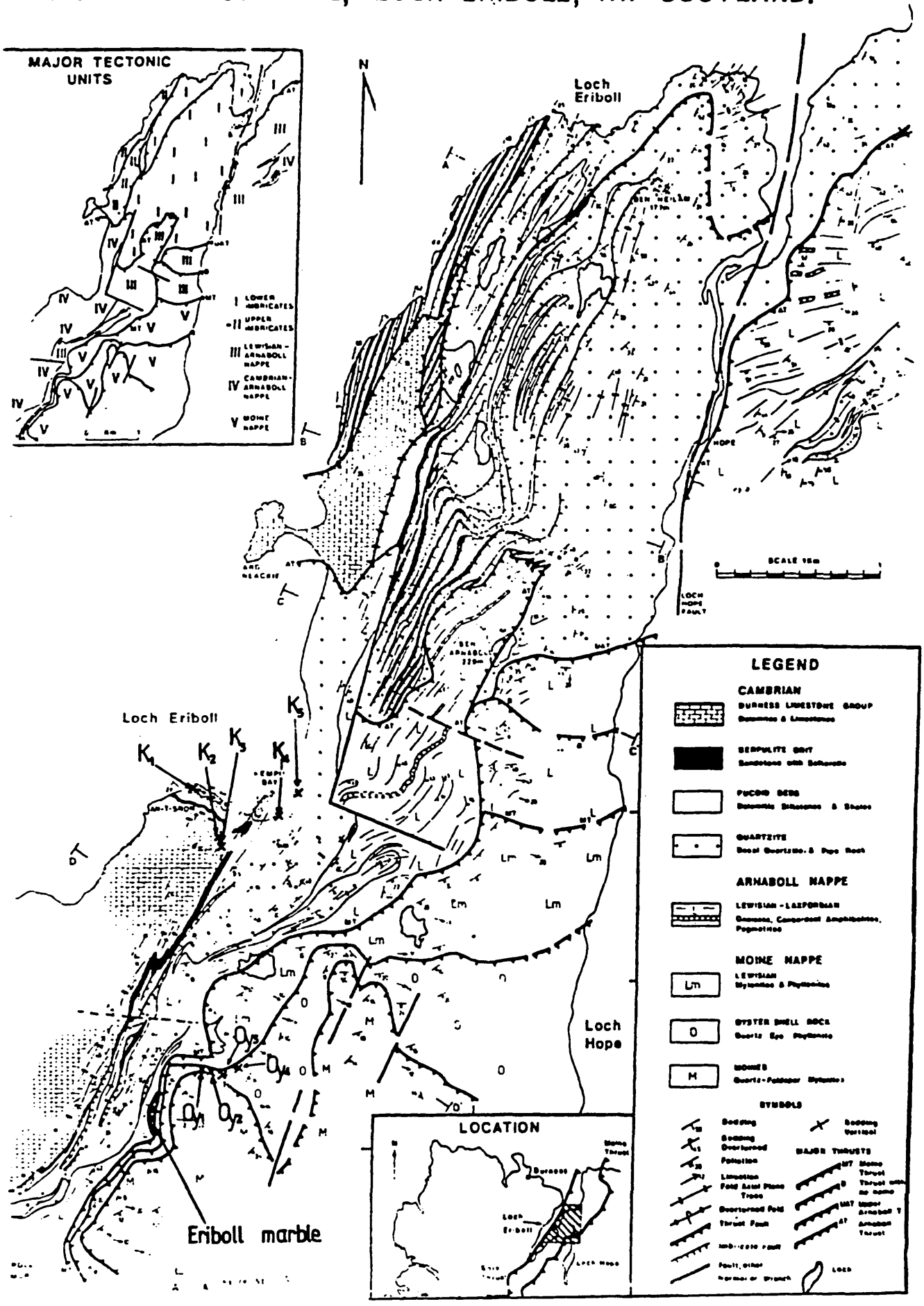

PLATE 3.4

a. The tectonic lens of Eriboll marble (arrowed) outcropping just below the Moine thrust (MT).

b. The lens is itself made up of smaller units of finely foliated chlorite marble, which seem to have been transported westward along chlorite-rich planes.

c. E S E - lineations (arrowed) are strongly printed on the fine folia, which are also folded producing three fold attitudes: SE, ESE and N/S- plunging minor folds (see Fig. 3.11c). The mylonitic foliation is also very fissile.

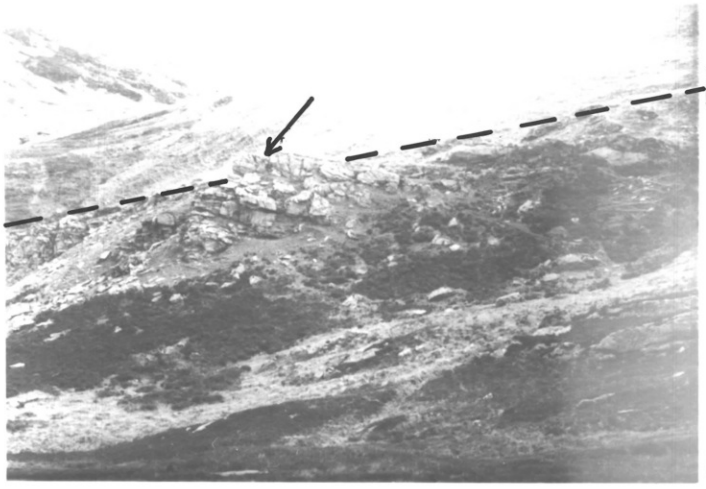

a

b

c

areas of sampling were the Oyster-Shell Rock just NE of the marble, and the Cambrian succession around Kempie Bay. The locations of the relevant samples are as follows:

Eriboll Marble:

Er. 7 - taken about 2 metres below the Moine thrust marked MT in Plate 3.4a. It is fairly deformed, but not greenish like most of the others.

The rest of the samples: Er 8, Er 9, Er 10, Er 11, Er 12, Er 13, Er 14, Er 15, Er 16, Er 17, Er 18, and Er 19 were collected along a line within the first 1m below the Moine thrust from north to south of the marble lens (Plate 3.4a).

Oystershell Carbonate:

OY1, OY2, OY3, and OY4 were four samples of a carbonate-rich band collected in Oystershell Rock just northeast of Eriboll marble (Fig.3.10). The samples were collected close to an unnamed thrust, but within 200m east of the Moine thrust.

Kempie Bay Samples:

The third group of samples from this area came from around Kempie Bay, that is north of Eriboll Marble and south east of Loch Eriboll.

K1, K2 and K3 are carbonate samples from this low strain area more than 1km west of the Moine thrust. They contain cleavage microstructure of possible importance in the deformation study of the carbonate rocks.

K4 and K5 - are samples of Pipe Rock collected also west of the Moine thrust, on the lower limb of a westward overturned

Fig. 3.11

Stereographic projection on the lower hemisphere of:

a. Poles to foliation (• on either side of the Moine thrust, and ▲ on either side of the Ben More thrust). Note how they plunge generally to the same west and WNW quadrants, although foliation near the Ben More thrust is slightly steeper-dipping than that near the Moine thrust.

b. Lineations close to the Moine thrust (in Moine mylonites and Durness carbonates). They plunge mainly less than 45^{o} to the ESE.

c. Folds in Moine rocks (▲), and all other rock types (•) in the two areas of study. Note that folds in the Moine rocks are confined in plunge mainly between east and south, while those in other rock types have more scatter.

d. Poles to tectonic seams or cleavage in carbonate rocks. Apart from a few NNW plunging poles, the majority plunge between west and WNW (see Plate 3.3d). Note that the poles to cleavage planes plunge in the opposite direction to the lineations.

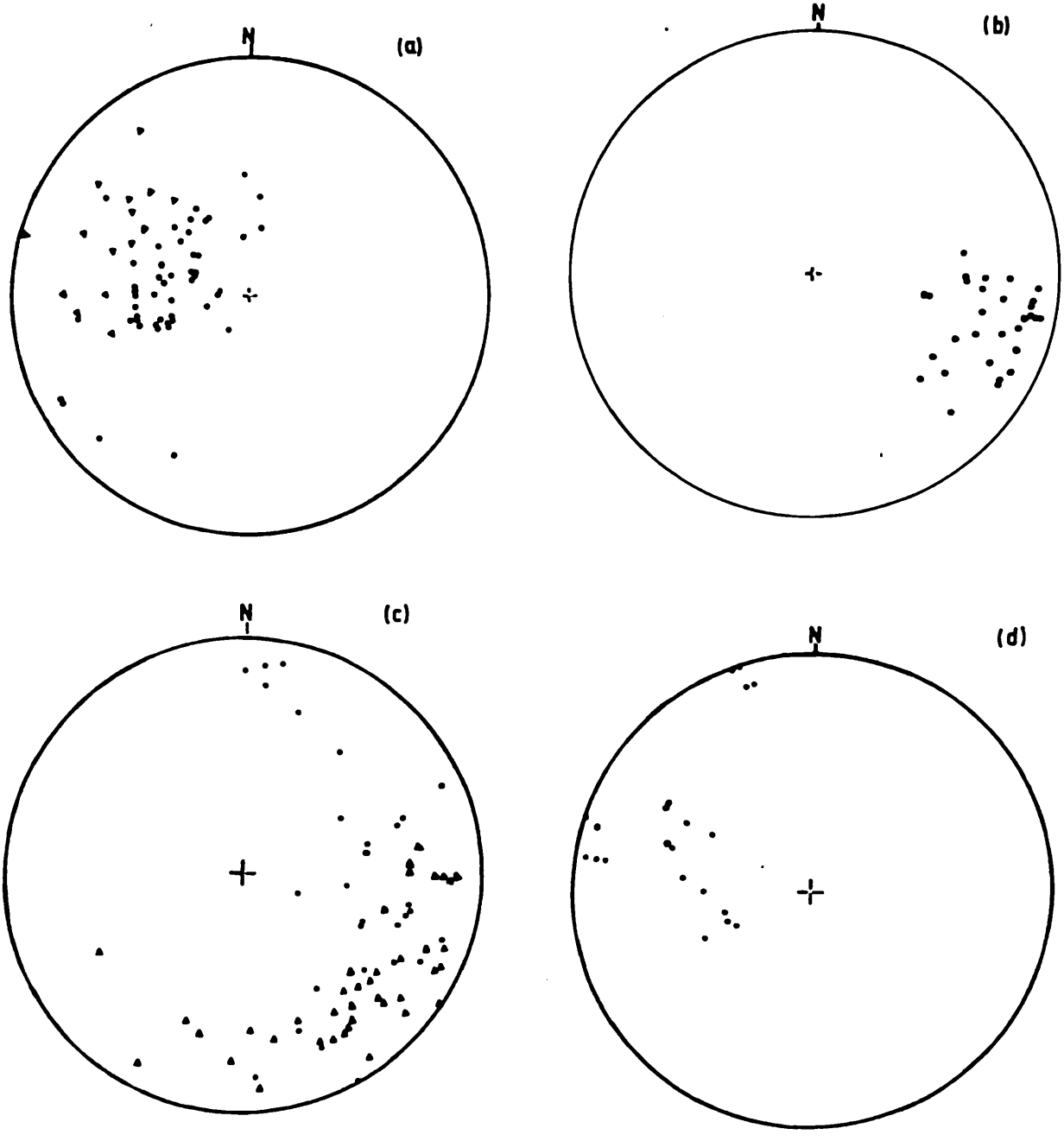
N
(a)
N
(b)
N
(c)
N
(d)

major fold. They both contain strained pipes and cleavage.

3.5 CONCLUSION

From the foregoing field evidence the following conclusions have been drawn about the deformation of the Durness Formation:

(i) Durness Carbonate deformation, especially below the Moine Thrust plane, varies from cataclasis at Knockan to crystal plasticity at Cnoc A' Chaoruinn, which goes further to produce mylonitization at Eriboll.

(ii) Mylonitization and Lineations in the carbonates were not found outside the Moine Thrust, although folds of varying orientations exist as far from the thrust as the foreland.

(iii) At least in sub areas B, C and D, there is no apparent relationship between the timing of mylonitization events in Moine rocks and in Durness Carbonates.

(iv) Movement along the Moine Thrust plane is likely to have outlived that on the Assynt Thrust as well as the intrusions of Loch Ailsh and Borolan in the south of Assynt. This conclusion was also arrived at by Milne (1978) using another set of evidence.

CHAPTER FOUR

STUDIES OF TEMPERATURES ASSOCIATED WITH THE DEFORMATION OF THE DURNESS CARBONATES

4.1.1 INTRODUCTION

The most intense deformation of the Durness Formation in the Moine Thrust Zone is along the individual fault zones, and this, particularly along the major thrusts, is accompanied by prograde metamorphism of the rocks below the thrusts including the Durness Carbonates. Some other aspect of metamorphism of the Durness Carbonates is associated with plutonic intrusives concordantly (sills) or discordantly emplaced at high levels, in most cases, before major thrusting began. In this chapter estimates are made of the temperatures associated with the metamorphism of the carbonate rocks as they underwent deformation along the major thrusts - particularly the Moine thrust. Estimated temperatures are compared with those earlier determined for the foreland, and models are postulated to account for the excess thermal energy partly responsible for this deformation-associated metamorphism. The experimental methods adopted, and the theoretical basis of the methods are first analysed.

4.1.2 Theoretical Background:

In a metamorphic environment dolomite $CaMg(CO_3)_2$ is capable of dissociation into a magnesian calcite, periclase and carbondioxide. The high temperature and low temperature equations for this behaviour are presented in subsection

2.5.1 of Chapter Two (see equations 2.4 and 2.5). Such an equilibrium thermal decomposition is driven forward by temperature increase and backward by increase in pressure, so that if the pressure on or of the system is known, it is possible to estimate the temperature of the system. The temperature is estimated from the $MgCO_3$ in solid solution with or dissolved in the calcite in equilibrium with dolomite, which was shown by Goldsmith and Newton (1969); and Goldsmith (1980) to be a function of the temperature at constant pressure. This geothermometer has been used by Sheppard and Schwarcz (1970), who fitted a mathematical equation to the curve of Figure 2.16; Hutcheon and Moore (1973); Moore and Kerrick (1976); Bickle and Powell (1977) and Rice (1977). Other means of temperature estimate like facies assemblage, stable phyllosilicate minerals or deformation mechanisms, in this case, of dolomite, could be used, but not with the same accuracy as the solvus geothermometer.

Analytical Facilities and Methods Used:

4.1.3 Rock Samples and Sampling Procedure

All rock samples collected in the field were fresh, oriented and their locations presented in maps of the separate field areas in Chapter Three, (Section 3.4). Those samples without lineations in them were oriented with an arrow pointing to N300°, approximately, parallel to the known movement direction, and opposite to the general plunge of the stretching lineations on the deformed rocks. The

lineation direction and attitude of the foliation planes are taken as co-ordinates in the study of the crystallographic fabric of crystallites, though they are not necessary in composite phase analysis or micro-chemical studies.

The aim in sample collection was to obtain samples representative of the entire area, from the relatively undeformed foreland to the high-strain area close to the thrust planes. This also included contact aureoles in carbonate rocks.

4.1.4 Analytical Facilities and Methods Used

Three analytical procedures were adopted for the study of temperatures associated with deformation of the Durness Formation, and are discussed below.

4.1.4.1 Whole Rock Composite Phase Analysis

This was done by means of a Phillips X-Ray powder Diffractometer with the following specifications:

Working Potential	=	34kv
Current	=	28mA
Radiation	=	filtered Co (Kα)
Scanning Speed	=	1°/min mostly, and ½°/min in a few check-up cases
Count Rate	=	400 c/sec mostly, but occasionally 800 c/sec was used
Time Constant	=	2

Oriented sample mounts were mainly used, with a few cavity mounts in some cases. Oriented mounts enhanced basal reflections of phyllosilicates, but did not drastically reduce reflections from other constituent minerals. Where reflections from other minerals were thought to be affected, cavity mounts were used in addition. The type of runs were Air Dry (A/D), Glycerated, 400°C (preheated and then cooled), and also 550°C (preheated and then cooled). The last three runs whenever used were mainly for verification.

The great advantage in using XRD for phase analysis soon became apparent because not only was stable phase variation more easy to appreciate on a strip chart but also because of the large sample size used, phases showed up which where very difficult to analyse using other methods. There is need to emphasize that the XRD in no way replaces completely other analytical facilities like the XRF or EPMA, but that they all complement each other.

4.1.4.2 Mineral Microchemical Studies

Those rock samples which contained both calcite and dolomite as revealed by the above technique were chosen for probe polishing. The very high standard of polishing required for backscattered imaging was often met by probe-polishing and for microchemical studies both the Cambridge Microscan-5 and the Jeol JXA-733 electron probe X-ray microanalysers were used.

Working Conditions with the Microscan-5:

Working Potential	=	15kv
Specimen Current	=	2-2.5 nA (for carbonates)
Electron Beam Spot Size on Specimen	=	1 - 2 μm

Excitation Area on Specimen	≏	10μm
Count Rate	=	(2 - 2.5) x 10^3 c/sec
Count Time	=	100 Live seconds
Dead Time	=	20 secs
Vacuum	=	10^{-5} Torr. (1.33 x 10^{-3} Pa)
Detector	=	Li-drifted Silicon solid state detector with Liquid Nitrogen cooler, EDS mode
Analyser	=	Link System 290

Working Conditions with the JEOL JXA - 733

Working Potential	=	15 kv
Specimen Current	=	2-2.5 nA
Operating modes used:		SEM, and Backscattered (compo);
X-ray measurement unit		LINK 860/500SR2
Analysing mode used		EDS

Back Scattered Electron Detector:

Silicon PN-junction detector (2 divisions annualr type)

Image processes: Topographic and compositional

Working pressure (specimen chamber) = 1x10^{-5} Torr (1.33x10^{-3} Pa).

The advantages of the Jeol-733 over the Cambridge Microscan 5 are many. The former is easier to use, and because of the backscattered viewing mode and wide range of maginifications available, the exact position of the electron beam with respect to the size of the specimen is no longer a problem. This viewing mode, enables the operator to choose parts of any crystal for analysis since features like reaction rims, zones, alterations and replacements are so well imaged.

4.1.4.3 Optical Microscopy

The third analytical procedure used was aimed at checking results arising from the above analyses. For this the Zeiss 3 light microscope was used in conjunction with the JEOL JXA-733 electron microscope. The former used ultra-thin thin sections, usually below 3μm in thickness. Ultra-thin thin sections are needed if dolomite and calcite are to display first order grey colour in transmitted light.

4.2 RESULTS OF THE WHOLE ROCK XRD PHASE ANALYSIS

The results of the analysis are presented as diffractograms of the air dry (A/D) samples. The results of follow-up tests on glycerated mounts as well as mounts heated to 400°C, and 550°C are not presented here since they were only used for checking up the results of the air dry runs. As far as the temperature study is concerned, using the calcite-dolomite solvus, the only important part of the diffractogram is that between $2\theta = 30°$ and 40°, i.e. the part containing the main calcite $(10\bar{1}4)$ and dolomite $(10\bar{1}4)$ peaks.

4.2.1 Results from the foreland, low strain areas and areas generally away from the thrust planes

Between $2\theta = 30° - 40°$ of Figure 4.1, the most important reflections are the 006 of mica, the $(10\bar{1}4)$ of dolomite, with the 101 of quartz and the main peak of feldspar (orthoclase or low microcline) crowding closer to the mica peak. The intensity of the dolomite peak varies, but generally the absence of the main calcite peak is diagnostic of this area.

FIG.4.1

X-ray diffractograms from the Foreland, low strain areas. Note the absence of the main calcite peak (10 $\bar{1}$4) between $2\theta = 30^{\circ} - 40^{\circ}$. The intensity of the dolomite peak (10 $\bar{1}$4) is variable, while the 006 of mica (illite) is usually very strong.

FIG. 4.2

Samples from the southern part of the Moïne Thrust show, between 2θ = 30° - 40°, a weak calcite (10 $\bar{1}$4) peak at d = 3.03Å. The dolomite (10 $\bar{1}$4) peak is still relatively stronger, while between 2°— 10° a chlorite (001) peak emerges, also characteristic of this area.

ch = chlorite, Fspar = feldspar qtz = quartz cc = calcite dol = dolomite.

4.2.2 Below the Moine thrust in the South

Below the Moine thrust plane at Knockan and Cnoc A' Chaoruinn ,the part of the diffractogram between 30° and 40° shows a remarkable change. Figure 4.2 shows the presence of the $(10\bar{1}4)$ calcite peak in D31 and C39, and the (004) of chlorite very close to $2\theta = 30°$. This is in addition to a generally very intense dolomite peak, very weak or no quartz and feldspar and varying amounts of mica. In D31 (Knockan) of Figure 4.2, the introduction of chlorite coincides with the disappearance of mica, such that even if some of the calcite was precipitated from solution, a lot of it would also have been produced from the dissociation of dolomite in situ, making some of the calcite usable for temperature studies. Although the chlorite peaks show a great increase in C39 (Cnoc A' Caoruinn), the $(10\bar{1}4)$ calcite peak does not reflect this increase in intensity.

4.2.3 Below the Moine Thrust at Eriboll

In the northern end of the Moine thrust zone, the Durness Formation just below the Moine thrust is characterized by very intense calcite $(10\bar{1}4)$ and chlorite peaks, with medium quartz, and little or no mica and dolomite peaks (Fig.4.3). The disappearance of mica is also coincident with the appearance of talc among the other minerals already mentioned. The increasing intensity of quartz with that of chlorite is as observed earlier by Fawcett and Yoder (1969), while the increasing intensity of calcite at the expense of dolomite could be explained by the tendency of

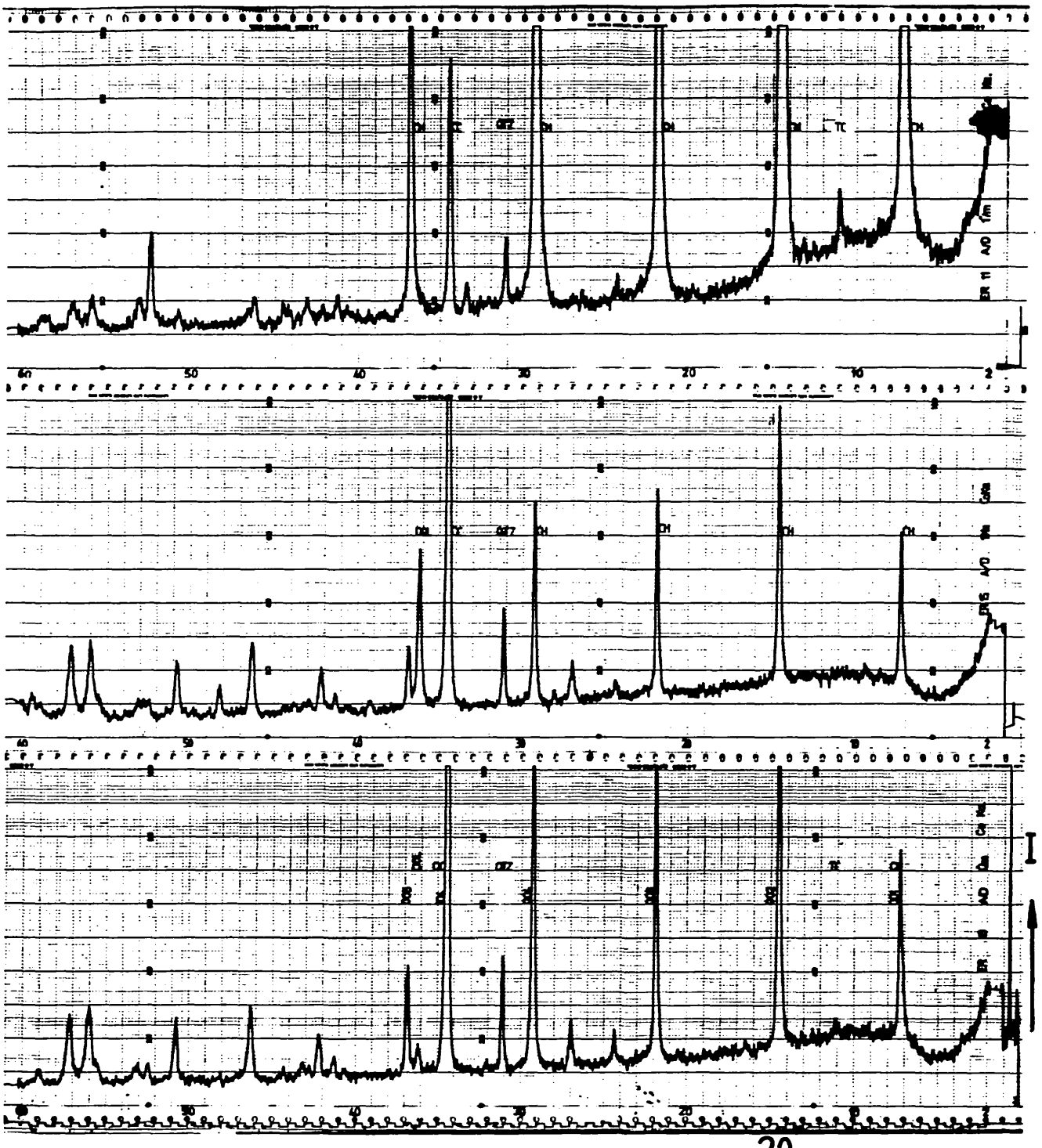

FIG. 4.3

Diffractograms of whole rock samples Er11, Er15 and Er19 from Eriboll. Note between $2\theta = 30^{o} - 40^{o}$ the presence of a very strong calcite ($10\bar{1}4$) peak, sometimes stronger than the dolomite ($10\bar{1}4$) peak. Between $2\theta = 2^{o} - 20^{o}$, this area is characterised by a strong chlorite (001) peak, absence of mica (002) and presence of a weak talc peak. ch = chlorite, tc = talc, qtz = quartz, cc = calcite, dol = dolomite.

dolomite to establish equilibrium by dissociating to produce calcite. The continuous presence of calcite and dolomite below the thrust plane suggests that the physical conditions have not pushed the equilibrium too far to the calcite field, hence a reasonably good field is provided for applying the calcite/dolomite geothermometer.

4.2.4 Near Intrusive Bodies

Carbonate samples taken from very close to intrusive igneous bodies produce diffraction peaks similar to 4.2.2 and 4.2.3 as well as some unique peaks. Figure 4.4 shows that very close to sills (A11) dolomite undergoes very little dissociation producing a little calcite and some of the Mg^{2+} ions take part in the building of chlorite lattices, hence equally little chlorite is present.

Around the Loch Ailsh Syenite, with higher heat extrusion to the surroundings, the dissociation of dolomite is so complete that brucite and calcite are produced (see B13 and C76 - Fig.4.4). In all cases there is the breakdown of the 9.9A mica mineral, and the formation of some antigorite (in B13 and C76) or chlorite (A11).

The presence of brucite [$Mg(OH)_2$] in carbonate rocks near igneous bodies and the absence of the 9.9A mica peak in the same rocks is likely to suggest that the breakdown of the latter mineral was too early and so rapid that when Mg^{2+} ions were supplied there were no mica lattice sites available for the generation of chlorite. This is unlike the thrust plane where the breakdown of dolomite and

FIG 4.4

Diffractograms of samples A11 (from close to a sill), B13 and C76 (close to the Lock Ailsh Syenite).

Note the strength of the calcite peak (10 $\bar{1}$4) between $2\theta = 30^{o} - 40^{o}$ and the presence of brucite (bc) which is absent along the Moine Thrust. Also while chlorite formed close to the sill, (A11), it could not form close to the syenite (B13, C76).

ch = chlorite, spt = serpentine, bc = brucite, cc = calcite dol = dolomite.

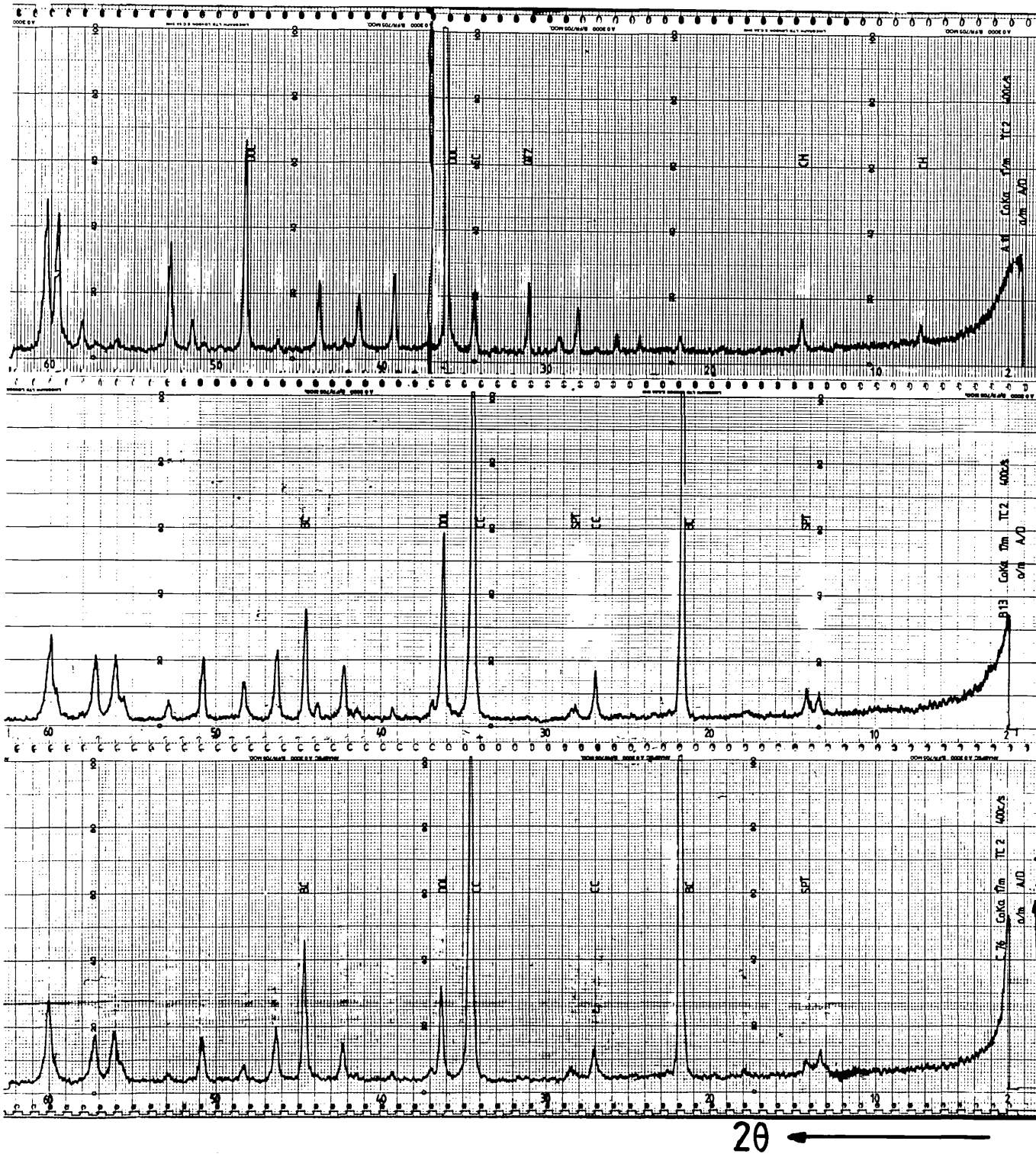
2θ

4.3 Addendum

Backscattered electron imaging of samples in thin sections made possible the differentiation of equilibrium from non-equilibrium calcite grains. While the former were uniformly disseminated, the latter were strung out mainly in veins, in the rock specimens. Also the $MgCO_3$ content of the non-equilibrium grains, particularly at Knockan, seemed to be lower than that of equilibrium grains.

supply of Mg^{2+} ions was going on hand in hand with the building of chlorite lattices from mica, and as a result no brucite was formed even at the Eriboll end of the thrust plane. This could suggest a tendency towards chemical equilibrium along the thrust plane, which is not obtainable near intrusive bodies.

4.3 RESULTS OF THE MICROCHEMICAL ANALYSIS OF CALCITE

To estimate the palaeo-temperatures associated with Moine thrusting using the calcite-dolomite solvus geothermometer only those carbonate samples showing appreciable amounts of calcite and dolomite were used. Since thermal effects associated with thrusting are most pronounced within one or two metres below the thrust plane, those carbonate samples showing the double phase assemblage were only obtainable close to the thrust plane.

4.3.1 EDS - Spectrum Analysis

The microchemical composition of calcite shows a fairly constant profile when the spectra of individual analyses from different samples are compared. Figures 4.5, 4.6 and 4.7 show typical spectra from Knockan (D31, Glencoul (ST 3) and Eriboll (Er-9) respectively. The dominant peak at 3.69 Kev is the CaKα peak, followed by a smaller Kβ peak at 4.01 Kev. These peaks cannot be compared in height, even when the livetimes are the same unless the original setting for the maximum spectrum height is made the same. The rest of the spectrum between 1-3.5 Kev is very important because changes in it, particularly changes in the magnesium peak at 1.25Kev are usable. Apart from calcium and magnesium, variable and often insignificant amounts of potassium, silicon, manganese and iron may be present. A comparison of Figures 4.5 and 4.7 shows a very

EDS Analysis, typical spectrum of calcite microchemistry in the Durness Formation from Knockan (sample D31). The small amount of Mg in the calcite is hardly shown on the spectrum.

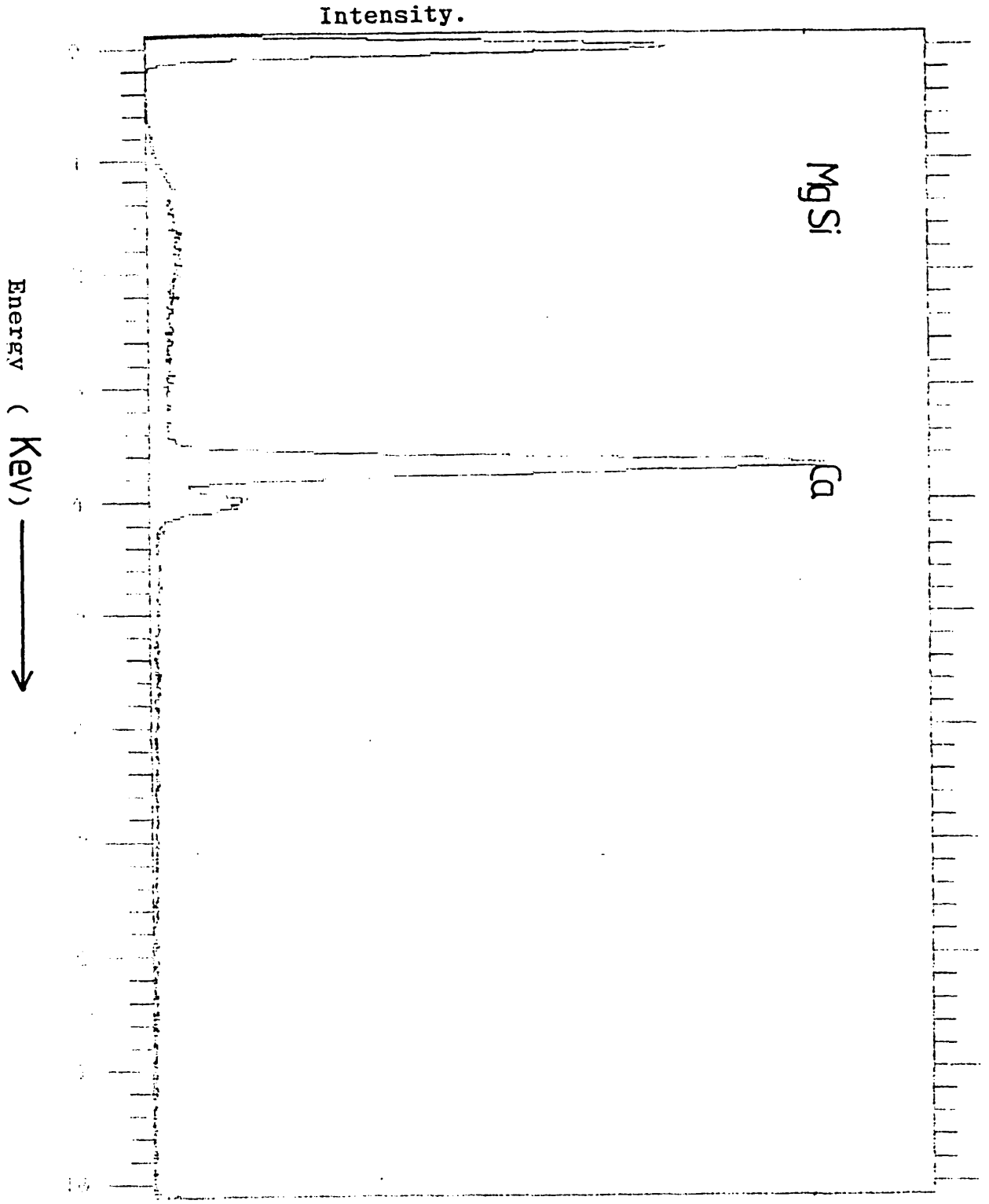

FIG. 4.6

EDS Analysis, spectrum of calcite microchemistry in the Durness Formation of Glencoul Area.

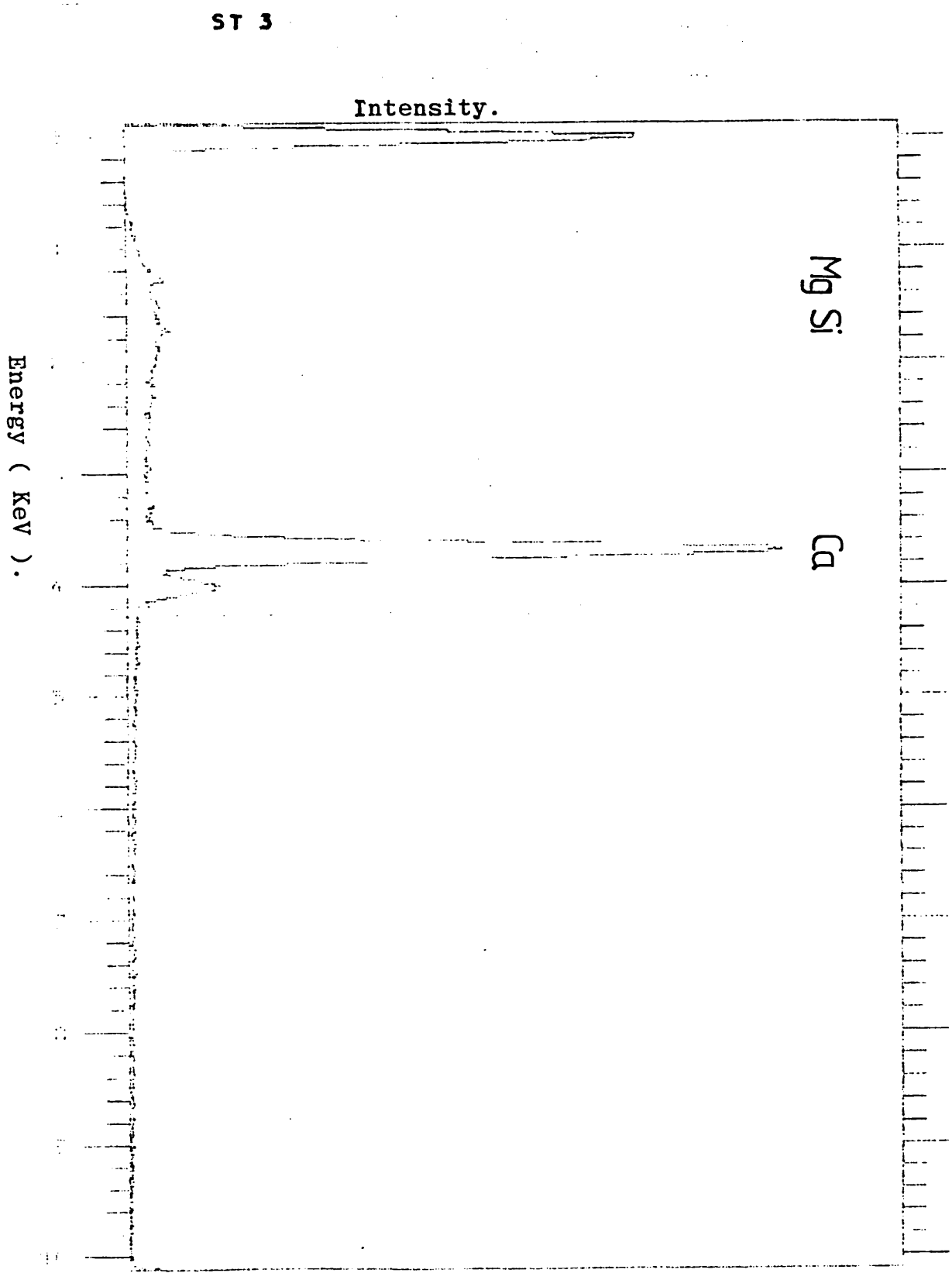

FIG. 4.7

EDS Analysis, spectrum of calcite microchemistry in the Durness Formation, Eriboll area. Calcite here seems relatively richer in Mg than the samples from the south.

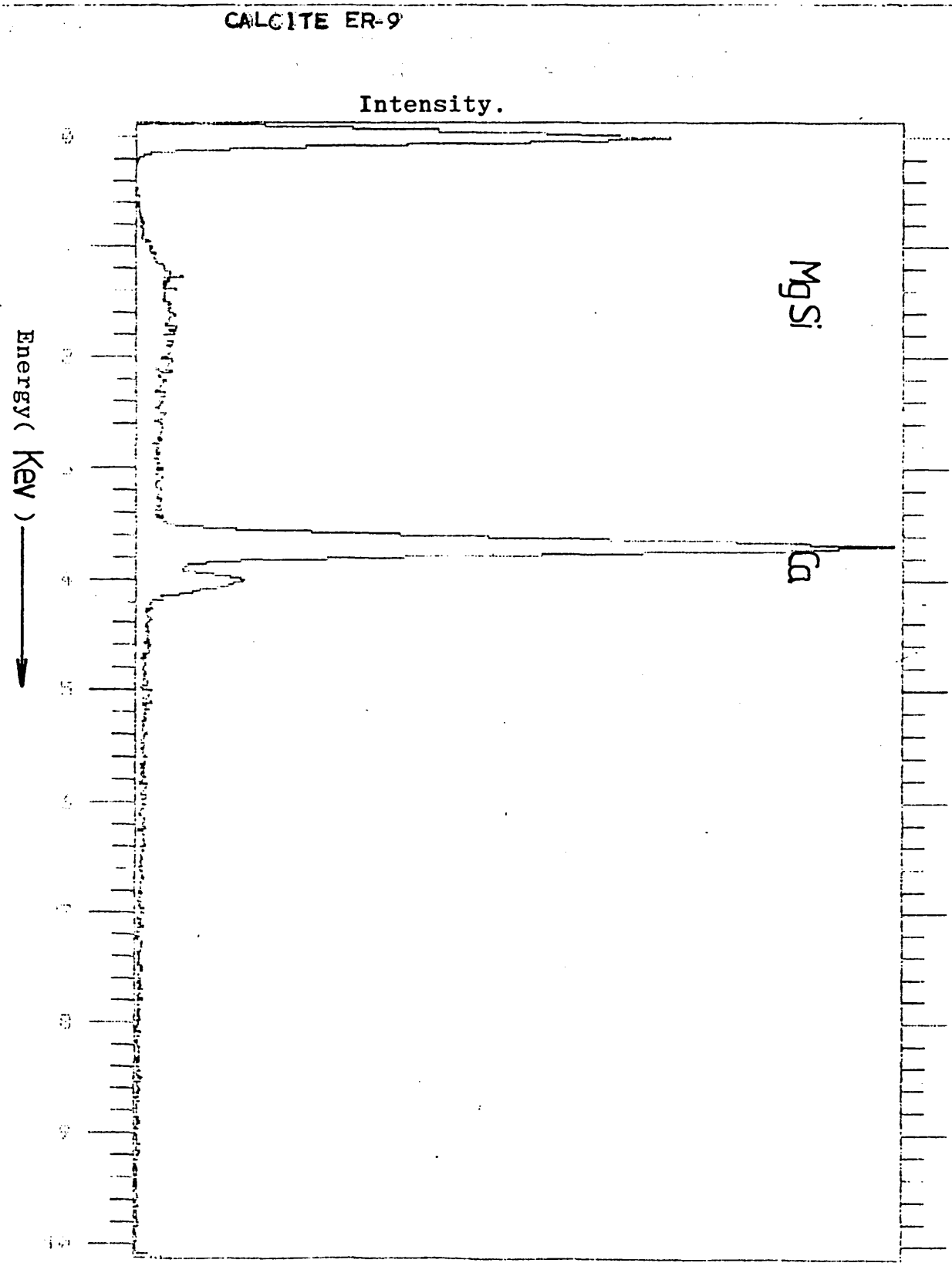

slight but noticeable difference in the MgKα (1.25 Kev) peak intensity. It is slightly more intense in Figure 4.6 than in Figures 4.5 and 4.7.

4.3.2 Results of the Microprobe Analysis

Tables 4.1 to 4.5 show the quantitative results of the electron probe microanalysis. Ten elements were normally analysed for, the percentage of oxygen estimated in most cases by difference. Only in analyses 1 and 2 of Table 4.1 was the percentage of oxygen computed by stoichiometry. The tables were compiled from the best analyses (in terms of total oxide) from each sample, and usually more than twenty analyses were aimed at per sample. Ideal solid oxide percentage varies between 54.5 - 57% (Deer et al. 1962). As the tables show the elements which have the most consistent occurence of anything above 5% confidence apart from calcium are magnesium, silicon, manganese and iron. Occasionally the presence of strontium is confirmed above the 5% confidence limit (Tables 4.4 and 4.5). Because of their ionic radii, only Mn^{2+} (0.83Å) and Fe^{2+} (0.80Å) can readily occupy the lattice positions of Mg^{2+} (0.78Å), while Sr^{2+} (1.175Å) may, with difficulty, substitute for Ca^{2+} or occupy sites in alternate planes to the Ca^{2+} planes such as are occupied by Mg^{2+}, and is therefore most likely to occupy cavities and voids not related to the regular lattice structure of calcite. It will require a Mg/Ca ratio of 1:1 for the Mg^{2+} ions to completely occupy all lattice positions in the plane alternate to the Ca^{2+} plane (see Fig.2.1), for every Ca^{2+} ion present in the lattice.

Table 4.1 Five typical chemical analyses of calcite from sample D31 from the Moine Trust as at Knockan.

Element	1		2		3		4		5	
	%ELMT	%OXIDE	%ELMT	%OXIDE	%ELMT	%OXIDE	%ELMT	%OXIDE	%ELMT	%OXIDE
Na	0.032	0.043	0.056	0.076	0.098	0.132	0.043	0.057	0.168	0.223
Mg	0.705	1.168	0.438	0.726	0.467	0.775	0.360	0.598	0.515	0.856
AL	0.026	0.050	-	-	0.059	0.111	-	-	0.110	0.208
Si	0.078	0.167	0.110	0.235	0.120	0.256	0.105	0.225	0.204	0.436
K	0.022	0.026	-	-	-	-	0.125	0.151	0.053	0.064
Ca	38.371	53.689	38.827	54.327	39.405	55.136	38.418	53.754	37.513	52.489
Ti	0.130	0.218	0.020	0.034	-	-	-	-	-	-
Cr	-	-	-	-	0.030	0.044	0.111	0.162	-	-
Mn	0.108	0.139	0.088	0.114	0.050	0.065	0.223	0.288	0.384	0.496
Fe	0.095	0.122	0.089	0.115	0.039	0.050	0.293	0.377	0.206	0.266
Total		55.622		55.629		56.569		55.612		55.088

Table 4.2 Five typical chemical analyses of calcite in sample C39 (Cnoc A' Chaoruinn). Sample C39 was taken from the Durness Formation below the Moine thrust.

Element	1		2		3		4		5	
	%ELMT	%OXIDE	%ELMT	%OXIDE	%ELMT	%OXIDE	%ELMT	%OXIDE	%ELMT	%OXIDE
Na	0.00	0.00	0.073	0.099	0.002	0.003	0.108	0.146	0.013	0.018
Mg	0.363	0.601	0.598	0.991	0.397	0.659	0.585	0.970	0.421	0.699
AL	0.041	0.077	-	-	0.069	0.131	0.058	0.105	0.015	0.027
Si	0.107	0.229	0.045	0.095	0.096	0.206	0.104	0.222	0.207	0.442
K	0.036	0.043	0.064	0.077	0.019	0.023	0.059	0.072	0.155	0.187
Ca	39.106	54.718	39.131	54.752	39.034	54.617	39.470	55.226	39.694	55.540
Ti	-	-	-	-	0.026	0.043	-	-	0.022	0.037
Cr	-	-	-	-	-	-	-	-	-	-
Mn	-	-	0.055	0.071	0.028	0.037	0.023	0.030	-	-
Fe	0.097	0.125	0.119	0.153	0.075	0.097	0.072	0.092	0.111	0.142
Total		55.792		56.237		55.815		56.863		57.093

Table 4.3 Five typical chemical analyses of calcite in Sample Er 9 (Eriboll)

Element	1		2		3		4		5	
	%ELMT	%OXIDE	%ELMT	%OXIDE	%ELMT	%OXIDE	%ELMT	%OXIDE	%ELMT	%OXIDE
Na	0.000	0.000	0.066	0.089	0.066	0.088	0.018	0.025	0.076	0.103
Mg	0.802	1.329	0.677	1.122	0.475	0.787	0.577	0.957	0.605	1.002
Al	0.065	0.123	0.045	0.084	0.008	0.014	-	-	0.047	0.089
Si	0.041	0.089	0.138	0.296	0.075	0.160	0.055	0.118	0.079	0.169
K	0.000	0.000	0.023	0.028	0.010	0.012	0.025	0.030	0.070	0.085
Ca	37.733	52.797	37.903	53.034	38.474	53.833	38.754	54.225	38.318	53.615
Ti	0.068	0.113	-	-	0.043	0.071	0.025	0.042	0.097	0.162
Cr	-	-	0.197	0.288	0.027	0.039	-	-	-	-
Mn	0.484	0.625	0.235	0.304	0.301	0.389	0.368	0.476	0.287	0.370
Fe	0.056	0.073	0.508	0.653	0.007	0.009	0.126	0.162	0.022	0.028
Total		55.148		55.898		55.402		56.288		55.864

Table 4.4 Five typical chemical analyses of calcite in sample Er-10 (Eriboll). Sample Er10 was taken from the Durness Formation below the Moine thrust.

Element	1		2		3		4		5	
	%ELMT	%OXIDE	%ELMT	%OXIDE	%ELMT	%OXIDE	%ELMT	%OXIDE	%ELMT	%OXIDE
Na	0.00	0.00	0.005	0.007	0.00	0.00	0.039	0.053	0.143	0.193
Mg	0.810	1.343	0.637	1.056	0.526	0.872	0.793	0.314	0.488	0.809
Al	0.031	0.059	0.00	0.00	0.013	0.024	0.060	0.113	0.048	0.091
Si	0.546	1.168	0.080	0.172	0.086	0.184	0.116	0.247	0.098	0.210
P	0.039	0.090	0.00	0.00	0.081	0.185	0.062	0.142	0.007	0.013
S	0.034	0.084	0.030	0.074	0.085	0.215	0.033	0.083	0.117	0.292
K	0.095	0.114	0.057	0.068	0.085	0.103	0.065	0.078	0.034	0.041
Ca	37.205	52.057	39.017	54.592	38.525	53.904	38.651	54.081	38.991	54.556
Sr	0.231	0.273	0.036	0.043	0.230	0.272	0.269	0.318	0.006	0.007
Ba	0.00	0.00	0.00	0.00	0.00	0.00	0.244	0.273	0.00	0.00
Mn	0.493	0.636	0.294	0.379	0.373	0.481	0.340	0.439	0.147	0.190
Fe	0.117	0.151	0.232	0.298	0.310	0.399	0.194	0.250	0.252	0.325
Co	0.00	0.00	0.00	0.00	0.00	0.00	0.00	0.00	0.00	0.00
Total		55.977		56.689		56.639		57.390		56.726

Table 4.5 Five typical chemical analyses of calcite in sample Er-11b (Eriboll), from the Durness Formation below the Moine thrust.

Element	1		2		3		4		5	
	%ELMT	%OXIDE	%ELMT	%OXIDE	%ELMT	%OXIDE	%ELMT	%OXIDE	%ELMT	%OXIDE
Na	0.161	0.217	0.187	0.252	0.024	0.032	0.049	0.066	0.00	0.00
Mg	0.585	0.971	0.645	1.070	0.704	1.167	0.747	1.238	0.794	1.316
Al	0.00	0.00	0.022	0.042	0.016	0.030	0.00	0.00	0.00	0.00
Si	0.057	0.122	0.042	0.090	0.120	0.256	0.069	0.148	0.058	0.125
P	0.00	0.00	0.029	0.066	0.00	0.00	0.00	0.00	0.00	0.00
S	0.022	0.054	0.062	0.155	0.00	0.00	0.035	0.087	0.004	0.010
K	0.010	0.012	0.105	0.126	0.033	0.039	0.082	0.099	0.042	0.051
Ca	38.803	54.294	38.241	53.506	39.253	54.922	39.494	55.260	39.504	55.274
Ti	0.006	0.010	0.105	0.176	0.055	0.091	0.00	0.00	0.082	0.137
Mn	0.867	1.119	0.834	1.077	0.580	0.749	0.369	0.477	0.280	0.361
Fe	0.382	0.492	0.327	0.421	0.149	0.191	0.272	0.350	0.240	0.308
Co	0.026	0.033	0.00	0.00	0.014	0.018	0.00	0.00	0.091	0.116
Sr	0.104	0.124	0.318	0.375	0.125	0.147	0.163	0.193	0.169	0.200
Ba	0.00	0.00	0.00	0.00	0.00	0.00	0.00	0.00	0.00	0.00
Total		57.448		57.356		57.643		57.917		57.897

As Tables 4.1 to 4.5 show, this ratio is very much below unity, hence there is no competition between Mg, Mn and Fe, to fill the alternate to the Ca^{2+} planes. This in effect means that any physical parameter estimated using the amount of Mg^{2+} or $MgCO_3$ as in this case, need not be corrected for the effects of other substituting elements. In addition, although all iron is analysed as Fe^{2+} due to the ZAF4 computer subroutine used, some of it would no doubt be in the Fe^{3+} state. The facilities used could not separate one valency from the other.

4.3.3 Estimate of the Percentage Molar $MgCO_3$ in Calcite and the Equilibrium Temperature

The method used for calculating the molar percentage $MgCO_3$ in calcite is described in Appendix 1, and is that normally used in analytical chemistry. Table 4.6 shows the moles percent $MgCO_3$ in calcite and temperature estimated from these using the equation of Sheppard and Schwarcz (1970). The equation relates the moles percent $MgCO_3$ in calcite to the equilibrium temperature T as follows:

$$\text{Log}_{10} \text{ Mole \% } MgCO_3 \text{ in calcite} = 1.727 \times 10^{-3} T - 0.223 \quad \ldots\ldots (4.1)$$

T is in °c.

This was suggested by Sheppard and Schwarcz (1970) as a best fit equation to the calcite-dolomite solvus curve of Goldsmith and Newton (1969) (Fig.2.16), and has been applied by Hutcheon and Moore (1973), and Moore and Kerrick (1976). The moles percent $MgCO_3$ and the corresponding temperatures estimated are also presented in histograms (Figures 4.8, 4.9, 4.10, 4.11 and 4.12 for samples D31, C39, Er9, Er10 and Er11b respectively).

Table 4.6 Temperatures (°C) estimated from Moles%$MgCO_3$ in Calcite (Ca $C0_3$) for the five samples: D31-Knockan; C39-Cnoc A Chaoruinn; Er 9, Er 10 and Er 11 - Eriboll. All samples from the Durness Formation below the Moine thrust.

M = Mean; SD = Standard Deviation.

Sample D31		Sample C39	
Moles% $MgC0_3$ in Calcite	Temperature (°C)	Moles% $MgC0_3$ in Calcite	Temperature (°C)
2.66	375.15	1.493	229.91
1.80	276.94	2.45	354.47
2.90	396.8	1.63	251.99
1.5	231.09	2.097	315.34
2.1	315.70	2.27	335.28
1.5	231.09	2.92	398.60
2.1	315.70	2.41	350.33
1.9	290.54	1.73	266.96
1.9	290.54	1.93	294.47
2.1	315.70	2.30	338.58
1.5	231.09		
2.2	327.40		
1.5	231.09		
M/SD			
1.97/ 0.44	294.53/ 54.64	2.123/ 0.43	313.59/ 52.37

Table 4.6(contd)

Er 9		Er 10		Er 11b	
Moles% $MgCO_3$ in Calcite	Temperature (°C)	Moles% $MgCO_3$ in Calcite	Temperature (°C)	Moles% $MgCO_3$ in Calcite	Temperature (°C)
1.69	261.08	3.04	408.73	2.99	404.56
2.99	404.56	2.90	376.8	2.76	384.43
1.68	259.59	3.17	419.26	2.87	394.26
2.59	368.44	3.33	431.64	2.94	400.32
1.74	268.41	2.57	366.49	1.94	295.77
2.95	401.0	2.62	371.34	3.26	426.30
2.53	362.55	2.16	322.79	2.89	396.00
2.37	346.12	2.69	377.97	3.07	411.20
2.49	358.54	3.26	426.30	2.65	374.20
2.0	303.43	2.90	396.8	2.41	350.33
2.4	349.28	2.01	304.69		
2.5	359.55	3.69	457.46		
2.8	388.05	2.32	340.76		
2.7	378.90	3.03	407.90		
3.3	429.37	2.87	394.26		
		3.09	412.83		
M/SD					
2.45/ 0.490	349.26/ 53.275	2.85/ 0.44	389.75/ 40.85	2.78/ 0.38	383.74/ 37.24

FIG. 4.8

Histograms of (a) moles % $MgCo_3$ in calcite against frequency, and (b) temperature against frequency, for sample D31 from Knockan.

Mm = mean of moles $\pm$ standard deviation

Tm = mean of temperatures $\pm$ standard deviation.

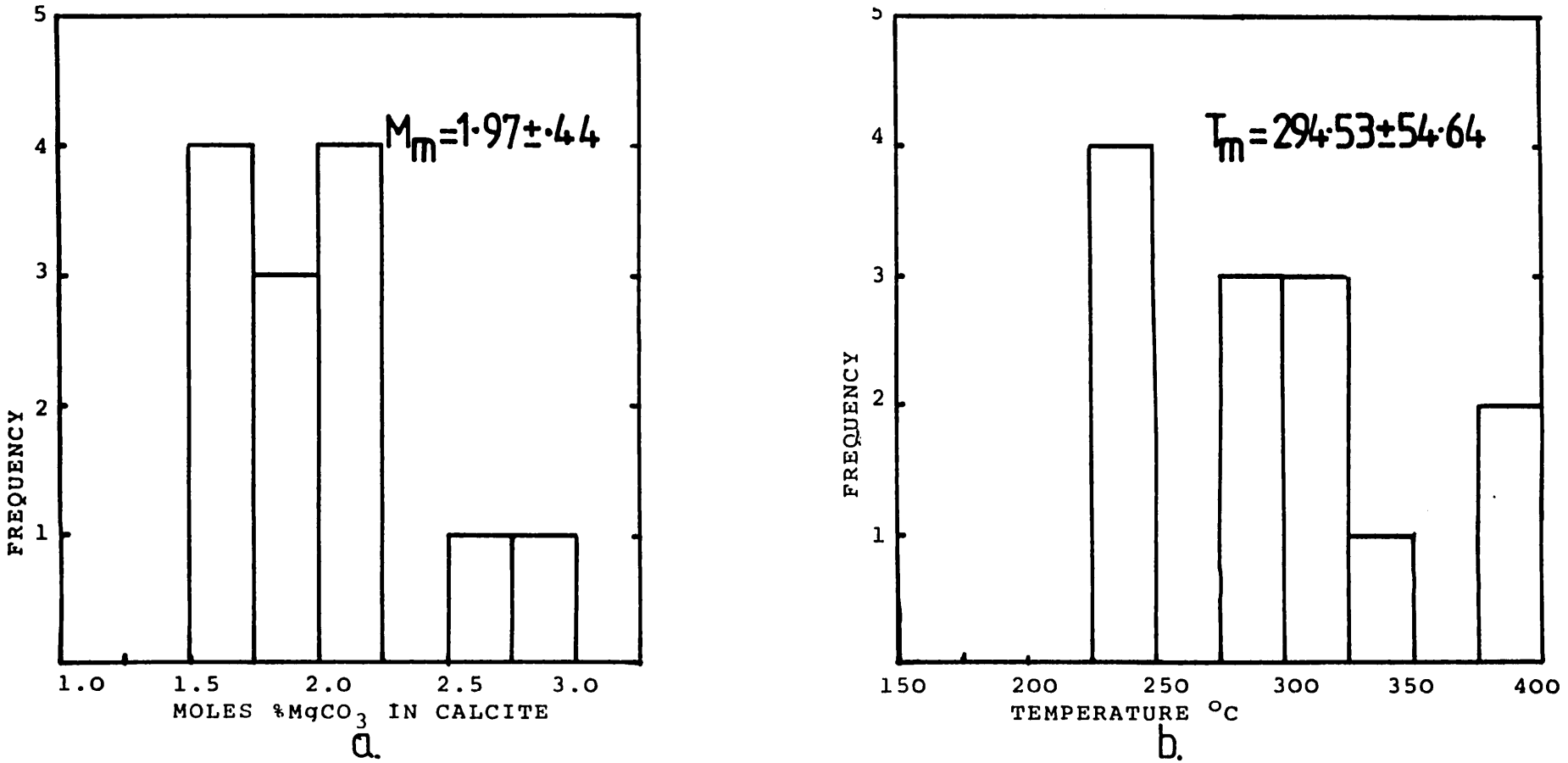

FIG. 4.9

Histograms of (a) moles % $MgCO_3$ in calcite against frequency and (b) temperature against frequency for sample C39.

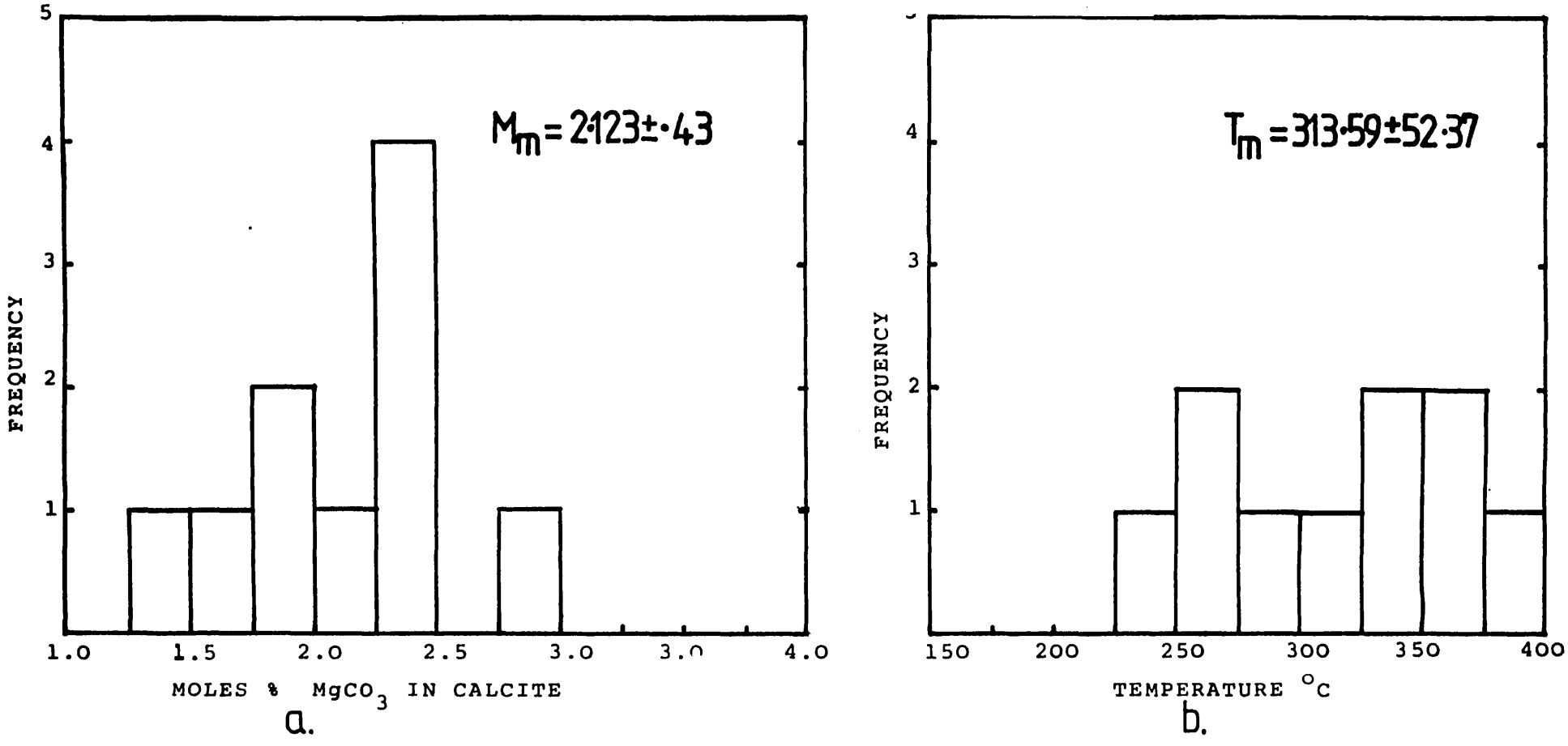

Mm = mean of moles $\pm$ standard deviation

Tm = mean of temperatures $\pm$ standard deviation.

FIG. 4.10

Histograms of (a) moles % $MgCO_3$ in calcite against frequency, and (b) temperature against frequency, for sample Er9 from Eriboll.

Mm = mean of moles $\pm$ standard deviation

Tm = mean of temperatures $\pm$ standard deviation.

Er 9

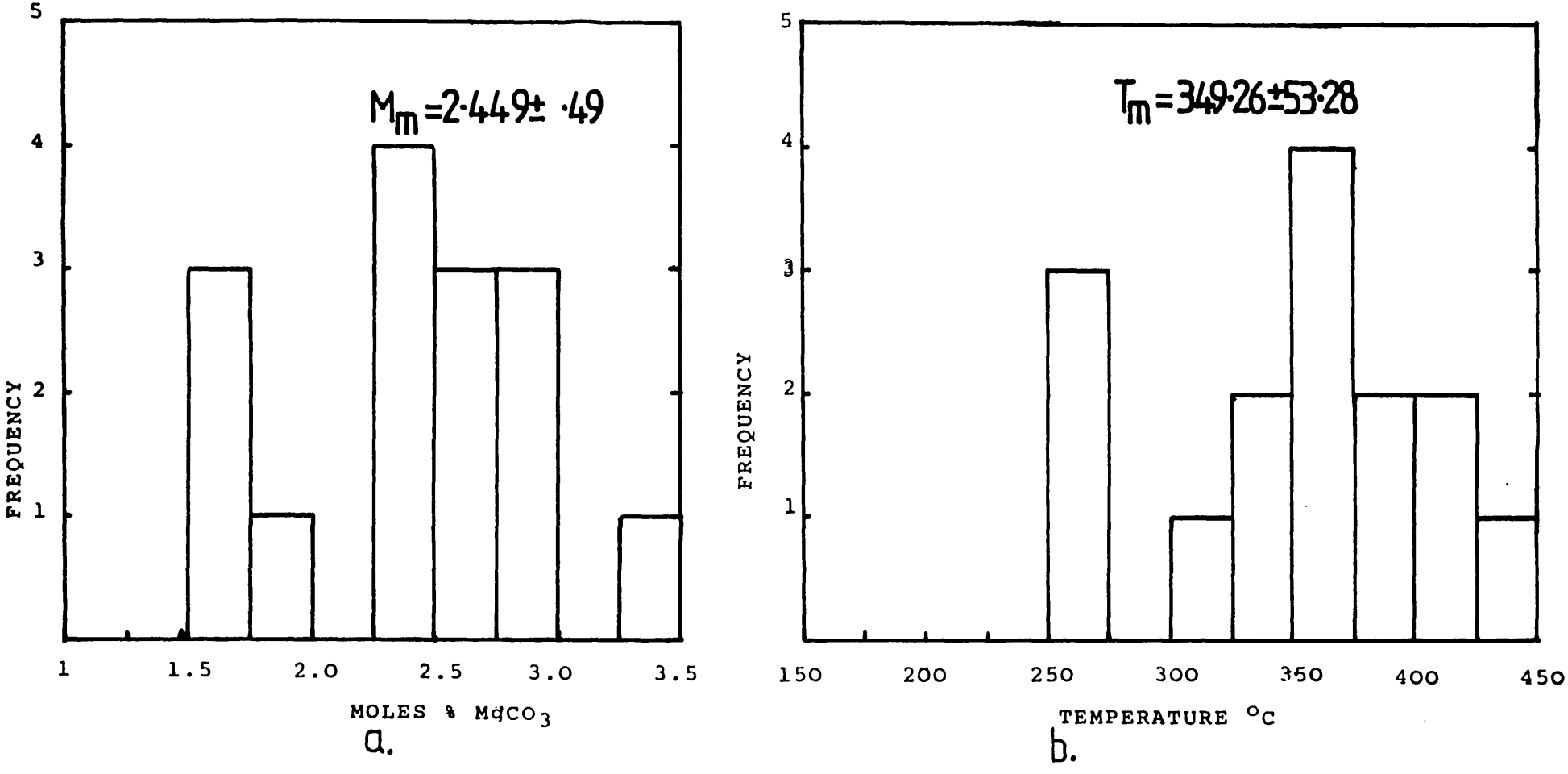

Fig. 4.11

Histograms of (a) moles % $MgCO_3$ in calcite against frequency, and (b) temperature against frequency, for sample Er 10 from Eriboll.

Mm = mean of moles $\pm$ standard deviation.

Tm = mean of temperatures $\pm$ standard deviation.

Er 10

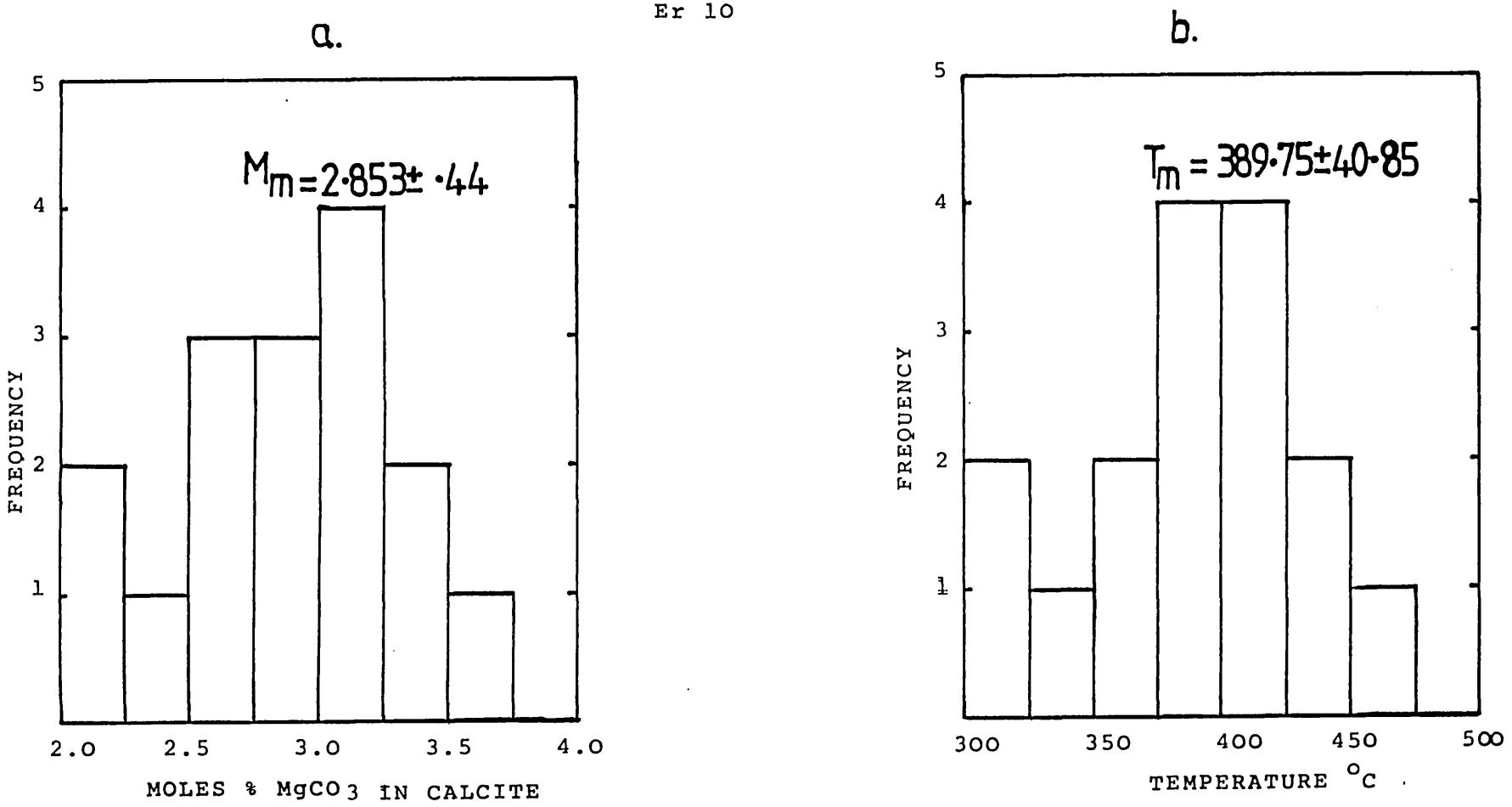

FIG. 4.12

Histograms of (a) moles % $MgCO_3$ in calcite against frequency, and (b) temperature against frequency, for sample Erllb from Eriboll.

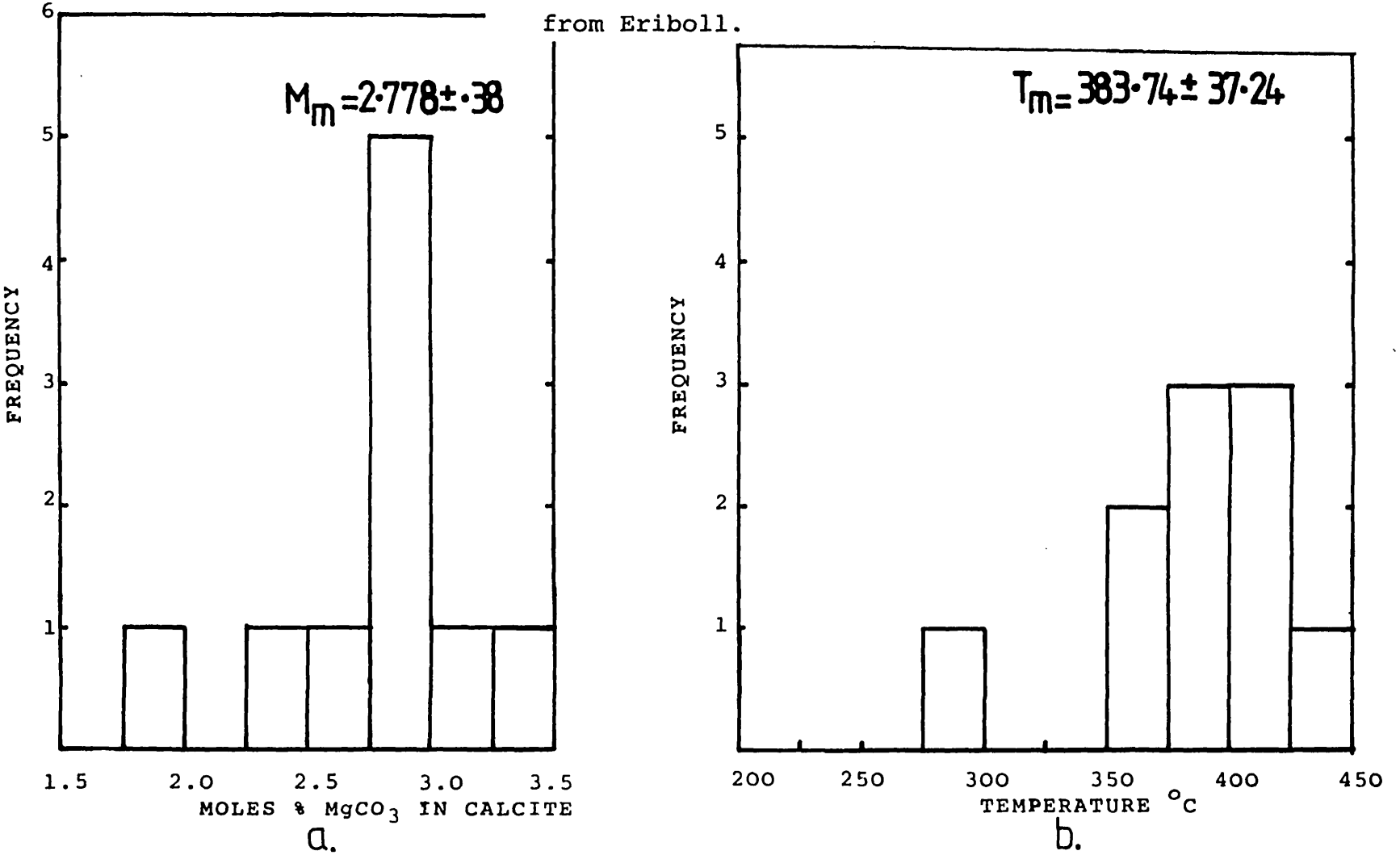

Mm = mean of moles ± standard deviation

Tm = mean of temperatures ± standard deviation.

4.3.4 Discussion of Results:

The analysis of temperatures associated with Moine thrusting has produced interesting results both from the points of view of metamorphism and tectonics. A comparison of Figures 4.8 and 4.9 shows that a positive temperature gradient exists below the Moine Thrust from Knockan in the west to Cnoc A' Chaoruinn in the east. The exact distance between sample location D31 (Fig.3.8), and C39 (Fig.3.7) is 10.49 km, giving a horizontal gradient of:

$$\frac{313.59 - 294.53°C}{10.94\ km} = \frac{19.06}{10.94} = \underline{1.74°C/km}$$

A comparison of D31 (Fig.4.8), and Er9, Er10 and Er11b shows a temperature difference of between 54°C and 95°C exists between Knockan in the south and Eriboll in the north of the Moine Thrust Zone. This is shown in Figure 4.13 if the mean temperature at the Eriboll end of the subMoines is taken as 374.00°C (mean of Er9, Er10, Er11b), the temperature difference between Knockan and Eriboll would then be 80°C approximately.

Temperature differences of approximately 20°C between Knockan and Cnoc A' Chaoruinn subMoines, and 80°C between Knockan and Eriboll subMoines are substantial enough to leave visible imprints of microstructural and metamorphic significance on the Durness carbonates. This evidence is reviewed in the following sections.

The presence of errors on the temperature estimates (e.g. ±55°C for D31, and ±52°C for C39) reduces the reliability and increases the complexity of the valuesof temperature differences and gradients. For example between D31 and C39, the round figure difference of 19°

is only halfway between 16° at the upper end of the error bars and 22° at the lower end. It emphasized therefore that exact values of temperature differences and gradients are not, in this section, as important as the indications of differences and gradients.

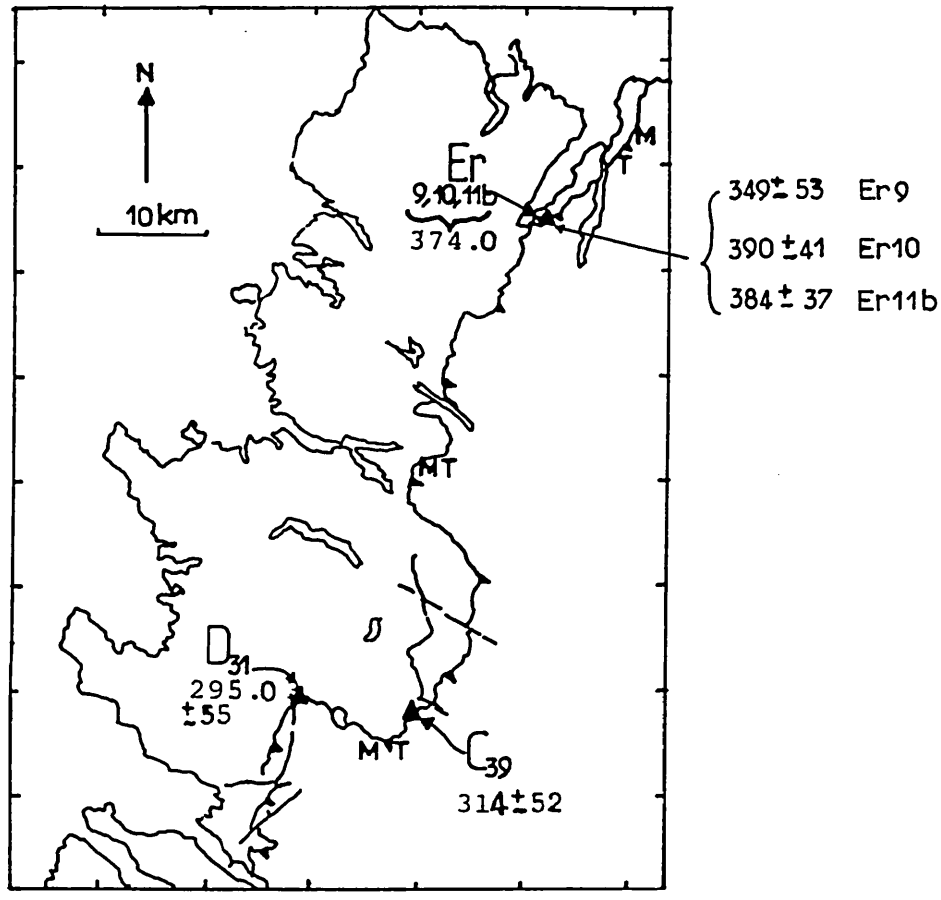

FIG. 4.13

The Moine Thrust zone showing the locations of samples used in temperature estimates.

C = Cnoc a' Chaoruinn

D = Knockan

Er = Eriboll

MT = Moine Thrust.

Values at localities, like 295.0 represent the temperature (°c) estimated for that locality.

4.4 EVIDENCE OF TEMPERATURE DIFFERENCE BETWEEN:

(i) the Caledonian Foreland and the Moine thrust zone;

(ii) the Moine thrust zone in the south and the MTZ in the north.

4.4.1 Between the Caledonian Foreland and the Moine thrust

The only palaeotemperature estimates in the foreland that may be reliable were made by Downie (1981). Using acritarch index fossils from the Fucoid Beds and a scale of colour index proposed by Staplin (1977), Downie estimated thermal indices and palaeotemperatures as follows:

		Thermal Index	PalaeoTemperature
An t-Sron-Eriboll	[NC446580]	±4.5	250°C
Skiag Bridge	[NC236241]	±3.7	200°C
Knockan Cliff	[NC189091]	±3.7	200°C
Ord Skye	[NC617134]	±3.2	150°C

With this data he had shown that even in the Caledonian foreland, there is a temperature difference of up to 50°C between Knockan and Eriboll, and that generally there is a temperature increase towards the north from Skye. Grant (pers.comm.) estimated a temperature less than 200°C using palinomorphs from the Torridonian at the foreland.

In Figure 4.1 the X-Ray diffractograms from the foreland and low strain areas are summarized. They are characterized by a medium to strong 0002 mica peak, a $10\bar{1}4$ dolomite peak of variable intensity, and some quartz and authigenic feldspar peaks. Characteristically absent from these diffractograms are chlorite peaks, showing that

PLATE 4.1

Backscattered electron micrographs of solution surfaces and their mineral content into the zone of metamorphism.

(a) Diagenetic stylolite (s--s) in dolomite in the Foreland carbonates. The stylolite is filled with iron and some titanium oxides, and mica (illite/Sericite). Stylolites in Foreland carbonates lack chlorite and the carbonates lack calcite. d - dolomite
Scale bar: 100μm

(b) Below the thrust at Knockan, chlorites (ch) have started to crystallize. The sites of easiest nucleation of chlorites are along diagenetic stylolites, consequently they are associated with the mica (m).
Scale bar: 10μm.

(c) Below the Moines at Cnoc a' Chaoruinn chlorite (ch) and K-feldspars (fsp) are well crystallized and thick, while mica is reduced to thin fibres in Durness carbonates. Some of the dolomite (d) also decomposed to calcite (cc).
Scale bar: 100μm.

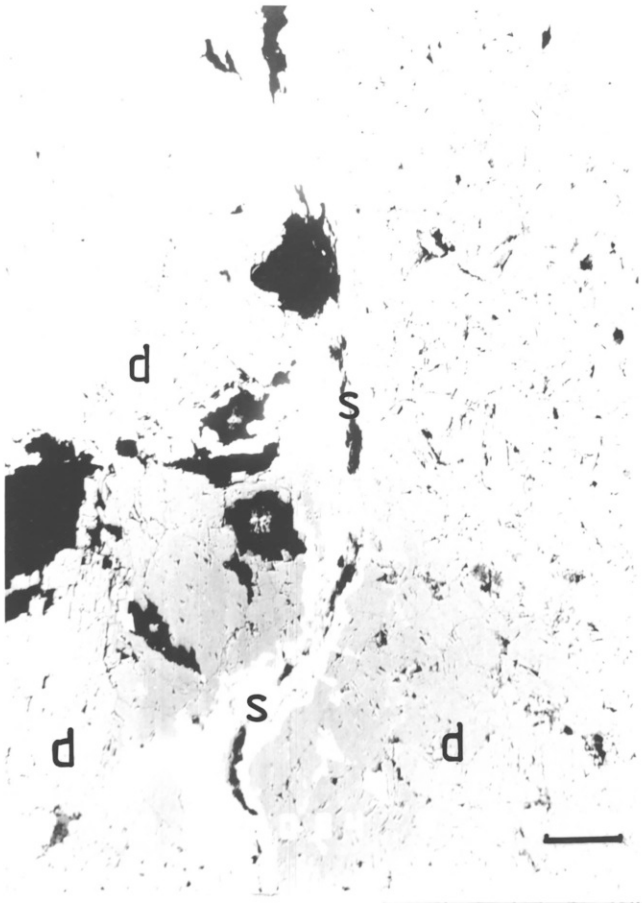

a

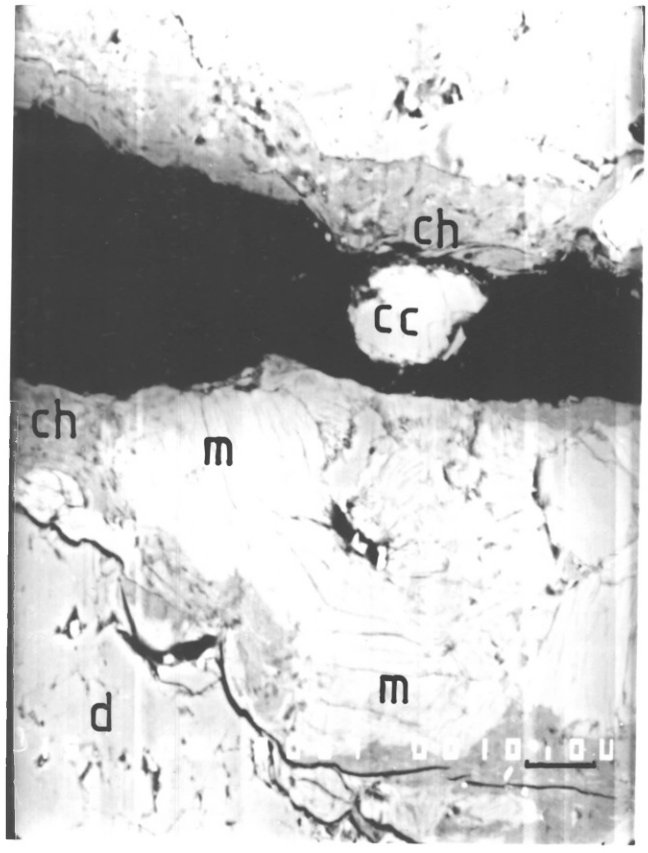

b

Plate 4.1

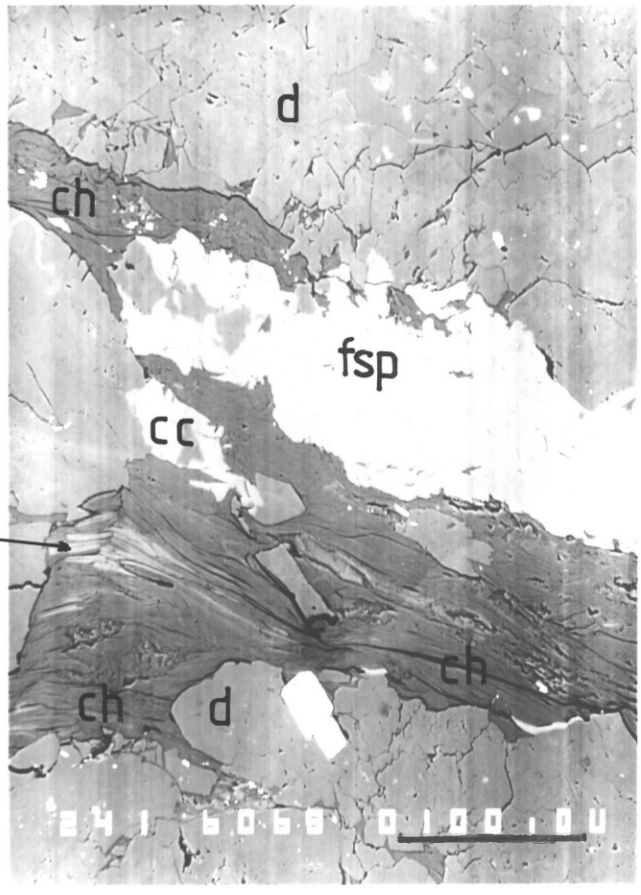

c

the thermally induced alteration of mica to chlorite found along the thrust plane does not obtain in the foreland.

Most of the mica found in the foreland samples is concentrated along diagenetic stylolites (see Plate 4.1a), as fine grained white mica with low basal (002) spacing, high Si:AL ratios and low K_2O values. The name illite/sericite has therefore been suggested for these foreland micas (Dunoyer de Segonzac, 1970).

An estimate of the Index of Crystallinity of the foreland illite/sericite micas gives values between 3.0 and 4 (Table 4.7). This is shown by Dunoyer de Segonzac (1970) to place this illite/sericite exactly within the metamorphic anchizone. This is the zone of transition between late diagenesis (main Index 5.5) and the "Chloritoschistose" epizone of maximum Index 2.5.

Table 4.7

Crystallinity Index (peak width at half maximum height of 10Å mica peak-in mm Weaver, 1960) measured from X-ray diffractograms of whole rock samples. Some of the diffractograms are shown in Figures 4.1 - 4.4

Foreland and Low Strain Areas	
Sample Number	Crystallinity Index (mm)
A14	3.5
A18A	3.0
(D)F.S.	4.0
A40	3.0
D54	3.5
Below the Moine Thrust	
Sample Number	Crystallinity Index
D1	3.25) Knockan
D24	2.0)
C39	3.0) Cnoc A'Chaoruinn
C88	2.0)

As mentioned above, nowhere in the foreland has the alteration from illite to chlorite been observed, except near intrusive bodies (Fig.4.4). Knipe (pers. comm.) showed by extensive work on slates that the temperature for that alteration might be up to 250°C. From the foregoing evidence it might be concluded that generally, maximum palaeo-temperatures in the Caledonian foreland especially the Cambro-Ordovician sequence, might not have exceeded 200 to 250°C.

Along and about 2m below the Moine thrust plane at Knockan, metamorphic conditions have changed a little from the foreland. As shown in sections 4.2 and 4.3, dolomite starts altering thermally into calcite, and the illite-chlorite alteration starts also (Plate 4.1b). Initially the proportion of chlorite to illite is very low, but towards the east this proportion increases to the extent that illite only forms thin fibres within thick bands of chlorite (Plate 4.1c).

Also the Index of Crystallinity of the mica below the thrust (Table 4.7) varies between 2.0 and 3.25. This is much lower than for the foreland samples and reflects the general crystalline nature of the mica.

From the foregoing, it does seem that the minimum temperature requirement of about 250°C for illite to chlorite alteration has been achieved along the Moine thrust plane, and therefore that the 295±55°C estimate from calcite-dolomite solvus at Knockan is reasonable. This temperature estimate plus the crystallinity index and mineral assemblage suggest that at the Knockan end of the Moine Thrust down to about 2m, the Durness Formation is in the upper epizone of metamorphism.

4.4.2 Data Between Knockan and Eriboll Adjacent to the Moine Thrust

(i) Structural Evidence:

That the microstructure below and above the Moine Thrust at Knockan is characterised by cataclasis has been known for a long time. The wedge of whitish dolomite just

below the Moine schists here decreases in thickness southwards and is permeated down to grain size level by large through-going fractures and micro-veins (Plates 4.2a, 4.2b). The network of fractures of very wide size range produces angular to subangular carbonate grains. Those fractures confined to individual grains tend to be smaller than the longer ones. Almost all fractures are healed, with a greyish, sometimes brownish carbonate cement. Fracture intensity increases and fractured grain size decreases towards the fault plane, while matrix cement concentration is higher near the fault plane, decreasing downwards towards a grain-supported breccia away from the fault plane.

The original diagenetic solution surfaces here have beeen transected and displaced by several later generations of fractures, while later generations of vein calcite grains show less weathering than the earlier ones. This microstructure is mostly found within two meters below the thrust plane and gives way about six meters from the thrust plane to a fairly intact dark-coloured foreland-type dolomite.

Below the thrust plane eastwards recrystallization takes place very rapidly wiping out the fractures and producing a mosaic of interlocking grains (Plate 4.2c).

Cataclasis may be an important mechanism in a shear zone because that is the only mechanism that can effectively move fluids about within the rock otherwise rock permeability is often too low to allow fluid movement in reasonable time (Price 1975; Norris and Henley, 1976). It is aided by high effective stresses, high strain rates, low

PLATE 4.2

a,b, and c optical photomicrographs of Durness carbonates below the Moine Thrust at Knockan. a and b, note the fracture intensity just below the thrust plane here. Fracturing is down to grain size level (a) 1m below the thrust plane. The cement is mostly carbonate, which as in (c) might re-crystallize to form fine grains. (b) is also within 1m of the thrust.

Scale bars: 1cm ,crossed polars.

c. About 1km east of Knockan Crag below the Moine thrust plane intense fracturinghas been replaced by re-crystallization producing a mosaic of interlocking grains. Only very few of the original fractures are still prominent. (c) is within 1metre of the thrust.

Scale bar: 1cm ,crossed polars.

Plate 4.2

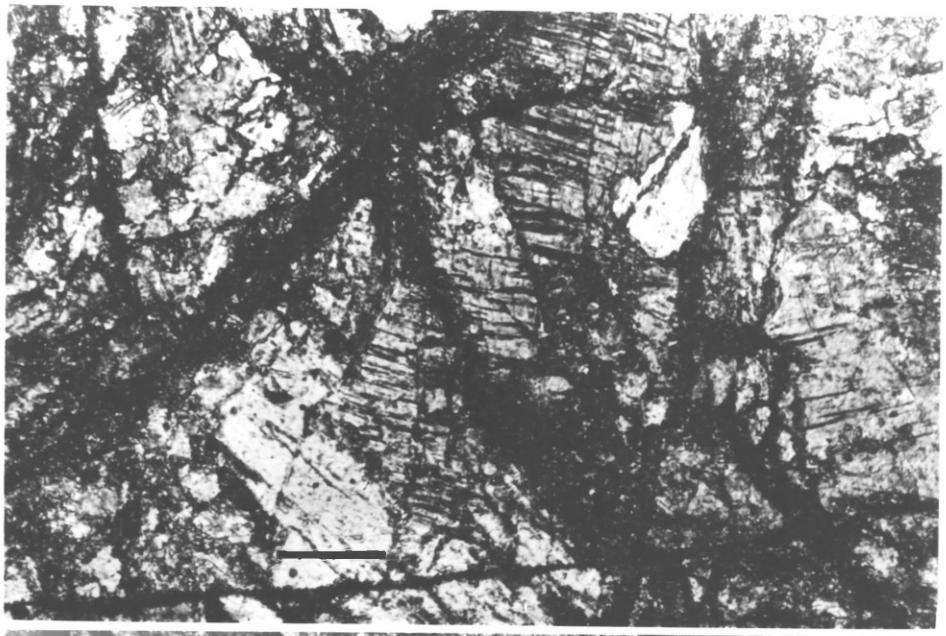

a

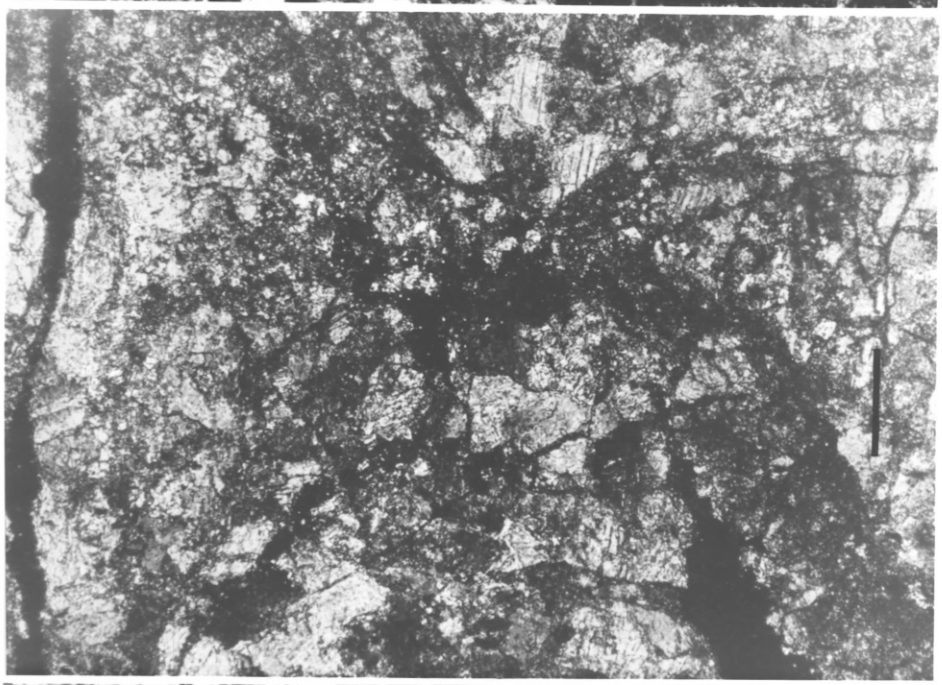

b

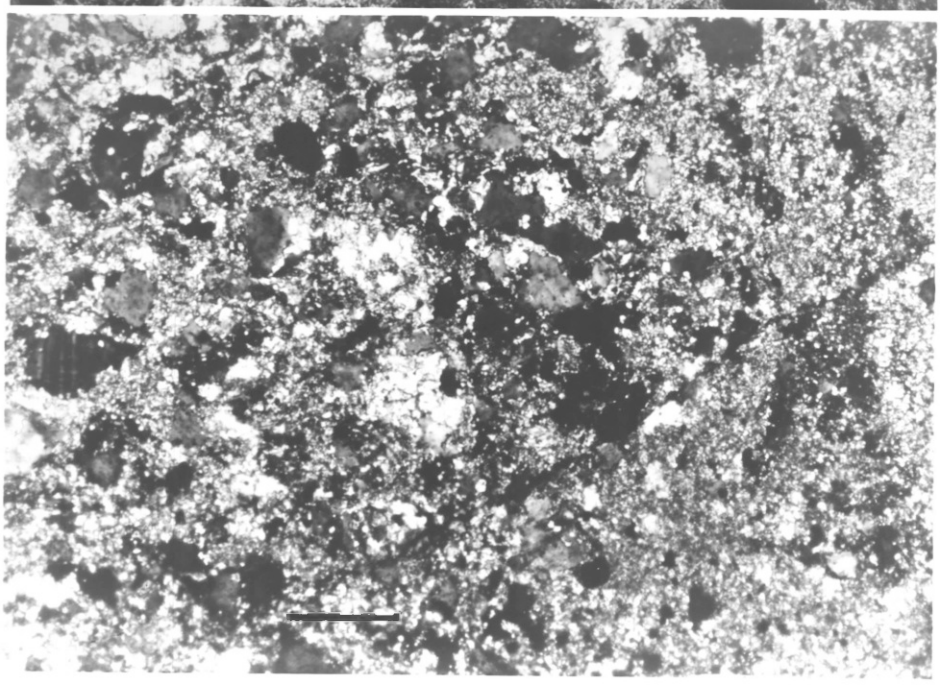

c

PLATE 4.3

Optical micrographs of mylonitized Durness carbonates at Eriboll. Below the Moine Thrust at Eriboll a fine mylonitic foliation has developed in the Durness carbonates. The dolomite and calcite grains are stretched out into ribbons of high strain (b), with chlorite and talc as the main phyllosilicates interleaving them. Later grains of mainly dolomite growing normal to foliation (d in a and c).

a,b,c, Photomicrographs in crossed nicols.

Scale bar: o.5 m. Calcite is stained dark by alizarine S.

Plate4.3

a

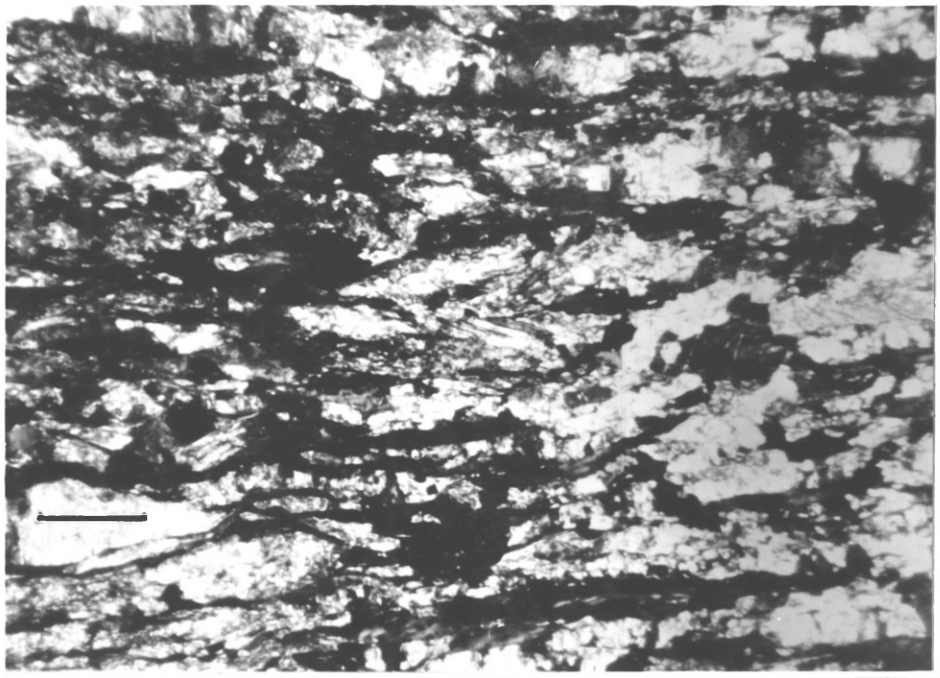

b

c

temperatures and is restricted to the upper 15km in most zones of continental deformation (Sibson, 1977; Turcote, 1983). In dolomite,cataclasis and kinking tend to precede or accompany c-slip at low laboratory temperatures - i.e. between 20° - 225°C (Barber et al. 1981), and according to the latter cataclasis and shear-fracturing must be counted as a significant deformation mechanism.

In contrast to the Knockan sub-area, the Durness Formation below the Moines at Eriboll is characterised by a fine foliation, defined by bands of dolomite, chlorite and calcite (Plates 4.3a, b, and c). The carbonate grains are commonly ribboned into fine grains of high aspect ratios typical of mylonites. This is also the area where dolomite shows extensive polysynthetic twinning, often with more than one set of twins (Plates 4.4a, b, and c), and affecting all generations of grains. There are limited indications of recrystallization mainly through subgrain rotation at grain boundaries (Plates 4.4a, and b). These recrystallized grains in most cases have the twinned microstructure.

Both single crystal and polycrystal deformation behaviour of dolomite suggest that twinning in dolomite is a fairly diagnostic medium-temperature deformation. Twins have not been observed in crystals deformed below 300°C, while at 350°C twinning of favourably oriented grains only becomes important (Barber et al., 1981). Between 400°C and 500°C dolomite twinning is ubiquitous, becoming less important but not completely wiped out above 500°C (Higgs and Handin,1959; Barber et al., 1981).

PLATE 4.4

Photomicrographs of carbonate rocks below the Moine thrust at Eriboll. All sizes and generations of dolomite grains are twinned and there is often more than one set of polysynthetic twins. In a and b some of the twinned grains have produced recrystallised grains (r) at the grain boundaries. Calcite is stained (dark) by alizarine S. 4.4a and 4.4c Scale bar: 0.5mm, 4.4b Scale bar: 0.2 mm. Crossed polars.

Plate 4.4

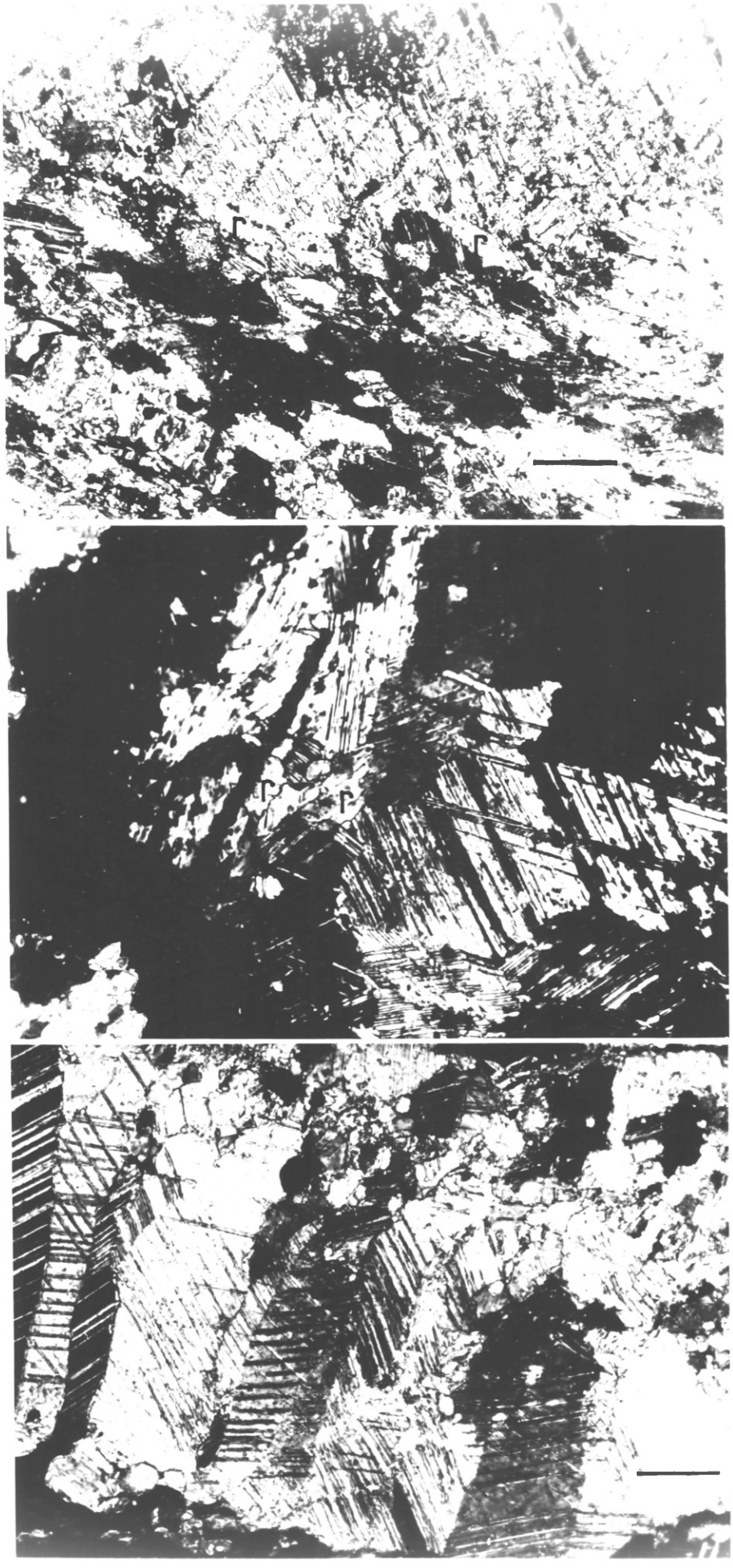

4.4.2 (i) Addendum

Although the effect of strain rate variation on the temperature of dolomite twinning has not been specifically investigated, the works of Higgs and Handin (1959) and Barber et al. (1981) at 1.6×10^{-4} and 1.3×10^{-5} respectively, gave the first indications that the temperature for the initiation of dolomite twinning may not be strain rate-controlled.

The mylonitic foliation and prevalent dolomite twinning at the Eriboll sub-area would suggest that the mean temperatures estimated for Er9 (349.00°C), Er10 (389.00°C) and Er11b (384.00°C), (Table 4.6) are of the right order.

(ii) Mineralogical and Microchemical Evidence:

A comparison of the X-Ray diffractograms from the Knockan end (Fig.4.2) and Eriboll end (Fig.4.3) of the subMoine Durness carbonates shows fairly interesting differences. While the former shows mainly strong illite and dolomite peaks, with weak chlorite and calcite and no talc, the latter shows strong chlorite and calcite with no illite and relatively weak dolomite peaks. Quartz peak intensities are known to go with chlorite intensity. Also new in Figure 4.3 is the talc peak at $2\theta = 11°$, this is best illustrated in Er11 of Figure 4.3.

As shown in Figure 2.19, even at low fluid pressures (~100 MPa) dolomite rocks will not produce talc below about 350°C. Hence while physical/chemical conditions are right for the generation of chlorite at Knockan (including 250°C and above temperatures), those same conditions allow the co-existence of illite and chlorite, being at the same time too low for the stability of talc. At Eriboll on the other hand, the physical/chemical conditions are rather too severe for the stability of illite, although right for chlorite and optimum for talc nucleation.

Other evidence of a microchemical nature is presented in Chapter Five, on the microchemistry of the chlorites generated in the carbonate rocks due to metamorphism. It is

p165 – K p comm

p212. not σ_3 but $\sigma_1 - \sigma_3$.

shown that Fe/Mg ratios in clinochlore increase from Knockan to Eriboll, i.e. with temperature. This is in agreement with Iwasaki's (1963) and Dunoyer de Segonzac's (1969, 1970) observations that Fe/Mg ratios increase with increasing metamorphism of chlorite in chlorite-bearing rocks.

4.5 POSSIBLE SOURCES OF THERMAL ENERGY FOR METAMORPHISM BELOW THE MOINE THRUST

In sections 4.2, 4.3 and 4.4 it was shown that the Durness Formation has undergone greenschist grade metamorphism along and close to the Moine thrust, and that the grade is higher at the Eriboll end than the Knockan end of the Moine Thrust. In this section models are proposed which are likely to account for the heat supply that produced the local change.

4.5.1 Lithostatic Geothermics

Given a maximum foreland temperature of 200°C at Knockan (Downie 1981) and assuming the Durine member of the Durness Formation was also in this temperature regime in pre-Caledonian times, what is the minimum height of Moine overburden necessary to trigger metamorphism in the carbonates below the thrust?

If it is assumed that normal geothermal gradient is as used by Sibson (1977), between 20 - 30°C Km^{-1}, (mean = 25°C Km^{-1}), the expected overburden will be a minimum of 2km to increase the temperature another 50°C to 250°C, which is in the range required to start chlorite crystallization. This would mean that the northern area of the thrust has been under

$\left(\frac{400 - 250}{25}\right)$ = 6km of Moine cover, (where 400°C is the approximate determined maximum temperature at the Eriboll end of the Moine thrust, and 250°C is Downie's estimate in the foreland of the north). This difference in thickness of Moine cover between the north and the south is what Coward (1982) alluded to and explained in terms of a possible steeper ramp climbed by the northern Moines. The change in thickness is supposed by Coward to have driven the northern zone further to the WNW.

Because of the greenschist grade of metamorphism resulting,

$$\lambda_v = 1 \quad \text{(Turner 1968, Sibson, 1977)}$$

where
$$\lambda_v = \frac{P}{\rho g z} \quad - - - - - - - - - - - - \quad (4.2)$$

and P is pore fluid pressure in a rock of density ρ at a depth z, and acceleration due to gravity is g. This means that the weight of overburden is approximately equal to the hydrostatic pressure and no matter how high the former is, it is "buoyed up" by fluids, reducing the effective overburden pressure to zero. Such a situation is not likely to contribute greatly to the rise in temperature expected from overburden pressure, though it might be ideal for fault propagation.

Also if depth of Moine cover alone could explain the subMoine metamorphism, then rocks much below the Moine thrust should also have been involved in this greenschist grade of metamorphism. Such evidence is lacking at the present level of exposure of the Moine thrust zone.

4.5.2 Thermal Equilibration following overthrusting

Another source of thermal energy following thrusting of the Moine nappe over the foreland carbonates could be the Moine rocks themselves. Being of higher metamorphic grade than the Cambrian-Ordovician suite and coming from a lower crustal level too, the base of the Moine schists resting on the former would immediately act as a source of radiant flux for physical/chemical processes below the thrust. This means that the attempt by the warmer schistose suite to establish thermal equilibrium with the colder top of the Cambrian-Ordovician suite, provided thrusting was rapid enough, resulted in "off-loading" of its excess heat, and a rapid gain in heat content of the colder rocks. The situation is illustrated in Figures 4.14 and 4.15, using the model developed by Oxburgh and Turcote (1974).

In Figure 4.14 a uniform stratigraphic column is assumed for both the mainland and what would later remain as a foreland (a). The geothermal gradient is such that $T_2 > T_1$ and is assumed, as shown in (d)(i), to be linear. In (b) the thrust is introduced, effectively separating an over-thrust suite A from a foreland suite B. The situation immediately after thrusting is represented in (c) showing an alternation of thermal surfaces T_1 and T_2, resulting in a saw-tooth form of geothermal gradient, as in (d)(ii). At any other time following thrusting the saw-tooth will gradually try to modify itself to produce a linear pattern as in (d)(iii), by heat exchange between the two surfaces in contact across the thrust plane.

FIG. 4.14

Model to explain thermal equilibration after overthrusting.

a. A uniform stratigraphic column with a uniform and linear thermal gradient as in (d) (i), is assumed for the N W highlands before thrusting began.
Temperature $T_2 > T_1$

b. The development of the Moine Thrust separates the mainland A from the foreland B.

c. At some time t_o of thrust propagation just before thermal equilibrium, there is a repetition of stratigraphy and isotherms (T_1 and T_2). This results in a compound geothermal gradient with a saw tooth, as in (d) (ii).

d.(iii) At time T_1 the decay of the saw tooth compound geothermal gradient will tend to create a new gradient, thereby increasing the temperature below the A - B interface. (adapted after Oxburgh and Turcote, 1974).

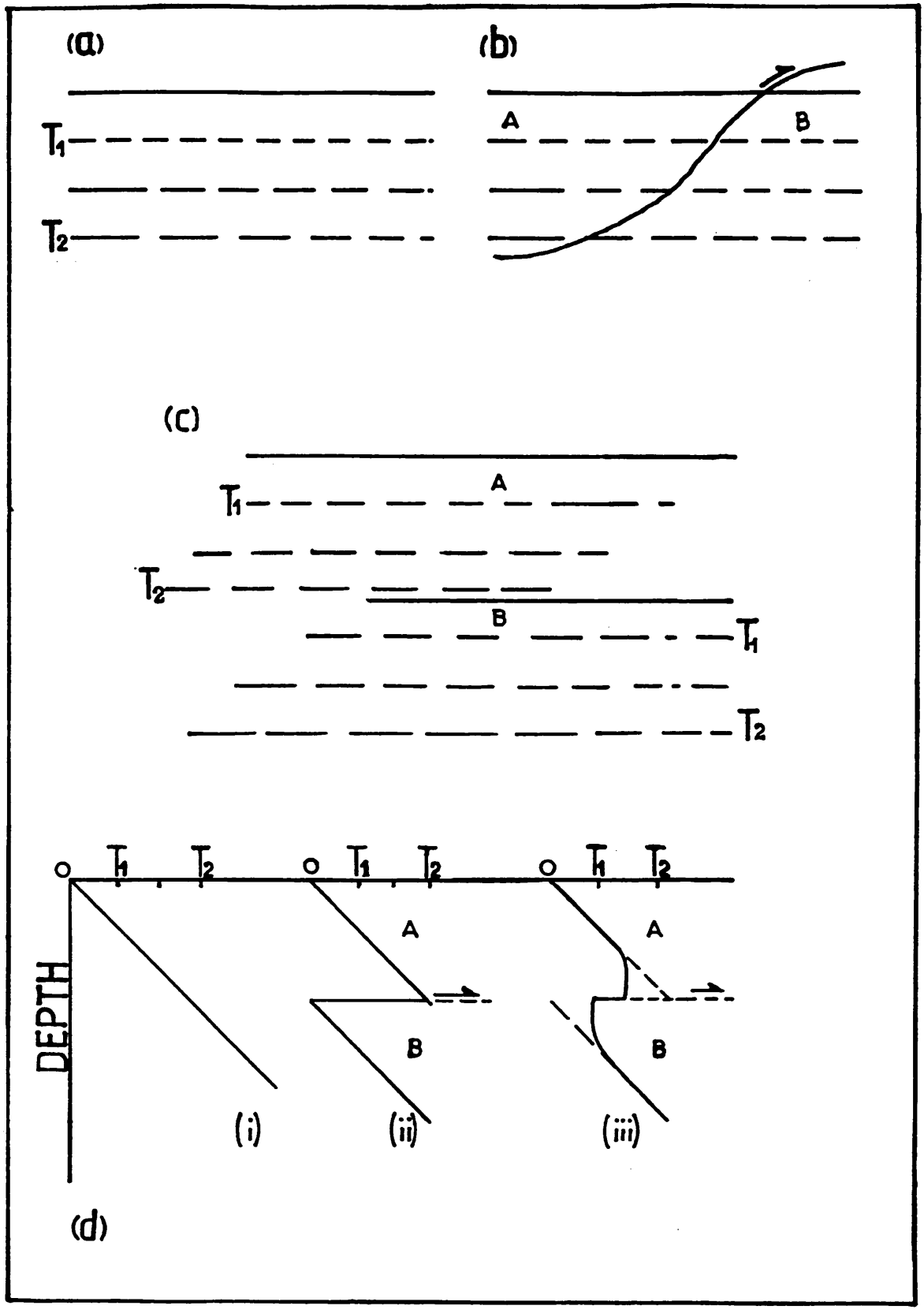
(a)
(b)
T1
T2
A
B
(c)
A
T1
T2
B
T1
T2
T1
T2
T1
T2
T1
T2
A
A
B
B
DEPTH
(i)
(ii)
(iii)
(d)

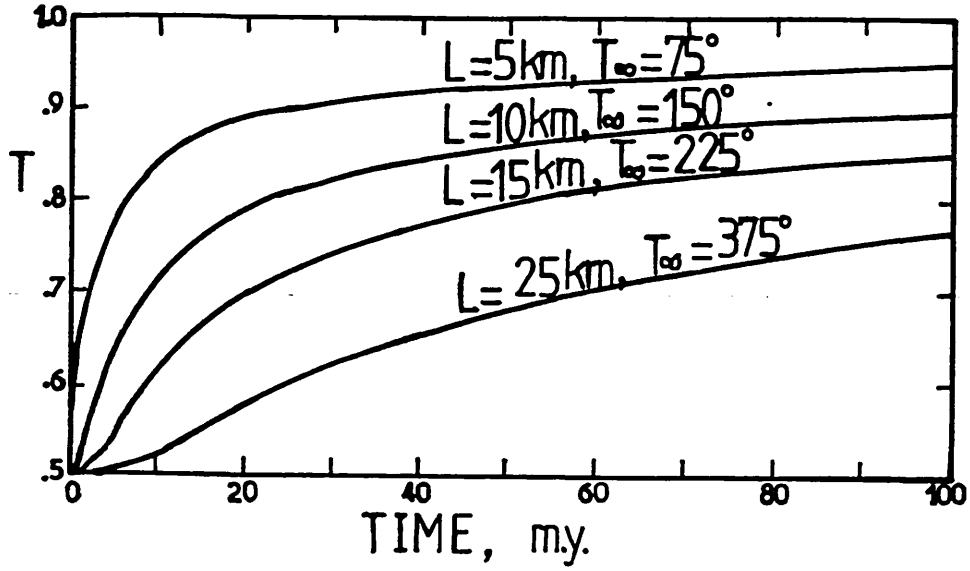

FIG. 4.15

Temperature T as a function of time on the interface between a thrust slab A and its basement B, as in Fig. 4.14, for slabs of 5, 10, 15 and 25km thickness. Equilibrium temperatures at the base of the slab are shown as T_∞ while T is the ratio of interface temperature at any instant to the equilibrium temperature. 0.5T is the temperature on the interface at the moment contact is made. Time elapsed after thrusting is given in million years, (after Oxburgh and Turcote, 1974).

In developing this model Oxburgh and Turcote (1974) assumed that all heat transfer across the thrust plane is by conduction and that the rate of thrusting is very rapid and, if possible, in one step. Even if some of the heat is transferred by fluid flow the heat quantity in question may be small since the fluids themselves are already warm coming from lower crustal levels. Even if the rate of thrusting is not very rapid, it may be partly compensated for by the rate of heat loss from the over thrust suite, which may not be very high either.

At any time (in million years) after thrusting, the interface temperature T at the thrust will, according to Oxburgh and Turcote (page 646), depend on the thickness of the overthrust slab-L. As shown in Figure 4.15 for different slab thicknesses (L between 5km and 25km) and assuming an initial contact (interface) temperature of 0.5T, different interface temperatures result after a particular time interval. The thinner the slab the more rapidly does it lose its heat, and hence the faster does the interface establish a thermal equilibrium. T_∞ are the maximum temperatures obtainable at the different interfaces when equilibrium has been established, and are equal to the initial temperatures at the bases of the thrust sheets of respective thickness.

At the present level of erosion of the Moine nappe the maximum thickness accorded it by Soper and Barber (1982) is approximately 30km. After intensive deep seismic investigation Brewer and Smythe (1984) reduced this depth to the zone of detachment to approximately 21km (see

Fig.3.2(a) and (b). Both models show the Moine nappe as a wedge of increasing thickness from a few metres at the western edge to its maximum thickness in the mainland. In both models also the Moine nappe is shown to interact with the Cambrian sediments of the foreland in the top 6km of the profile. From Figure 4.15, 6km of hot rocks would produce a maximum equilibration temperature of between 75°C and 150°C. Since the slide is so thin this equilibration temperature is likely to have been approached in the time interval since the Caledonian orogeny(~430my),(Coward, 1983). At depths below 6km (Brewer and Smythe, 1984), the Moine nappe interacts with the Lewisian gneiss and the heat transfer should therefore have a different sense.

4.5.3 Effect of Hydrothermal Fluids

The ingress of chemically active fluids in the Moine thrust zone probably during active thrusting has left effects which are difficult to mistake.

At Knockan the cataclasite below the Moines is held together by cement of hydrothermal origin (see S.S.4.4.2, Plates 4.2a, 4.2b). About two metres below the thrust where the original diagenetic solution structures are preserved, veins of different sizes and generations can be seen in fractures, joints and minor faults. These veins often contain calcite and/or quartz (Plates 4.5a, b) and are of hydrothermal origin.

At the Eriboll end about two metres below the thrust plane, a large amount of quartz and calcite were observed. The close association of this quartz with solution surfaces

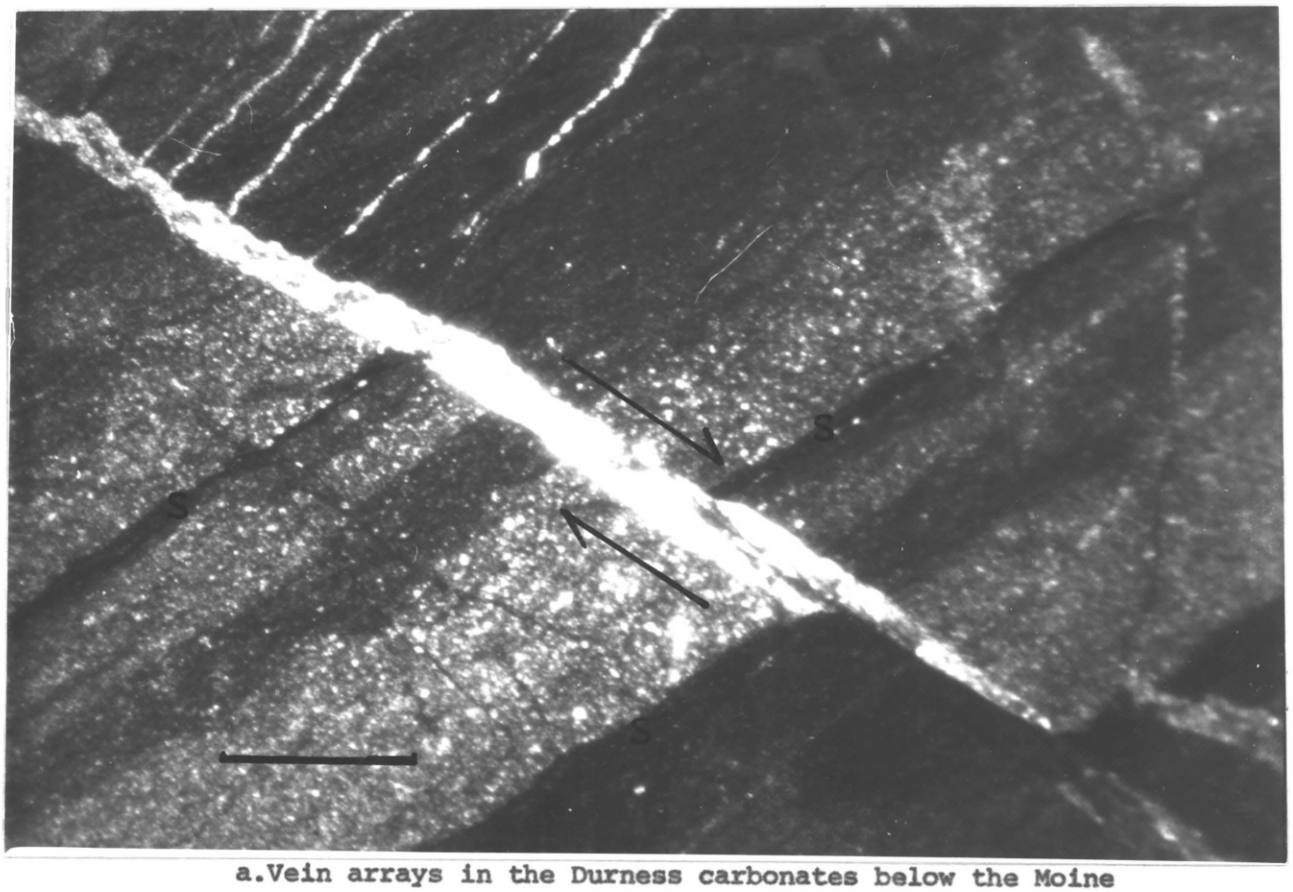

a.Vein arrays in the Durness carbonates below the Moine thrust at Knockan. Scale:1cm,crossed polars.

Plate 4.5

Some of the solution surfaces (S_1) have also been invaded by fluids during deformation, while strain was accommodated by either simple shear or pure shear or both.
Scale bar: 1cm, crossed polars.

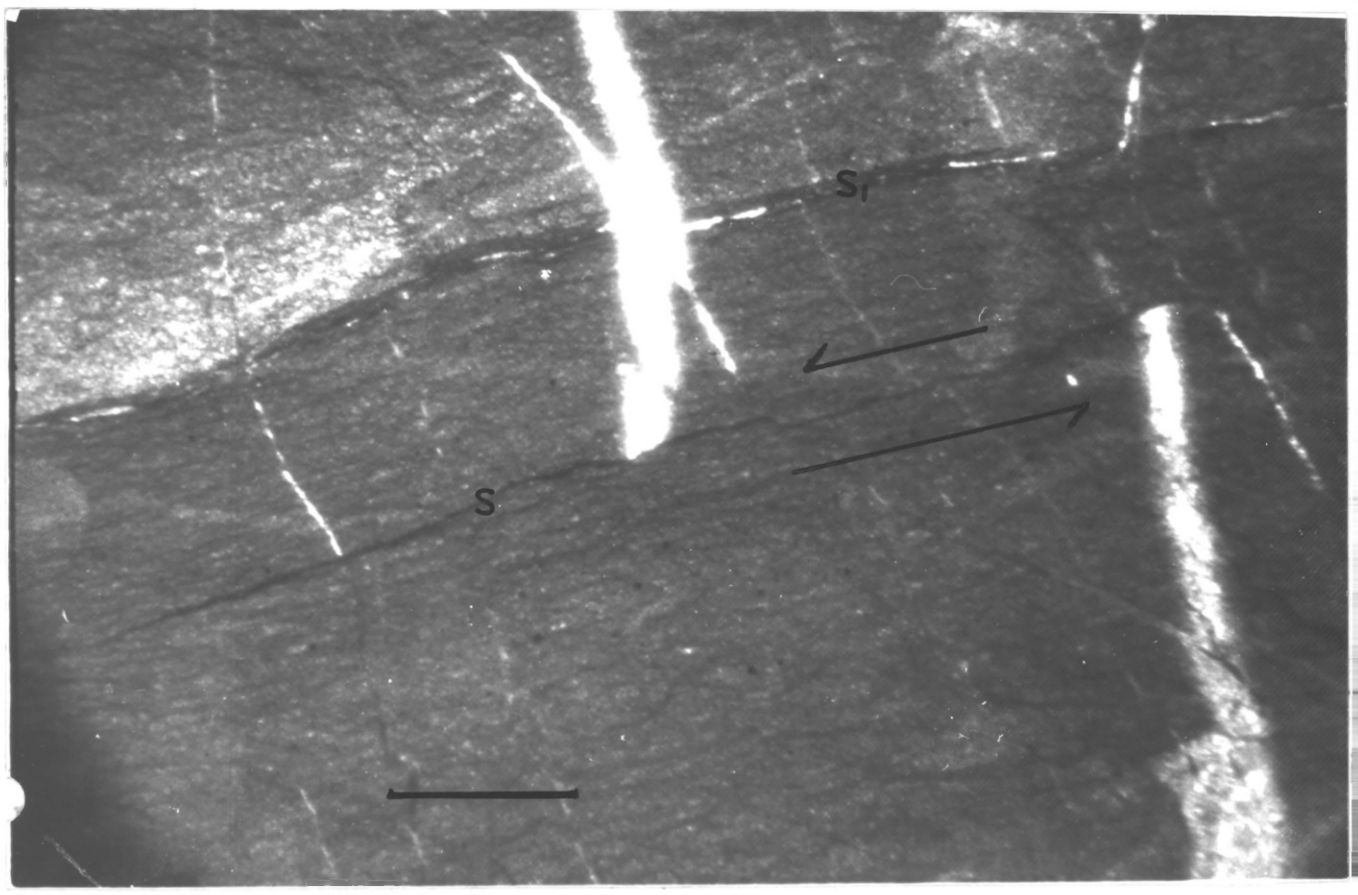

PLATE 4.6 Backscattered electron and optical micrographs of samle Er7 taken about 2m below the Moine Thrust plane at Eriboll.

a,b,c Backscattered electron micrographs,

Scale bars: 100μm.

d. Optical micrograph, crossed polars; Scale bar: 1 mm.

Large amounts of quartz (q) and calcite (cc) are deposited and strung out very close to diagenetic solution seams. These seams still contain white mica (m) which has not been altered to chlorite, an indication that the hydrothermal activity might have been at the lower temperature end. Note also the thickness of the seams (a and b), which might have resulted from expansion of the mica in the presence of undrained fluids.

Plate4.6

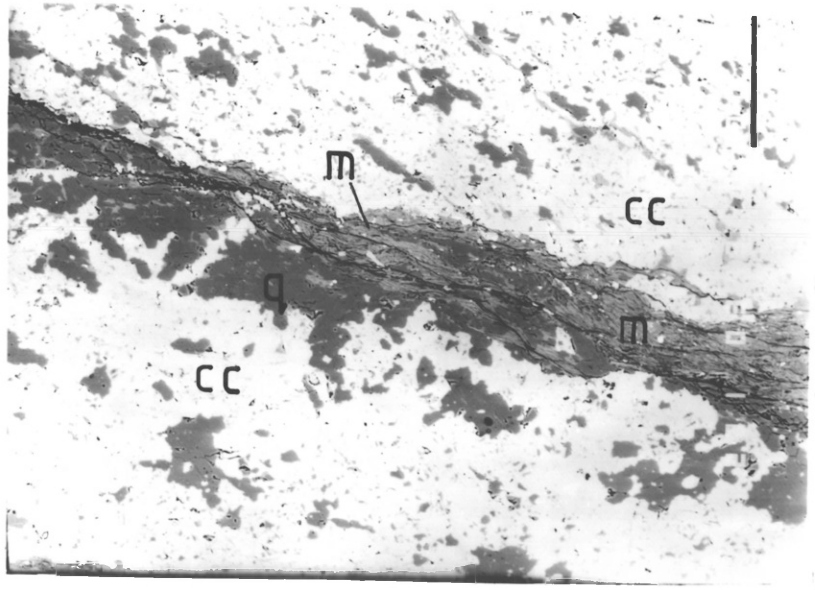

a

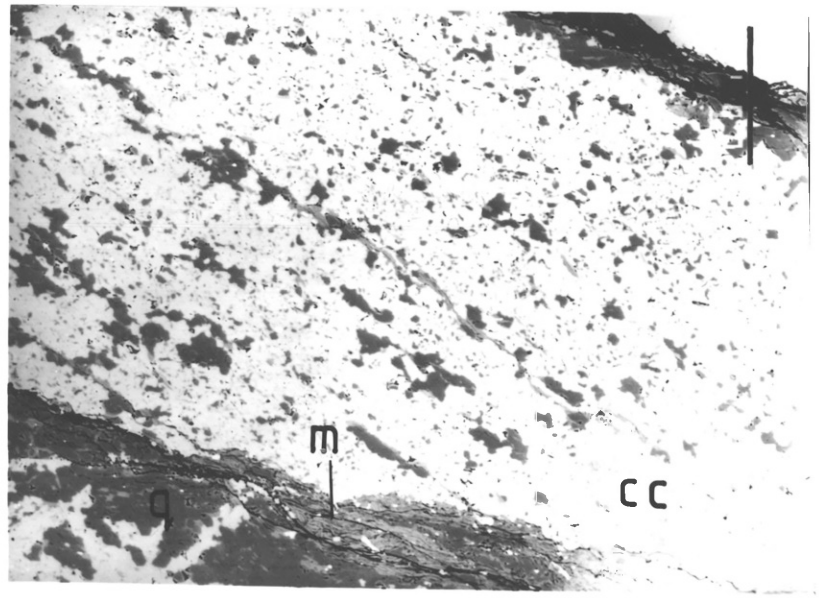

b

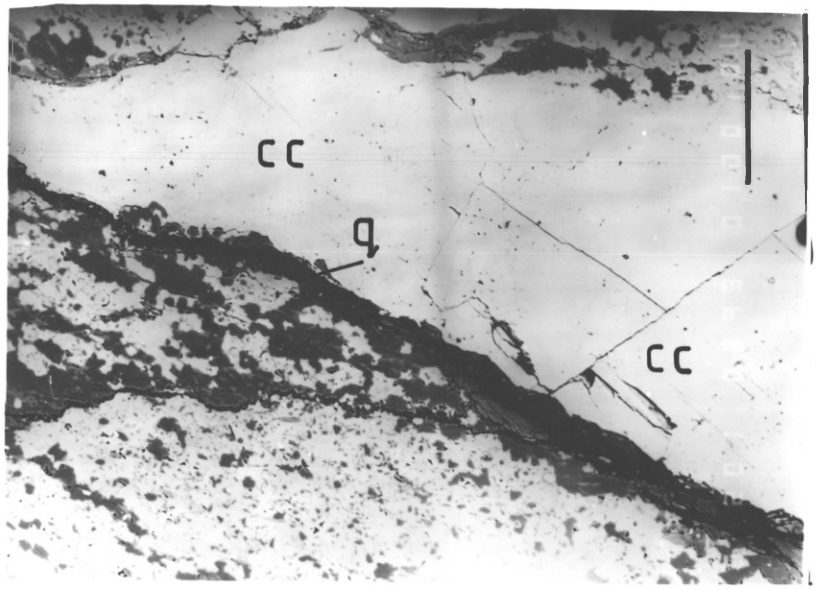

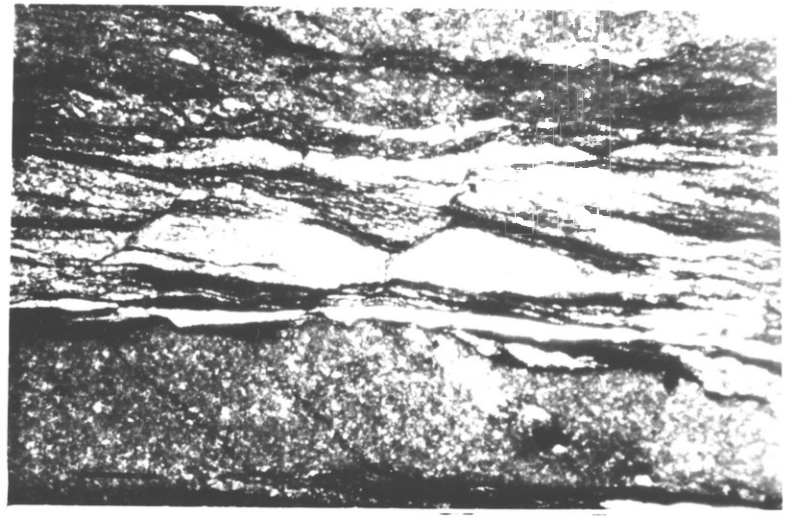

and fractures in the rock suggest a possible hydrothermal origin (Plate 4.6a, b, c and d). The ingress of such large scale, chemically charged fluids should have caused extensive destabilization of minerals like illite, but as shown in Plates 4.6a, b and c, no chlorite was produced, may be an indication that the fluids lost their heat quite rapidly away from the thrust.

Probably the most extensive evidence of hydrothermal fluid invasion in the Moine thrust zone is the zone of retrogressive metamorphism close to the thrust plane. Here Moine psammites which are of biotite garnet grade of meta morphism away from the thrust are converted to mylonites in the thrust zone with such minerals as biotite, feldspars, garnets wholy or partly converted to chlorite. Also characteristic of the mylonites is a depletion of potassium with respect to the psammites (Powell, pers. comm.). The presence of large bodies of undrained fluids after the last thrusting episode must have contributed in bulk material/ chemical transfer, and if these fluids came from reasonable depths in the crust, they are likely to have been warm and possibly transferred their heat to the host rocks.

An analysis of possible fluid pressures that accompanied Moine thrusting is presented in Chapter Five.

4.5.4 Deformation Feedback on Metamorphism

A deforming geological body acquires elastic and/ or plastic strain; the latter is stored with respect to the former. As a result the body gains in strain energy with respect to the free energy of the original system. The

elastic component of the strain energy is usually very small and can be neglected without adverse effects on total energy calculations. But, as Nicolas and Poirier (1976) showed, knowledge of the dislocation density of a deformed rock is necessary to facilitate the estimation of the stored plastic strain energy. A rock body undergoing deformation therefore acts as a medium where thermodynamic inputs (stress, strain, temperature and the extensive properties: entropy, volume and number of moles) are converted into energy. When the deformed rock crystals recover, recrystallize or dissolve, some of their stored energy is released to the "sink" (from neighbouring crystals to contiguous rock bodies).

Taking the Moine mylonites as an example, which are mainly a quartz mylonite, the stored plastic strain energy is given by Nicolas and Poirier (1976, p86) as:

$$W = \frac{\mu b^2}{4\pi(1-v)} \ln \frac{R}{bo} \quad \text{- - - - - - - - - 4.3}$$

where μ is shear modulus = 44GPa for quartz

b is Burgers vector = 0.5nm for quartz

v is Poisson's ratio≈0.3 for most materials.

R is distance between dislocations = $1/\sqrt{\rho}$, and

ρ is dislocation density

bo is core radius of dislocations = 2b

$$\text{Hence } W = \frac{\mu b^2}{8.8} \ln \frac{1}{2b\sqrt{\rho}} \quad \text{- - - - - - - - - 4.4}$$

ρ - a very difficult quantity to determine with reasonably high accuracy (Bailey and Hirsch, 1960; White, 1979a) was found to average about 5×10^7 cm^{-2} (White, 1979b) at Eriboll and to vary from 10×10^8 - $2.5 \times 10^8 cm^{-2}$ from Knockan Moine mylonites to Eriboll Moine mylonites (Weathers et al. 1979).

This suggests a mean dislocation density ϱ of 4.5×10^{8} as characteristic of deformed quartz in the Moine mylonites.

Therefore $W = 2.7313 \times 10^{-3}$ erg.cm^{-1}

For 4.5×10^{8} cm of dislocation line the energy stored in $1cm^{3}$ of quartz

$$W' = \varrho W = 4.5 \times 10^{8} \times 2.7313 \times 10^{-3} \text{ erg cm}^{-3}$$
$$= 1.2291 \times 10^{6} \text{ erg. cm}^{-3}$$
$$= 1.2291 \times 10^{-1} \text{J/cm}^{3}$$
$$= 2.7886 \text{ J. Mole}^{-1}$$
$$\text{or } 1.2291 \times 10^{5} \text{ J. m}^{-3}$$

Bailey and Hirsch (1960) observed from coldworked polycrystalline silver that experimentally measured values of stored energy are compatible with the observed dislocation distribution, provided the long range stresses associated with the networks are relatively small. They showed also that some of the stored energy was released during recovery, but much more during recrystallization. Earlier Clarebrough, Hargreaves and West (1955) had shown that the percentage of stored energy is independent of the method of deformation and that the energy stored is in general a more satisfactory criterion of the amount of deformation. They also showed that a considerable amount of the energy stored is released during recrystallization, followed by the return of the mechanical properties of the deformed metals to those of the undeformed state. Gross (1965) observed that although the activation energy for recrystallization in Solnhofen limestone is up to two times the normal level for metals, the proportion of the work of deformation which is stored in limestone is 50 to 100% greater than for the same metals.

If a highly deformed quartz/feldspar aggregate in the Moine mylonites undergoes dissolution, recovery and/or recrystallization, some amount of its stored energy less the activation energies for all or some of the above processes, will be released. This released energy could be transferred (mainly by conduction) to the carbonates and other rock types below the Moine thrust.

4.5.5 Heat from Retrogression in the Moine Mylonites:

The Moine thrust plane is bounded above by a mylonite zone of more than 600m (Soper and Wilkinson, 1975) and possibly up to 1km maximum thickness (Evans, pers. comm.) The Moine mylonites are derived from the Moine psammites mainly by plastic grain refinement processes in a non-hydrostatic stress state and it is fairly well agreed now that they might have been generated at the earliest stage of the Caledonian deformation (see Christie, 1963; Powell, 1974; Soper and Wilkinson, 1975; and also subsection 3.3.3)

It is also well known that biotite, muscovite and feldspars in the Moine psammites break down by retrogressive metamorphism to chlorite and greenish muscovites in the mylonites (Soper and Wilkinson, 1975; Evans and White, 1984). This behaviour is shown in Figures 4.16, 4.17 and 4.18. This is a series of diffractograms of Moine rock samples from the localities shown on Figure 4.19. The samples were not taken at regular intervals from the thrust plane, but in each series the first was taken from the Moine mylonites as close as possible to the thrust plane, while the last sample was collected from deep within the Moine psammites.

FIG. 4.16

X-ray diffractograms of Moine Schists at the Glencoul Area.

The Moine psammites ST 10 and ST 8 are mainly quartz, mica and feldspar rocks, while the Moine mylonites ST 7A show chlorite (14Å) in addition.

ch = chlorite, qtz = quartz.

Sample locations are as shown in Fig. 4.19

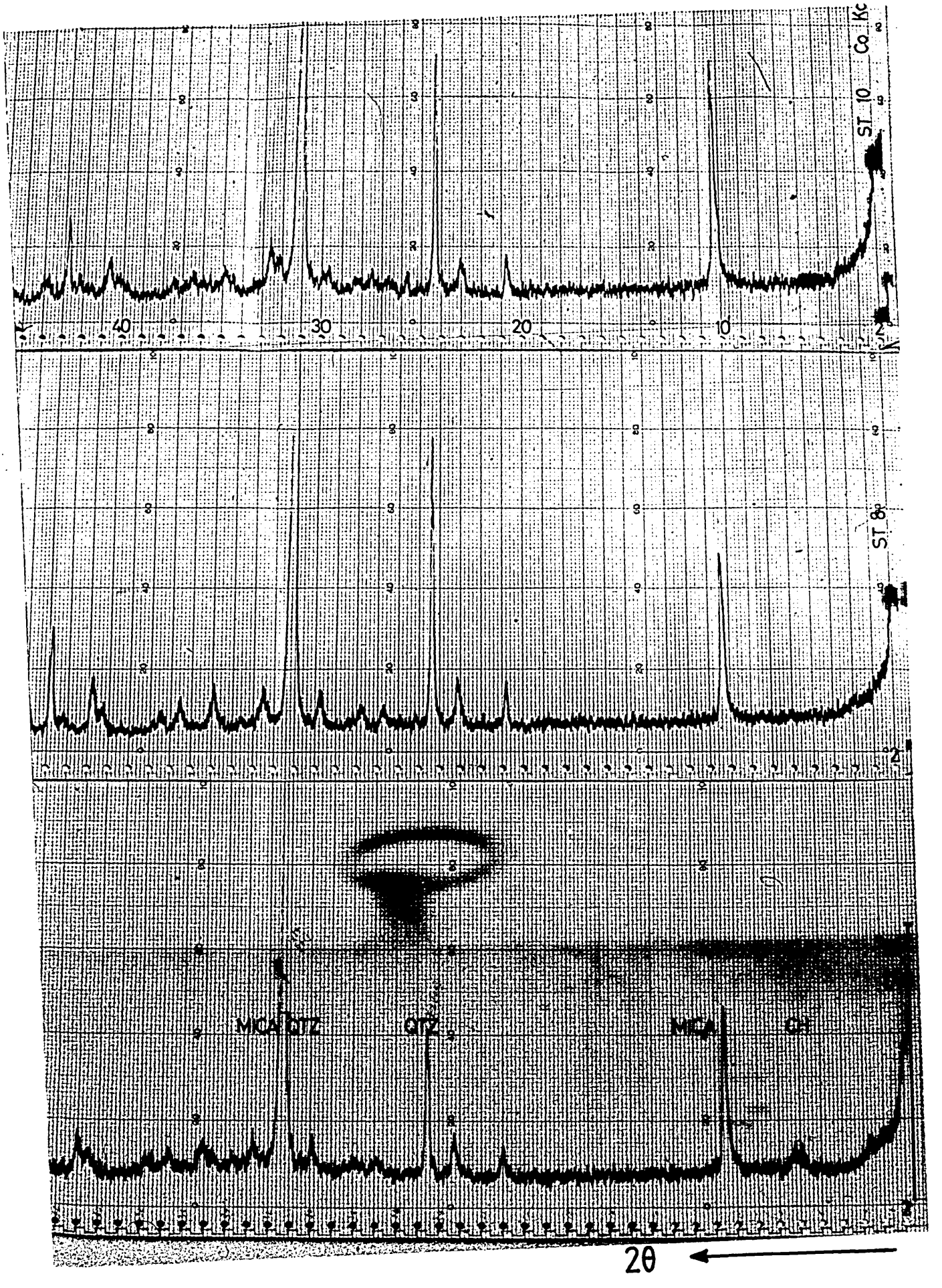
Co Kc
ST 10
40
30
20
10
ST 8
MCA
QTZ
QTZ
MCA
CH
2θ

FIG. 4.17

X-ray diffractograms of Moine Schists at Cnoc a' Chaoruinn area (see Fig. 4.19). C18D, C18C, C18B are all Moine psammites while C18A is a Moine mylonite sample.
Note the similarity in the phases of the psammitic rocks, and also the emergence of the (14Å) chlorite (ch) mineral in the mylonite sample.

ch = chlorite

qtz = quartz

alb = albite.

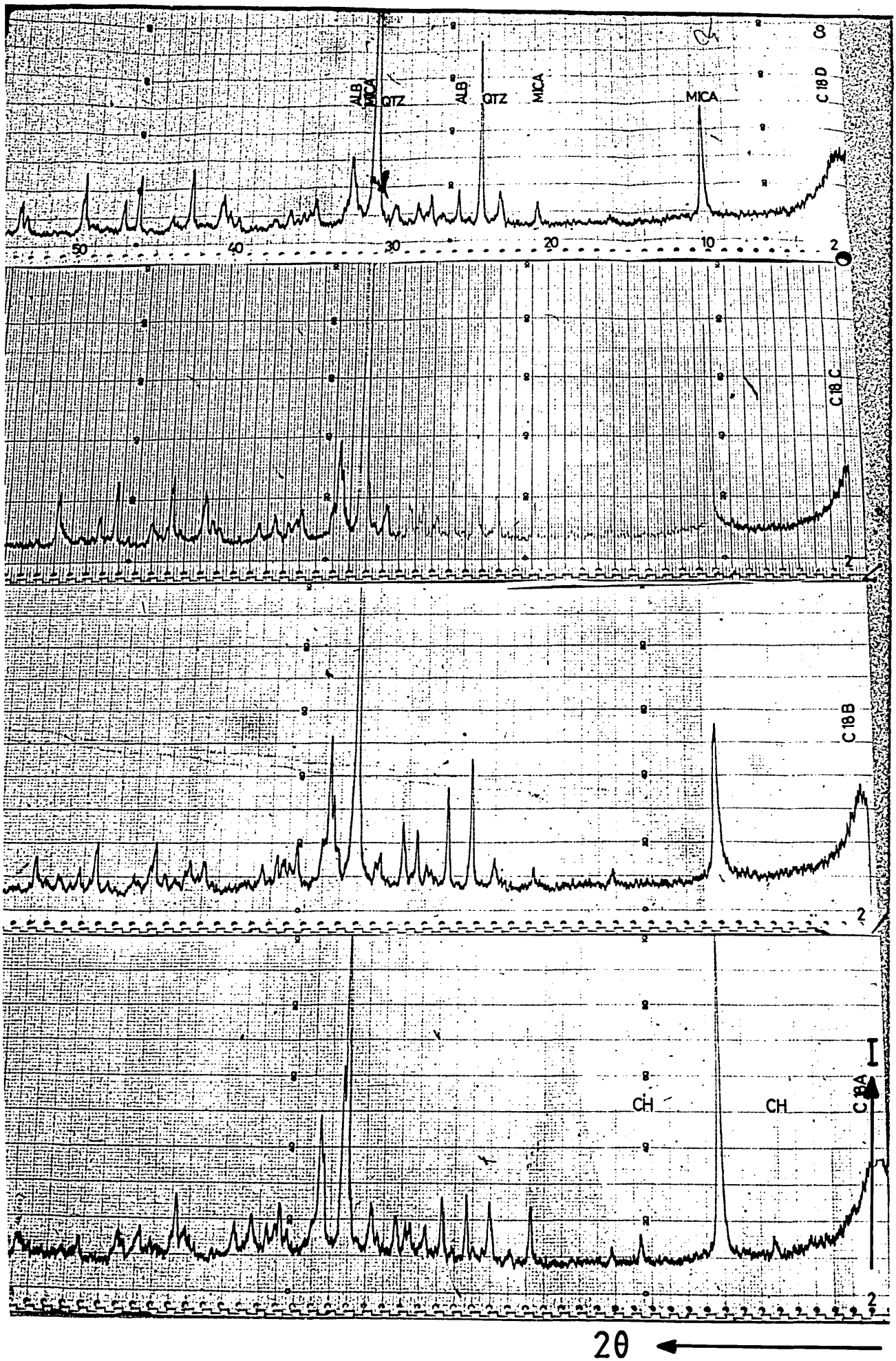
ALB
MICA
QTZ
ALB
QTZ
MICA
MICA
C 18 D
50
40
30
20
10
2
C 18 C
C 18 B
CH
CH
C 18 A
2θ

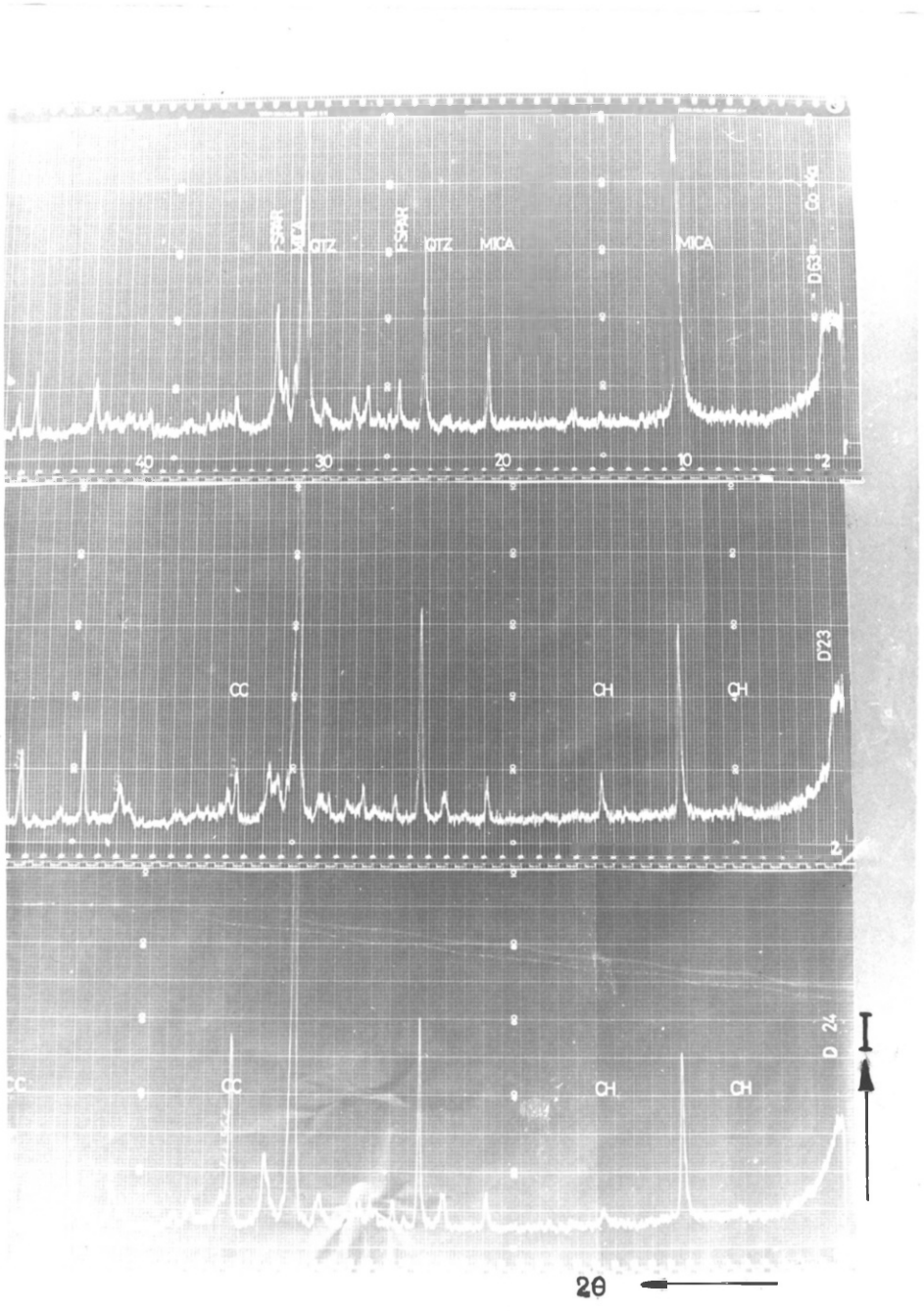

FIG. 4.18

A series of x-ray diffractograms of the Moine Schists at Knockan. D63 is from the Moine psammites and D23 and D24 are from the Moine mylonites (see Fig. 4.19). The main difference between D63 and D23 - D24 is the emergence of the small chlorite peaks at $2\theta = 7^{o}$ and 14^{o} in D23 and D24, while the mica peak in D63 is more intense than in D23 - D24. Biotite in the psammites is changing to chlorite in the mylonites.

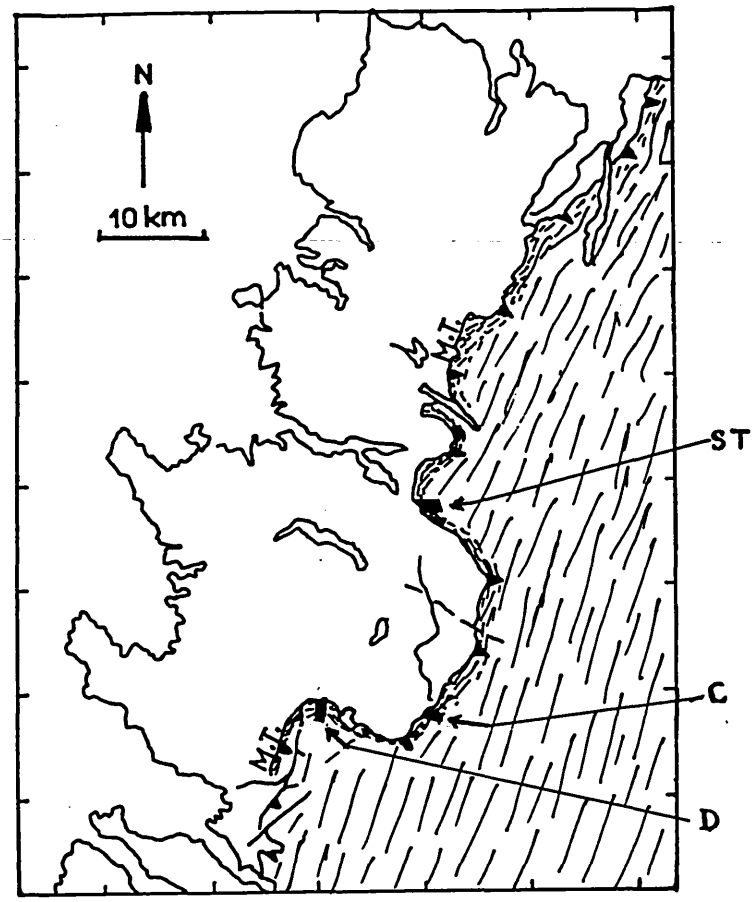

FIG. 4.19

The Moine Thrust Zone showing sample locations in the Moine Schists used for x-ray diffraction studies in Fig. 4.14 and 4.16.

ST is Glencoul area

C is Cnoc a' Chaoruinn

D is Knockan Area.

As shown in Figures 4.16, 4.17 and 4.18, the mineralogy is fairly common in the three profiles. The chlorite peak at 14Å ($2\theta=7°-8°$) characteristically occurs in the Moine mylonites. In Figure 4.16, for instance, the Glencoul Moines show the chlorite peak only in ST 7A - from the Moine mylonites, while ST8 and ST10 from the Moine psammites show fairly strong mica peaks ($\sim$10Å) and no chlorite. The 10Å mica peaks in the psammites are composite peaks of muscovite and biotite. The latter is easily imaged in backscattered electron microscopy and optical microscopy. Hence the process involves the chloritization of biotite within the mylonites in the Moine thrust zone where fluids aid in material transportation. Other chemical processes likely to take place here are the conversion of orthoclase feldspar to muscovite according to the equation:

$$6KAlSi_3O_8 + 4H_2O + 3Al^{3+} \longrightarrow 4KAl_3Si_3O_{10}(OH)_2 + 2K^+ + 6Si^{4+} \quad \text{---------4.5}$$

orthoclase → muscovite

and possibly the hydration of silica into muscovite in the presence of aluminium ions according to the equation:

$$3SiO_2 + 3Al(OH)_3 + K^+ + 9.731H_2O \rightarrow KAl_3Si_3O_{10}(OH)_2 + H^+ + 12.731H_2O \text{ (Powell, 1978)} \quad \text{----4.6}$$

The chloritization of biotite, on the other hand, was shown by Chayes (1955) to follow either of the steps:

(i) For iron-free biotite (eastonite):

$$K_2(Mg_5Al)(Al_3Si_5O_{20})(OH)_4 + 2H_2O + 4SiO_2$$

Eastonite

$$\longrightarrow Mg_5Al_2Si_3O_{10}(OH)_8 + 2KAlSi_3O_8 \quad \text{----------4.7}$$

Mg-chlorite orthoclase

(ii) For iron - containing biotite (annite):

$$2KFe_3^{+2}AlSi_3O_{10}(OH)_2 + 2H_2O \rightarrow Fe_5^{+2}Fe^{+3}AlSi_3O_{10}(OH)_8 + KAlSi_3O_8 + K$$

annite — iron chlorite — orthoclase

--------4.8

The potassium produced in reaction (4.8) would very readily be carried away in solution or be used up in reaction (4.6). Powell (pers. comm.) has observed that K/Ar ratios decrease very rapidly from the Moine psammites into the Moine mylonites, from whole rock chemical analysis. This is likely to lend credence to the possibility of K-dissolution following reaction (4.8).

4.5.4.1 Enthalpy Considerations

Taking reaction 4.8 and using the standard enthalpies of formation ΔH_f° (Helgeson, et al. 1978; Robie et al. 1978), we have:

$$2KFe^{+2}AlSi_3O_{10}(OH)_2 + 2H_2O \rightarrow Fe_5^{+2}Fe^{+3}AlSi_3O_{10}(OH)_8 + KAlSi_3O_8 + K$$

ΔH_f° : 2[-1232.2] +2[-68.32] = -2116.96 + [-949.19] +0 kcal

A B

-------4.9

Enthalpy change ΔH° of reaction is B-A

= -3066.15 - (-2599.04) = -467.11 kcal.

= -1961.86KJ = -980.93 KJ/mole of annite.

The exact quantity of heat released by the above process may be somewhat lower than the value of -980.93KJ/mole of chlorite. This is mainly due to the ΔH_f° of iron chlorite which is unknown and for which ΔH_f° of - 2116.96 Kcal of

PLATE 4.7

Backscattered electron micrographs of Moine mylonites. Scale bars: 1 mm.

a. A phyllosilicate band is imaged, showing the high proportion of Fe-Mg chlorite (ch), in a generally quartz-rich (Q) rock. The proportion of muscovite (m) is relatively low. (Gt) is garnet, undergoing alteration.

b. Outside phyllosilicate bands the mylonite is still up to about 20% rich in chlorite (ch), while quartz (Q) is still the dominant mineral in the groundmass.

Plate 4.7

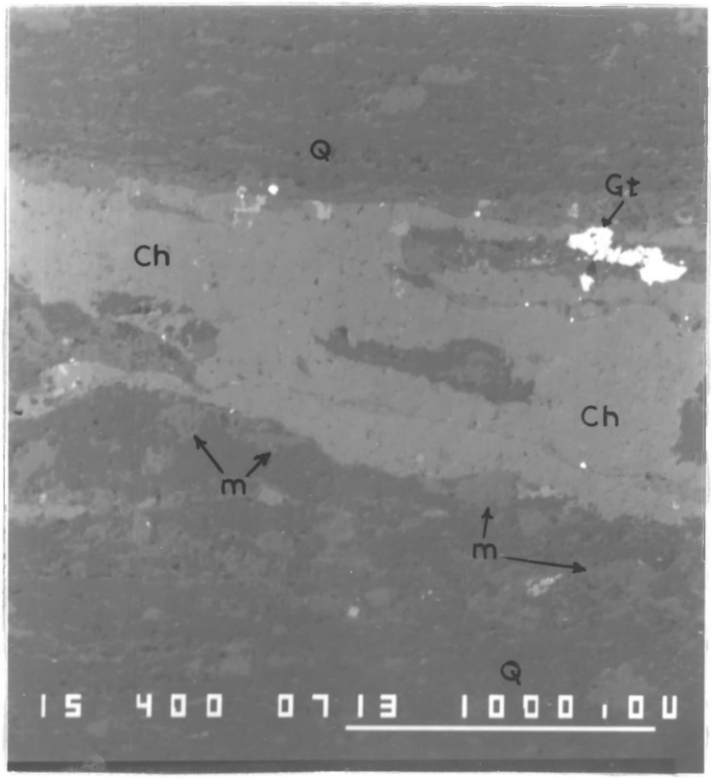

a.

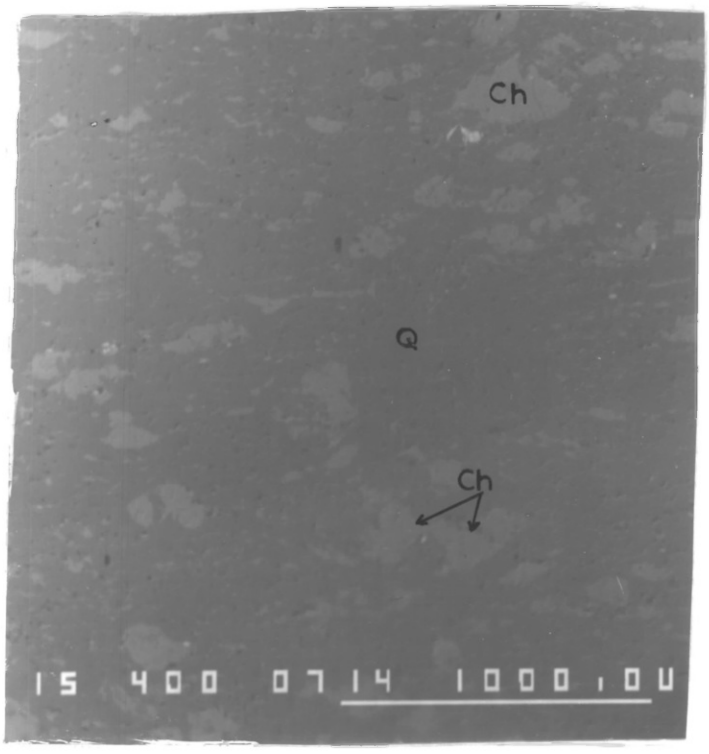

b.

Mg-chlorite has been used in equation (4.9). Also as shown in Figure 4.20, the chlorite variety in the Moine mylonites is neither a pure Mg- nor pure Fe- type, hence its ΔH_f° value would be lower than that for clinochlore but higher than that for pure Fe-chlorite (Kittrick, 1982). But reactions (4.8) and (4.9) suffice to show that the retrogressive chloritization of biotite in the Moine mylonites produces thermal energy of a certain amount. The precise amount will not only depend on knowledge of the exact thermochemical data for reactants and products, but also on the quantity of chlorite produced per unit volume of rock. In Plate 4.7a, a phyllosilicate-rich band in the mylonites is imaged to show a high proportion of chlorite (Ch)- compared to mica (m). Outside these phyllosilicate bands the chlorites and mica are also uniformly disseminated in a quartz matrix (Plate 4.7b). From the plates it seems about 20% of the rock is occupied by chlorite. Hence for every one cubic meter of the mylonites about 20% of it is chlorite.

The molecular volume of chlorite = $207.11 cm^3$

This value is only for Mg-chlorite, since that for Fe-chlorite and chlorites of intermediate composition are not known.

In 20% of $1m^3 = 10^6 cm^3$ the greatest volume of chlorite that the rock can contain is about $2 \times 10^5 cm^3$.

= 965.67 moles of chlorite/m^3

This value will of course depend also on the actual molar volume of the chlorite species, and for higher iron-containing chlorites with higher molar volumes, the total number of

FIG.4.20

Typical spectrum of chlorite in Moine mylonite generated in EDS. This iron-rich chlorite was in sample D24, a Moine mylonite sample from Knockan.

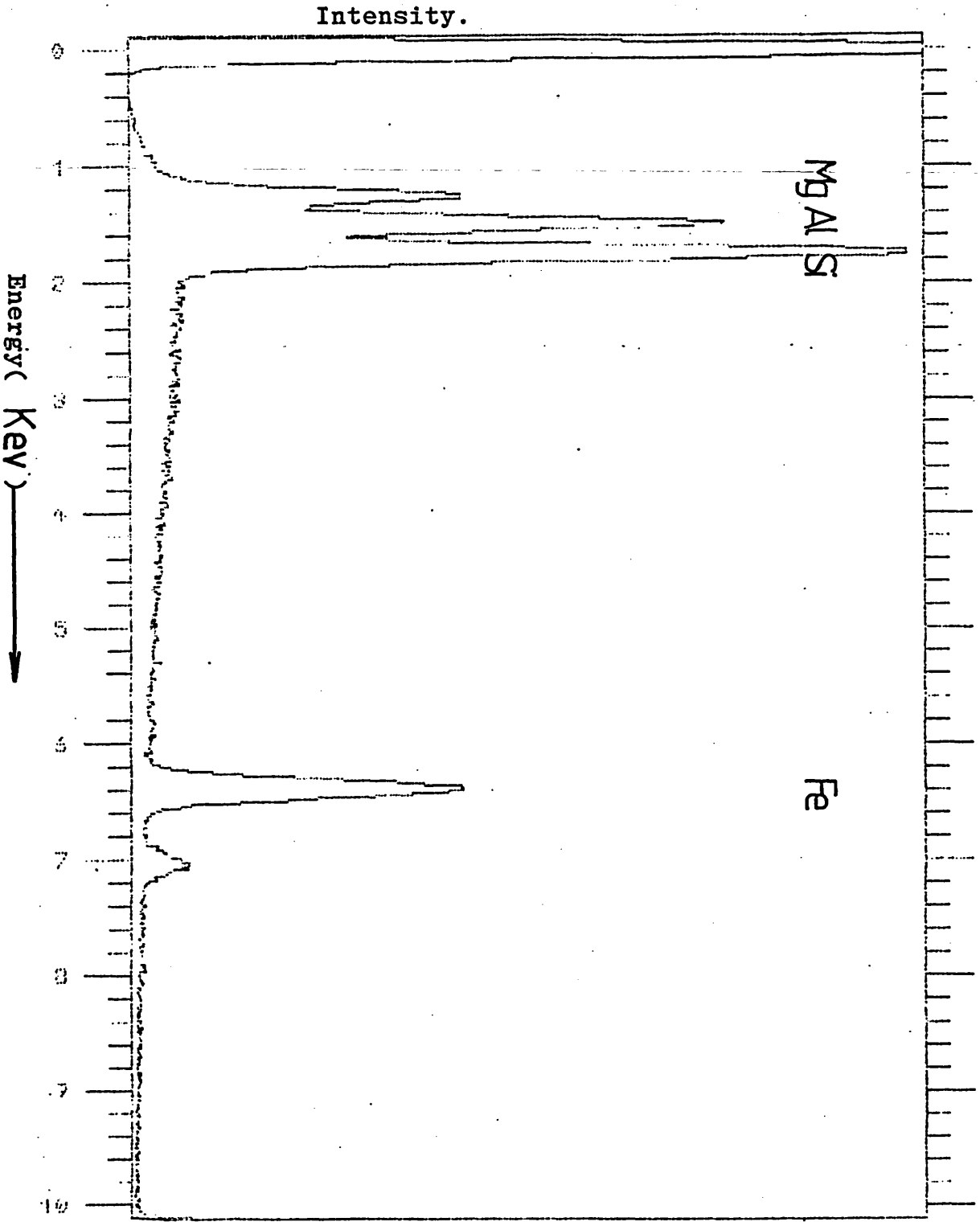

moles of chlorite would be lower than 966 per m^3. Assuming all this chlorite resulted from the chloritization of biotite, then the total heat produced by the process is

$$-980.93 \frac{KJ}{mole} \times 965.67 \frac{moles}{m^3}$$

$$= -947,254.67 \text{ KJ } m^{-3}$$

If all this energy was liberated instantaneously and in a pure (i.e.100%) quartz mylonite, and assuming no other heat source operated while the system was thermodynamically closed, the temperature of the quartz mylonite might rise by 87°K. As Plate 4.7 shows, the system is very far from monomineralic, the retrogressive alteration of geological materials is never spontaneous and the geological system was never closed. Also other sources of heat are known to operate in this thrust zone as elaborated in the rest of this section. As for retrogressive heat affecting the Durness carbonates, that will depend at least on rate of thrusting, rate of retrogression, method of heat transfer and rate of heat transfer.

4.5.6 Effect of Shear Heating

The heat dissipated on a fault, or shear zone, q per unit area, is related to the average slip velocity u and the shear stress by the equation:

$$q = \dot{u}\tau \text{ ----------4.10}$$

The relation is held by Oxburgh and Turcote (1970) to be valid for any type of creep process and also when the slip is due to granulation or small scale fracturing. Equation 4.10 proposes at least two constraints on the quantity of

heat generated or the efficiency of the system. At low shear stresses ~10MPa, and constant fault zone width very high slip rates can produce high frictional heat, while for small displacement rates (e.g. 3cm. yr^{-1}) only high shear stresses >100MPa can guarantee a large thermal output. Scholz (1979, 1980) showed that shear stresses less than about 100MPa cannot produce sufficient heat unless slip velocities exceed about 8-10cm/yr. He however adopted the "higher stresses/lower velocities" option. The other constraint on heat output is thefluid phase accompanying or resulting from thrusting. Sibson (1975) showed that the shear stress τ decreases as the displacement increases following the generation of pseudotachylite (frictional melt) at high temperatures. Also the rise in fluid pressure accompanying active faulting causes a drop in shear resistance or sliding friction. Hence the work dissipated in frictional traction over the fault surface - Ef (Sibson, 1977), which is the part of the total energy budget E convertible to heat, is reduced and the likelihood of shear heating decreases.

Evidence for shear heating comes from metamorphism adjacent to the fault for which field evidence points to the fault alone as the source of heat, and no other heat source can be inferred. Hence the presence of pseudotachylite on fault rocks - e.g. the outer Hebrides thrust (Sibson, 1975)

---

would indicate high thermal anomalies accompanying thrusting. Lackenbruch (1980) argued that large thermal

expansion of fluids in active fault zones coupled with additional pressure during post dilational microcrack closure would set up a hydraulic gradient to drive excess fluid from the heated zone. This chemically charged warm fluids on cooling in host rocks contiquous to the fault zone would deposit large amounts of minerals either as sandstone dykes or veins.

The Moine Thrust Zone has no evidence of abnormally high temperatures at least at the level exposed. No pseudotachylite has been found near the thrust plane, and rather than an abnormally high grade of metamorphism in the Moine mylonites close to the thrust, there is a low grade. The metamorphism below the thrust can be explained in other ways than by shear heating. White (1979b) estimated a regional shear stress of 17.5MPa using the quartz mylonites in the Moine Thrust Zone. This will give a temperature rise, $dT \approx 7°C \times \frac{u}{a}$ ----------4.11

Equation 4.11 is adapted from Lachenbruch's (1980 Equation 2c-p6098), with due allowance for a 17.5MPa (=175bar) shear stress. Thus only displacements u to fault zone thickness a ($^{u}/a$) > 15 will guarantee temperature increases up to 100°C.

Also as estimated in Chapter Five, fluid pressures are likely to have increased above 100MPa during Moine thrusting. These excess fluids are likely to have kept shear zone resistance down and therefore further reduced shear heating. Hence shear or frictional heating is not likely to have contributed much to metamorphism in the Durness formation below the Moine Thrust.

4.6 CONCLUSION

From the foregoing presentation it has been shown that:

(i) Prograde metamorphism of the Durness Formation accompanied and was closely associated with Moine thrusting. This is evidenced by the change in mineralogy, mica crystallinity index and deformation microstructure from the fore-land to the thrust plane.

(ii) The highest grade of metamorphism of the Durness Formation presently exposed is greenschist, with temperatures reaching approximately 390±41°C

(iii) A temperature difference of about 19°C exists between Knockan in the West and Cnoc A' Chaoruinn in the east. This gives a gradient of about 2°C/Km over the 10km distance, showing that temperature below the Moines rises, even if gradually, eastwards. This temperature difference and gradient are of course not very certain due to the presence of substantial errors on the estimated temperatures.

(iv) A temperature difference of about 100°C exists between Knockan and Eriboll, in the Durness carbonates below the Moine Thrust.

(v) Prograde metamorphism and neomineralization in the Durness formation could have been caused by a combination of:

(a) Thermal conduction from an overthrust Moine Nappe, in an attempt to establish thermal equilibrium and uniform geothermal gradients again after thrusting;

(b) ingress of warm silicic fluids accompanying thrusting;

(c) strain energy converted to heat in a highly deformed Moine mylonite zone undergoing cyclic recovery recrystallization and/or dissolution;

(d) heat energy from retrogression in the Moine mylonites, if the rate of thrusting was rapid enough.

These energy sources are shown in Figure 4.21, which is a model showing the interaction of Moine deformation with metamorphism in the Durness Carbonates. Figure 4.21 also models the spatial relationship of the two zones of active deformation and metamorphism bounding the Moine Thrust.

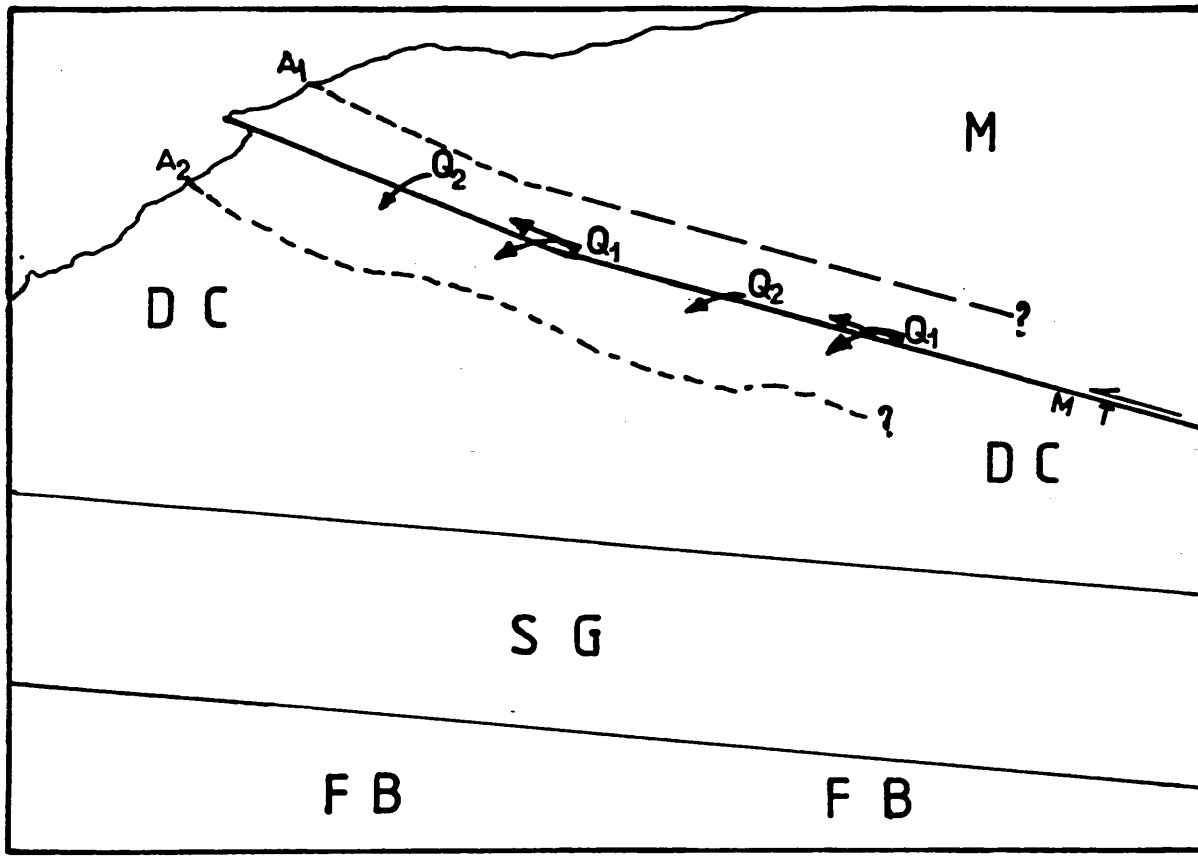

(not to scale)

KEY

M	Moine Psammites +Mylonites.
DC	Durness Carbonates.
SG	Serpulite Grit.
FB	Fucoid Beds

Fig.4.21 Model of the Moine Thrust Zone showing the interaction of Moine deformation with metamorphism of the Durness Carbonates. MT---Moine Thrust, A_1--A_2--the zone of interaction of deformation and metamorphism in Moine mylonites and Durness carbonates, respectively.
Heat sources are: Q_1 from warm fluids within the thrust zone, Q_2- from deformation within the Moine mylonite,+ post thrusting heat exchange by conduction,+ heat from retrogression.

CHAPTER FIVE

SOME EFFECTS OF THE METAMORPHISM ON THE DURNESS FORMATION

5.1.1 Introduction:

In this chapter the metamorphism of the Durness carbonates along the Moine Thrust is analysed in terms of its physical and chemical effects. These consist of the alteration of illite/sericite into chlorite below the Moine Thrust, the way the microchemistry of this chlorite product changes with respect to changes in temperature and the possible effect on fluid pressure along the thrust due to increase in temperature there with respect to the foreland. In subsections 4.4.1 and 4.4.2, it was pointed out that one of the main mineralogical differences between the Foreland/low strain areas and the Moine Thrust Zone as far as the Durness Formation is concerned is the alteration of low grade mica minerals (illite/sericite) into chlorite along the thrust zone. This chapter closely examines the chlorite product, particularly its microchemistry and how this varies from north to south along the thrust zone. A possible application of the newly acquired information to geothermometry is also suggested.

In section 5.5, the temperature increase found in the thrust zone with respect to the Foreland is used to compute fluid pressure increase that must have attended thrusting. This is done via physical equations first used by Raleigh and Evernden (1981). The application of this to the physical process of Moine transportation and deformation below the thrust plane are also discussed.

5.1.2 Background on the Structure of the Chlorite Lattice

The basic structure of chlorite was proposed by Pauling (1930) to consist of an alternation of a 2 : 1, or talc layer and a hydroxide sheet often called brucite layer or interlayer. The 2 : 1 layer is made up of two tetrahedral sheets, inverted with respect to one another, and one octahedral sheet; while the interlayer or brucite layer is made up of an octahedral sheet only (Fig. 5.1). Chlorite, mica smectite and talc are essentially similar in the structure of the 2 : 1 layer, while the interlayer is the main structural unit that imparts the differences in some characteristics, (e.g. d(001) to the four minerals. The main constituents of the octahedral sheets in both layers are Mg, Fe^{2+}, Al, and Fe^{3+}, but substitutions of Cr, Ni, Mn, V, Cu and Li in certain chlorite species are known. The main tetrahedral cation is Si, though R^{3+} substitution for Si^{4+} is primarily by Al, Fe^{3+} or B^{3+}. The negatively charged 2 : 1 layers have ideal composition $(R^{2+}, R^{3+})_3(Si_{4-x}R^{3+}_x)O_{10}(OH)_2$ and alternate regularly with positively charged interlayer sheets of ideal composition $(R^{2+}, R^{3+})_3(OH)_6$, (Bailey 1980), giving a general formula of the short form $X_m Y_4 O_{10}(OH)_8$ (Foster, 1962). The R^{2+} and R^{3+} refer to divalent and trivalent cations respectively, while X and Y represent octahedral and tetrahedral cations, respectively, and m is usually 6 or less.

5.1.3 Relevant aspects of changes in Chlorite Microchemistry

Although Winchell (1926) and Holzner (1938) held that all the Fe^{3+} in chlorites was formed by the secondary

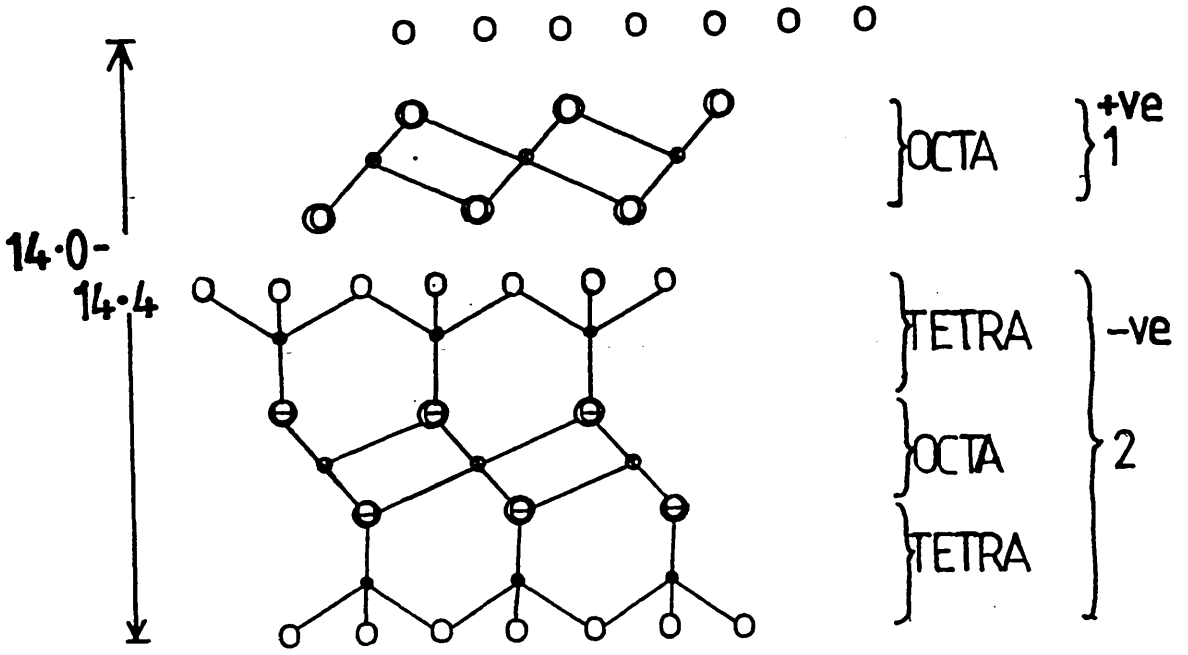

O	Oxygen
•	Tetrahedral cation
⊖	Oxygen + hydroxyl ion (in projection)
●	Octahedral cation
⊙	Hydroxyl group
OCTA	Octahedral sheet
TETRA	Tetrahedral sheet
1	Interlayer, brucite layer or hydroxide sheet
2	2:1 layer or talc layer

Fig.5.1

The structure of a chlorite lattice.

oxidation of Fe^{2+} according to the reaction:

$$2Fe(OH)_2 \rightleftharpoons 2FeO(OH) + H_2O, \quad ---- \quad 5.1$$

Foster (1962), in seeing no evidence for the above process proposed that any Fe^{3+} should be considered a normal constituent of chlorites like other layer silicates, such as biotite, and not as a product of secondary oxidation. Borggaard et al. (1982) after a series of oxidation and reduction experiments on iron-rich chlorite showed that essentially all of the Fe^{2+} of the original chlorite seemed to be located in the 2:1 layer, while octahedral Al and original Fe^{3+} was inferred to exist solely in the hydroxide sheet. They also showed that the conversion of Fe^{2+} to Fe^{3+} is reversible and appears to be associated with the release of hydrogen in apparent confirmation of equation 5.1. The released hydrogen often reacts with oxygen at the edges of the crystallites to form water, or the oxygen may diffuse into the 2:1 layer and react with the hydrogen. The fact that oxygen is low with respect to Fe^{3+} in such chlorites (Foster, 1962) could be indication that water really is formed as a by-product of the oxidation of Fe^{2+} to Fe^{3+} in chlorite.

The formation of water in chlorites following oxidation would be of great importance not only for lubricating movement planes in those phyllosilicates - an aid to grain boundary sliding - but would also bring about water weakening of materials like quartz. Although water tends to dissolve strained geological materials, thereby limiting grain size, it also acts as a grain growth medium, facilitating material transport (Tullis and Yund, 1982). Despite this latter behaviour, grain

sizes of geological materials close to phyllosilicates are generally known to decrease compared to those away from phyllosilicates in tectonites (White, 1979a, also see subsection 6.2.3).

The variation of the water content of chlorites with respect to their Fe/Mg ratios was shown by Foster (1964) to exhibit a strong relationship. She found that decrease in water content correlated with increase in Fe and decrease in Mg content. A similar decrease in H_2O (+F) content with decrease in MgO and increase in FeO characterizes the trioctahedral micas.

In 1962 Albee proposed without empirical or rigorously derived thermodynamic evidence that chlorites should have any proportion of Fe/Mg; that the exact value depends both upon the Fe:Mg ratio in the bulk rock, and upon the nature of the other minerals among which the Fe and Mg are partitioned. He also proposed that Mg - content in chlorites should increase as the grade of metamorphism increases. The only evidence these assumptions were based on was Nelson and Roy's (1958) and Turnock's (1960) experiments which indicate that the maximum stability temperature of Mg - chlorites is about 130°C higher than that of Fe - chlorites. On the other hand Iwasaki (1963), working on the metamorphic rocks of Eastern Shikoku - Japan, found that Fe^{2+} content of chlorites increased with metamorphic grade. Also Dunoyer de Segonzac (1969) showed that Fe/Mg ratio increased with increasing metamorphic grade.

Recently Velde and Rumble (1977) and Velde (1983) found from compiled microprobe chemical data of chlorites

that their chemistry is a function of the general geological conditions under which they form. They also showed that their Mg - Fe content might be used in metamorphic assemblages as a means of estimating P - T conditions if the chlorites are in equilibrium with another ferro-magnesian phase. This is partly because the alumina content will not interfere with the partitioning of the divalent ions between different phases.

In this chapter the relationship of Fe/Mg in chlorites with respect to temperature is presented, and its geothermometric application is suggested.

5.2 RESULTS OF THE STUDY

5.2.1 Samples Studied

Although sixteen samples were studied for their phyllosilicates, only five were selected for detailed analysis of their chlorite content. These samples were obtained directly below the Moine Thrust plane in the Durness Formation as follows:

D31c	-----	Knockan
C39	-----	Cnoc a' Chaoruinn
Er9	-----	Eriboll
Er10	-----	
Er11b	-----	

Their exact locations and sample descriptions are as outlined in Chapter Three, Section 3.4

The samples selected were those that contained at least ten percent chlorite (with or without mica) and were well placed relative to the thrust, while at the same time forming a series from Knockan to Eriboll. Samples from Glencoul

PLATE 5.1

Backscattered electronmicrographs (a, b and d), and optical micrograph (c) of Durness Carbonates from the Moine Thrust Zone.

The transition from Knockan (a) through Cnoc a' Chaoruinn (b) to Eriboll (c) - (d) is marked by gradual increase in the chlorite - Ch - component of the Durness Carbonates, and decrease of the white mica (M) component. At the Eriboll end chlorite bands are so thick (c) and pervasive throughout the whole rock (d) that the white mica component is absent very close to the fault.

Scalebars:

a	-	10 μm
b	-	100 μm
c	-	2 mm
d	-	100 μm

F = Orthoclase feldspar.

Dol = Dolomite

Cc = Calcite

PLATE 5-1

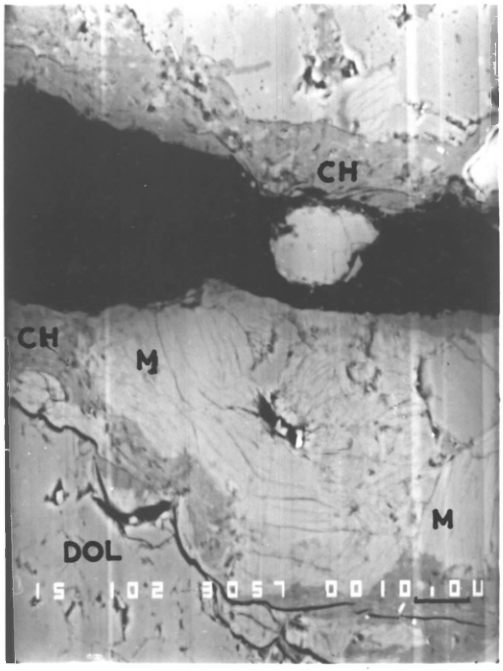

a

b

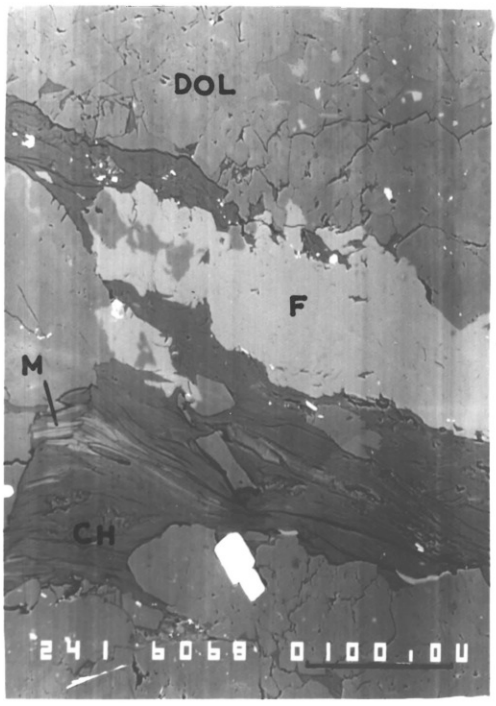

c

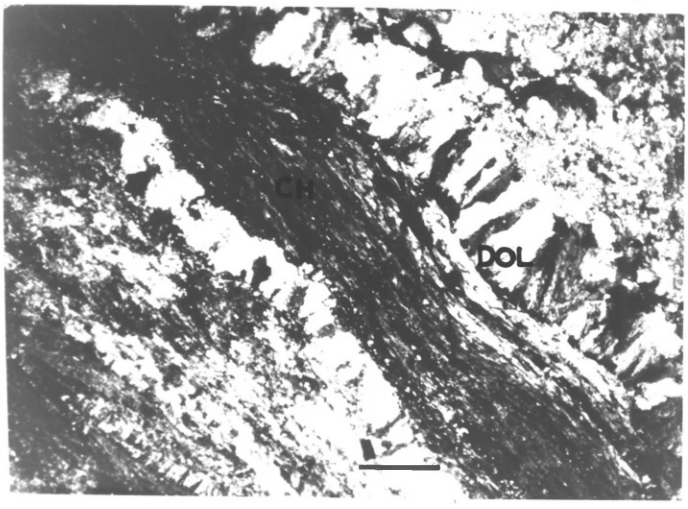

d

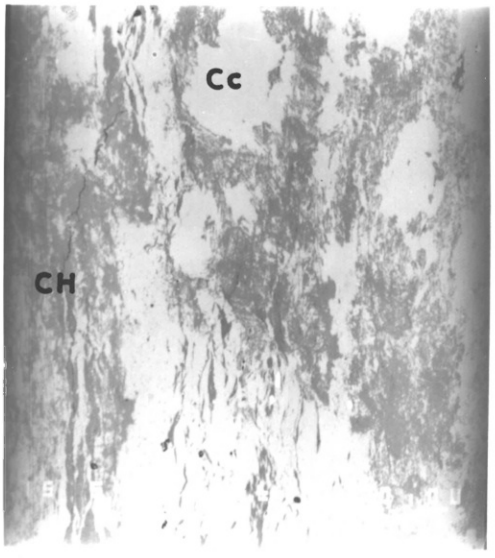

were not included due to lack of chlorite in them.

5.2.2 Results of X-Ray Diffraction Studies

The diffractograms presented in Chapter Four (Section 4.2) were used in the analysis shown in Table 5.1(a+b). As shown in Table 5.1, there is a transition zone between the Caledonian Foreland/low strain zone and the Eriboll end of the Moine Thrust. This transition is characterized by the occurence together of mica and chlorite, and it coincides with the southern end of the Moine Thrust from Knockan to Cnoc a' Chaoruinn. The Eriboll end of the thrust zone is characterized by very strong chlorite reflections, while the Foreland low strain zone gives very strong mica (illite/sericite) reflections. This is also shown on Plate 5.1 where the transition from Knockan (Plate 5.1a) through Cnoc a' Chaoruinn to Eriboll (Plates 5.1c+d)are marked by gradual disappearance of the mica portion and replacement by chlorite.

5.2.3 Spectrum Analysis

The spectrum generated by the line printer in the electron probe microanalyser is fairly similar for sample D31c chlorites (Fig. 5.2) and sample Er9 (Fig. 5.3). These chlorites as shown are mainly Mg-chlorites called clinochlore (Dana, 1892; Foster, 1962), and differ from chlorites in the Moine mylonites (Fig. 4.18) by the weakness of the Fe peak. A comparison of Figures 5.2 and 5.3 shows among other things the stronger Fe peak (at approximately 6.4 kev) in Figure 5.3 than Figure 5.2. This correlates somewhat with the d(001) of chlorite shown in Table 5.1. d(001) of chlorite is 14.3Å in D31c and only 14.0Å in Er9. The well known reduction of d(001) of chlorite with increase in Fe content was attributed by Shirozu (1960) to Al substitution for Si as more Fe is admitted into the chlorite lattice.

Fig. 5.2 EDS spectrum of chlorite.
The chlorite type in the Durness Formation at Knockan has strong Mg and very weak Fe peaks.

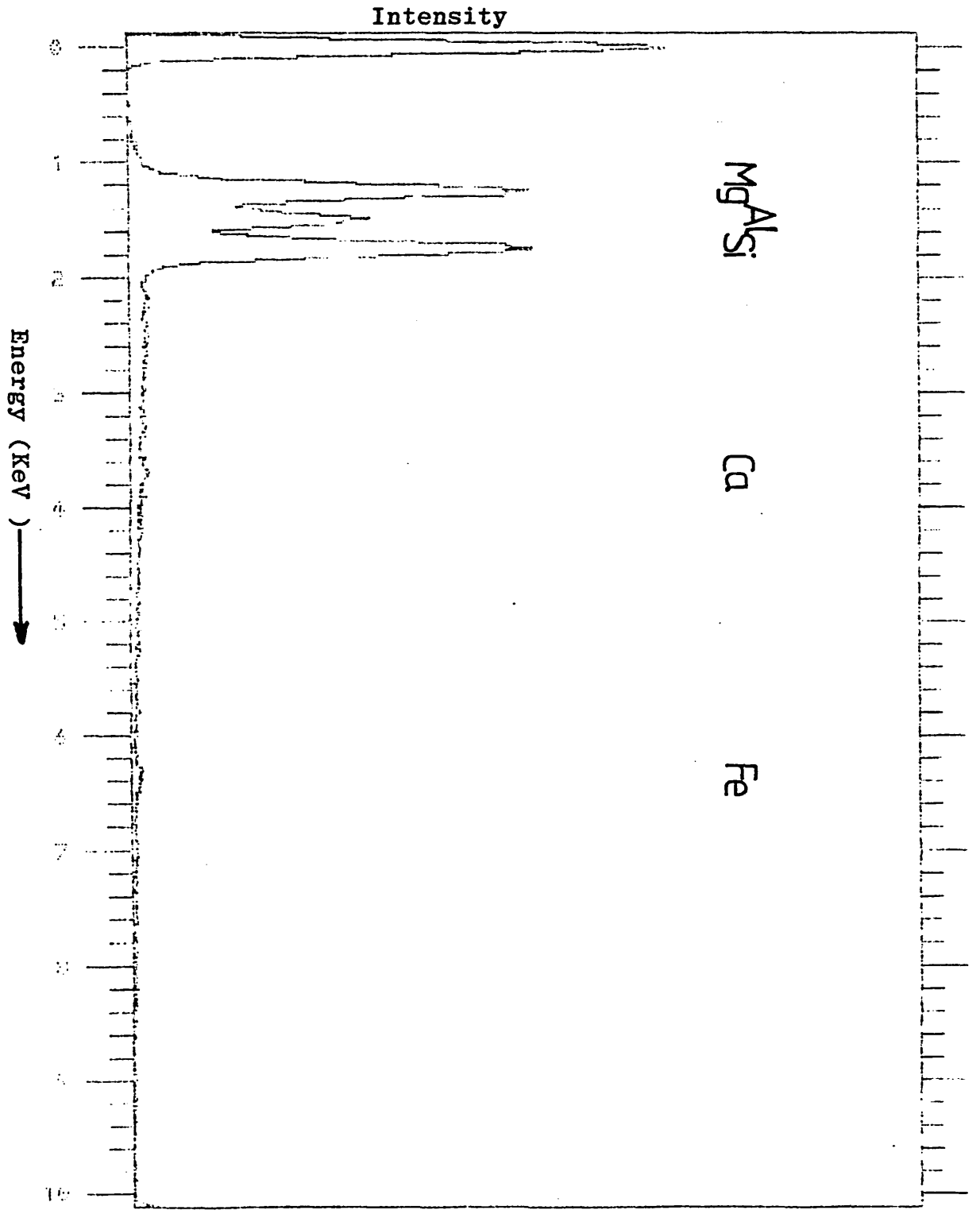

Fig. 5.3 EDS spectrum of chlorite. Clinochlore within the Eriboll marble shows a stronger Fe peak than that at Knockan.

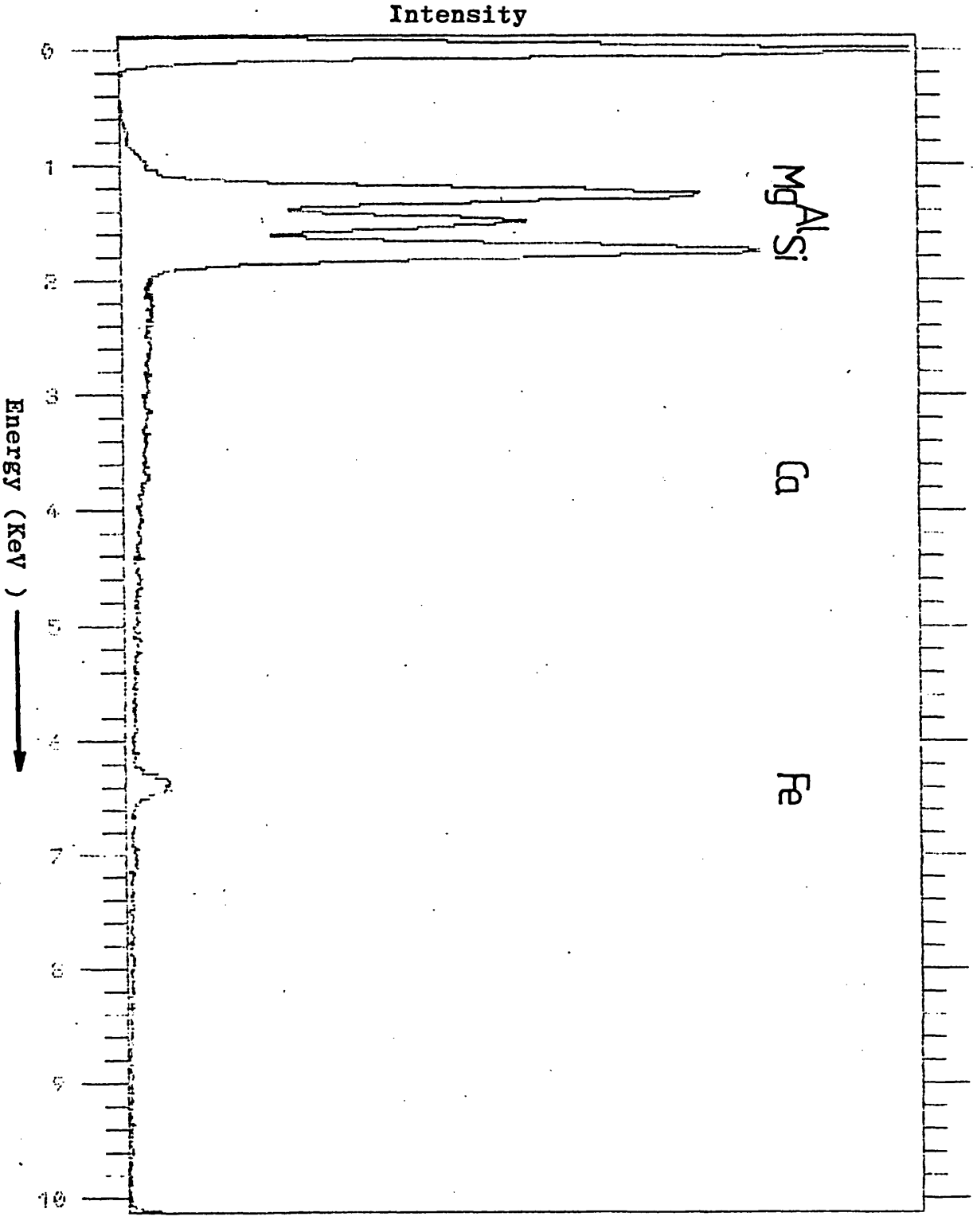

Sample No.	General Location	d(001)Å illite/ sericite	Relative Size of d(001) peak	d(001)Å chlorite	Relative Size of d(001) peak
A14	Foreland	9.93	strong		
A18	"	10.035	strong		
A99B	"	9.97	very strong		
A98	"	9.93	very weak		
A40	"	9.97	medium strong		
B5		9.97	very strong		
C18A	Moine Thrust South	9.92	very strong	I4.2	weak
C39	"	9.88	weak	14.1	strong
C83	"	9.97	very strong	14.2	weak
C88	"	9.92	strong		
D31C	"	9.93	very weak	14.3	very weak
D1	"	9.97	strong	14.2	very weak
Er-8B	Moine Thrust North			14.0	medium strong
Er-9	"			14.0	weak
Er-11	"			14.1	very strong
Er-19	"			14.1	strong

TABLE 5.1(a)

Basal reflections d(001) of illite/sericite (mica) and chlorite, from the Foreland to the Moine Thrust Zone. Note the transition from an illite/sericite - only Foreland to chlorite - dominant phyllosilicates in the north - the south along the Moine Thrust is from Knockan to Cnoc a Chaoruinn. Also d(001) - chlorite becomes smaller towards the north. Data from whole-rock and clay-fraction x-ray diffractograms.

Sample No.	Crystallinity Index of 14Å (Chlorite) mineral - mm	
D1	3.0	south
D31C	4.0	
C39	3.0	
C83	4.0	
Er8B	2.25	north
Er9	2.50	
Er15	2.0	
Er19	2.25	

TABLE 5.1(b)

Crystallinity indices of the 14Å (chlorite) mineral - as peak width (mm) at ½ peak height. Note the decrease in index towards the north.

5.2.4 Results of Microchemical Studies

Results of the microchemical analyses are presented in Tables 5.2, 5.3, 5.4, 5.5 and 5.6. Microchemical analysis of chlorites was done mainly using the JEOL 733 Superprobe with analytical facilities and conditions as outlined in subsection (4.1.4). The optimum specimen current used was between 3 and 4 nA. All estimates of H_2O content were done by difference (100 - Total % Oxide), while total iron content (Fe) was estimated rather than Fe^{2+} and Fe^{3+} separately. Foster (1962) analysed 150 chlorite chemical studies from many parts of the world and showed that total H_2O varied from 9 - 15% and depended strongly on Fe content. The water contents estimated in the analyses presented in the Tables (5.2 - 5.6) fall within this range. It was also this range that differentiated the acceptable results from the unacceptable ones, hence although up to thirty analyses per sample were usually aimed at, only those with range of H_2O composition between 9 - 15% and lower than 0.5% K_2O were used in most cases.

5.2.5 Discussion of Results

There is no place in the chlorite lattice for large cations like Na^+ (0.95 - 0.98Å), K^+ (1.33) and Ca^{2+} (0.94 - 0.99) and any analyses containing more than 0.5% of Na_2O, K_2O or CaO would, according to Foster (1962) suggest interlayering or admixture with mica and/or montmorillonite. There is some amount of sodium in most analyses and the mean value of percentage Na_2O tends to decrease from 0.74% (Sample D31) to 0.28% (Sample Er11b). The values of K_2O are generally low, except in Sample C39 where a mean value of 0.599 was obtained.

	1		2		3		4		5		6	
ELMT	%OXIDE	FORMULA	%OXIDE	FORMULA	%OXIDE	FORMULA	%OXIDE	FORMULA	%OXIDE	FORMULA	%OXIDE	FORMULA
Na	0.102	0.028									1.508	0.417
Mg	34.67	7.279	34.436	7.248	35.313	7.551	35.778	7.759	36.784	8.162	33.310	7.090
Al	17.14	2.845	17.090	2.844	17.803	3.010	17.211	2.951	18.586	3.261	18.657	3.140
Si	33.67	4.742	34.002	4.801	34.691	4.976	35.163	5.116	33.832	5.036	33.289	4.752
K							0.210	0.039	0.134	0.025		
Ca	0.29	0.044	0.346	0.052	0.207	0.032	0.275	0.043	0.588	0.094	0.142	0.022
Ti												
Fe^{+}	1.32	0.155	1.420	0.168	1.068	0.128	1.582	0.192	1.970	0.245	1.244	0.149
H_2O*	12.76		12.508		10.778		9.741		8.086		11.759	

	7		8		9		10		MEAN	MEAN½
ELMT	%OXIDE	FORMULA	%OXIDE	FORMULA	%OXIDE	FORMULA	%OXIDE	FORMULA	%OXIDE	FORMULA
Na	0.373	0.101	1.963	0.550	2.482	0.685	1.013	0.286	0.744	0.103
Mg	33.307	6.906	32.756	7.054	32.781	6.950	33.488	7.269	34.262	3.648
Al	17.751	2.910	18.464	3.144	16.639	2.789	17.245	2.960	17.658	1.486
Si	33.116	4.606	34.335	4.960	33.787	4.805	35.987	5.240	34.187	2.428
K	0.103	0.018	0.102	0.019	0.100	0.018	0.044	0.008	0.116	0.021
Ca	0.220	0.033	0.168	0.026	0.264	0.040	0.454	0.071	0.296	0.0217
Fe^{+}	1.161	0.135	1.485	0.179	1.390	0.165	1.809	0.220	1.445	0.087
H_2O*	13.947		10.727		12.537		9.729		11.257	

Half Cell Formula: $Mg_{3.648}\ (Si_{2.428}\ Al_{1.486}\ Fe_{0.087})\ O_{10}\ (OH)_8$

TABLE 5.2 Sample D31 (Knockan) - chlorite microchemistry showing ten of the analyses, the mean percentage oxide and the half cell formula. Percentage of water estimated by difference.

	1		2		3		4		5		6	
ELMT	%OXIDE	FORMULA	%OXIDE	FORMULA	%OXIDE	FORMULA	%OXIDE	FORMULA	%OXIDE	FORMULA	%OXIDE	FORMULA
Na	0.503	0.138	0.571	0.160	0.518	0.146	0.738	0.208	0.266	0.076	0.466	0.132
Mg	32.466	6.850	31.789	6.864	33.719	7.283	32.537	7.056	32.809	7.209	31.983	6.972
Al	18.501	3.087	17.367	2.965	19.195	3.278	20.027	3.434	19.995	3.474	19.763	3.406
Si	31.186	4.414	33.102	4.795	33.383	4.837	32.670	4.752	34.873	5.140	35.025	5.122
K	0.378	0.068	0.899	0.166	0.236	0.044	0.300	0.056	0.875	0.165	0.891	0.166
Ca	1.758	0.267	2.356	0.366	0.143	0.022	0.239	0.037	0.297	0.047	0.097	0.015
Fe^{+}	1.715	0.203	2.367	0.287	2.060	0.250	2.752	0.335	2.057	0.254	2.114	0.259
H_2O^{*}	13.353		11.548		10.515		10.537		8.807		9.506	

	7		MEAN	MEAN ½
ELMT	%OXIDE	FORMULA	%OXIDE	FORMULA
Na	0.695	0.198	0.537	0.076
Mg	33.455	7.330	32.680	3.540
Al	20.132	3.488	19.283	1.652
Si	33.440	4.915	33.383	4.427
K	0.613	0.115	0.599	0.056
Ca	0.267	0.042	0.737	0.057
Fe^{+}	2.006	0.247	2.153	0.131
H_2O^{*}	9.331		10.514	

Half Cell Formula: $(Mg_{3.540}\ Al_{0.079}\ Fe_{0.131})\ (Si_{2.427}\ Al_{1.573})\ O_{10}\ (OH)_8$

TABLE 5.3 Sample C39 (Cnoc a' Chaoruinn) - chlorite microchemistry showing some of the analyses, the mean percentage oxide and the half cell formula. Percentage of water estimated by difference.

	1		2		3		4		5	
ELMT	%OXIDE	FORMULA	%OXIDE	FORMULA	%OXIDE	FORMULA	%OXIDE	FORMULA	%OXIDE	FORMULA
Na			0.254	0.090			0.417	0.152	0.569	0.200
Mg	30.677	8.548	31.541	8.535	33.159	9.048	30.690	8.578	31.967	8.631
Al	19.657	4.331	20.448	4.375	20.095	4.335	19.234	4.250	20.636	4.406
Si	32.351	6.047	32.751	5.945	32.141	5.883	31.877	5.976	32.392	5.867
K	0.039	0.009			0.107	0.025	0.073	0.018		
Ca	0.419	0.084	0.526	0.102	0.359	0.070	0.599	0.120	0.215	0.042
Ti	0.087	0.012			0.022	0.003				
Mn	0.147	0.023			0.139	0.021	0.080	0.013	0.143	0.022
Fe	4.642	0.726	5.700	0.865	3.741	0.573	5.608	0.879	5.684	0.861
H_2O*	11.98		8.78		10.24		11.42		8.39	

	6		7		8		9		10	
ELMT	%OXIDE	FORMULA	%OXIDE	FORMULA	%OXIDE	FORMULA	%OXIDE	FORMULA	%OXIDE	FORMULA
Na	0.345	0.125	0.306	0.113	0.263	0.091	0.811	0.282	0.396	0.146
Mg	30.616	8.507	29.948	8.469	32.740	8.702	31.248	8.348	30.897	8.776
Al	19.113	4.199	19.049	4.259	20.811	4.374	19.900	4.204	19.129	4.296
Si	32.328	6.026	31.730	6.019	33.056	5.894	34.046	6.102	31.034	5.914
K	0.066	0.016	0.037	0.009			0.107	0.024	0.042	0.010
Ca	0.897	0.179	0.357	0.073	0.226	0.043	0.245	0.047	0.132	0.027
Ti			0.118	0.017	0.107	0.014			0.011	0.002
Mn	0.186	0.029					0.053	0.008	0.112	0.018
Fe	5.538	0.863	5.903	0.936	5.568	0.830	6.238	0.935	5.182	0.826
H_2O*	10.91		12.55		7.23		7.35		13.07	

	11		12		13		MEAN	MEAN ½
ELMT	%OXIDE	FORMULA	%OXIDE	FORMULA	%OXIDE	FORMULA	%OXIDE	FORMULA
Na	0.613	0.226			0.364	0.059	0.334	0.074
Mg	31.285	8.872	35.273	7.951	32.067	4.017	31.701	4.290
Al	19.179	4.300	20.753	3.699	19.706	1.952	19.824	2.126
Si	31.201	5.935	26.796	4.052	31.823	2.674	31.810	2.003
K			0.109	0.021	0.136	0.015	0.080	0.017
Ca	0.169	0.034	1.168	0.189	0.251	0.023	0.428	0.084
Ti	0.064	0.009	0.078	0.009			0.070	0.009
Mn	0.041	0.007	0.076	0.010	0.101	0.007	0.108	0.017
Fe	3.987	0.634	6.288	0.795	5.169	0.363	5.327	0.405
H_2O*	13.46		9.46		10.38		10.402	

Half Cell Formula: $(Mg_{4.290}\ Mn_{0.017}\ Ti_{0.009}\ Al_{1.029}\ Fe_{0.405})\ (Si_{2.903}\ Al_{1.097})\ O_{10}\ (OH)_8$

TABLE 5.4

Sample Er - 9 (Eriboll) - chlorite microchemistry showing thirteen of the analyses, the mean percentage oxide and the half cell formula. Percentage of water estimated by difference.

	1		2		3		4		5		6	
ELMT	%OXIDE	FORMULA	%OXIDE	FORMULA	%OXIDE	FORMULA	%OXIDE	FORMULA	%OXIDE	FORMULA	%OXIDE	FORMULA
Na			0.210	0.079			0.152	0.056	0.336	0.123	0.171	0.062
Mg	25.937	6.974	28.664	8.261	30.807	8.653	29.381	8.259	28.279	7.999	30.719	8.608
Al	15.707	3.339	18.551	4.227	18.892	4.196	18.160	4.036	18.703	4.183	19.964	4.423
Si	41.657	7.513	30.795	5.953	32.079	6.045	33.274	6.274	32.841	6.232	31.330	5.890
K	0.041	0.009	0.050	0.012							0.055	0.013
Ca	0.420	0.081	0.174	0.036	0.185	0.037	0.257	0.052	0.236	0.048	0.099	0.020
Ti	0.183	0.025			0.036	0.005	0.047	0.007	0.090	0.013	0.034	0.005
Mn	0.058	0.009	0.133	0.022	0.099	0.016						
Fe	5.611	0.840	8.581	1.387	5.714	0.900	6.629	1.045	7.097	1.126	5.791	0.910
H_2O*	10.39		12.84		12.19		12.10		12.42		11.84	

	7		8		9		10		11		12	
ELMT	%OXIDE	FORMULA	%OXIDE	FORMULA	%OXIDE	FORMULA	%OXIDE	FORMULA	%OXIDE	FORMULA	%OXIDE	FORMULA
Na	0.502	0.181	0.520	0.188	0.217	0.079	0.566	0.205	0.585	0.213	0.181	0.065
Mg	31.077	8.602	30.719	8.539	30.819	8.605	31.518	8.750	30.215	8.460	30.708	8.454
Al	19.433	4.253	19.470	4.279	19.547	4.316	19.418	4.263	19.507	4.318	19.356	4.213
Si	32.012	5.944	31.702	5.911	31.636	5.926	31.718	5.907	30.807	5.786	32.064	5.921
K	0.057	0.014					0.042	0.010	0.048	0.011		
Ca	0.093	0.018	0.331	0.066	0.252	0.051	0.159	0.032	0.290	0.058	0.160	0.032
Ti	0.155	0.022			0.012	0.002			0.137	0.019	0.404	0.056
Mn	0.094	0.015	0.094	0.015	0.101	0.016			0.098	0.016	0.432	0.067
Fe	6.159	0.956	6.705	1.046	6.134	0.961	5.796	0.903	8.059	1.266	7.379	1.140
H_2O*	10.42		10.46		11.28		10.78		10.25		9.32	

	13		MEAN	MEAN ½
ELMT	%OXIDE	FORMULA	%OXIDE	FORMULA
Na	0.644	0.183	0.314	0.130
Mg	31.078	6.802	29.994	4.114
Al	19.122	3.309	18.910	2.052
Si	30.835	4.527	32.52	2.993
K	0.040	0.007	0.048	0.006
Ca	0.269	0.042	0.225	0.022
Ti	0.083	0.009	0.118	0.008
Mn	0.131	0.016	0.138	0.011
Fe	6.544	0.803	6.631	0.511
H_2O*	11.25		11.195	

Half Cell Formula: $(Mg_{4.114}\ Mn_{0.011}\ Ti_{0.008}\ Al_{1.045}\ Fe_{0.511})\ (Si_{2.993}\ Al_{1.007})\ O_{10}\ (OH)_8$

TABLE 5.5

Sample Er - 10 (Eriboll) - chlorite microchemistry showing thirteen of the analyses, the mean percentage oxide and the half cell formula. Water percentage estimated by difference.

	1		2		3		4		5		6	
ELMT	%OXIDE	FORMULA	%OXIDE	FORMULA	%OXIDE	FORMULA	%OXIDE	FORMULA	%OXIDE	FORMULA	%OXIDE	FORMULA
Na	0.219	0.061	0.419	0.116	0.290	0.080	0.245	0.068	0.332	0.092	0.165	0.045
Mg	29.960	6.200	30.569	6.536	30.376	6.447	28.756	6.123	30.146	6.405	29.298	6.206
Al	19.406	3.285	19.086	3.227	19.071	3.200	17.274	2.908	18.527	3.113	19.029	3.187
Si	28.918	4.153	29.522	4.235	29.798	4.243	32.258	4.608	29.054	4.141	29.056	4.129
K	0.071	0.013			0.039	0.007						
Ca			0.152	0.023	0.042	0.006	0.213	0.033	0.192	0.029	0.150	0.023
Ti	0.078	0.008	0.055	0.006			0.032	0.003			0.087	0.009
Mn	0.139	0.017	0.241	0.029	0.193	0.023	0.091	0.011	0.250	0.030	0.128	0.015
Fe	8.217	0.987	6.456	0.774	6.261	0.745	7.452	0.890	6.907	0.823	7.449	0.885
H_2O*	13.81		13.43		13.93		13.62		14.38		14.54	

	MEAN	MEAN ½
ELMT	%OXIDE	FORMULA
Na	0.278	0.039
Mg	29.851	3.160
Al	18.732	1.577
Si	29.768	2.126
K	0.055	0.005
Ca	0.150	0.011
Ti	0.063	0.003
Mn	0.174	0.010
Fe	7.124	0.425
H_2O*	13.952	

TABLE 5.6

Sample Er - 11b (Eriboll) - chlorite microchemistry showing some of the analyses, the mean percentage oxide and the half cell formula. Water percentage estimated by difference.

Half Cell Formula: $(Mg_{3.160}\ Mn_{0.010}\ Ti_{0.003}\ Fe_{0.128})\ (Si_{2.126}\ Al_{1.577}\ Fe_{0.297})\ O_{10}\ (OH)_8$

Most of the K_2O in Sample C39 must have come from mica which is in very close admixture with chlorite (Plate 5.16). The value of 0.737 for mean percentage CaO in Sample C39 could be attributed to the presence of $CaCO_3$ in the system, with which the chlorite is likely to be in non-chemical admixture.

The variation of the main elements Mg, Al and Fe with respect to Si are expressed as A, F', M, where

$$A = \frac{Al_2O_3}{SiO_2}$$

$$F' = \frac{FeO}{SiO_2}$$

$$M = \frac{MgO}{SiO_2}$$

and $A + F' + M = 100$

The AF'M values of acceptable analyses are presented per sample in Figure 5.4. The most noticeable feature of Figure 5.4 is the gradual increase in F' value with increase in temperature. The temperatures for Samples D31c , C39, Er9, Er10 and Er11b are as determined in Chapter Four, using the calcite/dolomite solvus geothermometer. If the relationship between FeO/SiO_2 and temperature in this chlorite is a true one, then it is most likely to be more easily expressed in terms of FeO/MgO against temperature. This is shown in sub-section 5.3

5.2.6 Estimate of Half Cell Formula and Type of Chlorite

The half cell structural formula can be estimated either from the full formula given in the printout following

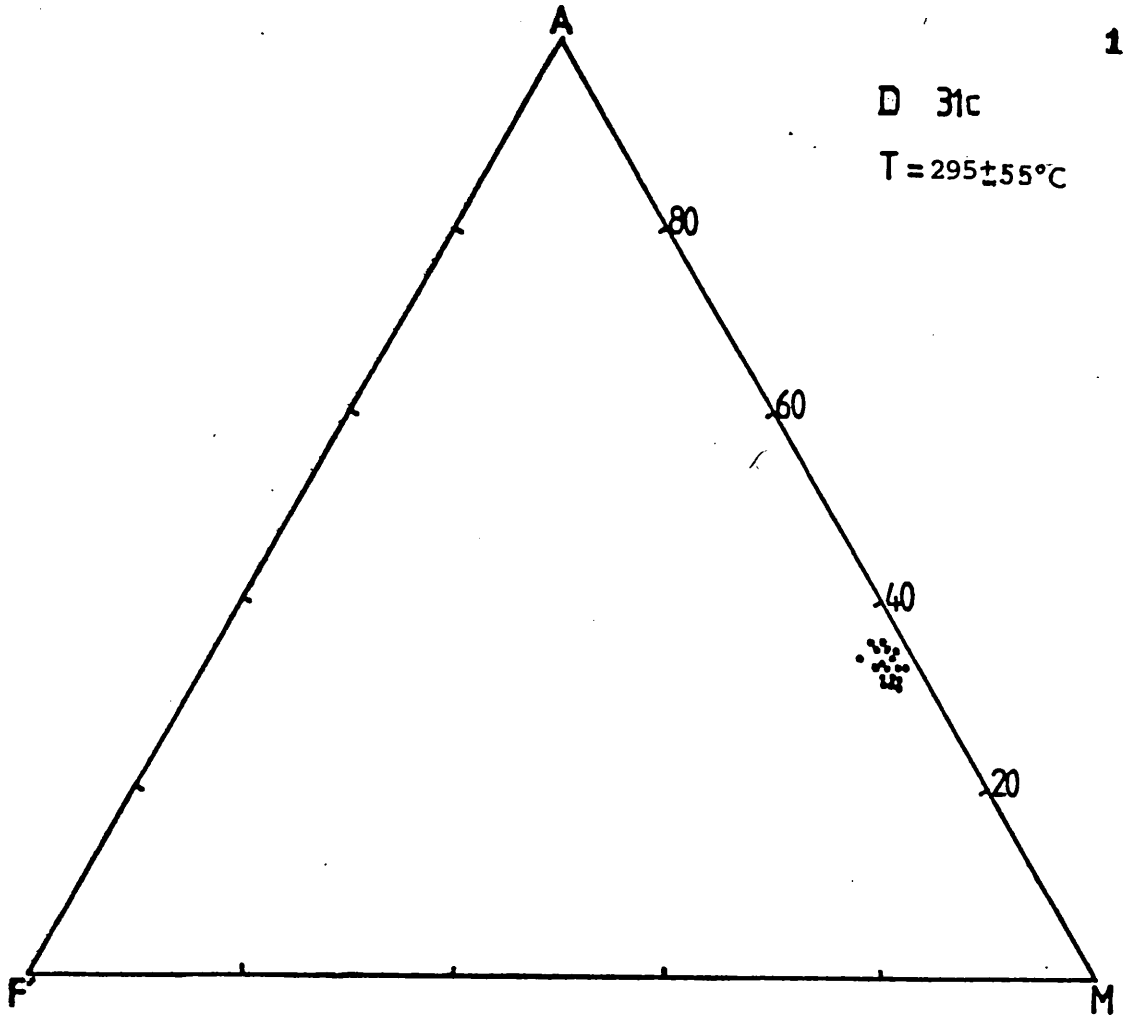

[a]

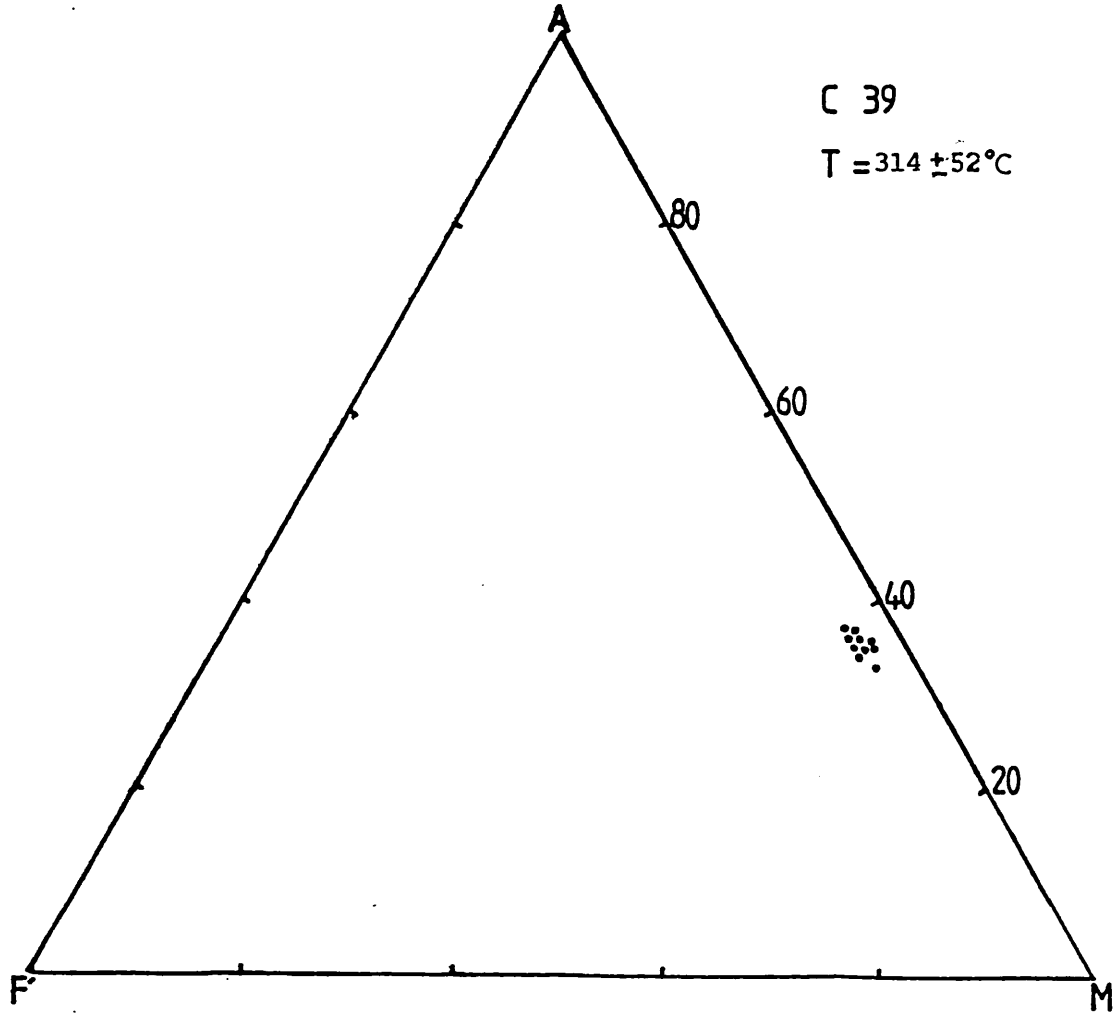

[b]

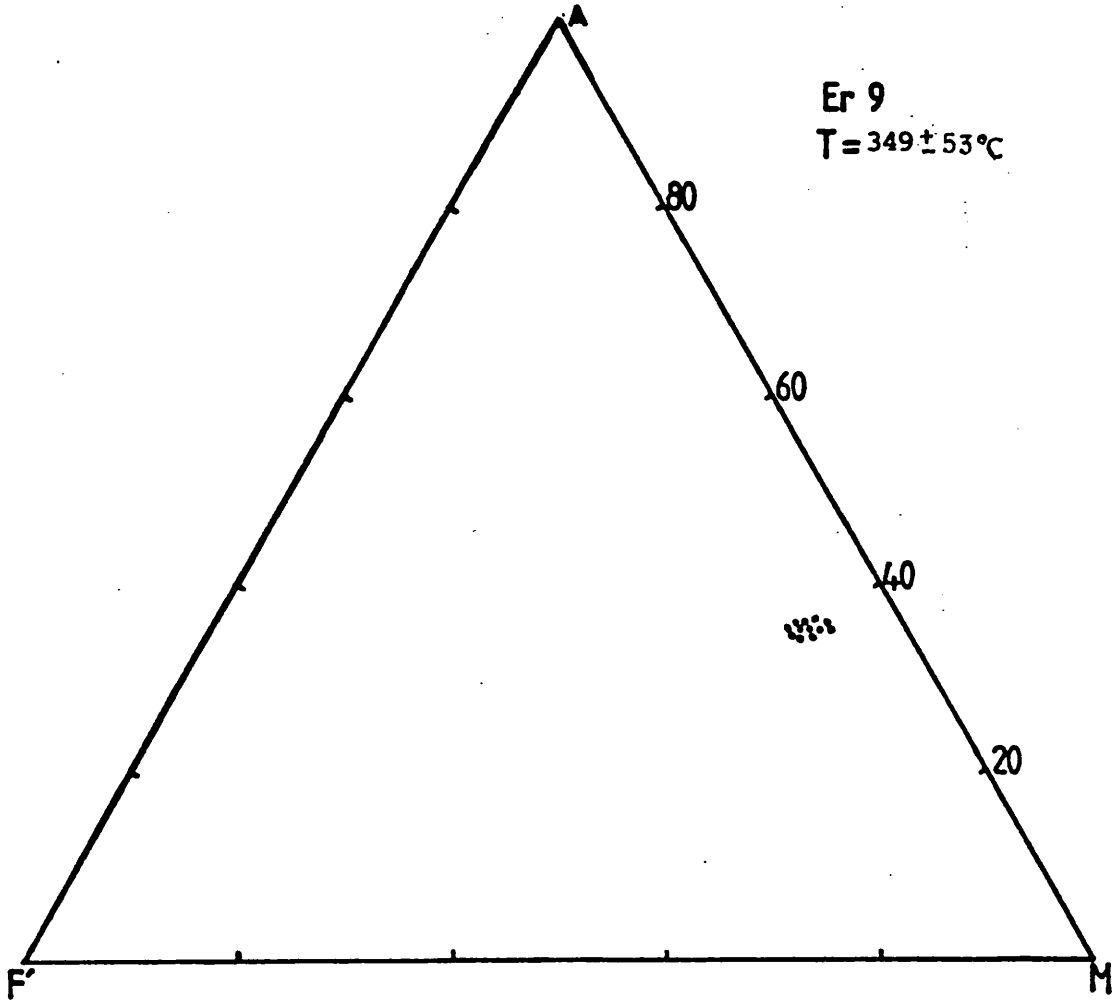

[c]

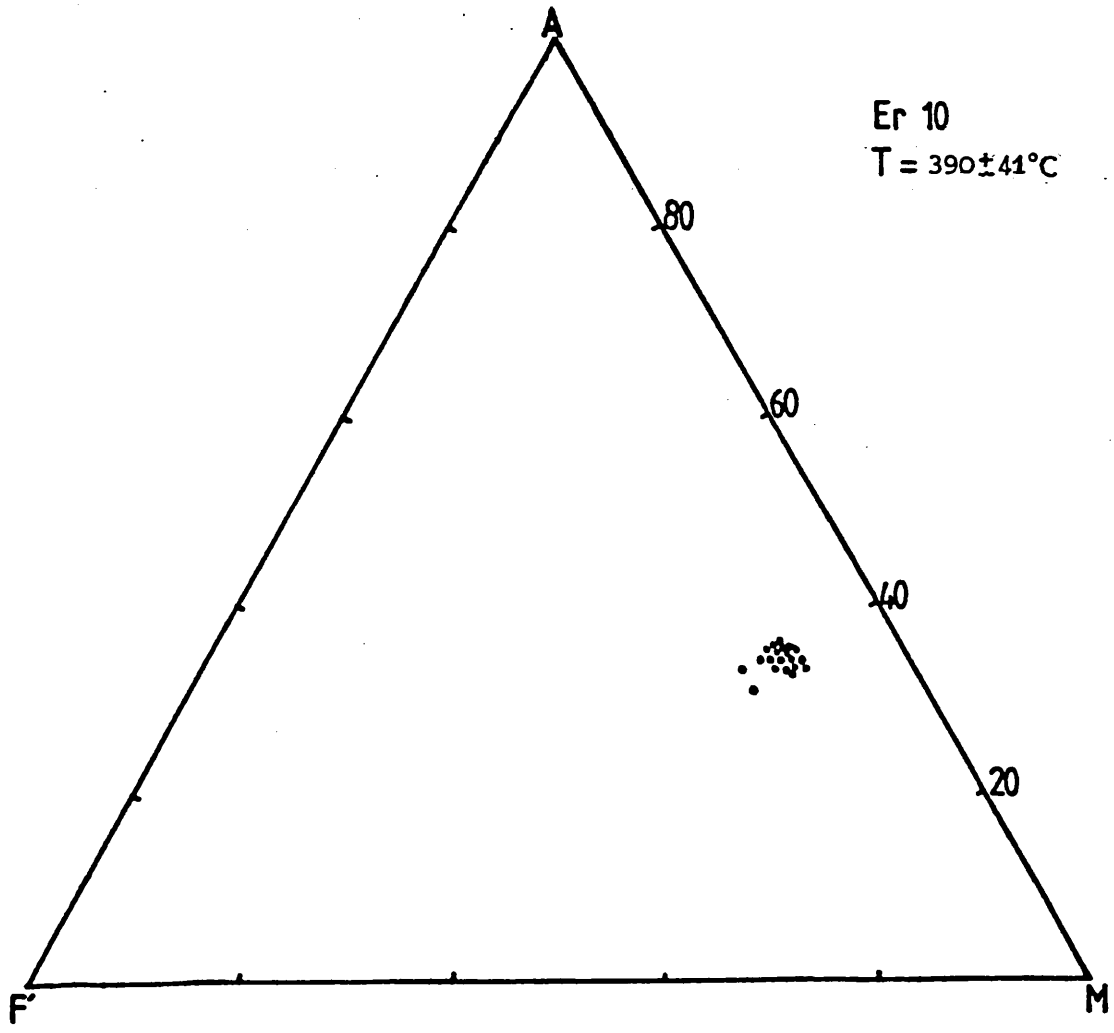

[d]

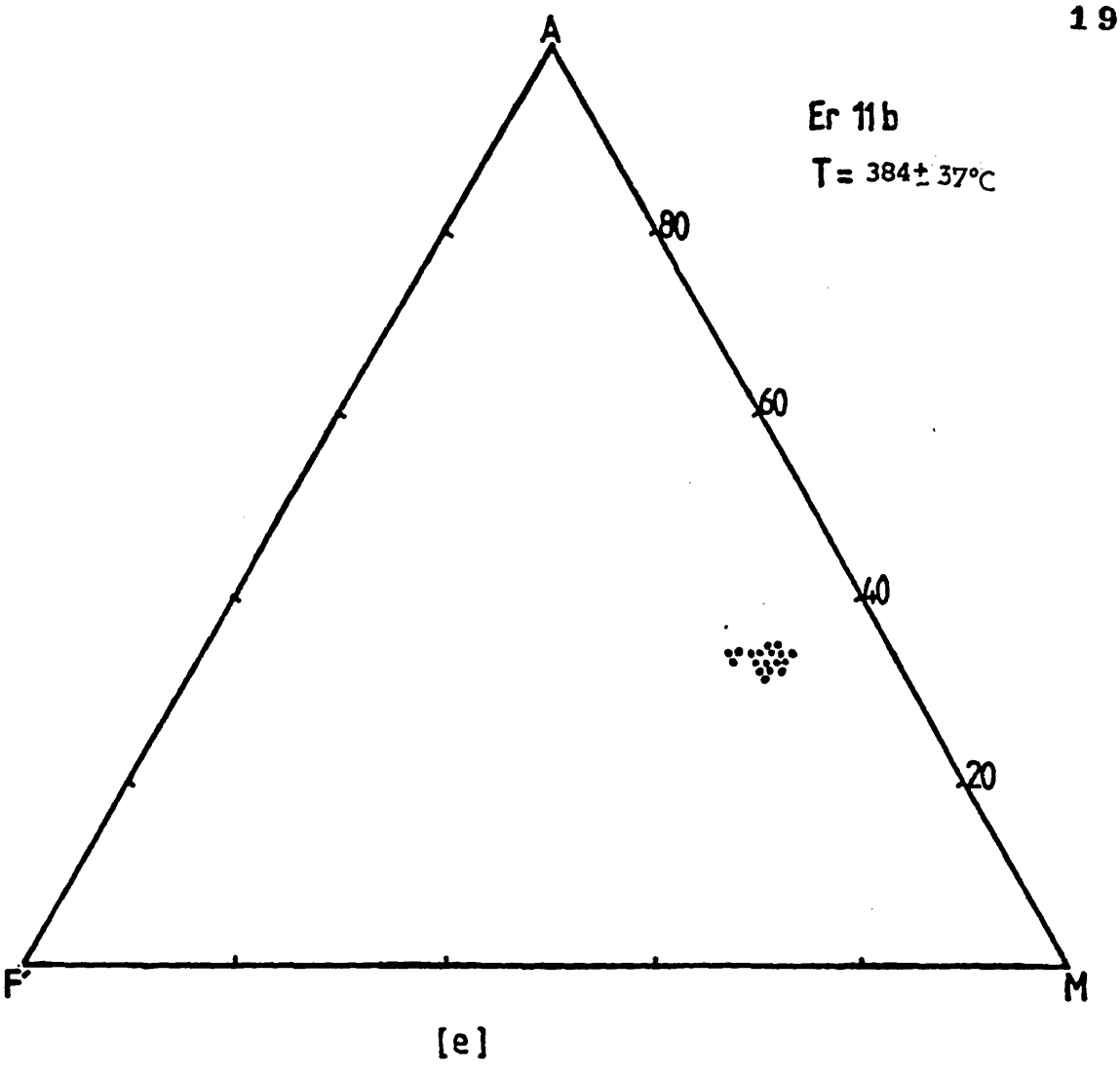

Fig.5.4

Chlorite microchemistry in AF'M space, and its variation with change in temperature.

(a) D31c-Knockan.

(b) C39 -Cnoc a' chaoruinn.

(c) Er-9 -Eriboll.

(d) Er-10 "

(e) Er-11b "

Note the gradual increase in F' towards Eriboll, and with change in temperature.

the EDS - X-ray analysis, or using the method suggested by Foster (1962). The formulas were estimated on the basis of the theoretical O(OH) content of the unit cell of chlorite being $O_{20}(OH)_{16}$. Also using the general formula $X_mY_4O_{10}(OH)_8$ for the half cell, m is usually 6 or somewhat less, but not more (Foster 1962). The half cell formulas resulting are therefore:

(i) Sample D31: $(Mg_{3.648}(Si_{2.428}Al_{1.486}Fe_{0.087})O_{10}(OH)_8$

(ii) Sample C39: $(Mg_{3.540}Al_{0.079}Fe_{0.131})(Si_{2.427}Al_{1.573})O_{10}(OH)_8$

(iii) Sample Er9: $(Mg_{4.290}Mn_{0.017}Ti_{0.009}Al_{1.029}Fe_{0.405})$
$(Si_{2.903}Al_{1.097})O_{10}(OH)_8$

(iv) Sample Er10: $(Mg_{4.114}Mn_{0.011}Ti_{0.008}Al_{1.045}Fe_{0.511})$
$(Si_{2.993}Al_{1.007})O_{10}(OH)_8$

(v) Sample Er11b: $(Mg_{3.160}Mn_{0.010}Ti_{0.003}Fe_{0.128})$
$(Si_{2.126}Al_{1.577}Fe_{0.297})O_{10}(OH)_2$

The high Mg - content of these chlorites necessitates the application of the species name - Clinochlore, after Bayliss (1975).

5.3 TEMPERATURE DEPENDENCE OF FeO/MgO RATIOS

The relationship of the ratio FeO/MgO to the rock temperature is shown in Figure 5.5. There is a slight indication of linear dependence between 280°C and about 400°C, giving a computed equation of the form;

$$T\ (^{\circ}C) = 278.27 + 456.33\ FeO/MgO \quad - - - - \quad 5.2$$

Sample Number	Mean %Mg	Mean %Fe	Mean %MgO	Mean %FeO	$\frac{\bar{Fe}}{\bar{Mg}}$	$\frac{\bar{FeO}}{\bar{MgO}}$	Temp. (^{o}C)
D31C	19.983	1.203	32.866	1.440	0.060	0.044	$295.0^{\pm}$ 55
C39	19.848	1.668	33.358	2.146	0.084	0.064	$314.0^{\pm}$ 52
Er9	18.796	4.106	31.167	5.283	0.218	0.170	$349.0^{\pm}$ 53
Er10	17.956	5.208	29.774	6.700	0.290	0.225	$390.0^{\pm}$ 41
Er11b	17.670	5.488	29.299	7.061	0.311	0.241	$384.0^{\pm}$ 37

TABLE 5.7

Mg and Fe data from Tables 5.2 to 5.6, used for constructing Fig. 5.6.

if the error bars are not considered. The presence of error bars on the estimated temperatures, as shown in fig. 5.5, suggests a band rather than a unique line of relationship between T(^{o}C) and FeO/MgO. Within this band the actual intercept on the T axis may be more or less than 278, while the gradient of the line, if it is unique, may not be exactly 456.

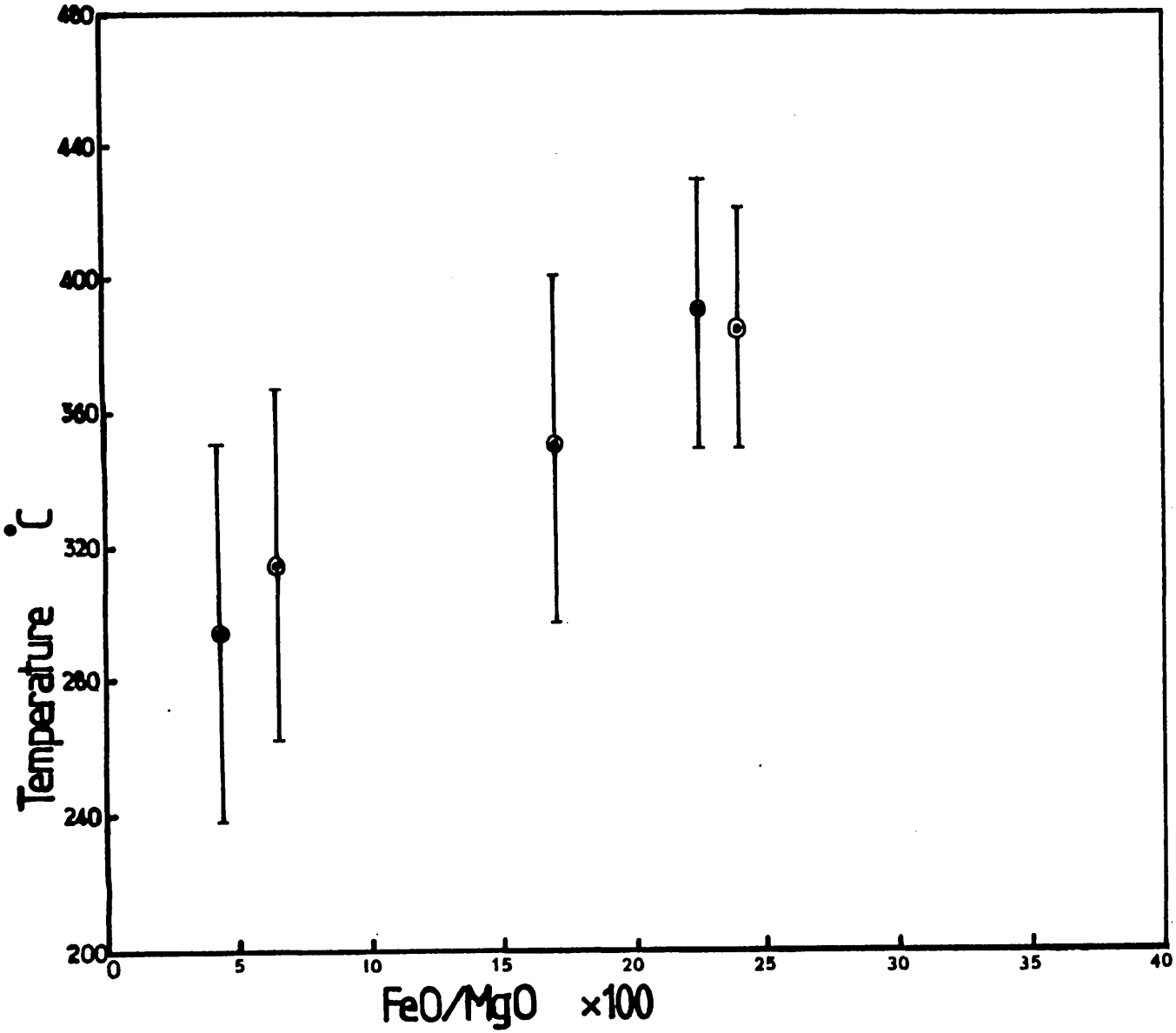

Fig.5.5 Plot of the FeO/MgO ratios in chlorite against temperature estimated from calcite/dolomite geothermometry in chapter four. Vertical bars represent standard deviation ,asshown in Table 5.7 .

However, Eqn. 5.2 suggests that no iron will be incorporated in a lattice of clinochlore at temperatures below or up to 278°C. Above this temperature, provided the availability of Fe is guaranteed, the intake of Fe should increase linearly (or nearly so) with temperature. Table 5.7 is the data source for Figure 5.5

5.4 APPLICATION OF THE TEMPERATURE DEPENDENCE OF FeO/MgO RATIOS

Chlorite has a very wide stability range - from conditions on the bottoms of modern estuaries (Powers, 1957), through the whole of the greenschist facies range to about 710°C (Nelson and Roy, 1958), or 720°C (Yoder 1952, Fawcett and Yoder 1966) under laboratory conditions. Chlorite stability in natural rocks has not been reported at these high temperatures.

The upper limit of stability reported from experiments can be pushed up to over 800°C by increasing the water vapour pressure in a laboratory synthesis over 600MPa (Fawcett and Yoder, 1966). The synthesis of chlorite was thought to always proceed by the nucleation of the 7Å polymorph ("aluminous serpentine", Yoder 1952; "septechlorite", Nelson and Roy, 1958 Turnock, 1950), which slowly converted to the 14Å normal chlorite. But more recent observations show that pre-tectonic or syn-tectonic replacement of white mica by chlorite could take place all the way from burial (Craig et al. 1982), to metamorphism (Weber, 1976; 1980).

As Table 5.1 and Plate 5.1 show, chlorite in the Durness Formation is mainly found along the Moine Thrust, apart from local occurences near intrusive bodies. In both

situations they are genetically related to the original mica (illite/sericite). They nucleate on or replace the mica, being aided in the process by ingress of Mg^{2+} ion-containing fluids during deformation. The presence of these fluids over such a long zone and for what must have been a very long time (since upper Ordovician times) probably resulted in an equilibrium between the chemistry of the respective minerals and the environment. Hence application of the newly derived T/Mg/Fe relationship would only yield meaningful results in a metamorphic environment where there appears to have been chemical equilibrium and where one of the phases is clinochlore.

Secondly, since total pressure, water pressure and oxygen fugacity are known to affect the stability of chlorite species, it is very likely that pressure will also affect the FeO/MgO ratios in ways that could make meaningless any determinations of temperatures by means of this method. Estimates of tectonic stress in the Moine Thrust Zone have produced values lower than 100MPa as the deviatoric stress (White, 1979; Wheathers et al, 1979), and this will be taken as the upper boundary condition for equation 5.2.

Hence, if the stress in the environment is estimated to be about 100MPa and there are indications that the mineral system maintained equilibrium with the environment, given, of course, that the rock contained clinochlore in the first instance, it may be possible to estimate rock paleotemperatures, using equation 5.2, or a modification of it, from the microchemical analysis of this chlorite phase.

5.5 ESTIMATE OF FLUID PRESSURE ACCOMPANYING THE LAST PHASE OF MOINE THRUSTING

5.5.1 Introduction

Evidence presented in Chapter Four (see Plates 4.5 and 4.6) suggests that fluids must have accompanied or aided the emplacement of the Moine Thrust, at least during the last phase of the orogeny. Also the preceeding analysis in this Chapter showing a gradual and progressive readjustment in chlorite material microchemistry close to the thrust plane, may indirectly suggest the presence of a fluid medium to contain and exchange chemical species with the evolving minerals. The bulk of the fluids would, for kinematic and tectonic reasons, be confined to that part of the thrust plane (above and below) which takes active part in basal sliding. It is possible, by using thermomechanical relationships, to estimate fluid pressure values, the accuracy of which will depend on the accuracy of the equations, and the dependability of the physical parameters used.

5.5.2 The Argument

The physical statements adopted in this analysis (see equations 5.3 and 5.4 below) are the same as, and are based on the argument developed by Raleigh and Evernden (1981, P175). The basic assumption is that a pore in the Durness carbonates within or very close to the datum on which the Moine Thrust was later placed, contained fluid (water) of volume V_1, pressure P_1 and temperature (of Foreland) T_1. Due to thrusting there was a volume change, dV of both rock pore and the water in it due to temperature increase of dT, and pressure increase dP,
It is assumed that the volume change of the water and the pore (rock) are equal, that is, no voids developed in the rock as a result of thrusting, it is possible that for the

water

$$dV = V\alpha_w dT - V\beta_w dP \quad ---- \quad 5.3$$

and for the rock

$$dV = V\alpha_r dT - V\beta_r dP \quad ---- \quad 5.4$$

α_w and α_r are the thermal expansion eoefficients of water and rock, while β_w and β_r are the compressibilities of water and rock and dP is rise in fluid pressure.

In the compressibility equation of Birch (1966)

$$\beta = -\frac{1}{V}\left(\frac{dV}{dP}\right)_T = 1/\rho \left(\frac{d\rho}{dP}\right)_T \quad ---- \quad 5.5$$

dV/dP is intrin sically negative, hence β is a positive number having the dimension of reciprocal of stress or pressure (MPa^{-1}). For this reason - $V\beta_r dP$ is used as the last term in equation 5.4, rather than the positive term as used by Raleigh and Evernden (1981). Combining equations 5.3 and 5.4,

$$V\alpha_w dT - V\beta_w dP = V\alpha_r dT - V\beta_r dP \quad ---- \quad 5.6$$

$$dT(\alpha_w - \alpha_r) = dP(\beta_w - \beta_r) \quad ---- \quad 5.7$$

$$\frac{dP}{dT} = \frac{\alpha_w - \alpha_r}{\beta_w - \beta_r} \quad ---- \quad 5.8$$

$\alpha_w \gg \alpha_r$, and $\beta_w \gg \beta_r$ (Birch, 1966, Kennedy and Holser, 1966; and Skinner, 1966). Hence at moderate confining pressures,

$$\frac{dP}{dT} \approx \frac{\alpha_w}{\beta_w} \quad ---- \quad 5.9$$

As shown by Kennedy and Holser (1966) α_w/β_w falls between 15 and 20 bar/^oC, hence for any increase in temperature the corresponding fluid pressure increase to keep dP/dT between these limits can be calculated

5.5.3 Addendum

In chapter four it was shown that estimated temperatures are associated with substantial errors. Such errors pose the major problem of affecting dT and hence dP in ways that are difficult to predict. The values of temperature used in these fluid pressure estimates should be regarded as average values, and accordingly the fluid pressures calculated may not be taken as exact values.

5.5.3 Estimate of Fluid Pressure

In order to estimate the rise in fluid pressure accompanying thrusting by means of Equation 5.9, the temperature estimates of Downie, (1981) for the Foreland will be used in conjunction with the temperatures of the Moine Thrust Zone estimated in Chapter Four. Downie estimated a temperature of 200°C for the Foreland at Knockan (see Subsection 4.4.1). This was shown in Chapter Four to increase to 295° in the Durness carbonates of the Moine Thrust Zone of the same area. Hence

$$dT = 95^{\circ}$$

and $$dP = 95^{\circ}C \times 15 \frac{bars}{C} = 1.425 \text{ k bars}$$

$$= 142.5 \text{ MPa}$$

At the Eriboll end on the other hand,

$$dT = 124^{\circ}C$$

and $$dP = 124^{\circ}C \times 15 \frac{bars}{C} = 1.860 \text{ k bars}$$

$$= 186.0 \text{ MPa}$$

5.5.4 Estimate of Confining Pressure during the last phase of Thrusting

When a body of hydrothermal solution accumulates on a fault zone with a pressure greater than the pore water (hydrostatic) pressure, extension fracturing of the rock (hydraulic fracturing) occurs. While the external normal stress tends to keep a fracture closed, the pressure of the fluid on the plane tends to open the fracture, although the shear stresses along the fracture are unaffected by the fluid pressure (Price, 1966; Phillips, 1972). The limiting condition for hydraulic fracturing at depth is when the pore fluid pressure approaches the confining pressure (Price, 1975),

particularly for rocks of low tensile strength. Generally rock failure by hydraulic fracture in the brittle field obeys the following laws:

$$\sigma_3 - P \geq -T \qquad ---- \qquad 5.10$$

and $$\sigma_1 - \sigma_3 \leq 4T \qquad ---- \qquad 5.11 ,$$

Price (1966, 1975); Price and Hancock (1972). Equation 5.10 means that extension failure occurs perpendicular to the axis of least principal stress when the pore fluid pressure P exceeds the magnitude of σ_3 by an amount equal to or greater than the tensile strength T of the rock. Equation 5.11 on the other hand means that the differential stress $(\sigma_1 - \sigma_3)$ must be small enough to render shear impossible. As shown by Phillips (1972, see also Fig 5.6) the Mohr stress circle that satisfies equation 5.11 touches the failure envelope on the abscissa (-Ve T), and gives τ (shear stress) values of about T. Since the tensile strength of rocks is usually very low (2 to 10 MPa, Handin 1966), the shear stress is accordingly kept very low.

In subsection 5.5.2 the simple starting assumption was made that the pore of volume V_1 and initial pressure P_1 was situated in the Durness carbonates within or very close to the datum on which the Moine Thrust was later placed - that is the top of the Durness Formation. Price (1975) showed that hydrostatic pressure in the pore fluids as far down as the water table is one atmosphere (0.10 MPa), and could be regarded as zero pressure.

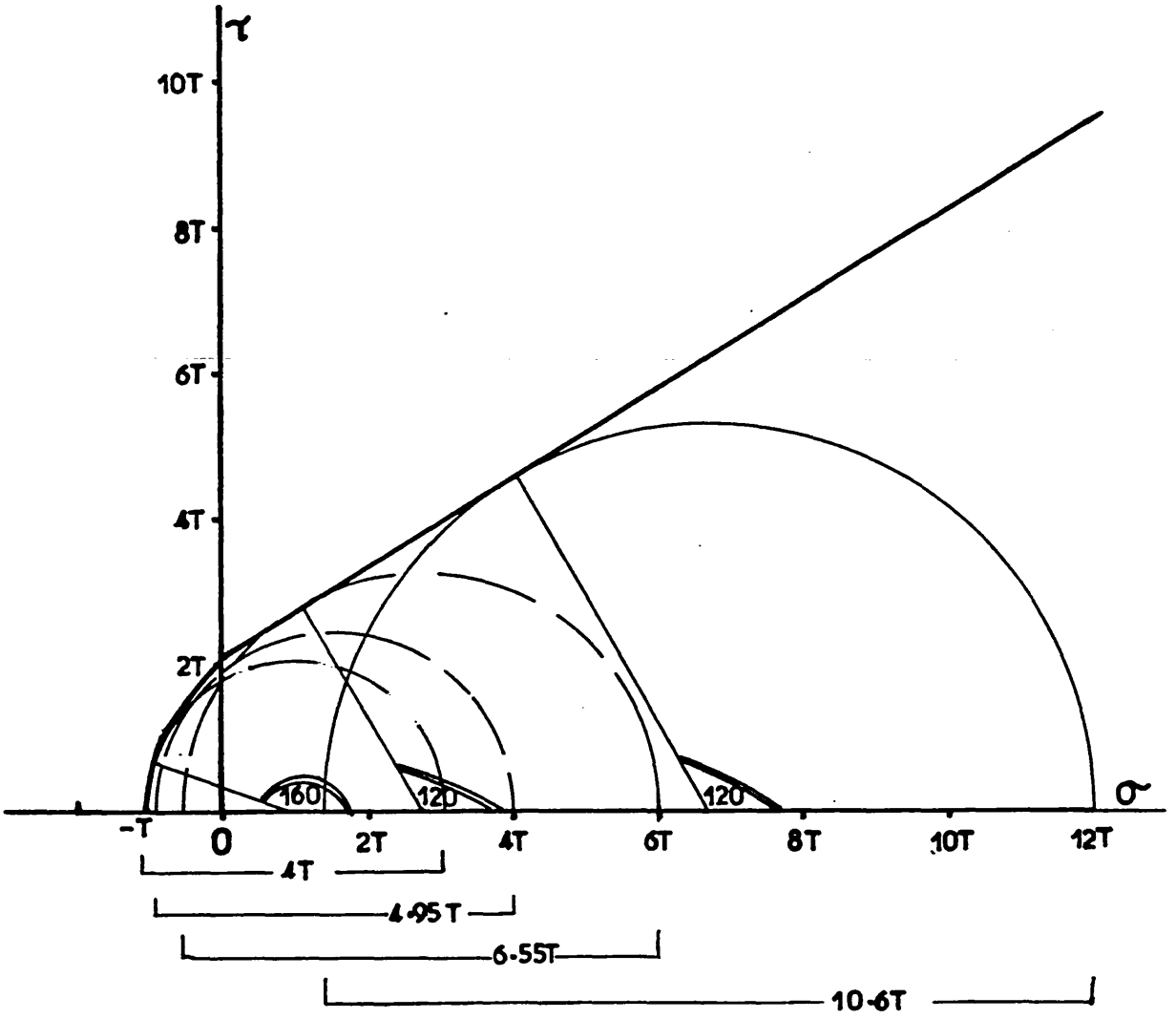

Fig. 5.6 Stress circles representing some effective principal stresses and differential stresses required to bring about the formation of normal faults dipping at 60° or steeper angles.

Hence $P_1 \approx 0 - - - - 5.12$

and $dP_k = P_{2k} = 142.5$ MPa at Knockan

also $dP_e = P_{2e} = 186.0$ MPa at Eriboll

Taking T, the tensile strength of the rock, as 10 MPa, and using Equation 5.10 the confining pressure

$$\sigma_3 = P - T$$
$$= 142.5 - 10$$
$$= 132.5 \text{ MPa at Knockan and}$$
$$186.0 - 10 = 176.0 \text{ MPa at Eriboll}$$

These values cannot be very exact given that the value of T used is not exact and Equations 5.3 to 5.9 may not represent the complete manner of interaction between temperature, pressure and volume in fluid-filled fractures. But the difference in confining pressure between these two ends of the Moine Thrust Zone is consistent with other observations (see for example Coward, 1982).

5.5.5 Discussion:

Apart from the effects of high stress, high strain rates, low temperatures and low confining pressures, the only other physical parameter of well known effect on cataclasis of rocks is fluid pressure. Hydraulic fracturing of rocks leaves a network of fractures and/or veins, and these fractures may be down to the level of a grain size.

Tectonic events, like overthrusting, cause perturbations in the thermal history of rock masses (Roberts, 1972; Oxburgh and Turcotte, 1974; Bickle et al., 1975; Norris and Henley, 1976). The effect on the underthrusted rocks will be to increase pressure very rapidly and then to increase temperature at nearly constant pressure (see Norris and Henley, 1976- Fig. 2). Thus, thermal expansion will be

PLATE 5.2

Optical micrographs of Durness Carbonates. Below the Moine Thrust at Knockan, the Durness Formation is characterised by a dense network of fractures. Some of these are through-the-grain fractures (a), while others contain vein minerals (calcite + quartz, b + c) evidence of fluid activity accompanying thrusting.

Scalebars: a - 0.5 mm
b - 2 cm
c - 2 cm

PLATE 5·2

a

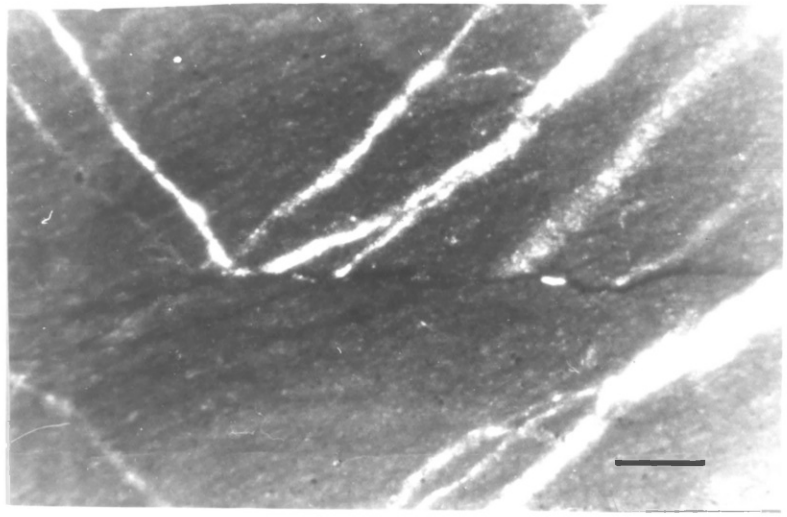

b

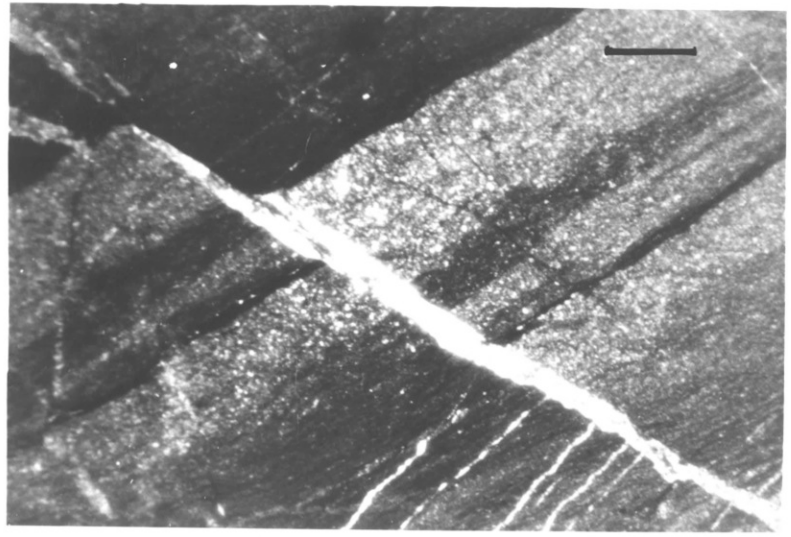

followed immediately by fluid invasion which might produce hydraulic fracturing, vein systems and the eventual loss of water from the rocks. The overthrust rocks on the other hand experience a rapid drop in pressure almost at constant temperature. Both the temperature and pressure then continue to drop uniformly (Norris and Henley, 1976) as uplift and erosion continue. As shown by Margara (1974) subsurface water in rocks undergoing uplift and erosion tends to shrink in volume, allowing fluids from adjacent unaffected areas to move in. The transportation and release of these highly charged fluids into higher crustal levels at low temperatures and pressures results in the deposition, particularly in the fractures, of materials hitherto held in solution, so forming veins of quartz, calcite,etc. (Phillips, 1972; Price, 1975).

In the Durness carbonates below the Moine Thrust at Knockan, fracturing down to grain size level was found to occur very close to (within 1 m) the thrust plane. These fractures are generally stained, and/or healed with calcite-rich cement (Plate 5.2a, b, c). The veins do not normally run along the bedding planes (Plate 5.2b, c), but could transect and displace original bedding (Plate 5.2c) or themselves get transected and displaced by later movements along solution surfaces (Plate 5.2b).

The situation is quite different at the Eriboll end of the thrust zone. Here the higher fluid pressures meant that fluids can actually invade and physically open up bedding planes and solution surfaces (Plate 5.3a). As shown in sub-section 3.4.7, Sample Er 7 from which Plate 5.3a, b was

produced, was collected about 2m below the Moine Thrust at Eriboll. It is obvious that these fluids carry large quantities of quartz and calcite, and the manner of deposition of the quartz in particular close to solution surfaces (Plate 5.3b) makes the genetic relationship of the quartz veins to the solution surfaces strong. Apparently only very high fluid pressures of the type that affected this area are strong enough to "heave up" and sustain the lithostatic load, thereby allowing later generations of dolomite grains (Plates 5.3c, d, e) to grow normal to the original foliation. A detailed description of this peculiar microstructure is presented in Chapter Six.

5.6 CONCLUSION

The occurrence of chlorite below the Moine Thrust in Durness carbonates has enabled a study of the dependence of the microchemistry of the mineral on temperature.

The study confirms earlier observations that the ratio FeO/MgO of chlorites may be an increasing function of grade of metamorphism. It, however, leads to the establishment of a relationship between FeO/MgO and average temperature, of the form:

$$T(^{o}C) = 278.27 + 456.33\ FeO/MgO$$

The importance of this equation is its applicability in paleo-temperature estimate of rocks containing clinochlore. The method of derivation of the equation using natural geological data only may be found to give it advantage over other geo-thermometers fabricated in geological laboratories. But because of the presence of error bars on estimated temperatures, the exactness of this equation cannot be stressed, and it may not therefore be applied in its present form.

PLATE 5.3

Optical micrographs (a, c, d, and e) in crossed polars and Backscattered Electron micrograph (b) of Durness Carbonate from the Moine Thrust Zone at Eriboll.

(a and b) - large amounts of quartz (qtz) and calcite (Cc) are deposited very close to diagenetic solution surfaces and fissures parallel to the foliation.

(c, d and e) - later minerals (mainly dolomite and quartz) tend to grow normal to foliation, and also normal to the earlier formed minerals. See Also Plate 6.13

In c and d the growing dolomite crystals abut on chlorite, while in e they abut on pyrite grains.

Scalebars:

a	-	2.5 mm
b	-	100 μm
c	-	1 mm
d	-	1 mm
e	-	200 μm

PLATE 53

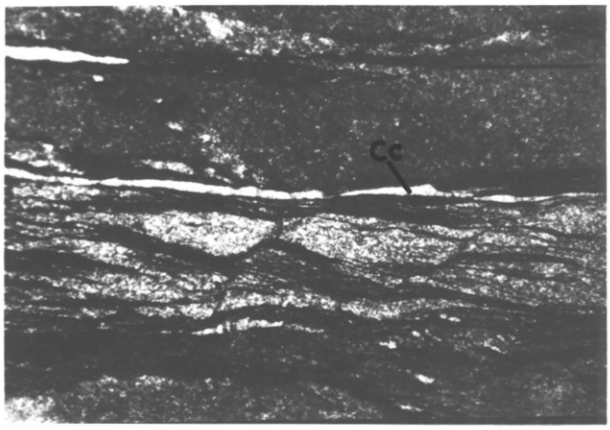

a

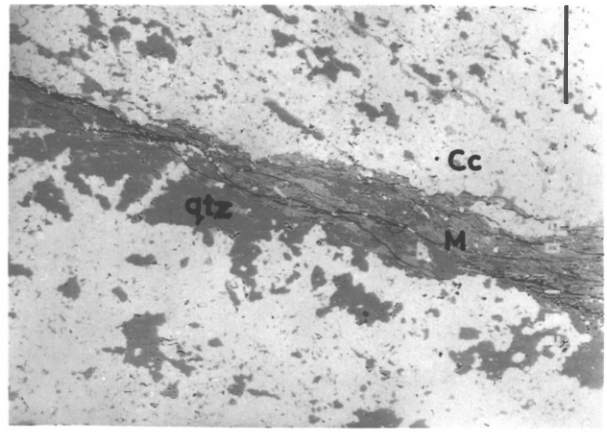

b

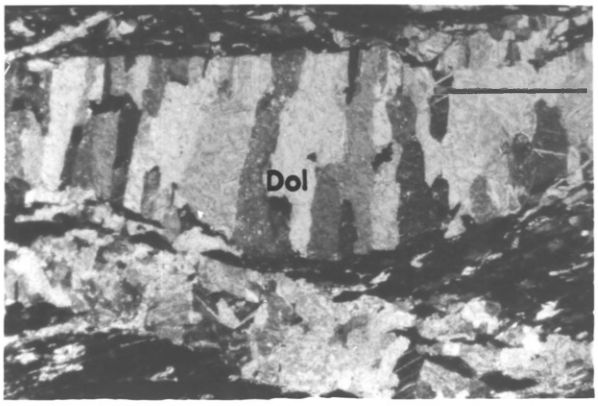

c

d

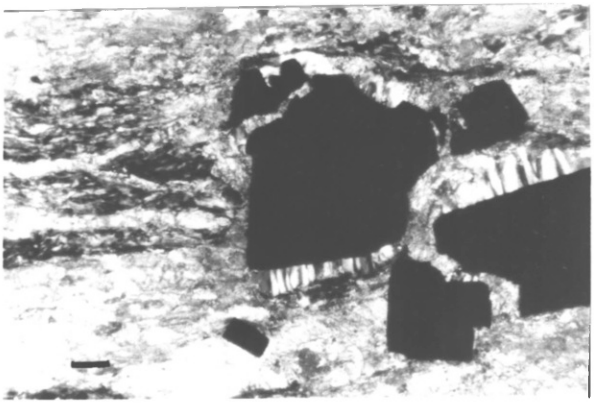

e

At low temperatures chlorites tend to establish equilibrium with the chemical environment by incorporating a limited number of each species of cations, allowing this number to increase, for certain elements, as the temperature increases, while still keeping their 14Å basal characteristic.

Fluid pressures, although transient, have been high during Moine thrusting. The last phase of thrusting might have been aided by fluids of minimum pressure up to 143 MPa and possibly as high as 186 MPa.

Fluid pressure difference between Knockan and Eriboll could have been up to 40 MPa. This difference is likely to have contributed to the change in style of deformation and resultant microstructure in the Durness carbonates of these areas. A detailed analysis of the microstructure follows in Chapter Six.

The confining pressure during the last phase of thrusting in the Moine Thrust Zone might have ranged from 133 MPa to 176 MPa, the upper limit believed to have prevailed at Eriboll.

CHAPTER SIX

MICROSTRUCTURE, FABRIC AND STRESS ANALYSES IN CARBONATE ROCKS OF THE DURNESS FORMATION

6.1.1 Introduction

In this chapter the microstructural evolution of the Durness Formation is traced from the Caledonian Foreland to the Moine Thrust Zone. Those aspects of the foreland-type microstructure that have been passed on to higher strain regimes are discussed and their effect analysed. Along the thrust zone microstructures characteristic of the north and of the south are compared, while differences between the east (Cnoc a' Chaoruinn) and the west (Knockan) are also brought out.

A comparative analysis of crystallographic fabric from the south (Assynt) to Eriboll is presented. In this analysis the area around Knockan is left out due mainly to the extent of cataclasis in the carbonate rocks here. The chapter also deals with estimates of the tectonic stresses that are likely to have propagated the Moine nappe and thereby developed the thrust. This is made possible by means of steady state (equilibrium) grain size analysis in the carbonate rock. The estimated values of stress are compared with earlier estimates using similar and other microstructural parameters in the thrust zone. Finally an analysis of tectonite fabrics from selected areas of carbonate deformation is presented.

PLATE 6.1

Stylolites in Foreland carbonate.

a. Diagenetic stylolites and seams stand out in the dolomitic carbonates of the foreland. They are clay-filled, and may become faulted, warped (see S arrowed) or passively transported with the host rock. Scale: Lens cover is 5cm across.

b and c Backscattered electron micrographs of stylolites in carbonate rocks. Note the sharp terminations of the host rock grains (b) and the branched nature of the "mainstream" sylolite (c). The main stylolites contain iron and some titanium oxides and iron sulphides (brightest), and white mica (grey). Scale: 100 μm

d. Backscattered electron micrograph close up view of the branches or "tributaries". They wind along grain boundaries only, carry metallic ores (iron and titanium oxides and iron sulphides) instead of white mica (m). Scale bar: 10 μm.

PLATE 6·1

a

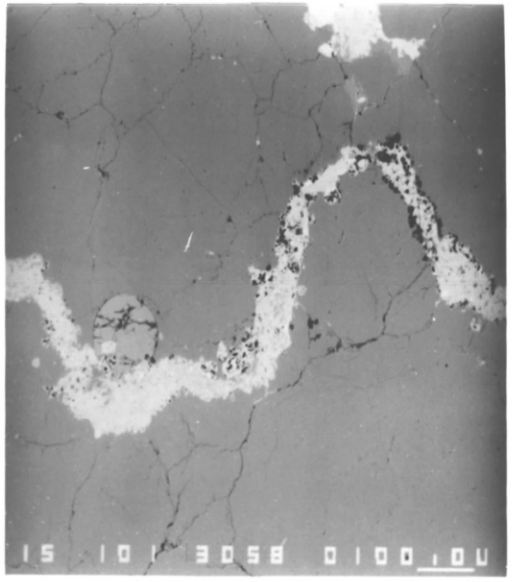

b

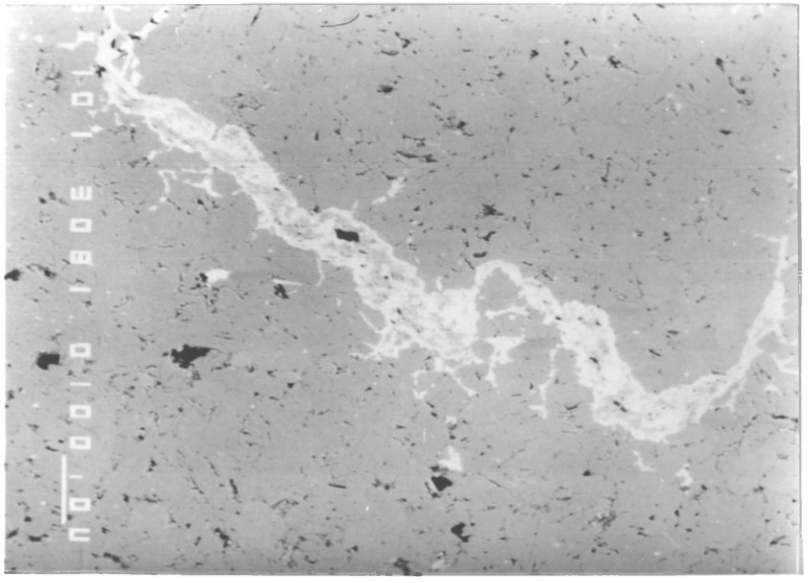

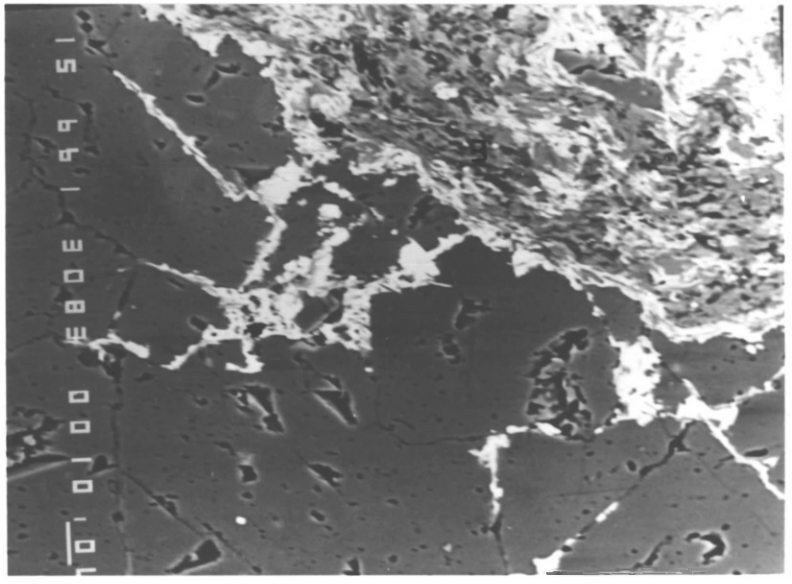

6.1.2 Microstructures of the Foreland and low Strain Carbonate Rocks

Typical of the Foreland and very low strain areas are solution surfaces, which very often stand out because of the clay concentration within them (Plate 6.1a). Whether occuring at the Durness beach, Eriboll, Assynt foreland or very close to the thrusts, these solution features preserve the same basic characteristics. They commonly occur parallel to bedding and may tilt with bedding in response to later deformation. They may become compacted where the rock has been overlain by later nappes (Plate 4.5a, b; see s - s), fractured and/or invaded by tectonic-associated fluids or warped into simple folds with the host rock (Plate 6.1a; see s).

Backscattered scanning electron microscopy and x-ray diffraction show the host rock to be dolomite and the material in the solution seams and stylolites (Plate 6.1b, c) to be mainly illite/sericite mica and oxides of Fe and Ti with Fe sulphides. Solution surfaces range in thickness from about 2 microns up to 2.5cm, normal to bedding, and may be branched as in Plate 6.1d. The branches ("tributaries") which are often short compared to the length of a particular stylolite, contain metallic ores only, unlike the main stylolite. Etched samples in SEM (Plates 6.2a, b) show the clay-filled solution seams to be bounded on both sides by zones that do not respond to etching in dilute hydrochloric acid and stand out almost at the same level as the clays in the seams. They are carbonate/clay zones supported by the "tributaries" of metallic ores. Also the clay bodies are the zones where undissolved tests of microfossils are concentrated during the pressure solution process.

PLATE 6.2

Solution features in dolomite rocks.

a and b Electron micrographs of solution seams in carbonate rocks. Etched samples like these reveal the presence of bounding walls on either side of the clay-filled seam. These walls are more resistant to etching than the carbonate host rock, but less than the clay within the seam. The holes in the seams were left by microfossil tests.
Magnification: x 720.

c and d Optical micrographs (crossed polars) of Foreland dolomite rocks. Grain size is fine to medium (0.062 - 0.25mm) with no deformation features. The grains are equiaxed.
Magnification: (c) x 63, (d) x 40

PLATE 6·2

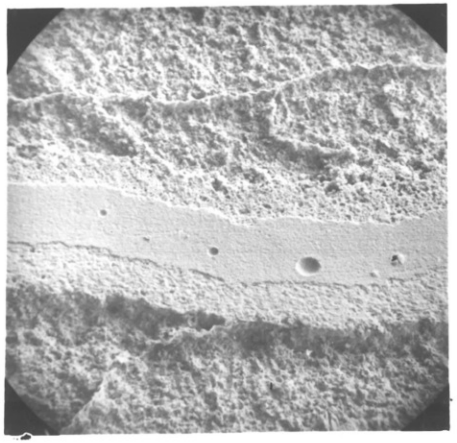

a

b

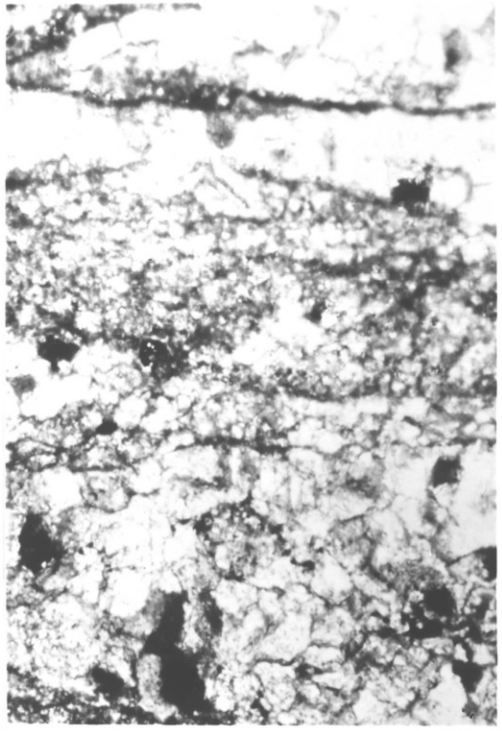

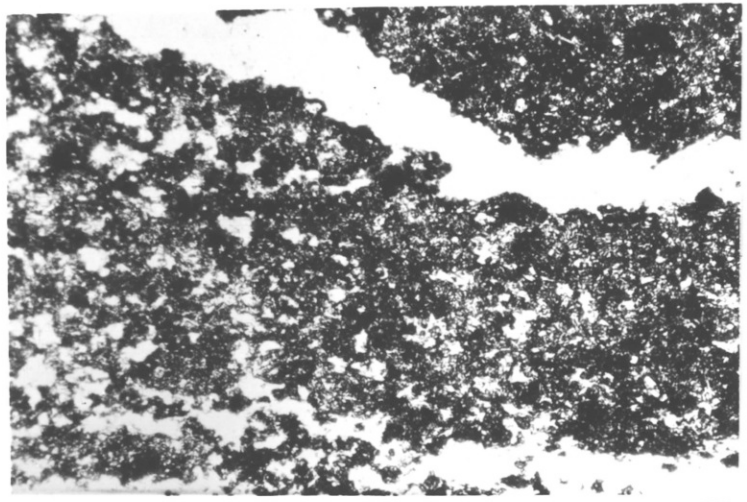

d

Grain size ranges from medium (0.062 - 0.25mm, Folk 1959) to very fine authigenic crystalline dolomite (Plate 6.2c, d).

The solution features are interpret ed as diagenetic and pretectonic in origin formed while the Durness Formation was undergoing induration. The tributaries of metallic ores might suggest mechanical and solution transportation for the Ti component due to low solubility (Rose et al, 1979), while the Fe component could have been transported in solution along grain boundaries into the main stylolites.

6.2 MICROSTRUCTURES OF INTERMEDIATE STRAIN AREAS

6.2.1 The Durness Carbonates of Kempie Bay Area

Samples K_1, K_2 and K_3 taken from the Durness Formation near Kempie Bay, Loch Eriboll (Fig. 3.10), show interesting microstructural features. The location of the samples is more than 1 km west of the Moine Thrust in part of the Sole nappe affected by minor to intermediate folding and minor thrusts and backthrusts. The attitudes of the folds (orientation of hinge lines), the thrusts and bedding are all sympathetic or closely related to the trend of the Moine Thrust Zone in this area (McClay and Coward, 1981) and hence any microstructures developed in the rocks in relation to these minor to intermediate structures (like cleavage) could be related to some phase of activity on the Moine Thrust. The cleavage found in samples K_2 and K_3 dips to the south east and is of crenulation type, (Cosgrove, 1976; Hobbs et al, 1976; Gray, 1979; see also Plate 6.3a)

6.2.1.1 Detailed Description of Cleavage Microstructure

In hand specimens this cleavage is fine, sharp and

PLATE 6.3

Cleavage microstructure in Durness Formation of the Kempie Bay Area.

a. A cleavage (c1) imposed on crenulations or minor folds within the low strain carbonate rocks of Kempie Bay - Eriboll area.
Scale bar: 100 μm, electron micrograph.

b. The cleavage lamellae consist of very fine-grained white mica (illite/sericite) anastomosing around elongate grains of feldspar (F) and dolomite (D). The cleavage lamellae are usually at a high angle to bedding.
Scale bar: 10 μm, electron micrograph.

c. Outside the cleavage the original bedding consists of elongate grains of dolomite, quartz and feldspar with a little mica. Dolomite grains are usually zoned , (see D), with the rims being more Ca-rich.
Scale bar: 100 μm, electron micrograph.

d. Feldspar grain (F) in cleavage lamella has been rotated and/or dissolved parallel to the lamella. Just outside the lamella, dolomite, (D), quartz and feldspar (F) are often broken up into lozen-shapes as they rotate into the lamella.
Scale bar: 10 μm, electron micrograph.

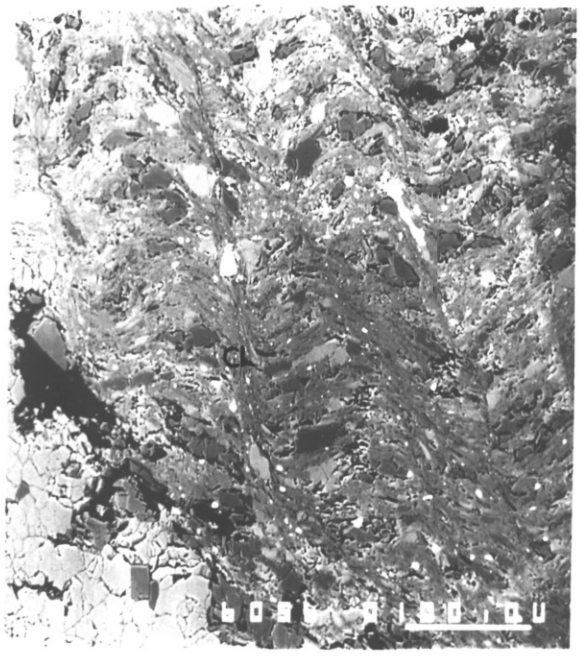

a

b

PLATE 6·3

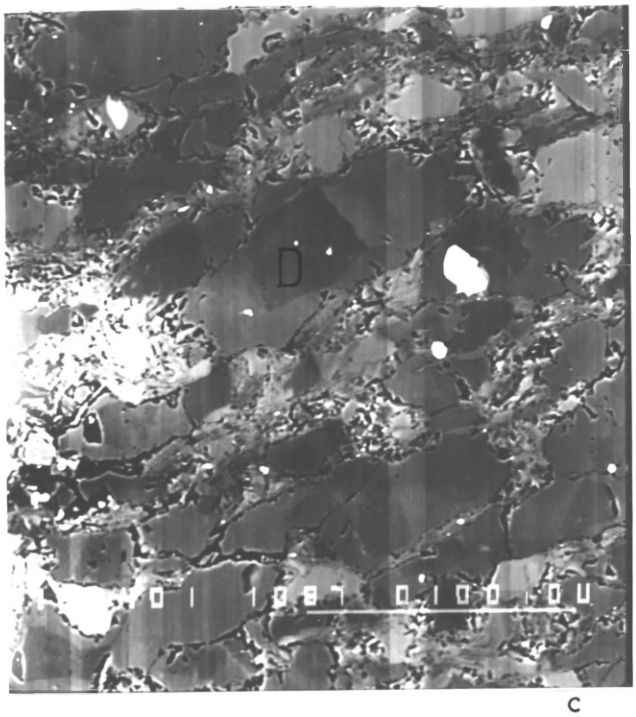

c

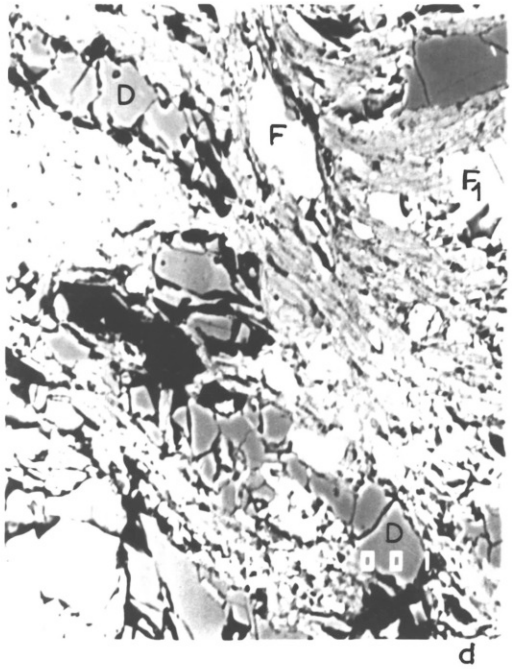

d

defines narrow zones, and is therefore called discrete crenulation cleavage after Gray, (1977b , 1979). In some cases a microfolding/cleavage relationship could be seen, as in Plate 6.3a, while in others microfolding in the vicinity of the cleavage lamella is not obvious. Grain orientations in the cleavage lamellae are at high angles to bedding (in the microlithon). High magnifications show the lamellae to consist of very find grained illite/sericite mica anastomosing around elongate grains of feldspar and dolomite mainly (Plate 6.3b). Outside the lamellae (that is in the microlithons) dolomite, quartz and feldspar grains elongate parallel to bedding with small amounts of mica. The dolomite grains are often zoned with high Mg cores and high Ca rims, (Plate 6.3c). The absence of calcite and chlorite here are evidence that processes going on in this environment are lower temperature than along the thrust (compare with Plate 4.3, and Plate 6.8b).

A study of the chemistry of feldspars and mica in both cleavage and microlithon is presented in Table 6.1. As shown in A, there is a relative enrichment in Ti in the feldspars of the microlithons compared to the feldspars of the lamellae. Table 6.1B on the other hand shows a slight increase in Si and K in the microlithon relative to the cleavage lamellae. This slight increase in Si in the microlithon could be explained by faster dissolution of Si from the cleavage planes (or P layers of Gray, 1979; Stephens et al. 1979; Knipe, 1981 and Weber, 1981) and deposition of same in the microlithon. The behaviour of K as shown in Table 6.1 is inconsistent with earlier observations (see Gray, 1979; Stephens, 1979, and Knipe 1981). Potassium content is known to increase into the cleavage planes

A

ELMT	K-feldspars within cleavage lamellae 1 % Oxide	2 % Oxide	3 % Oxide	4 % Oxide	5 %Oxide	ELMT	K-feldspars in the microlithon 1 % Oxide	2 % Oxide	3 % Oxide	4 % Oxide
Mg			0.340			Na	0.320			0.400
Al	18.705	18.663	18.847	17.976	18.404	Al	19.106	18.639	18.441	18.902
Si	65.910	65.544	65.038	65.618	64.614	Si	65.374	64.469	64.644	64.769
K	16.612	16.832	16.381	16.345	16.107	K	16.666	14.761	16.176	16.537
Ti	0.199				0.263	Ti	0.262	0.360	0.214	0.275
TOTAL	101.43	101.04	100.61	99.94	99.39	TOTAL	101.73	98.23	99.48	100.88

B

ELMT	Mica (illite) in cleavage lamellae 1 % Oxide	2 % Oxide	3 % Oxide	4 % Oxide	5 % Oxide	ELMT	Mica (illite) in the microlithon 1 % Oxide	2 % Oxide	3 % Oxide	4 % Oxide
Mg	3.962	3.696	4.177	4.300	5.981	Mg	2.683	2.929	3.249	4.835
Al	26.898	27.703	28.397	28.627	25.941	Al	28.101	26.001	30.994	28.251
Si	46.557	46.094	47.335	46.287	46.542	Si	50.329	53.227	49.281	48.850
K	9.825	7.281	9.640	7.111	10.368	K	10.474	11.541	10.221	10.530
Ti	0.477	3.563	0.303	0.441	0.438	Ti	0.197	0.392	0.475	0.430
Fe	1.264	0.900	1.114	0.947	2.808	Fe	0.656	0.909	1.511	1.508
TOTAL	88.98	89.24	90.97	87.71	92.08	TOTAL	92.44	95.00	95.73	94.40

TABLE 6.1 Comparison of microchemistry of K-feldspars and mica (illite) within cleavage lamellae and outside the lamella (microlithon) in Durness Carbonate samples of Kempie Bay area. (A) Note the higher percentage of Ti in K-feldspars in the microlithon, comparaed to the lamellae. (B) Si and K percentages appear slightly higher in the microlithon than in the lamellae

hence the decrease shown in Table 6.1 may be a local effect, due to material inhomogeneity.

The feldspar grain in Plate 6.3d presents a little evidence that although cataclasis is high outside the lamellae, within the lamellae grain reorientation could be assisted by simple shear, as in a microshear zone.

In plates 6.3d and 6.4, the intervening area between the lamellae and the foliation was closely studied to determine the reorienting mechanism in such a low temperature area. In Plate 6.3d elongate grains of dolomite and feldspar in the intervening areas between the lamellae and the microlithon are seen disolved and fractured into lozenges, with a lot of voids in between. This is also illustrated in Plate 6.4 which shows extensive bedding plane flattening in these carbonate rocks. Plate 6.4b, c and e show some grain fracturing just outside the cleavage lamella. This is also the zone of mixed grain shapes, corresponding neither to those in the lamella nor in the microlithon. Hence it may be said that the low temperature of the deformation environment here has affected the reorientation mechanism of grains in rocks developing cleavage. Apart from solution with or without plastic strain, more evidence may yet emerge that cataclasis does indeed contribute to grain reorientation in very low temperature cleavage development.

6.2.2 The Loch Ailsh Marbles

Of the carbonate samples collected north and northwest of Loch Ailsh, only samples B43, B45, B45e, B5 and B6 (Fig. 3.6) produced microstructures of importance in this study. In Chapter three it was shown that movement on the Moine Thrust still continued after the emplacement of the Loch Ailsh syenites.

PLATE 6.4

A cleavage and its contact zones in dolomite rock. Contact zones between a cleavage lamella in (a) and the bedding are imaged in (b), (c) (d) and (e).

b. Note the presence of reaction rims in dolomite grains. The greyish rims are more Ca-rich, while the darker cores are more Mg-rich. Grain shape in the contact zone between the lamella and the microlithon is neither bedding-parallel nor cleavage-parallel.

c and d Some of the grains in the contact zone are either curved (as in c) or fractured (see arrows in d) in order to reorientate parallel to cleavage. The fracturing intensity diminishes away from the cleavage.

e. Grains in the microlithon become more tappered and refined as they approach the lamella. This applies to fractured and unfractured grains, see also b and d. Scale bar: 100μm.

PLATE 6·4

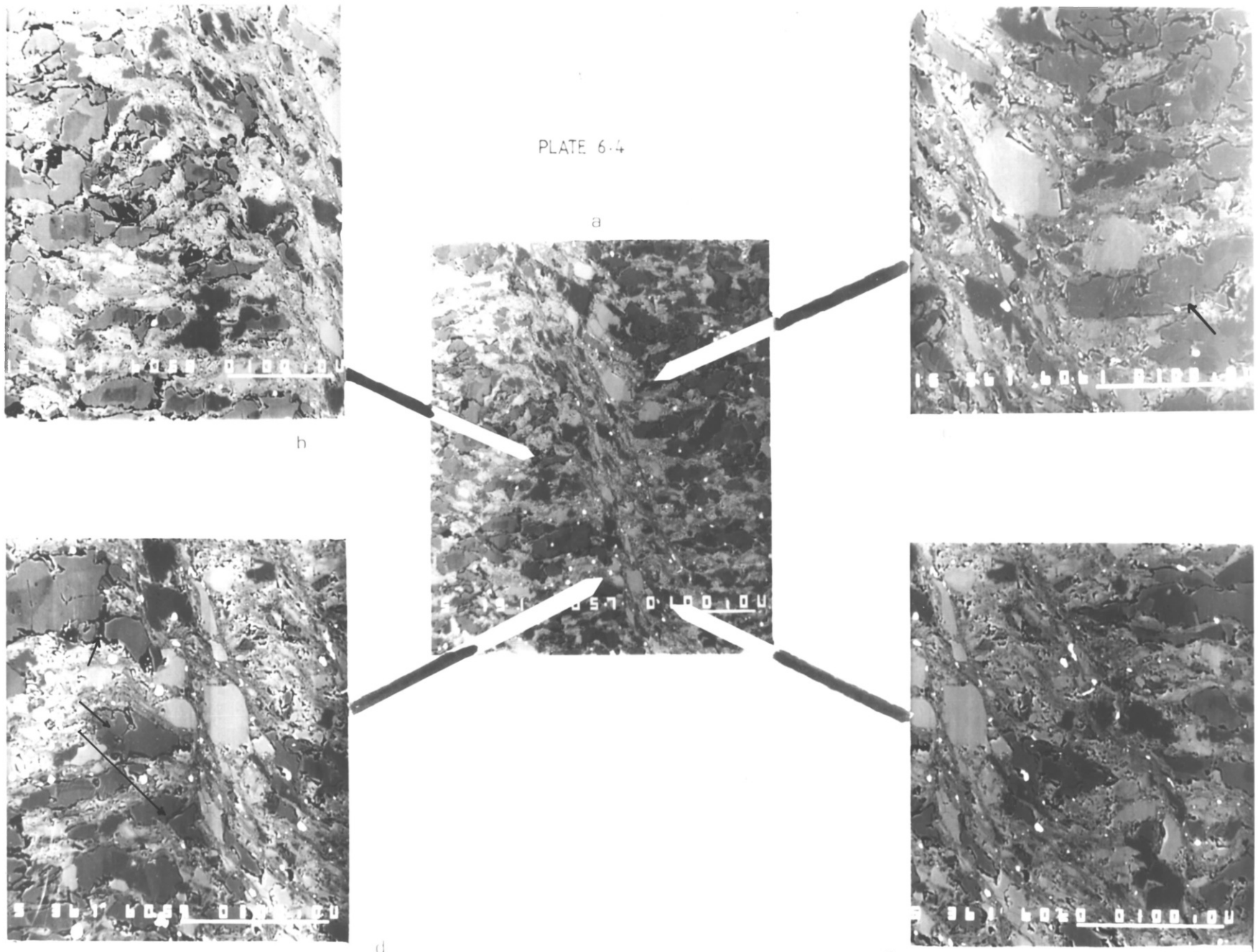

This magmatic intrusion/orogeny relationship is important in this area because the heat from the former caused extensive crystallization and neomineralization in the country rocks including the Durness Formation, prior to later deformation. Because of this difference in mineralogy and grain size compared to the carbonates along the Moine thrust plane slight differences in deformation mechanisms should be expected.

The deformation in this environment can be invoked to explain the splicing of mica in original diagenetic solution seams into fibres (Plate 6.5a), and at the same time producing a very closely fitted fabric with statistical grain elongation in a direction parallel to the E.S.E. lineations (Plate 6.5b). Grain boundary terminations are not always at trip le junctions, and some grains interpenetrate along their lengths (Plate 6.5c). A new type of clay mineral, uncommon either in the foreland or along the Moine thrust plane, also developed in this area (Plate 6.5, d and e). These are the long thin rods of attapulgite (palygorskite). The thicker bundles grow through grain boundaries, while the grain bodies may be pierced through by single strands or rods (Plate 6.5d). This interaction produces the well-known grain size reduction (of dolomite grains) near these clay minerals (see White, 1979a).

6.3 MICROSTRUCTURE OF HIGH STRAIN AREAS: ALONG THE MOINE THRUST IN THE SOUTH

6.3.1 Knockan Area

As shown in figures 3.4 and 3.8, the Knockan area, including the cliff - Knockan Crag - is the southwestern extreme of the zone of dislocation in Assynt. Here the Moine Thrust overlies a wedge of whitish-coloured, cataclased dolomite which is itself lying over highly fractured, dark-

PLATE 6.5

Lock Ailsh Marble.

a. Splicing of white mica m in a diagenetic solution seam possibly during movement. The fibres of mica minerals are easily invaded by fluids which cause alteration and neomineralisation.
Scale bar: 10 μm, electron micrograph.

b. A tightly fitted fabric produced from strain and possibly pressure solution, with grain elongation in the NE direction.
Scale bar: 30μm, electron micrograph.

c. Grain boundary interpenetration is common in the carbonate grains, although some tripple junctions do exist still.
Scale bar: 3μm, electron micrograph.

d and e A new clay mineral, uncommon in the foreland and along the thrust zone, is developed here. It consists of rods of attapulgite (palygorskite). Where these rods are densely developed they "choke up" the carbonate grains reducing grain size (as in d).
Scale bar: d - 20μm
e - 6μm

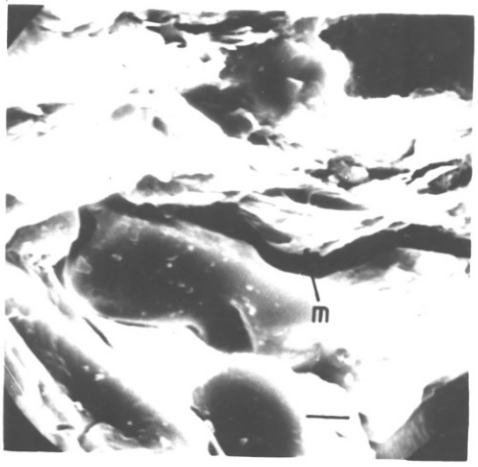

a

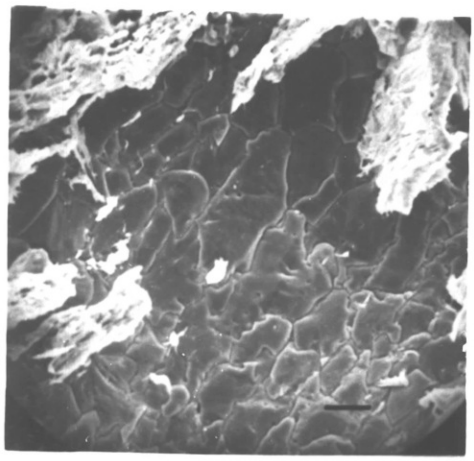

b

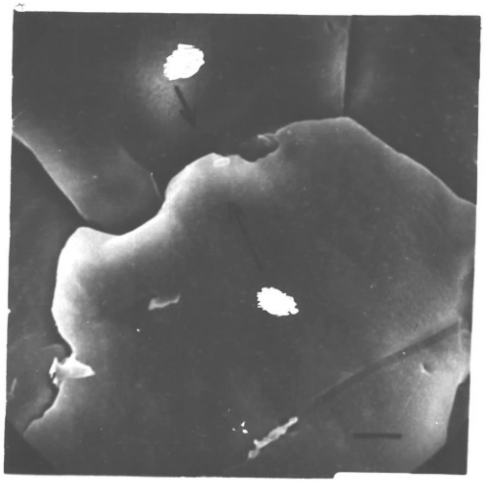

c

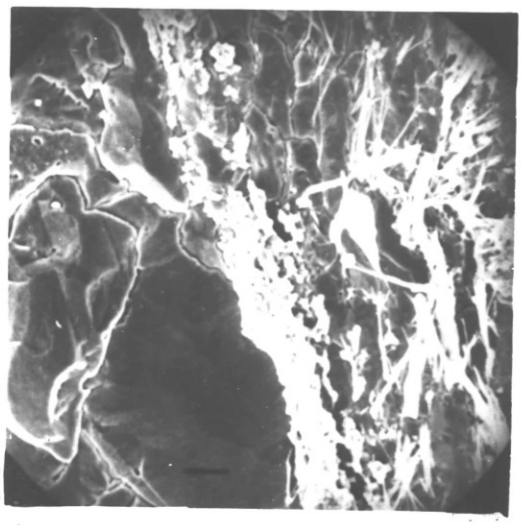

d

e

coloured, foreland-type dolomite (Plate 3.3, a and b). The wedge of dolomite decreases in thickness south and south-eastwards, being overlain here by a cataclasite resulting from intense fracturing of Moine mylonites. The description of a vertical profile of the carbonates beneath the thrust plane in this area is presented below in zones with contrasting micro-structure.

6.3.1.1 Zone A

This is a cataclasite extending from the thrust plane proper to about 1m below (Plate 6.6a). A network of fractures of a very wide size range permeates the entire rock producing very angular to subangular carbonate grains. The fractures are normally healed either with a greyish, sometimes brownish carbonate cement (Plate 6.6a, b) or newly nucleated carbonate crystals (Plate 6.6c, d). Fracture intensity increases and fractured dolomite grain size tends to decrease towards the fault plane, while matrix cement concentration is higher near the fault plane decreasing downwards towards a grain- supported breccia away from the fault plane. Vein calcite grains are usually highly weathered and the veins cross-cut showing that they probably belong to different generations.

The original diagenetic solution surfaces here are commonly transected and displaced by fractures, while in a few undisturbed segments nucleation and growth of chlorites took place during metamorphism (Plates 5.1a, 6.6e).

6.3.1.2 Zone B

This extends from 1 - 2m below the thrust plane, and is characterised by much lower fracture intensity. Grain size is ultrafine marking the inception of crystallization from the

PLATE 6.6

Durness carbonates below the Moine Thrust - Knockan.

a. From within 1m of the thrust plane. Note the intense fracturing even down to grain size level. Grain size is a mixture of fairly large old and deformed grains with small newly formed grains. Scale bar: 1mm, optical micrograph, crossed polars.

b, c and d. Fracture healing is by greyish or brownish carbonate cement as in (a), or nucleation of fine crystals of mainly calcite (c and d). Crystallization in fractures (veins) and in original diagenetic solution seams (c, d and e) is dominant in this area.

Scale bar: b = 1mm) Optical micrographs in
c = 1mm) crossed polars.
d = 1mm)

e. Chlorite (Ch) nucleates in diagenetic solution surfaces which have not been disturbed by tectonics.
Scale bar: 1mm, optical micrograph in crossed polars.

PLATE 6-6

a

b

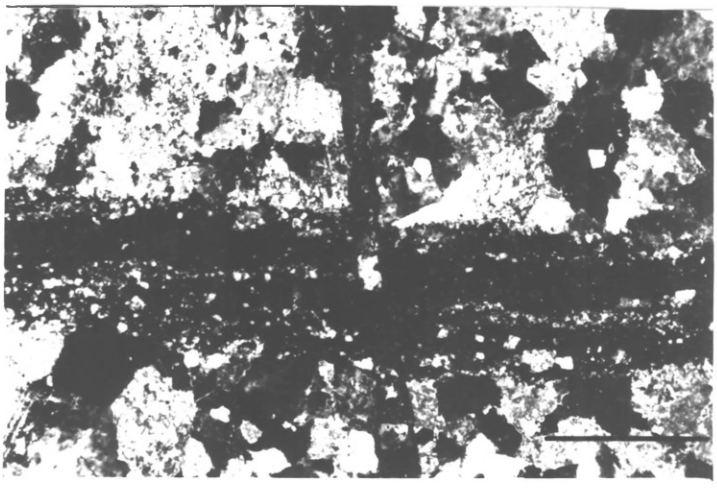

c

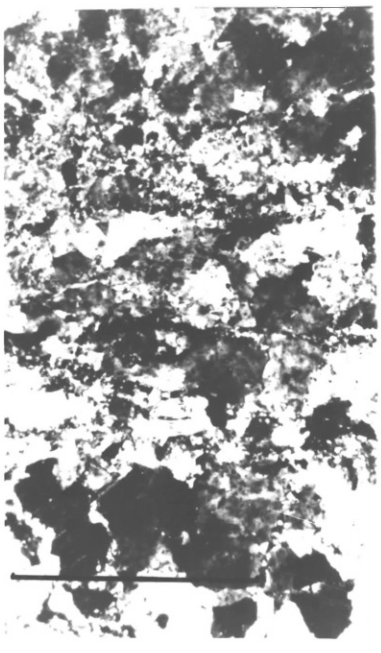

d

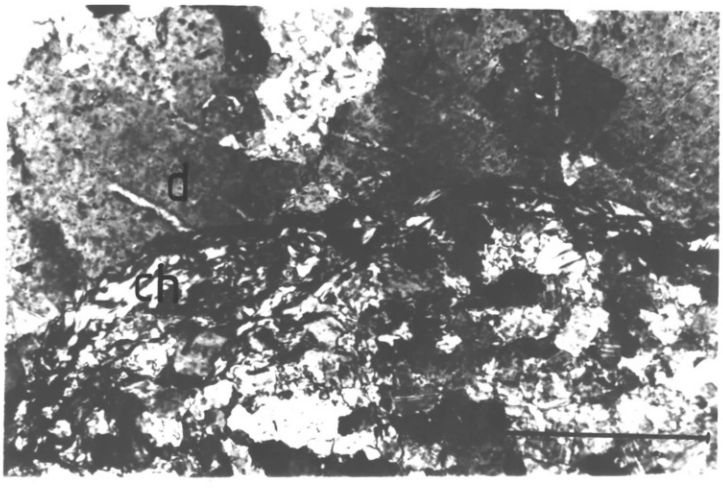

e

original carbonate matrix. A network of spaced calcite veins transects both bedding and solution surfaces (Plate 6.7a, b). Some of the veins are also displaced by later movements along bedding and solution surfaces (Plate 6.7b, c), showing that under a shear stress regime solution surfaces are used as movement horizons to accommodate strain.

Also common in this zone is the very close arrangement of bedding - parallel solution surfaces (Plate 6.7a, c). Also bedding - parallel linear arrangements of pyrite microgranules give a dark colour banding to the rock. The range in vein width and the way these veins cross cut is an indication that the carbonates beneath the thrust here experienced several cycles of fluid pumping during the last phase of tectonic activity.

Recrystallization and grain growth increase towards the top of the zone partially wiping out sedimentary and diagenetic structures.

6.3.1.3 Zone C

From two to three metres below the thrust is a zone of complete recrystallization with a nearly uniform fine grained mozaic of mainly dolomite, and a little quartz. All diagenetic solution seams together with fractures carried over from earlier deformations have either healed or are sites of formation of very fine crystals. Most of the earlier coarse grains in veins have been recrystallized producing a nearly uniform texture all through. There is a characteristic absence of chlorite and calcite in this zone.

6.3.1.4 Zone D

This zone extends from three to four metres below the thrust, and consists of fairly uniform crystallized grains,

co-existing with old solution surfaces. Recrystallization and healing of fractures has almost wiped out all original fractures and diagenetic seams. A little mica and chlorite occur in some of the seams, emphasizing another secondary use of solution surfaces, as sites for nucleation of new minerals. This is the greatest depth where the products of metamorphism have been revealed, both by x-ray diffraction and extensive microscopic analysis. Hence it could be said that the maximum depth of the zone of prograde metamorphism associated with the thrust at Knockan is about four metres.

6.3.1.5 Zone E

Below four metres from the thrust plane there is a fairly coarse-grained cataclasite in which the last generation of fractures was healed by growth of calcite micrograins into the fractures or by the deposition of a brownish, iron-containing cement within the fractures. There is a characteristic absence of quartz in veins, unlike the other zones, and the veins are calcite-filled. Some of the dolomite grains show centrally placed alteration haloes made up of calcite. All diagenetic structures have been wiped out by crystallization, though there is no evidence in the rock of the development of a new foliation.

6.3.1.6 Zone F Foreland Dolomites

Since the whitish-coloured carbonates described above are smeared out into a wedge the total thickness diminishes south and south-eastwards. Along the vertical profile sampled, the dark foreland carbonates are only about 6 metres below the Moine thrust plane (Plate 3.3a, 6), and extend for another four metres to the top of the Serpulite Grit. It is uniformly crystallized, intensely fractured, producing several generations

PLATE 6.7

Microstructure in the Druness carbonate within 1-2m of the thrust plane.

(a), (b) and (c)

1 - 2m below the thrust plane. A network of spaced calcite veins cross-cuts the formation. These veins fill fractures along which there has been displacement (as in a), or which became displaced by later movement along earlier solution surface - S (in b and c). The high incidence of cross-cutting veins in this area suggests high fluid activity during a cyclic sequence of tectonic pulses.

Scale bar: a = 1cm) Optical micrographs in
b = 1cm) crossed polars.
c = 1cm)

d. One mile east of the cliff below the thrust, fractures are almost completely healed, grain size ranges from 1mm to much less. There is no foliation, and grain boundaries are very serrated.

Scale bar: 1mm, optical micrograph, crossed nicols.

PLATE 6-7

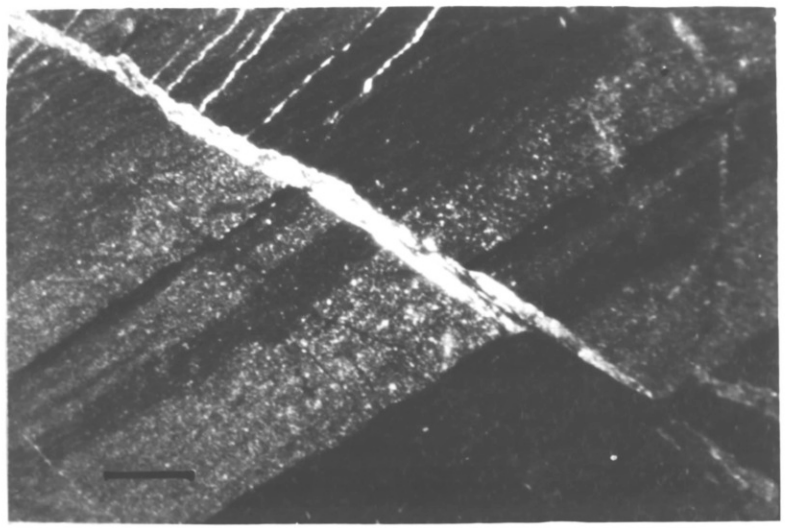

a

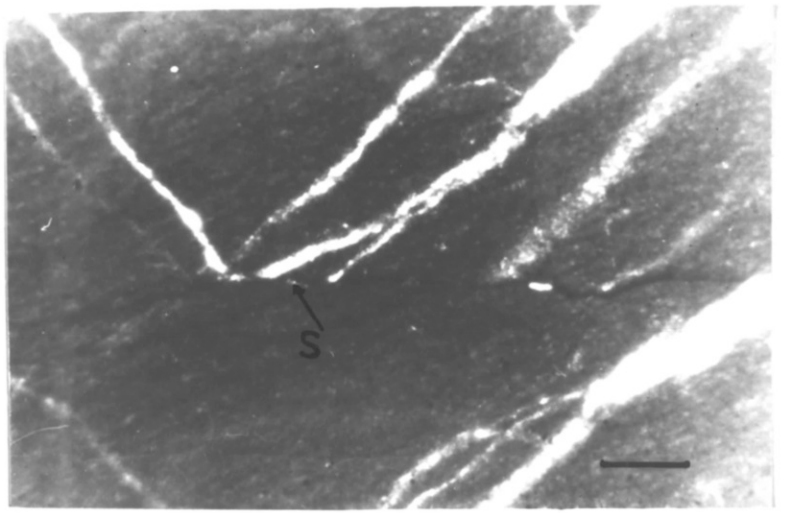

b

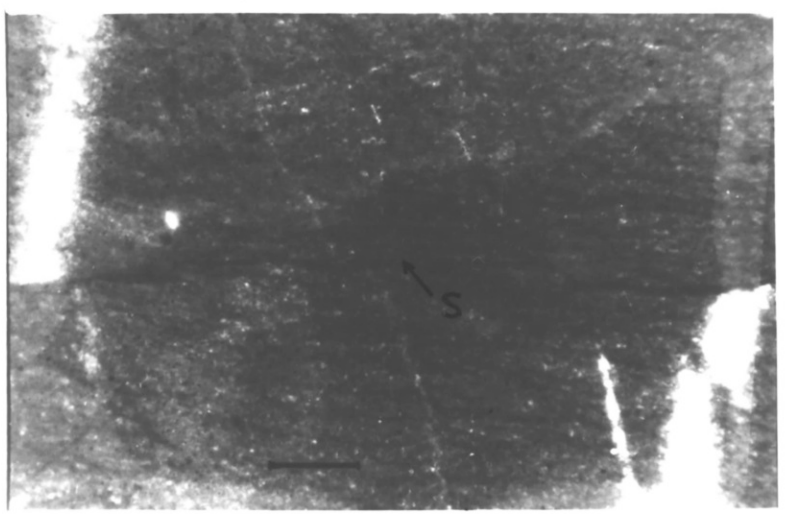

c

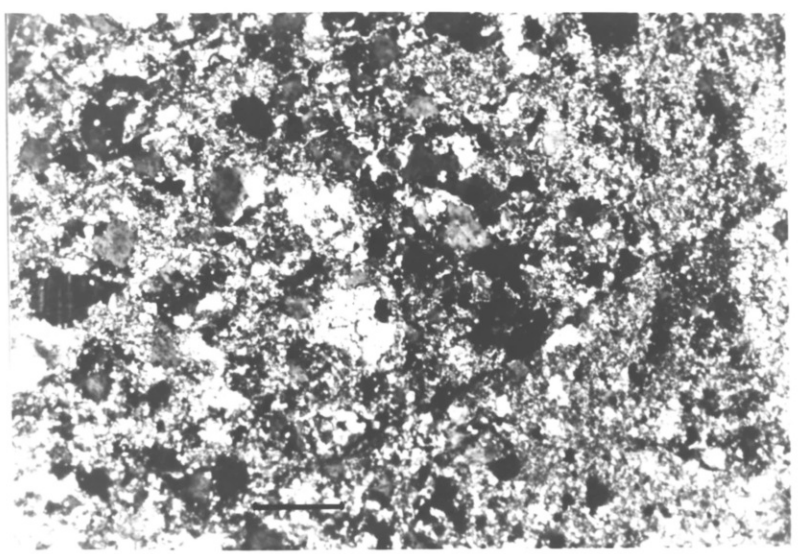

of fractures, but no foliation. Despite the total recrystallization, the rock still maintains its dark greyish colour due, probably, to the presence of opaque impurities.

More than 1km east of this vertical profile, along the top one metre of the carbonates a foliation is still lacking, though fracture intensity and width have diminished greatly (Plate 6.7d). The repeated fracturing and recrystallization have produced a microstructure in the carbonates that is non-steady state that is, not in equilibrium with the stress, and cannot therefore be used to estimate the stress magnitudes.

6.3.2 Cnoc a' Chaoruinn Area

Ten kilometres to the east of Knockan Crag below the Moine thrust plane is the area of fairly complex deformation described in subsection 3.4.4. Here the Lower Assynt thrust, the BenMore and Moine thrusts outcrop together in a small area (Figs. 3.4; 3.7) and with their imbricate thrusts impart an element of complexity to the area. Apart from differences in temperatures between this area and Knockan (see Subsection 4.3.4), there also exist important microstructural differences.

Here, compared to Knockan, a reasonable foliation has developed in addition to a fairly obvious though weak lineation described in Chapter 3. The foliation could be described as incipient, with bands of phyllosilicates and carbonates, alternating (Plates 6.8a, b). The phyllosilicate bands which are mainly inherited from stylolites and diagenetic solution seams contain fibres of mica and chlorite. These bands range in thickness between 2.5μm and 100μm normal to foliation.

The rock is about 70% dolomite, with calcite, quartz authigenic feldspars and phyllosilicates making up the other

30%. The main opaque minerals present are oxides of iron and titanium and sulphides of iron (Plates 6.8b, 6.8c).

6.3.2.1 Grain Shape and Boundaries

Grains are generally of equant shapes, but in some cases only slightly so (Plates 6.8a, 6.8d). The longer dimensions are not always parallel to foliation. There is some amount of grain boundary interpenetration where the grains have serated edges (Plate 6.8d) but the tendency towards straight boundaries is quite obvious. Grain width ranges between 37 - 40μm, normal to foliation.

6.3.2.2 Other Strain Features

Undulatory extinction affects mainly the largest grains (like q in Plate 6.8c), and quartz more than dolomite. Twinning is very scarce here, averaging about one in three hundred grains, and increasing very gradually eastwards below the thrust. $r(10\bar{1}4)$ cleavage dominates in 30 - 40% of dolomite and calcite grains, being mainly along one plane. Maybe because of the low strain, and/or low temperatures, subgrains and recrystallized grains are generally not present.

Calcite/dolomite microstructure here is interpreted to have gone beyond the brittle field into what may be regarded as a ductile state with possible equilibrium relationship to stress and has therefore been used in stress estimates. The results are presented in Section 6.5

6.3.3 The Glencoul Area

Samples collected within the imbricate structure below the Moine Thrust in this area (see Fig. 3.9) showed microstructures different from the southern areas. Like the rest of the south, ubiquitous twinning is not observed in dolomite, but there is a better development of foliation, especially in the Fucoid Beds (Plate 6.9a). This is aided principally by the higher concentra-

PLATE 6.8

Lineated and foliated dolomites - Cnoc a' Chaoruinn.

a and c A foliation has developed in this area consisting of bands of mica - m, bounded by dolomite/calcite as in (a) or quartz q (in c). Note undulatory extinction of quartz grain - q. In some places the alteration of mica to chlorite - Ch and the formation of feldspars - fp (b) are quite common.

In (d) serrated grain boundaries result in inter-penetrated grains, where the phyllosilicate content is low. This is different from (a), where grain boundaries are more straight.

(a), (c) and (d) - optical micrographs in crossed polars.
Scale bars: 1mm each.
(b) - electron micrograph (backscattered.
Scale bar: 100μm.

PLATE 6-8

a

b

PLATE 6.9

Fucoid Beds, sample ST-3, within the imbricates below the Moine Thrust at Glencoul (see fig. 3.9 for location and Appendix 2 for grid reference).
Quartz appears dark due to ultrathinning. Note the "drawing out" of quartz into ribbons, while dolomite grains are still irregular in shape with serrated edges, and often interpenetrating (see d and a), there is a greater percentage of white mica in this rock than in the Durness carbonates.

a. There is fairly extensive subgrain formation, especially in quartz (see q in (a). Some of these have further rotated to form recrystallized grains. Twinning of dolomite is very rare, hence most of the low temperature strain here must have been taken up by quartz and grain boundary sliding in mica.

Scale -(a), c and (d) = 1mm) Optical micrographs in
(b) = 63μm) crossed polars.

PLATE 6-9

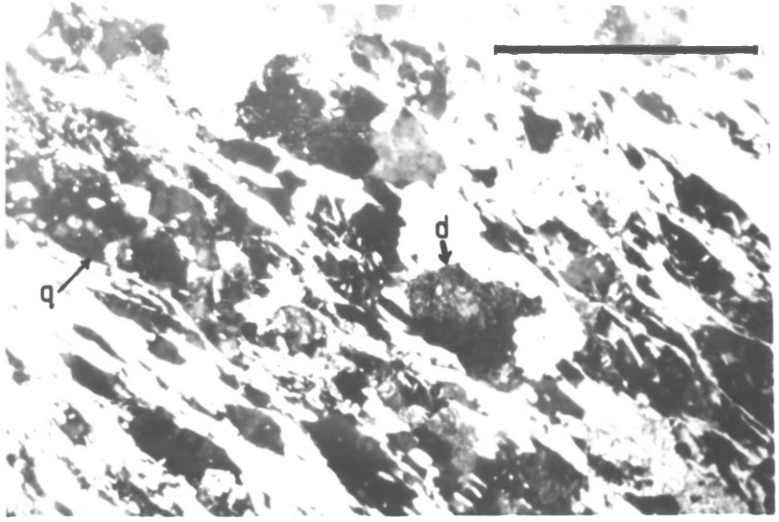

a

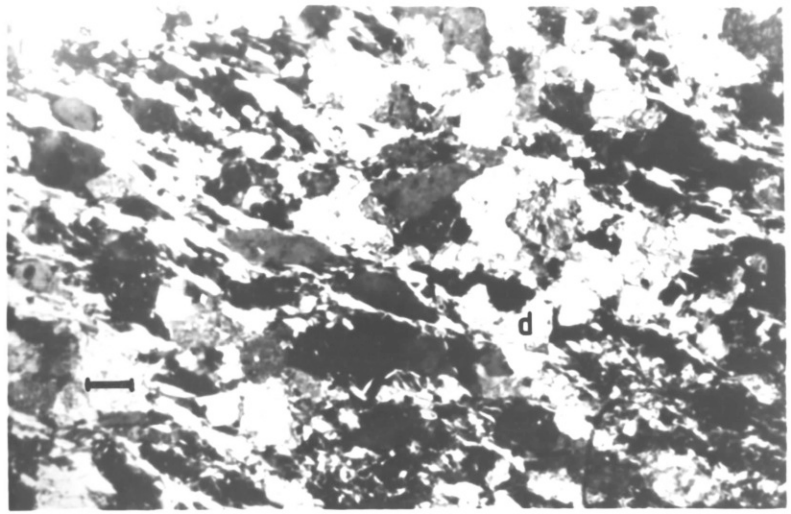

b

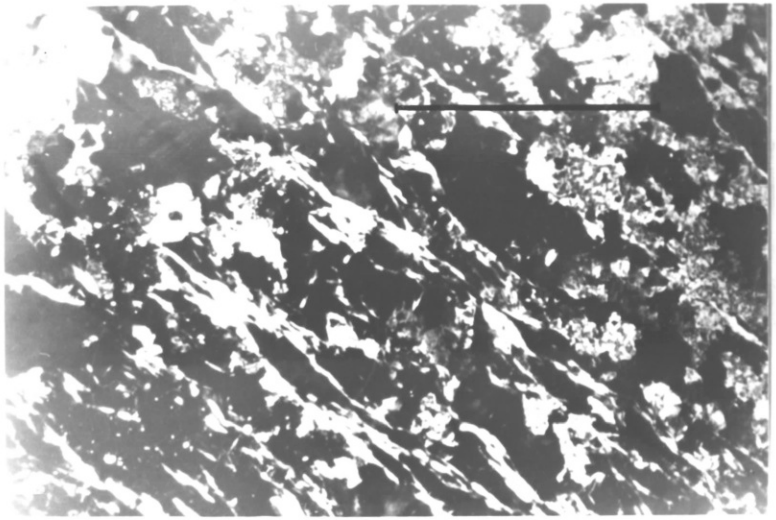

c

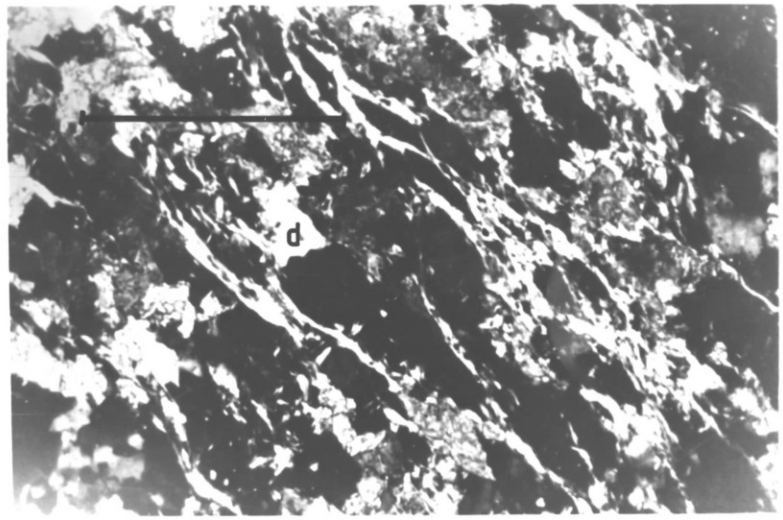

d

tion of white mica and quartz than in the Durness Formation. The quartz, as shown in Plates 6.9a, b, c and d, forms ribbons much more easily than dolomite or feldspar and as a result has better developed pressure shadows. Quartz (which appears dark due to ultrathinning) shows fairly extensive subgrain formation and some recrystallization (see q in Plate 6.9a), while the grains that have not started recrystallizing show extensive deformation bands. Dolomite on the other hand shows very little subgrain formation and correspondingly little recrystallization. Its grain boundaries are more serated and less regular due mainly to interpenetration with other dolomite grains (see d in Plate 6.9a), with quartz (see d in Plate 6.9b and d) and with feldspars.

Grain size ranges from 37 - 45μm for the dolomite grains, the lower end size range being in those samples with higher mica content. The absence of twinning is partly compensated by the presence of single sets of cleavage which bear no constant relationship to the foliation.

6.4 MICROSTRUCTURE OF HIGH STRAIN AREAS: ALONG THE MOINE THRUST IN THE NORTH

Intensely deformed outcrops of the Durness Formation below the Moine Thrust in Eriboll have been referred to by Peach et al. (1907), and given a brief description by Soper and Wilkinson (1975, see also subsection 3.4.7). No detailed microstructural description of this type locality has been done despite its potential for aiding the unravelling of the history of Moine thrusting. The microstructures described below are of Durness Carbonates from the locality referred to as "Eriboll Marble" in Fig. 3.10.

PLATE 6.10

A very fine mylonitic foliation in the Eriboll marble.

A very fine mylonitic foliation has developed in the Durness carbonates here. It is made up of bands of carbonate (dolomite and calcite) minerals interleaved with chlorite and talc. The two generations of dolomite grains are d_1 - parallel to foliation, and d_2 - normal to it ((b) and (c)).

Dolomite grains, unlike in Assynt, are ribboned (see (a) and (d)), and twinning is ubiquitous (c and d).

For d_1 type of grains, grainboundaries are parallel to foliation, and grain interpenetraion is not as common as in Assynt.

Scale bars: (a), (b) and (c) = 0.5mm) Optical micrographs
(d) = 1mm) in crossed polars.

NOTE: Calcite has been stained ark by Alizarine S.

PLATE 6-10

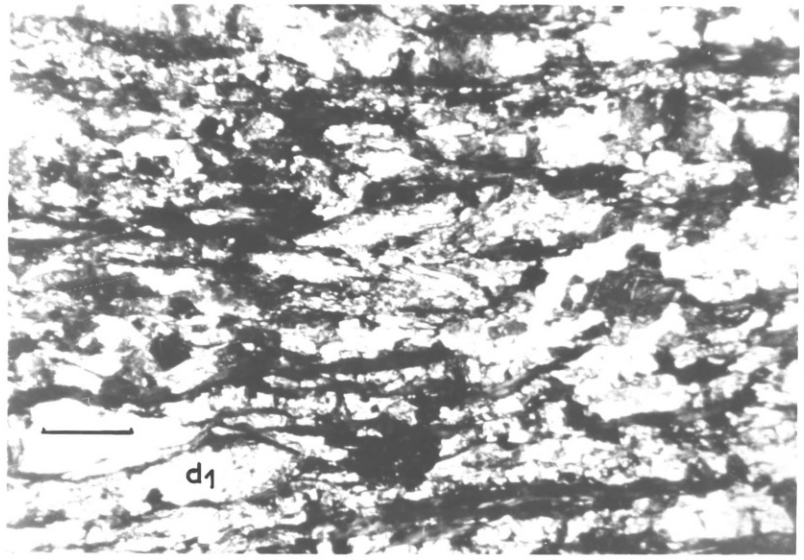

a

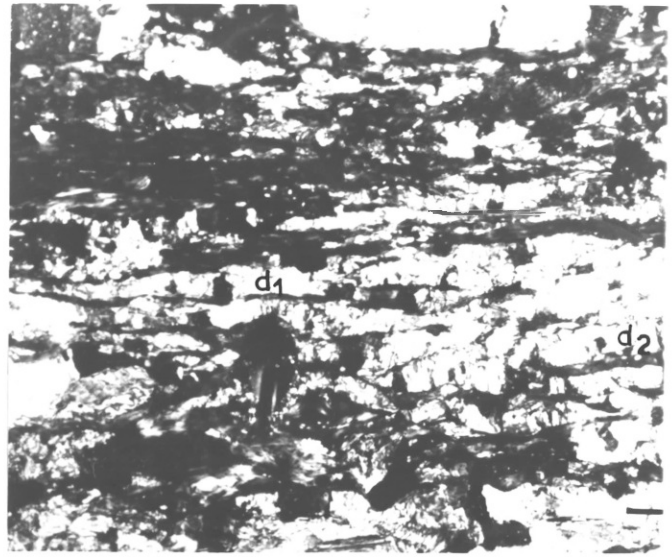

b

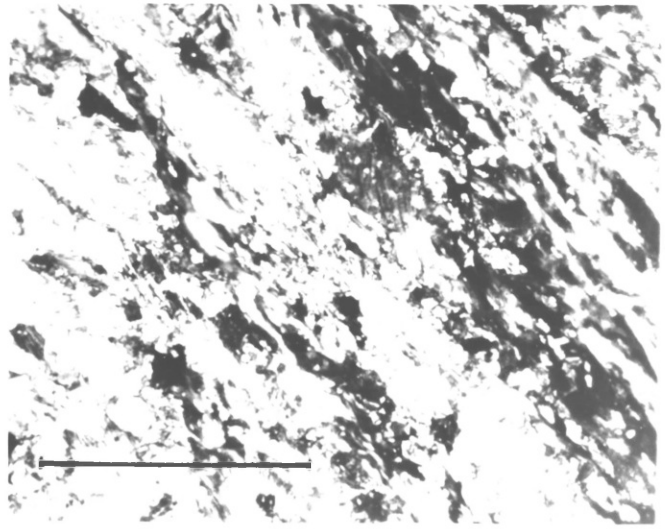

6.4.1.1 Foliation

A very fine schistose foliation has been developed in the carbonates of this part of the Moine Thrust Zone (Plate 6.10a, b, c and d). Bands or ribbons of calcite and/or dolomite alternate with laths of chlorite and talc mostly without mica. Plates 6.10a and b are very much like the mylonitic quartzite from the Moine Thrust Zone described by Christie (1963, see Plate 9). Two generations of dolomite grains are generally displayed here; an earlier, highly strained, often ribboned and twinned type, which is parallel to foliation; and a later type normal to the foliation, with or without twinning. These latter grain shapes are described later in this section. In Plates 6.10b and c the two types of grain orientations are shown to coexist very closely. The very fine grained nature of this rock, the fine or very close schistose banding present and the presence of high strains which have resulted in twinning and ribbon textures of the carbonate grains, are all factors which justify the term "mylonite" to be applied here too.

6.4.1.2 Grain Boundaries

Although grain boundaries are straighter and more parallel to foliation here than anywhere in the south, on closer view the larger grains show extensive grain boundary recrystallization, producing serrated edges and a mortar texture (compare Spry, 1969, Plate XXXVIII). The recrystallized grains are invariably twinned and may have their longer dimensions parallel to the foliation (Plates 6.11a, b).

Grain size ranges from 23μm to 50μm, normal to foliation for twinfree dolomite grains and is between 30μm and 40μm for the twinned calcite grains.

The grain size

PLATE 6.11

Twinning in calcite and dolomite.

Twinning in calcite and dolomite is ubiquitous at the Eriboll area of the Moine Thrust Zone. The smaller grains develop single twin sets (see S_1 in b,c, and d) while the porphyroclasts _ S_2 - normally have two or more sets of twins.

Twin sets in c and d suggest simultaneous, rather than sequential development of f - twins in dolomite, hence one set normally rotates the other (earlier) set (see c).

Recrystallization around the boundaries of the largest grains is most noticeable, replacing the porphyroclasts with finer, often twinned grains. The resulting grain boundary (of the porphyroclast) is serrated (see a, b and e).

Optical micrographs, in crossed polars, and alizarin.

Scale bars: a,b,c and d = 1mm

e = 0.5mm.

PLATE 6-11

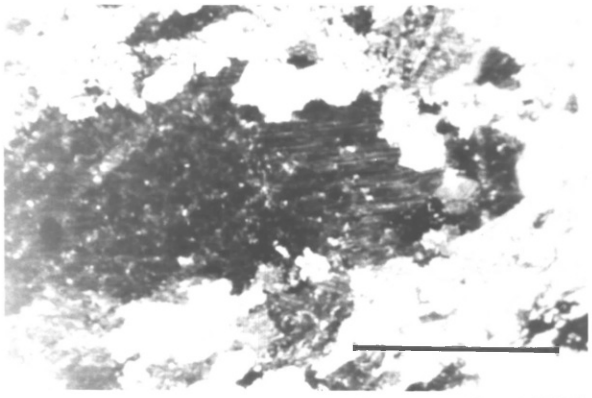

a

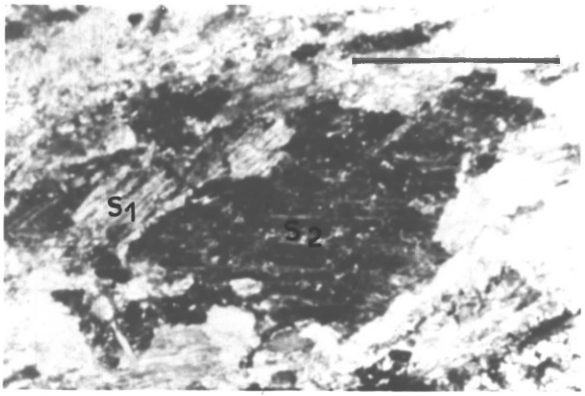

b

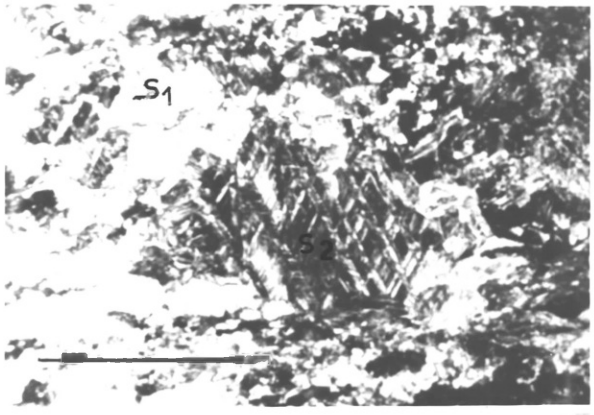

c

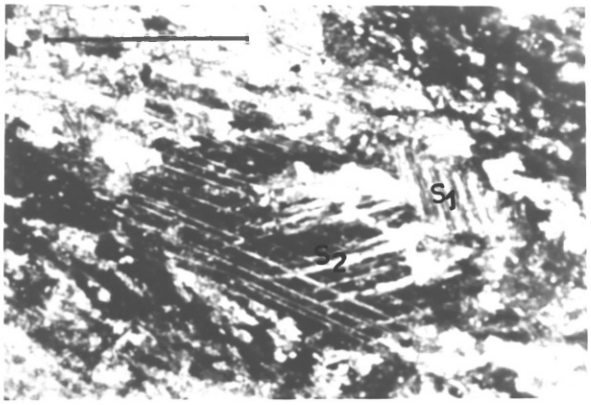

d

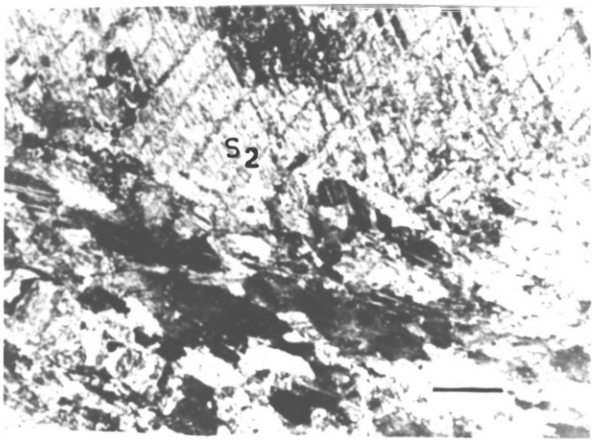

e

has been used to estimate the possible stress magnitudes.

6.4.1.3 Twinning

Twinning in the Durness Carbonates below the Moine thrust in this area is ubiquitous, affecting both calcite and dolomite grains of both foliation - parallel and foliation - normal generations (Plates 6.11c, d and e) and also of different sizes. Twinning is polysynthetic, with most calcite and dolomite grains having one set of narrowly spaced twins. Occasionally, the very large dolomite grains have two sets of twins, but these are in the minority, or a set of cleavage may be superimposed on already twinned grains. These cleavage/twin planes together with the grain boundaries are the sites for nucleation of new grains.

6.4.1.4 Recrystallization

Apart from grain boundary chemical reactions producing zoned dolomite grains (Plate 6.4b), grain boundary sliding to accommodate large imposed strains, grain boundaries also lend themselves as sites of recrystallization of new grains (Plate 6.11a,b, c and e). Newly recrystallized grains tend to acquire twins easily and to elongate out under the strain. Although they are likely to have recrystallized as fine equiaxed grains under syntectonic conditions (Roberts and Ahlblom , 1978), they are soon flattened out or elongated due to subsequent deformation (Nic olas and Poirier, 1976). The recrystallization process is therefore very likely to be syntectonic, and the grains of equilibrium size. The other type of recrystallized grains nucleate mostly in the highly strained junctions between twins and imposed cleavage (Plate 6.12a and b). In Plate 6.12a, a large relict dolomite grain has been twinned on two sets of f twin planes, the earliest set running left to right of the photo.

PLATE 6.12

Intracrystalline recrystallization (a and b) occurs at high strain junctions.

These junctions are formed as in:

a. By superposition of a late r cleavage - cl - on two earlier f-twin sets (east-west set, north-west - south-east set), and in

b. two r cleavage sets (north-south set and north-west - south -east set), on two earlier twin sets (north east south west set and north west - south east set). These very high strain intersections along the cleavage lamellae become centres for nucleation of new grains. Growth of these new grains would require diffusion or transfer of material within the porphyroclast to the nucleated grains - a solid state process. These intracrystalline grains are generally smaller than those at the grain boundaries.

In c and d relicts - c - of the larger porphyroclasts are being progressively reduced by rotation of sub grains s into new grains.

Optical micrographs in crossed polars with alizarin s staining.
Scale bars: 200μm.

PLATE 6-12

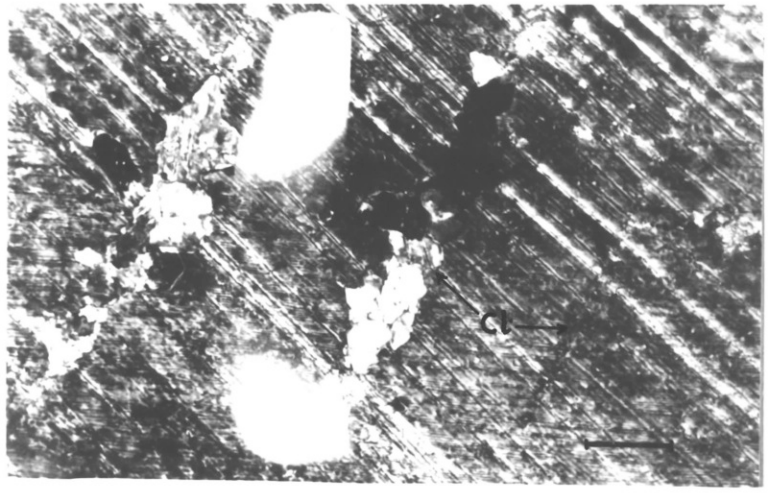

a

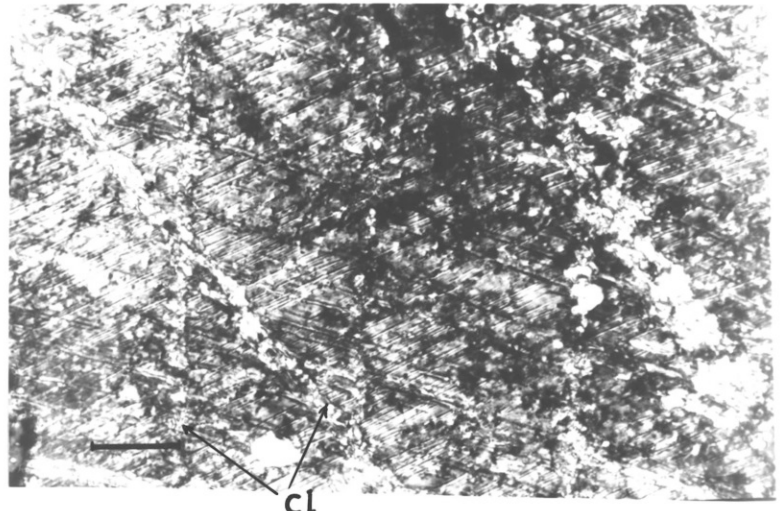

b

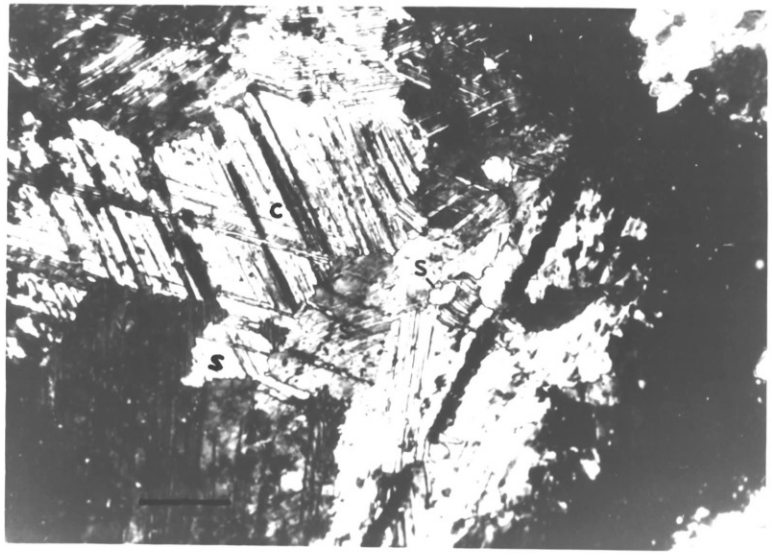

c

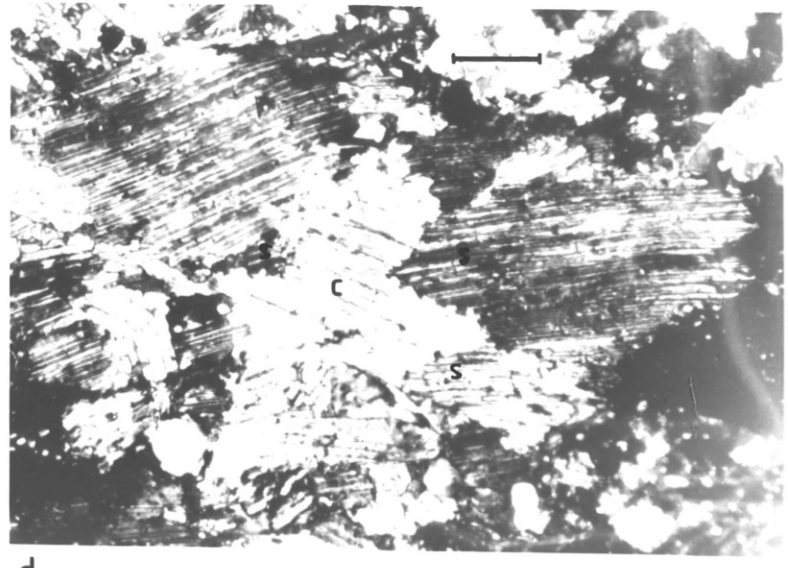

d

The coupling of deformation strains resulting from twinning with those resulting from cleavage produced very narrow zones of high strain energy concentration. Since recrystallization is a strain energy reduction mechanism (Mercier et al; 1977), it is not surprising therefore that these zones of high strain are sites of new grain nucleation.

In Plate 6.12b there are at least two sets of r cleavage imposed on two sets of f twins and the same recrystallization process takes place along the former. The intensity of intracrystalline recrystallization is not comparable to grain boundary recrystallization, and grains produced in the former tend to be smaller than in the latter. This could partly be explained in terms of difference in activation energy between intracrystalline and boundary diffusion. After the nucleation of a new grain, be it within the porphyroclast or at the boundary, the rate of grain boundary migration V_{gb} of the new grain is a function of the driving force F and the grain boundary mobility M as:

$$V_{gb} = MF^n \quad ----- \quad (6.1)$$

(See also Nicolas and Poirier, 1976; equation 4.41). This thermally activated process involves the transport of atoms across the grain boundary by diffusion. The mobility:

$$M = Mo \exp -\frac{(\Delta H_{gb})}{KT} \quad ----- \quad (6.2)$$

for diffusion at the boundary of the porphyroclast, while

$$M = Mo \exp - \frac{(\Delta H_b)}{KT} \quad ----- \quad (6.3)$$

is the mobility of the migrating species within the porphyroclast. ΔH_{gb} is the activation energy for grain boundary migration, while ΔH_b is that for bulk migration. K and T are Boltzmann's constant and the temperature respectively. At a particular temperature

PLATE 6.13

The fibrous dolomite grains.

These grains usually grow at a high angle to the foliation (a and b), although deformation may bend (d) and/or twin them (c and d).

Their constant attachment to a phyllosilicate (chlorite and talc) substratum (a,b,c and d) suggests a genetic relationship between them.

Plates (e) and (f) - quartz and calcite grains growing as fibres on pyrite grains also grow in a similar manner - normal to foliation. In (f) a quartz grain growing on a pyrite face traces the path of growth. Note that optical continuity between both ends is only slightly off.

As shown in (b) and (d) some grains are terminated along their length by other more successful ones. This may suggest growth of favourably nucleated grains.

Optical micrographs in crossed polars.
Scale bars: (a), (c) and (f) = 0.5mm
(b), (d) and (e) = 1mm

PLATE 6-13

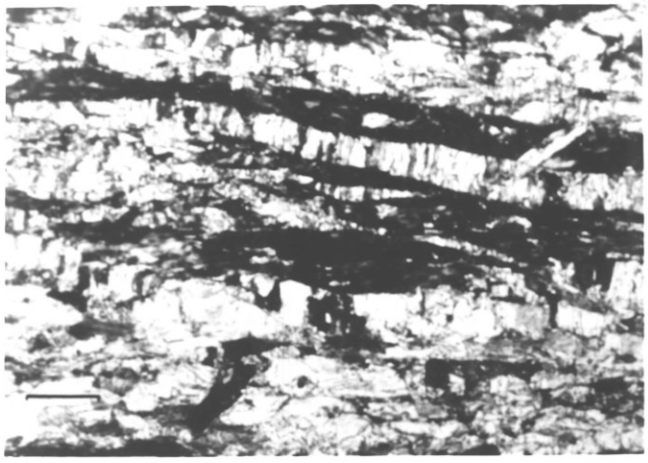

a

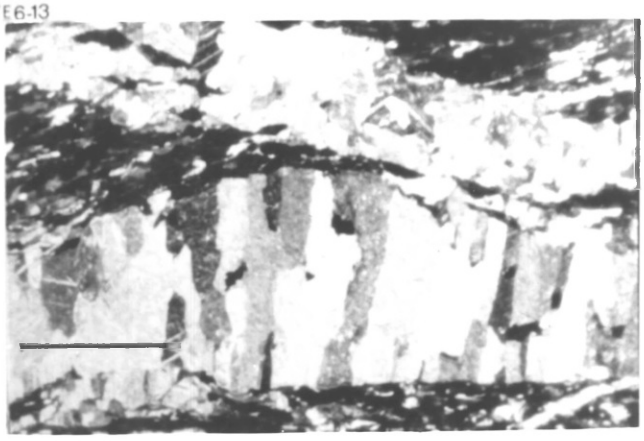

b

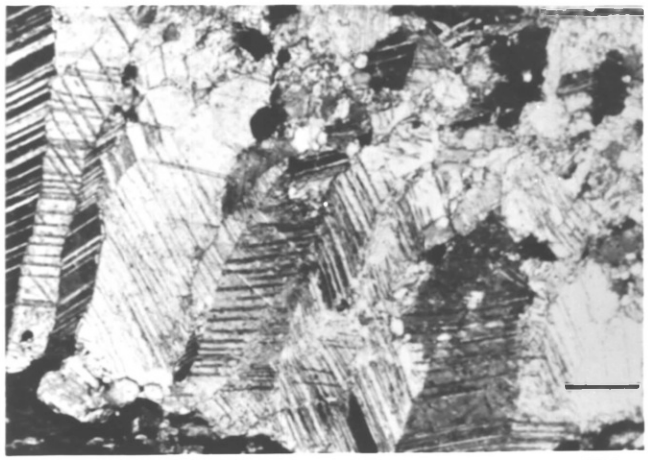

c

d

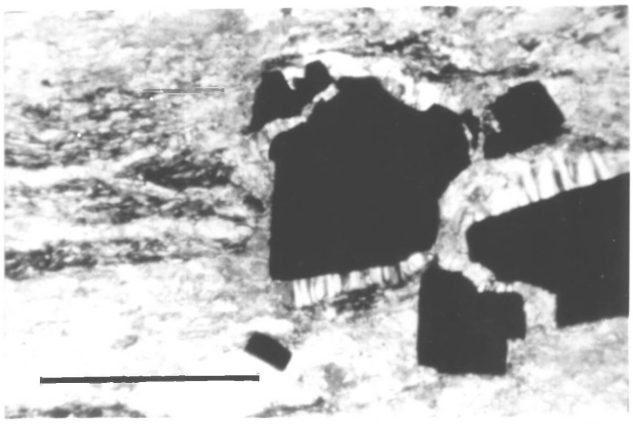

e

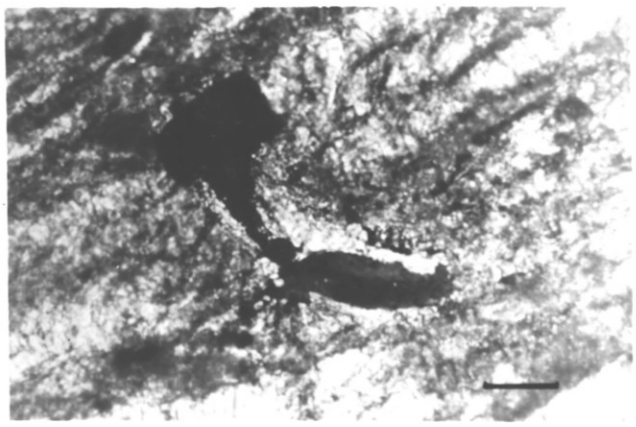

f

$\frac{1}{2}\Delta H_b \leqslant \Delta H_{gb} \leqslant 2/3\Delta H_b$ (Ashby, 1972; Rutter, 1976; White, 1976; Roberts and Ahlblom, 1978), hence grain growth would be more difficult within the porphyroclast than at its boundary. That intracrystalline recrystallization was only found in the larger porphyroclasts is as predicted by Roberts and Ahlblom (1978).

6.4.1.5 The Fibrous Carbonate Microstructure

Apart from the foregoing, the other microstructure of interest at Eriboll comprised the fibrous carbonate crystals growing at a high angle ($\sim 90^{\circ}$) to the foliation (Plate 6.13a,b). They were partly discussed in section 5.5 in terms of fluid pressure requirements for their growth. These grains have a fairly constant spatial relationship to the phyllosilicate bands of chlorite and talc. They appear to grow from the phyllosilicates, spatially, while the latter grew as long plates parallel to the foliation. Some phyllosilicate plates may have two such overgrowths above and below, but it is rare to find grains growing in the same way in the carbonate bands (i.e. in the non-phyllosilicate bands of the foliation). The suggestion is therefore that there is a genetic relationship between these carbonate grains and the dominantly chloritic phyllosilicates.

Occasionally these fibrous crystals are twinned (Plate 6.13c and may be bent (Plate 6.13d), but generally they tend to grow parallel to other later minerals (like calcite and quartz) growing in abutment to pyrite crystals (Plate 6.13e, f).

Chemically these fibrous grains are dolomite grains and they do not respond positively to any staining tests (e.g. they are not stained by alizarine S).

Although the mineralogical system under the Moines is unstable with respect to dolomite (which is altering to calcite - see chapter four) and mica (altering to chlorite - see chapter five), the persistently foliation-normal nature of the fibrous

crystals suggests a late development after the last tectonic phase. Earlier growth of the grains would have caused extensive bending of the fibres in response to the prevailing shear stress.

In section 5.5 this microstructure was used as evidence to support the inference of high fluid pressure (186 MPa) in this environment. Such a fluid pressure, which is a combination of water and carbon dioxide from the reaction:

Dolomite ⟶ Calcite + Periclase + Carbon Dioxide - - - - - (6.4)

could very easily trigger the reverse reaction: (see Fig. 2.15)

Calcite + Periclase + Carbon Dioxide ⟶ Dolomite - - - - - (6.5)

The dolomite produced in (6.5) could then be the late phase that grew as fibrous crystals.

6.5 ESTIMATES OF STRESS BY MEANS OF DEFORMATION MICROSTRUCTURE IN THE DURNESS CARBONATES

6.5.1 Introduction

Since Turner (1962) first described petrofabric techniques for mapping principal stress orientations (using calcite twin lamellae), and relative stress magnitudes, a lot of information has been made available by geologists, ceramicists, and metallurgists aimed at relating stress during material deformation to the resulting microstructure. Although the standard microstructural features in use today are dislocation density, subgrain size and recrystallized grain size in a steady state tectonite (deformed at a constant stress and strain rate in the secondary creep field), other parameters that have been considered and/or used are deformation twinning in carbonate rocks (Jamison and Spang, 1976; Tullis, 1980) and diopside (Raleigh and Talbot, 1967), as well as insitu measurements (Merrill, 1964; Potts, 1964). In situ techniques normally measure borehole deformation (strain) which is

then converted to the stress around the borehole via sufficient knowledge of the elastic moduli of the rock. They are more appropriate in the fields of rock engineering and mining, and will therefore not be considered further here. Paleopiezometers that use deformation microstructures are based on the apparent correlation between flow stress and microstructures produced in experimental deformation studies of several crystalline materials.

Attempts have been made in the recent past by workers in the Moine Thrust Zone to estimate stresses associated with the emplacement of the Moine nappe (Weathers et al., 1979; White, 1979a,b,c). But these have mainly used one mineral type - quartz. In this section calcite and dolomite microstructures (grain sizes) from below the Moine thrust will be used to estimate the paleostresses responsible for the last phase of Moine thrusting and the information obtained will be compared to earlier estimates in other rock types.

6.5.2 Models of Flow Stress and Microstructure

6.5.2.1 Dislocation Density / Differential Stress

The underlying assumption in relating flow stress to dislocation density is that a steady state density of dislocations is enclosed within a grain volume of deformed rock mineral by the applied stress ($\sigma_1 - \sigma_3$). Each dislocation elastically strains the lattice of the crystal, and as a result has a stress field associated with it (Nicolas and Poirier, 1976; Kohlstedt and Weathers, 1980). Nearby dislocations exert forces on one another through their stress fields, and the sum total of the stress fields constitutes the internal stress field.

When the applied stress equals the internal stress, any excess dislocations newly generated are annihilated or absorbed into low-angle boundaries. Since the internal stress exerted by one dislocation on its nearest neighbour is inversely proportional

to their separation (Kohlstedt and Weathers, 1980).

$$\sigma_{int} \propto \frac{\mu b}{r} \qquad ----- \qquad 6.6$$

where μ and b are shear modulus of the material and the Burgers vector respectively. The dislocation density ρ is simply related to the spacing between them by the equation:

$$\rho \simeq 1/r^2 \qquad ----- \qquad 6.7$$

Hence $(\sigma_1 - \sigma_3) = \sigma_{int} = k\mu b\rho^{\frac{1}{2}}$ --- 6.8

where k is a material constant of magnitude 1 to 3 (see also McQueen and Jonas, 1975; Mercier et al. 1977; White, 1979a; Weathers et al, 1979; Christie and Ord, 1980; Kohlstedt and Weathers, 1980). Although 6.8 is empirically derived, Mercier et al. (1977), Christie and Ord (1980) and Kohlstedt and Weathers (1980), have obtained linear relationships by plotting convenient arrangements of the right against the left side, using laboratory data determined for quartz and olivine. Hence the empirical equation 6.8 is said by Kohlstedt and Weathers (1980) to provide a good basis for estimating paleostresses, although the inequality of applied to internal stress in naturally deformed rocks may, according to White (1979), limit its applicability.

6.5.2.2 On the Stress Dependence of Subgrain Size

The size of subgrains is a function of stress mainly, and a relationship of the form:

$$(\sigma_1 - \sigma_3) = \frac{\mu b}{d^v} \qquad ----- \qquad 6.9$$

has been used by Raleigh and Kirby (1970), Mercier et al. (1977), Twiss (1977), White (1979a), Kohlstedt and Weathers (1980) and Edwards et al. (1982).

$\sigma_1 - \sigma_3$ = differential stress

l and v are material constants

μ = shear modulus

b = Burgers vector

d = Subgrain size

Subgrains (or cells in low temperature deformation) form because a uniform array of dislocations tend to cluster together in order to reduce the total free energy (Twiss, 1977; Edwards et al. 1982). According to Twiss, the subgrain walls coexist with a steady state density of dislocations in the volume. Subgrains produced during cold working at high strains resemble both morphologically and structurally the subgrains produced during creep, although the high stresses and low temperatures in the former case result in smaller sizes for subgrains, which also contain high dislocation densities (White, 1979a). There is a continuous dislocation interaction between the matrix of the subgrain and its boundary throughout the deformation, such that at low strains subgrains are bounded by hedges of dislocations. The latter, as shown by White (1979a), reorganise into walls of dislocations as strain increases.

By means of rigorous theoretical treatment, Edwards et al. (1982) derived a stress/subgrain size relationship of the form

$$\frac{\sigma_1 - \sigma_3}{\mu} = \left[\frac{64}{\pi g A(1-v)} \frac{D_2}{D_1} bcj\right]^{1/n} \left(\frac{L}{d}\right)^{1/n} \left(\frac{b}{d}\right)^{3/n} \quad - - - \quad 6.10$$

where $\sigma_1 - \sigma_3$, μ , b and d have the same meaning as in 6.9 and

A and n are dimensionless constants

Cj = number of jogs per unit dislocation length

D_1 = coefficient of diffusion for creep

D_2 = coefficient of diffusion for dislocation climb in the boundary

g($o < g < 1$) is determined by the local geometry of deformation

L = the mean slip distance

V = Poisson's ratio, and π has its usual value $\frac{22}{7}$

Equation 6.10 resembles or reduces to equation 6.9 if

$$\mathbf{l} = \left[\frac{64}{\pi g A(1-v)} \frac{D_2}{D_1} bcj \frac{L}{b}\right]^{1/n} \quad \text{and}$$

V in (6.9) = $4/n$

The material constants $\mathbf{l}$ and v in equation 6.9 have values of 10 - 100 and ~ 1 respectively for geological materials (Twiss, 1977; White,1979a; Etheridge and Wilkie, 1981; Edwards et al; 1982).

6.5.2.3 <u>On the Stress Dependence of Recrystallized Grain Size</u>

At least three mechanisms of dynamic recrystallization have been outlined (see Mercier et al., 1977; Roberts and Ahlblom, 1978; Kohlstedt and Weathers, 1980), and these will be considered under low temperature and high temperature subheadings.

(i) At low temperatures and/or low stresses subgrain boundaries may continuously rotate to form grain boundaries. The misorientation across a subgrain boundary progressively increases with continued deformation as dislocations from the subgrain matrix are incorporated into the boundary. At about 7^{o} misorientation the boundary energy approaches its maximum value (Kohlstedt and Weathers, 1980), and is, for all purposes a

grain boundary. This mechanism of subgrain - rotation recrystallization has been identified in naturally deformed rocks (White, 1973b, 1976b; Poirier and Nicolas, 1975).

(ii) At high temperatures and high stresses, new grain boundaries do form by the migration of a small portion of an existing high-angle grain boundary. As the boundary migrates or bulges into the region of higher dislocation density, it absorbs the dislocations on its way thus reducing the strain energy in the grain. With further deformation the bulge pinches off at the base to form a new grain which is relatively strain free (Hobbs et al. 1976; Mercier et al. 1977; Kohlstedt and Weathers, 1980).

(iii) A third mechanism of recrystallization is outlined by Mercier et al.(1977) to consist of the generation of new nuclei preferentially at intersections of subgrains and grain boundaries. Since the driving force for growth of the new grains is the energy difference between the new grain and the old grain/subgrain pair, the direction of growth is normal to the new grain boundary (see Fig. 6 of Mercier et al. 1977). This third mechanism may not be very different from (i) and (ii).

Even though recrystallization lowers the strain energy of the deforming material, it still needs to be thermally activated hence the observation of dolomite recrystallization above 700°C by Wenk and Shore (1975). Unlike recovery which begins very rapidly and decreases with time, recrystallization starts slowly, builds to a peak and then decreases with time, unless the deformation continues, when both processes may repeat themselves in cycles.

Due to the continued generation of dislcoations during deformation an equilibrium or steady state condition obtains when the reduction in free energy due to decrease in dislocation

density is balanced by the increase in free energy due to strain and the increased grain boundary area. At that state, the grain size D is a monotonic function of the differential stress:

$$\frac{D}{b} = Kn \left[\frac{(\sigma_1 - \sigma_3)}{\mu}\right]^{-n} \quad ----- \quad 6.11$$

(Twiss, 1977, 1980; Kohlstedt and Weathers, 1980). n and Kn are constants of magnitude 1.47 and 4.60 respectively, calculated by Twiss (1977) on the basis of combined data for nine deformed materials. Equation 6.11 could be dimensionally represented by:

$$(\sigma_1 - \sigma_3) = m\, D^{-w} \quad ----- \quad 6.12$$

showing the stress dependence of the reciprocal grain size -D (mm) through a constant m. The value of m varies from one material to another and also according to the ratio of internal to applied stress within the deforming matrix. Calcite, for instance, has m = 7.5 with w = 0.68 and quartz has m = 5.5 (Twiss, 1977; Weathers et al. 1979; White, 1979a; Christie and Ord, 1980). Mercier et al. (1977) have obtained the relation:

$$(\sigma_1 - \sigma_3) = 381.D^{-0.71} \quad ----- \quad 6.13$$

on the basis of deformed wet quartzites. $(\sigma_1 - \sigma_3)$ is in megapascals and D is in microns. Similarly Friedman and Higgs (1981), obtained a relation of the form:

$$(\sigma_1 - \sigma_3) = 13.8D^{-0.70} \quad ----- \quad 6.14$$

from the simple shear deformation of calcite polycrystals. The stress is in MPa, while D is in millimeters. As Christie and Ord (1980) showed, although the relationships derived by Twiss, (1977) and Mercier et al, (1977), have different values for m and w (in equation 6.12) the real difference between the two functions is small, amounting to differences in estimated flow

stress of less than a factor of 2, for a particular grain size.

6.5.3 Problems and Inadequacies with stress estimates using the stress/microstructure relationship.

If dislocation densities, subgrain sizes and/or recrystallized grain sizes in deformed or deforming minerals are functions only of the prevailing stress, one would expect the result (stress) to be the same no matter the material analysed in a given tectonite or the method (equation) used. But inconsistencies in results to date indicate that there may be difficulties right through from the equations and constants, methods of measuring the microstructural parameter in question, as well as inadequate knowledge of the effect of the total physical/chemical environment or system on the microstructure/s being analysed in geological materials (see White, 1979a, b; Weathers et al. 1979; Christie and Ord, 1980; Etheridge and Wilkie, 1981).

5.5.3.1 Difficulties with measurement of ρ, d and D

It has been shown by White (1979a) that measurements of ρ, d and D using different instruments should not be used together since the constants k, l and m in equations 6.8, 6.9 and 6.12 respectively do vary from one instrument to another. An accurate determination of dislocation density is an immensely difficult task due mainly to the numbers involved, the difficulty of getting all dislocations on a plane into contrast and counting errors due to overlap of dislocations (Christie and Ord, 1980). On the other hand, grain and subgrain sizes determined by transmission electron microscopy are very different from those measured in optical microscopy. It is necessary to use one instrument for a given microstructure, at a time.

6.5.3.2 Difficulties with the physical equations

To the extent that discrepancies exist in the coefficients and powers of the physical equations proposed either from theoretical treatment or empirical derivation, will little differences result from stress values determined using such equations (compare Mercier et al. 1977; Twiss, 1977 and Friedman and Higgs, 1981; see also S.S. 6.5.2.3). Some of the estimates of stresses recently published show wide differences for different microstructural parameters in the same rocks (see White, 1979a; Wheathers et al. 1979; Christie and Ord, 1980; Etheridge and Wilkie,1981). Some of these differences will, no doubt, have their roots in the basic inadequacies of the paleopiezometers.

The way temperature and strain rate affect dislocation density, subgrain and grain sizes of geological materials has not been widely exposed yet, but indications are that there is a dependence of subgrain and grain size at least on temperature (TaKeuchi and Argon, 1976; Mercier et al. 1977; Roberts and A hlblom, 1978; White, 1979a; Tullis and Yund, 1982). TaKeuchi and Argon (1976) showed that d/b is not only a function of τ/μ at a constant temperature, but also between 400°C and 800°C for LiF, d/b increases with temperature at constant τ/u . This demonstrated the inadequacy of their relation (see TaKeuchi and Argon, 1976, equation 11, p.1551):

$$\tau = K\frac{\mu b}{d} \qquad - - - - - \qquad 6.15$$

which equates the shear stress resolved on single crystal planes τ , to the subgrain size d, Burgers vector b, shear modulus μ and a constant K(10-100). The similarity of equation 6.15 to 6.9 is obvious, though the former relates shear stress, while the latter relates deviatoric stress, to subgrain size. Also using LiF, they showed that the dislocation density is a

a function of the reciprocal temperature at constant shear stress:

$$(\rho^{b^2})_{\tau/\mu} \propto \frac{1}{T} \quad - - - - - \quad 6.16$$

Since ρ, d and D are related for a particular material, it has been suggested (White, 1979a) that a temperature dependence of one could also mean a dependence for the other parameters. This is supported by Mercier et al's (1977) formulation of temperature dependence of grain size by the equation:

$$D = 1.13\sigma^{-1.4} \exp(13500/RT) \quad - - - - - \quad 6.17$$

where D is grain size, σ is deviatoric stress, R and T are the universal gas constant and temperature respectively. Also Roberts and Ahlblom (1978) showed that the parameter Z (Zener - Hollomon parameter), increased as the dislocation density, but decreased as the subgrain and grain sizes increased. Z is defined as:

$$Z = \dot{e} \exp(Q/RT) \quad - - - - - \quad 6.18$$

where $\dot{e}$ is the strain rate and

$$Q = -R\left[d\ln\dot{e}/d(1/T)\right]_{\sigma_{max}} \quad - - - - \quad 6.19$$

They proposed a decrease in grain size with decrease in strain rate at a constant temperature, that is the effect of strain rate on grain size is noticeable when the temperature is held constant, and vice versa. This is analogous to the twinning behaviour of calcite in temperature/strain rate space (Spiers, 1981).

6.5.3.3 Problems connected with the Geological Environment

The geological environment is one in which deformed rocks are not monominerallic, their immediate past history is not easy to decipher and what contributions other deformation mechanisms have made to the present microstructure cannot be exactly assessed. The presence of a second phase, e.g. phyllosilicates, does actually inhibit grain growth to an

equilibrium size (White, 1979a; Etheridge and Wilkie, 1981; see also Plate 6.5d). Clay minerals are usually associated with water (interstitial and bound water) and how this water in the vicinity of deforming crystallites affects grain size is not yet known.

Deforming rocks often go through cycles of high stress and stress relaxation, such that minerals of high strain go through periods of reduced strain, allowing other minerals to pick up strain (White and White, 1984). This cyclic behaviour was definitely not incorporated in formulations of steady state equations, and the way it affects the ratio of internal to applied stress within the deforming grains is yet to be understood.

6.5.4 On measured Grain Sizes

For the present study the microstructural parameters measured were recrystallized dolomite and calcite grains and twinned calcite grain sizes. Attempts to use twinned calcite grain size to estimate stress proved abortive. The stress/twinned calcite grain size relationship suggested by Spiers (1981) produced an equation similar to 6.12, Stresses estimated using the equation always produced results more than an order of magnitude higher than those estimated with untwinned grain sizes, for the same rock sample.

As shown in Figure 6.1, mean untwinned calcite grain sizes (utw) in three of the four samples studied tend to be smaller than the twinned calcite (tw) grains in the same samples. Untwinned calcite in Oyster Shell rock (OY1) and OY4) and the Durness Carbonates (Er10 and Er12) do not seem to show any marked difference in grain sizes. Figure 6.2 shows the

Fig. 6.1

Calcite grain size in Oystershell rock (OY1, OY4) and Durness carbonates (Er - 10, Er - 12). Closed circles = tw are for twinned grains and open circles = utw are for untwinned grains. Bars above and below the points represent standard deviation.

All sizes of twinned and untwinned calcite and dolomite grains were measured by the intercept method using an optical microscope. Usually 150 to 200 measurements were made per sample, from which the mean and standard deviation were calculated.

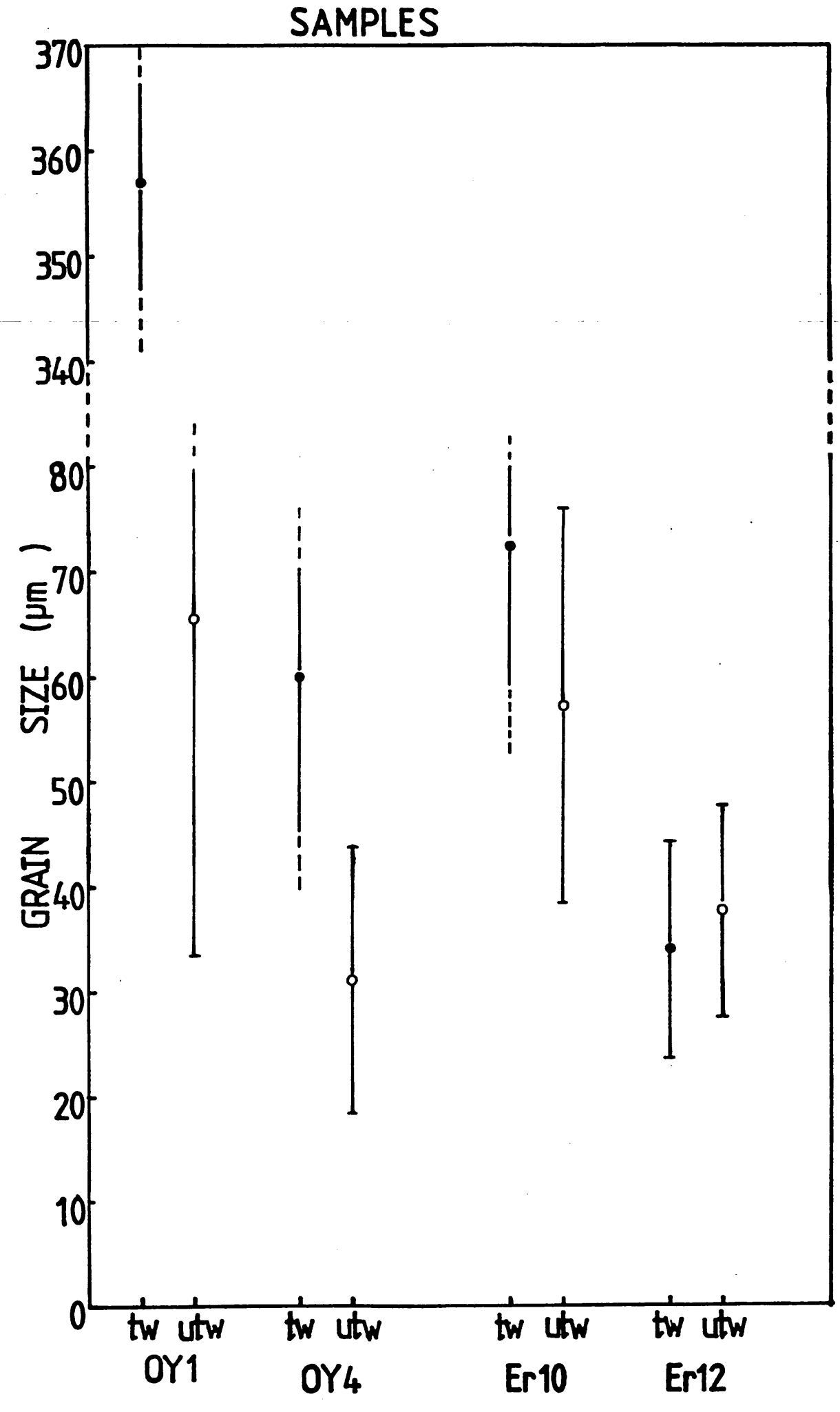
SAMPLES
GRAIN SIZE (µm)
370
360
350
340
80
70
60
50
40
30
20
10
0
tw utw tw utw tw utw tw utw
OY1
OY4
Er10
Er12

Fig. 6.2

Twin-free recrystallized dolomite grain size from the south C88, C89, C105 (Cnoc a' Chaoruinn), through Glencoul ST_7 and ST_{12}, to the north Er - 9, Er - 17 (Eriboll).

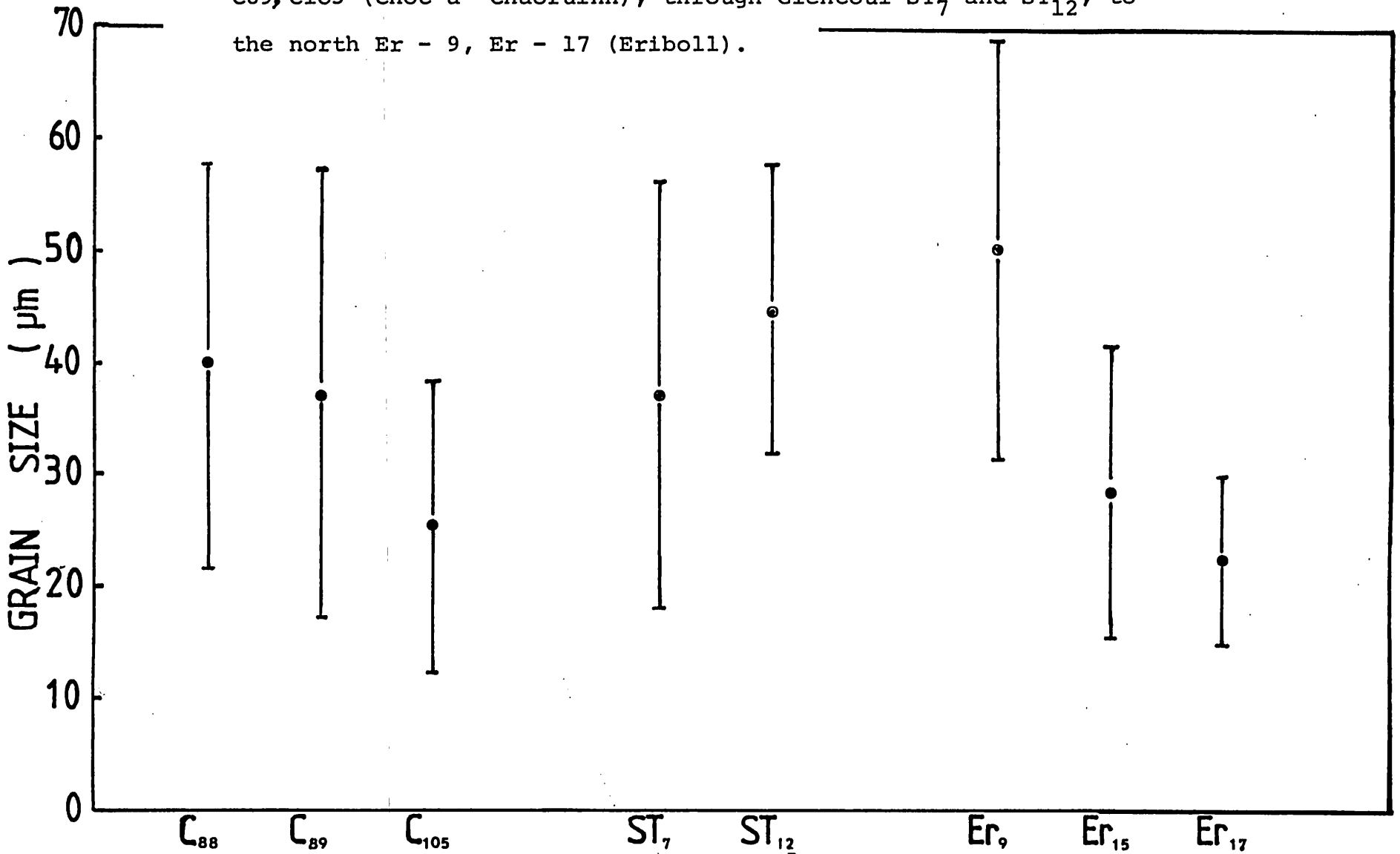

variation of twin-free dolomite grain size from Cnoc a' Chaoruinn (C88 - C105), through Glencoul (ST_7 - ST_{12}) to Eriboll (Er_9 - Er_{17}). Carbonate grain sizes measured at Knockan could not be included in the figures or used in the stress estimates for the reason that the cataclastic nature of the deformation at Knockan will not always allow the application of laws based on steady state creep.

As shown in Figure 6.2, mean dolomite grain size tends to be between 20 μm and 40 μm, without a consistent tendency for recrystallized grains to decrease towards the north (Eriboll).

6.5.5 On Choice of Equations and Parameters

For estimates of stress using dolomite and calcite equilibrium grain sizes, the equations of Twiss (1977) were used (see Twiss, 1977, equation 11). He showed that

$$\sigma = Bd^{-0.68}, \text{ where } B = K\Gamma b^{0.68} \quad ---- \quad 6.20$$

σ is the differential stress ($\sigma_1 - \sigma_3$) in MPa, d is the grain size in (mm), K = 2.3988 ≈ 2.40.

$$\Gamma = \frac{\mu}{1-V}$$ where μ is shear modulus, and

V is Poisson's ratio, and

b is the most common Burgers vector for the material under consideration. For calcite, B = 7.5 (Twiss, 1977), while for dolomite the value of B is unknown. It is necessary to estimate B for dolomite in order to set up a usable stress/grain size relationship.

Using physical data from Birch (1966) on Bethlehem dolomite (U.S.A.),

E = Young's Modulus V = Poisson's Ratio (unknown)

G = Rigidity Modulus μ = Shear Modulus

K = Bulk Modulus = $^1/_\beta$ β = Compressibility

b = Burgers Vector

E	G	$\beta = {}^1/_K$	V(estimated)
0.710	0.323	1.19	0.36
0.930	0.362	1.19	0.32
0.916	0.398	1.19	0.32

Table 6.2

$$V = \frac{3k - E}{6k} \qquad \text{- - - - -} \qquad 6.21$$

Using the values of E and $\beta = {}^1/_k$ to find V,

(1) $V = \frac{3 \times 0.84 - 0.710}{6 \times 0.84} = 0.36$

(2) $V = \frac{3 \times 0.84 - 0.930}{6 \times 0.84} = 0.32$

(3) $V = \frac{3 \times 0.84 - 0.916}{6 \times 0.84} = 0.32$

0.33 = average value of V.

$$\mu = \frac{E}{2(1+V)} \qquad \text{- - - - -} \qquad 6.22$$

$= 3.2009 \times 10^4$ MPa (average)

$$T = \frac{\mu}{1 - V} \quad \text{(Twiss, 1977)} \qquad \text{- - - - -} \qquad 6.23$$

$= \frac{32009}{0.67000} = 4.7775 \times 10^4$ MPa

Log K = 0.38 (from equation 6.20, also see Twiss 1977)

$\therefore$ K = 2.40

b = 4.81 Å = 4.81×10^{-7} mm for dolomite (Paterson, 1976)

$\therefore$ B (equation 6.20) becomes

$B = 2.3988 \times 4.7775 \times 10^4 \times (4.81 \times 10^{-7})^{0.68}$

$= 5.7950$

Table 6.3

Estimates of paleostress (MPa) associated with Moine thrusting using equilibrium calcite (Cct) and dolomite grain size.

Sample Number	Source (Rock & Area)	Mean Grain Size (Twinned Cct) (μm)	Mean Grain Size (untwinned Cct) (μm)	Mean Grain Size (untwinned Dolomite (μm)	Stress from equil. Cct grains (MPa)	Stress from equil. dolomite grains (MPa)
OY1	Oystershell Rock - Eriboll	358.43	65.00		48.07	
OY4	Oystershell Rock - Eriboll	59.99	31.18		73.16	
Er10	Marble - Eriboll	72.27	57.60		52.42	
Er12	Marble - Eriboll	33.67	37.40		69.81	
Er9	Marble - Eriboll			50.30		44.26
Er15	Marble - Eriboll			28.58		64.97
Er17	Marble - Eriboll			22.52		76.48
ST7	Durness Carbonates_ Glencoul			36.79		54.74
ST12	Durness Carbonates_ Glencoul			44.50		48.10
C88	Durness Carbonates_ Cnoc a'Cha.			39.83		51.72
C89d	Durness Carbonates_ Cnoc a'Cha .			36.96		54.54
C105	Carbonates _ Cnoc a'Cha.			25.13		71.20
Mean Stress					60.87	58.25

Therefore the stress/grain size relationship for dolomite becomes:

$$\sigma = 5.795 \times d^{-0.68} \quad ----- \quad 6.24$$

and for calcite, using Twiss's (1977) relationship

$$\sigma = 7.5 \times d^{-0.68} \quad ----- \quad 6.25$$

These are the equations to use in the stress estimates by means of dolomite and calcite recrystallized grain size. The accuracy of the value B as determined above depends on the accuracy of the elastic constants of dolomite grains measured in the laboratory. At the moment, data on elastic properties of dolomite grains are very rare and there is a tendency to use what is available, rather than choose the best values as in other minerals.

6.5.6 Result of Stress Analysis

Using equations 6.24 and 6.25 estimated stresses from twelve carbonate samples are presented in Table 6.3. These range from 44.26 MPa (Er9) to 76.48 MPa (Er17), with an average of 58.25 MPa for dolomite and 60.87 MPa for calcite. These ranges and averages are quite within those estimated by White (1979b - 50 - 100 MPa), despite his warning not to rely very much on the values, Wheathers et al. (1979), and Ord and Christie (1984) all of whom used recrystallized quartz grain size in the Moine Thrust Zone. The newly determined differential stress suggests a shear stress of between 22 to 38 MPa and possibly up to 40 MPa.

6.6 ANALYSIS OF THE CRYSTALLOGRAPHIC FABRIC OF DOLOMITE AND CALCITE IN TECTONITES OF THE DURNESS FORMATION.

6.6.1 Introduction

In this section a dynamic analysis of the crystallographic preferred orientation of the deformed carbonates is presented. This consists mainly of the c-axis fabric of dolomite tectonites

in the south (Assynt) and c-axis fabric of both calcite and dolomite tectonites from the Eriboll end of the thrust zone.

The microstructure of the carbonate rocks the fabric of which is hereby presented has been described in sections 6.3 to 6.4 of this chapter. This fabric analysis excludes the dominantly cataclastic rocks of Knockan and the undeformed or low strain rocks of the foreland. It starts from the eastern bend of the Moine Thrust at Cnoc a' Chaoruinn northwards through Glencoul to Eriboll, within the thrust zone. Temperatures are those determined, using the calcite/dolomite geothermometer, where possible (see Chapter Four).

6.6.2 Method of Analysis

Most of the samples studied had extension lineations clearly printed on them, and orientated thin sections were cut parallel to the lineations and normal to the foliation, i.e. XZ sections according to the tectonic scheme shown in figure 6.3b. In this scheme X marks the direction of maximum finite elongation and Z is the direction of maximum finite shortening. Y, the intermediate axis, accordingly refers to the direction of intermediate strain. This representation therefore places the XY plane of the finite strain ellipsoid on the foliation.

The second type of sections were cut normal to lineations and normal to foliation i.e. YZ sections, and were used mainly to supplement or corroborate information from XZ sections. In both sections the two fabric elements L and S (Fig. 6.3c) define a reference frame to which the crystallographic fabrics of the carbonate tectonites are related.

In samples with no noticeable lineations, sections were cut parallel to N120° - 300° which is approximately parallel to the lineations and the movement direction of the overlying

Fig. 6.3

(a) Fabric of a non-tectonite and its typical random pattern of c-axes.

(b) X,Y and Z are the principal directions of the finite strain ellipsoid. X is the direction of maximum finite elongation, while Z is the direction of maximum finite shortening. Y is the intermediate strain axis, and the foliation - s is accordingly an XY plane.

(c) Fabric of a tectonite and one common pattern of c-axes crystallographic preferred orientation. l and s are lineation and foliation respectively.

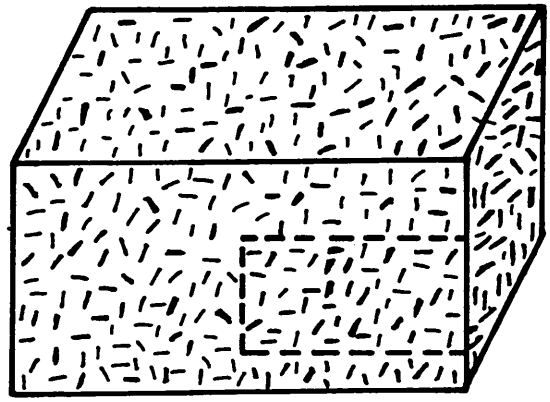

(a)

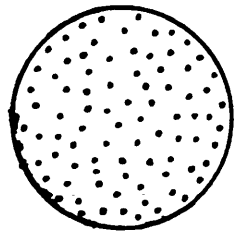

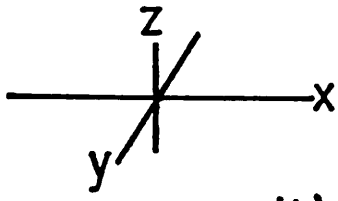

(b)

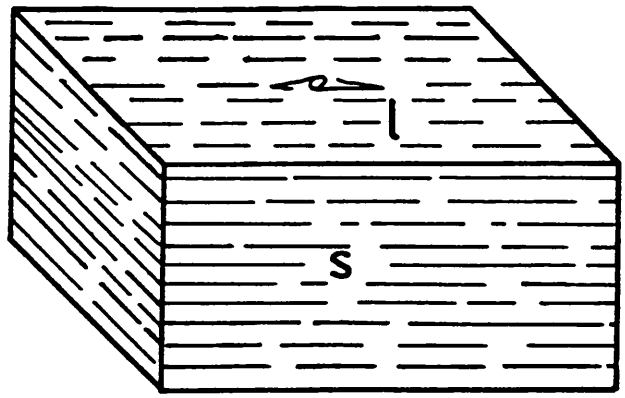

(c)

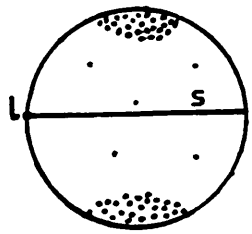

Moine nappe (Coward et al. 1980).

Ultra-thin thin sections of the carbonate samples were prepared using the method of Lindholme and Dean (1973). This three-stage lapping technique uses 1,200 grit aluminium oxide powder for the final lapping, producing thin sections of about 3μm thickness. Although the method often produced wedge-shaped sections, only where such sections were judged to be representative of the sample were they used for fabric analysis. The study of crystallographic fabric was done by means of a universal stage attached to a normal petrological microscope.

Fabric data were plotted by projection using the lower hemisphere of a Schmidt net, while counting and contouring were done by means of a Kalsbeek counting net as suggested by Ragan (1973).

6.6.3 Results of Fabric Analysis

6.6.3.1 Dolomite C-Axis (0001) crystallographic preferred orientation

As figure 6.4 shows the c-axis fabric of dolomite tectonites below the Moine thrust displays a detectable variation from Cnoc a' Chaoruinn to Eriboll. From a pseudo-orthorhombic symmetry with peripheral girdles (C - 39 and C - 84), there is a slight tendency towards concentrations at high angle to the foliation as the traverse is followed eastwards (C - 89). This trend is not quite so well followed by ST - 12 as ST - 7 from the Glencoul area. The tendency towards foliation normal point maxima (characteristic of carbonates) is best displayed by Er - 17 and Er - 15 from Eriboll, compared to the samples from the south. In all cases there is a strong tendency for c-axis of deformed dolomite grains to lie at a high angle to the foliation(s). This also includes a tendency of non-parallelism with the lineation which itself lies on the foliation. The lineation (l) position

Fig. 6.4

Dolomite c-axis crystallographic fabric from Cnoc a' Chaoruinn to Eriboll along the Moine Thrust (MT) Zone. Lower hemisphere projection using a Schmidt net. Contours are 2,4,6,8, 10% and above per 1% area. Temperatures estimated by calcite/dolomite geothermometry (see Chapter 4).

The top of the fabric diagram corresponds to the top of the sample, while the top arrow of the simple shear couple is parallel to the tectonic transport direction. A sinistral sense of shear is inferred.

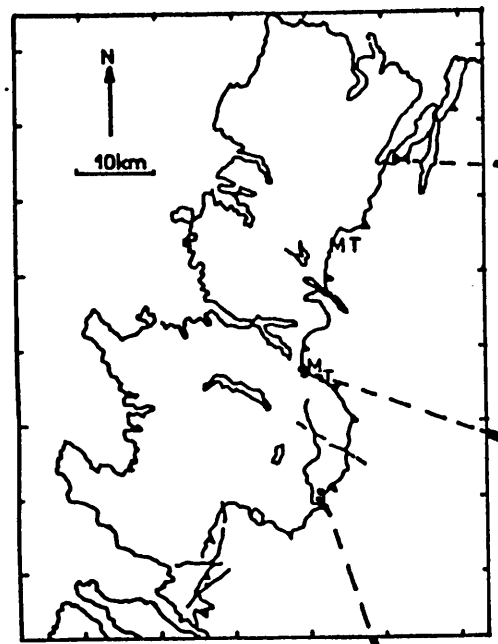

T ≙ 400°C

Er-15 · Dol (150)

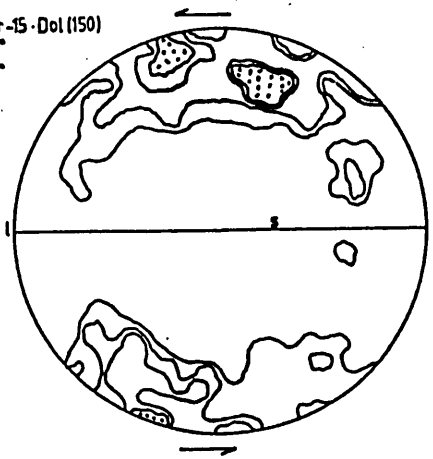

Er-17 Dol (150)

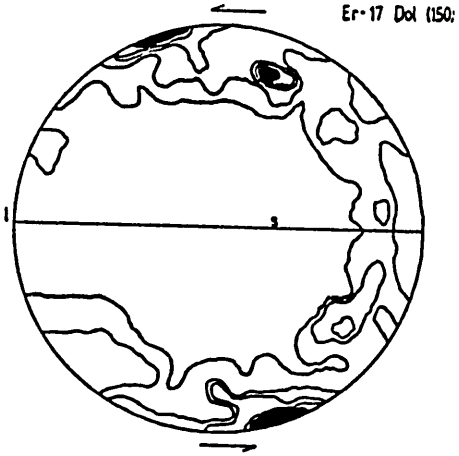

ST-7 Dol (150)

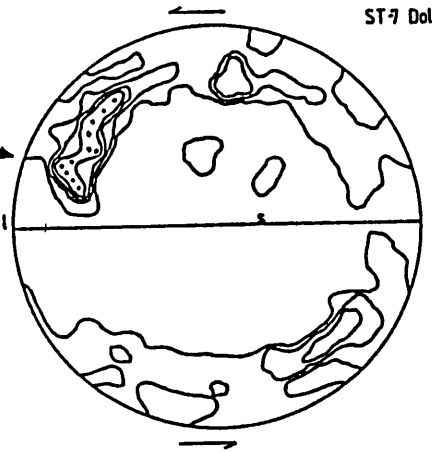

ST-12 Dol (150)

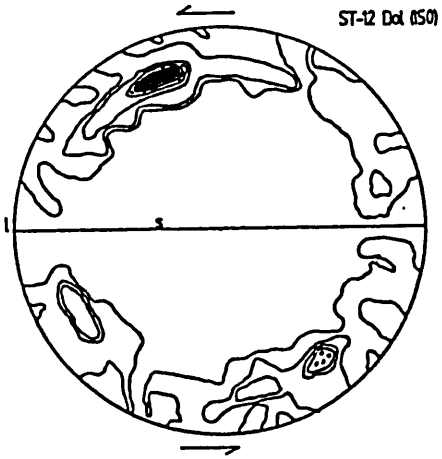

C-39 Dol (150)

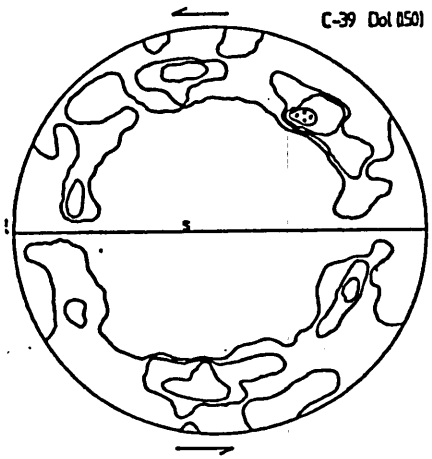

T≙314°C

C-84 Dol (150)

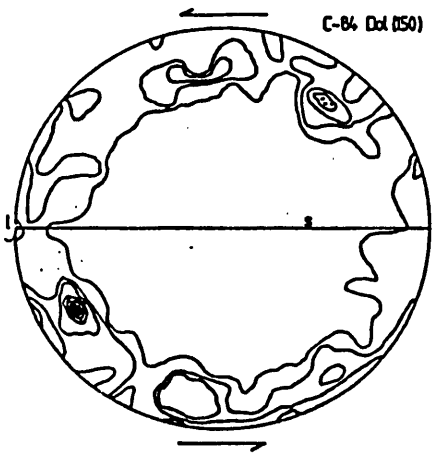

C-89 Dol (150)

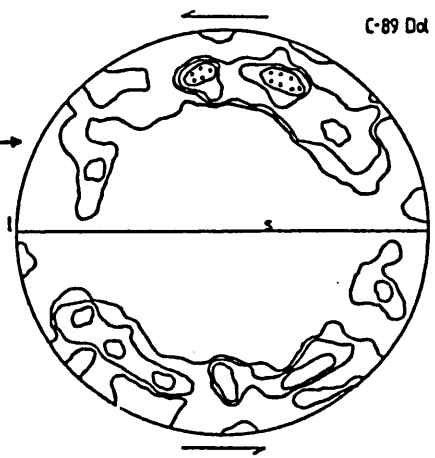

adopted in all the diagrams is that towards the transport direction (WNW) with respect to the rest of the rock geometry, as opposed to the plunge (ESE) direction.

Also noteworthy is the symmetry of the fabric with respect to the foliation plane and lineation direction. In all the fabric diagrams it is quite easy to insert at least two planes of symmetry one of which is invariably the foliation plane (S). In the symmetry analyses it is the skeletal outline or main features rather than density distribution that is relied upon, because as suggested by Paterson and Weiss (1961) and Lister and Williams (1979) a final fabric which is symmetric with respect to the skeletal outlines, may be asymmetric when density distribution is considered. Law et al. (1984) also found very high symmetry of c-axis fabrics with respect to the foliation and lineations. They analysed quartz c-axis fabrics of both porphyroclasts and recrystallized grains in the lower and upper Arnaboll nappes below the Moine thrust plane of Eriboll area. As shown in Figures 6.5 and 6.6 the symmetry displayed by dolomite is not similar to that of calcite. The calcite fabrics are more oblique with respect to the foliation and lineation, much in the same way as recrystallized quartz fabrics of Law et al. (1984) are oblique in comparison to the fabrics of quartz porphyroclasts. This analogy is easier to understand if it is realised that both recrystallized quartz and calcite in this part of the Moine thrust zone are solid state derivatives or products from porphyroclasts of quartz and dolomite respectively, even if the former is physical and the latter is chemical in nature.

The tendency for c-axis fabrics of dolomite to change from peripheral girdles to pseudo-maxima at a high angle to foliation (compare C - 39 to Er - 15, Fig. 6.4), correlates well

Fig. 6.5

Comparison of dolomite (a) and calcite (b) fabrics from the same tectonite (Sample Er - 15). Note the asymmetry of the point maxima in (b), while (a) shows better symmetry with respect to s. Contours are 2,4,6,8, 10% and above per 1% area.

Dolomite - 150 grains , calcite - 110 grains.

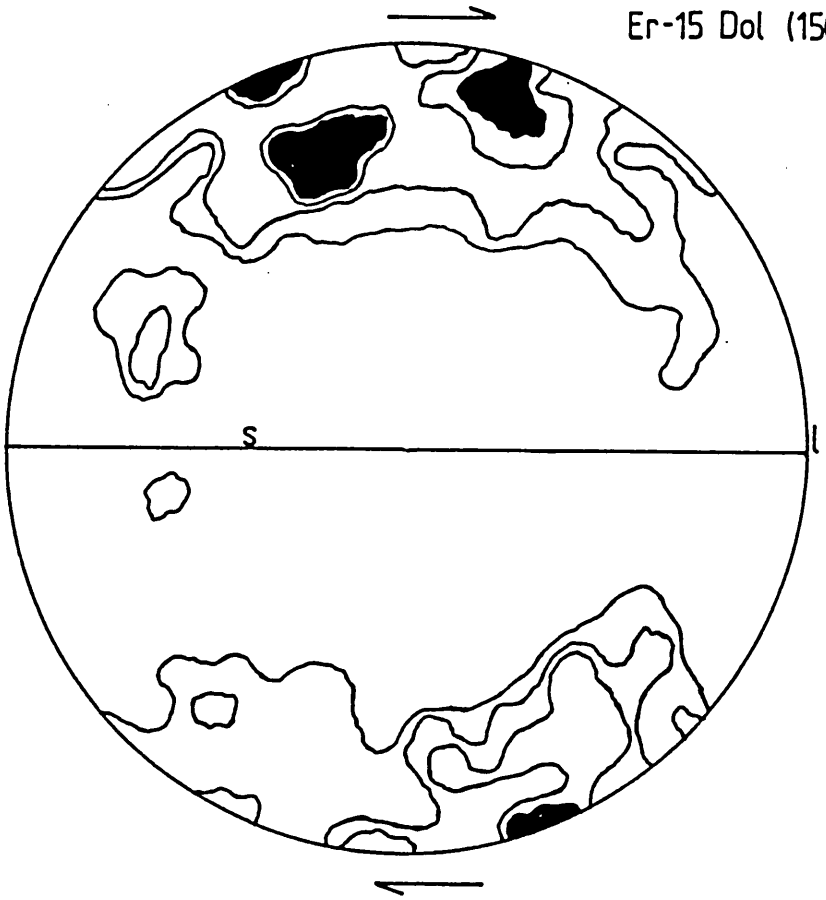

a

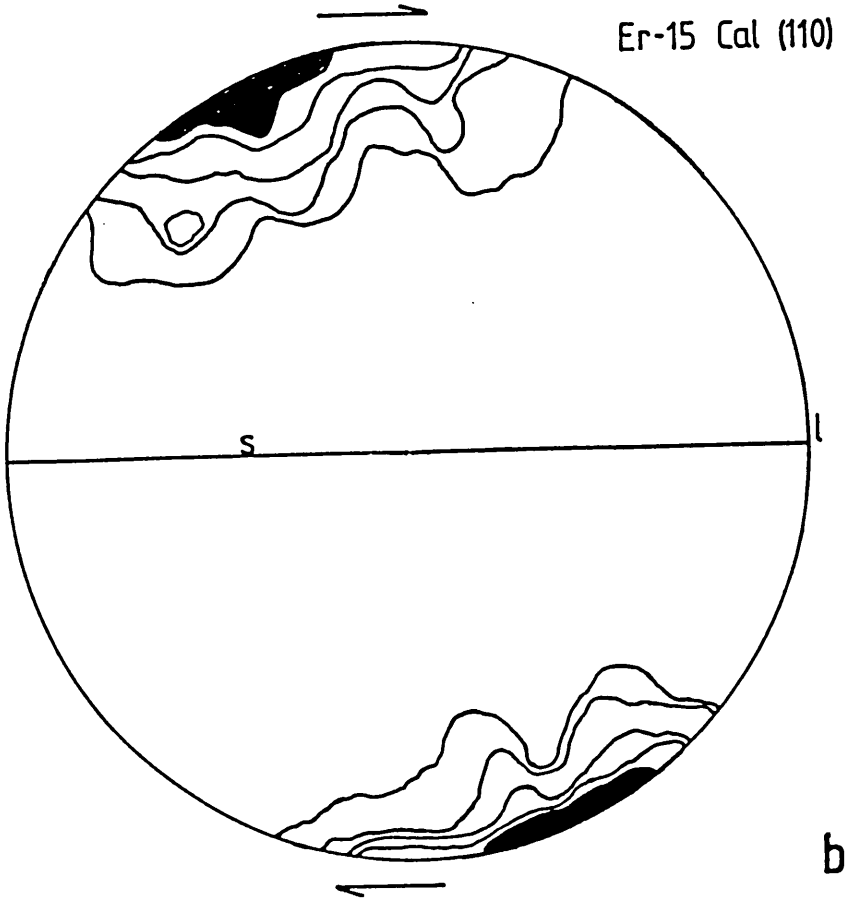

b

with rise in temperature from 314°C to 400°C (see Chapter Four for method of estimate). The significance of this correlation is discussed later.

6.6.3.2 Comparison of Dolomite and Calcite Fabrics from the same Tectonites

Neumann (1969), made a comparison between dolomite and calcite fabrics from naturally deformed neighbouring layers of interlaminated marble and dolomite. The specimens were collected 30cm apart. In this subsection the fabrics of calcite and dolomite from the same rock samples are presented. The samples analysed were mainly from the Eriboll end of the Moine Thrust Zone, where the proportions of calcite to dolomite, as can be seen in optical microscopy, are sufficient for comparison. By controlled staining with Alizarine S the calcite could be just differentiated from the dolomite without excessive depreciation in optical transmissibility.

As shown in Figures 6.5 and 6.6 calcite and dolomite fabrics from the same rock samples are dissimilar. Although both have c-axis maxima at high angles to the foliation, calcite fabrics are more asymmetric than dolomite with respect to the foliation. Secondly, while dolomite tends to split up into several discrete maxima, calcite tends to form a single maximum density. That both samples Er - 15 and Er - 17 show stronger maxima for calcite than dolomite can be related directly to the strength of the two materials, dolomite being stronger than calcite (Mercier et al. 1977; Barber, 1977). Neumann (1969) noticed similarities in calcite and dolomite fabrics from which the conclusion was advanced that the orienting mechanism must be one that produces similar results in both minerals.

The fabrics of Figure 6.5b and 6.6b are similar to

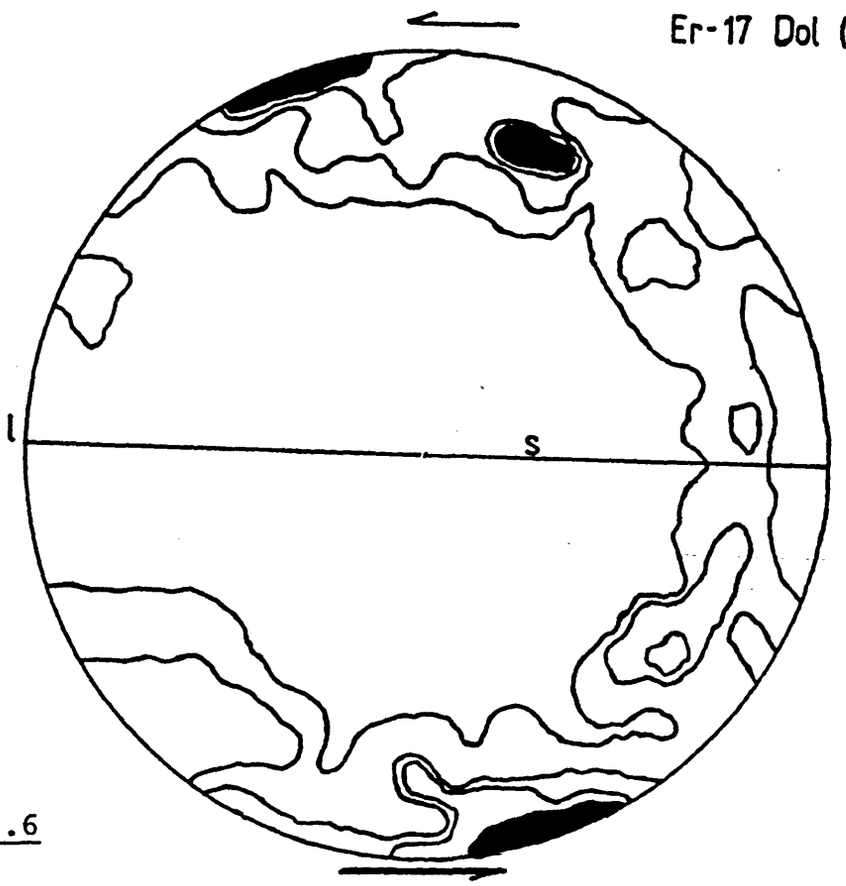

a

Fig. 6.6

Comparison of tectonite fabrics of dolomite (a) and calcite (b) from the same sample (Er - 17). Contour intervals 2,4,6,8, 10% and above per 1% area.

Dolomite - 150 grains , calcite - 110 grains

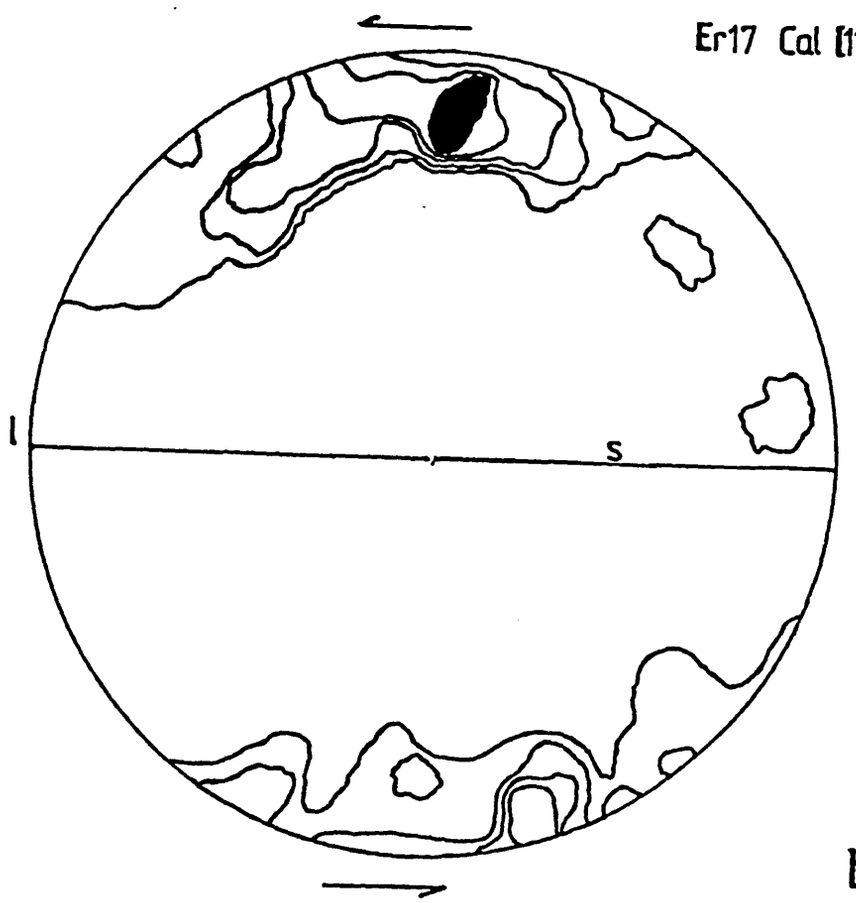

b

those obtained by Rutter and Rusbridge (1977) from non-coaxially deformed Carrara marble at 400°c. The strain rate of the laboratory deformation was $10^{-5}sec^{-1}$, while the confining pressure ranged between 150 MPa and 300 MPa. They concluded that such fabrics could result from simple shear polyphase or non-coaxial deformation involving large strains. Earlier Wenk et al. (1968) and Wenk and Shore (1975) obtained similar oblique fabrics from natural calcite mylonites.

6.6.4 Interpretation of Fabrics of Dolomite and Calcite

Crystallographic fabric analyses in dolomite tectonites since Sander (1930), Fairbairn and Hawkes (1941), Fairbairn (1942), Christie (1958) to Trommsdorff and Wenk (1965) and Neumann (1969) have produced a similar or recurring pattern: a c-axis maximum or tendency towards a c-axis maximum at a high angle to the foliation. The problem has always been what explanation would suffice for this fabric since knowledge of the physics of dolomite deformation is still evolving. Unlike in the past, the present approach towards deformation studies combining high resolution electron microscopy with material deformation (single and polycrystalline) studies - is likely to speed up understanding of the operating mechanisms during plastic deformation in dolomite. At this level of understanding it seems the most important questions yet to be answered are:

(i) At what level of resolved shear stress a particular glide system is likely to start making meaningful contributions to preferred orientation in dolomite, and

(ii) How interacting glide systems under a particular set of physical conditions affect the crystallographic fabric particularly in dolomite.

In Chapter Two (see Fig. 2.10) it was reviewed that

at low temperatures (<100 - 500°c) the greatest contribution to the deformation of dolomite is likely to come from c-slip or basal slip in an a direction. Within this temperature range the critical resolved shear stress τc is below 100 MPa. The likelihood of this slip system operating at higher temperatures and influencing c-axis fabric (>500°c) is not, apparently, very reduced by the known effect of temperature on it (Wenk and Shore, 1975; White and White, 1980). The known effect of twinning is limited to the 400 - 500°c temperature range, with possible extensions to 350°c and above 500°c (Fig. 2.10c). f($\bar{2}$021) slip - the other well known slip system in dolomite (Barber et al. 1981) has a very high CRSS value at low temperatures - 150 MPa, which drops to 100 MPa at 700°c (Fig. 2.10b)

As Wenk and Shore (1975) showed from laboratory deformation of dolomite, the fabric patterns expected and their relative intensities depend on temperature, confining pressure, strain rate, total strain and possibly strain path. Hence it is not sufficient to interprete the fabric transition from Cnoc a' Chaoruinn to Eriboll (Fig. 6.4) in terms of the known temperature difference alone. Although C - 39 (T = 314°c), C - 84 and C - 89 suggest temperatures in the range where basal slip is dominant, their fabric patterns are too complex to interprete in terms of basal slip alone. The sample from Eriboll, Er - 15 in particular, may show higher, but not exclusive activity on the basal plane. The microstructure shows twinning activity is also considerable. Hence the fabric patterns at the Eriboll end may suggest a combination of basal (0001) slip and f ($02\bar{2}1$) twinning.

Host grain c-axis fabrics symmetric with respect to the foliation and lineation have been interpreted as indicating a

coaxial deformation history (Rutter and Rusbridge, 1977; Lister, 1978; Law et al. 1984) or the result of plane strain. The non-coaxial fabrics of the late-stage mineral - calcite may indicate a progressive overprinting of non-coaxial deformation over an earlier coaxial type, (see also Ramez and Murrell, 1964; Law et al. 1984).

Comparing the fabrics of Figures 6.4, 6.5 and 6.6 in terms of symmetry with respect to the foliation and lineation, to those of Law et al. (1984), a few interesting observations tend to emerge;

(i) Below the Moine nappe from Assynt to Eriboll the fabrics of deformed host grain quartz and dolomite tend to be symmetric with respect to the foliation and lineation.

(ii) The fabrics of recrystallized quartz are like those of recrystallized calcite to the extent of their asymmetry with respect to the foliation and lineation, compared to host grain quartz and dolomite fabrics.

6.6.5 Fabric of the Fibrous Dolomite Microstructure

6.6.5.1 Introduction

In section 6.4 the microstructure of a late-forming set of fibrous dolomite grains was presented. They were shown to be the result of nucleation and growth on a phyllosilicate base, as opposed to nucleation and grain growth during recrystallization. The selective presence of this dolomite microstructure only at the Eriboll end of the Moine thrust was also cited as evidence in Chapter Five for the presence of very high fluid pressures accompanying Moine thrusting at Eriboll. In this subsection the fabric of the fibrous dolomite grains is presented and an interpretation is offered.

Fig. 6.7

a, b and c - growth fabrics of late dolomite grains in samples Er - 9, Er - 19 and Er - 15

(a) 200 grains of dolomite in sample Er - 9

(b) 150 grains of dolomite in sample Er - 19

(c) 200 grains of dolomite in sample Er - 15

(d) Recrystallization fabric of dolomite grains in sample Er - 15 for comparison with (c) from the same sample. 150 dolomite c-axes.

Contour intervals: 2,4,6,8, 10% and above per 1% area

a

Er-9 Dol (200)

c-axes of crystalites normal to the foliation(s).

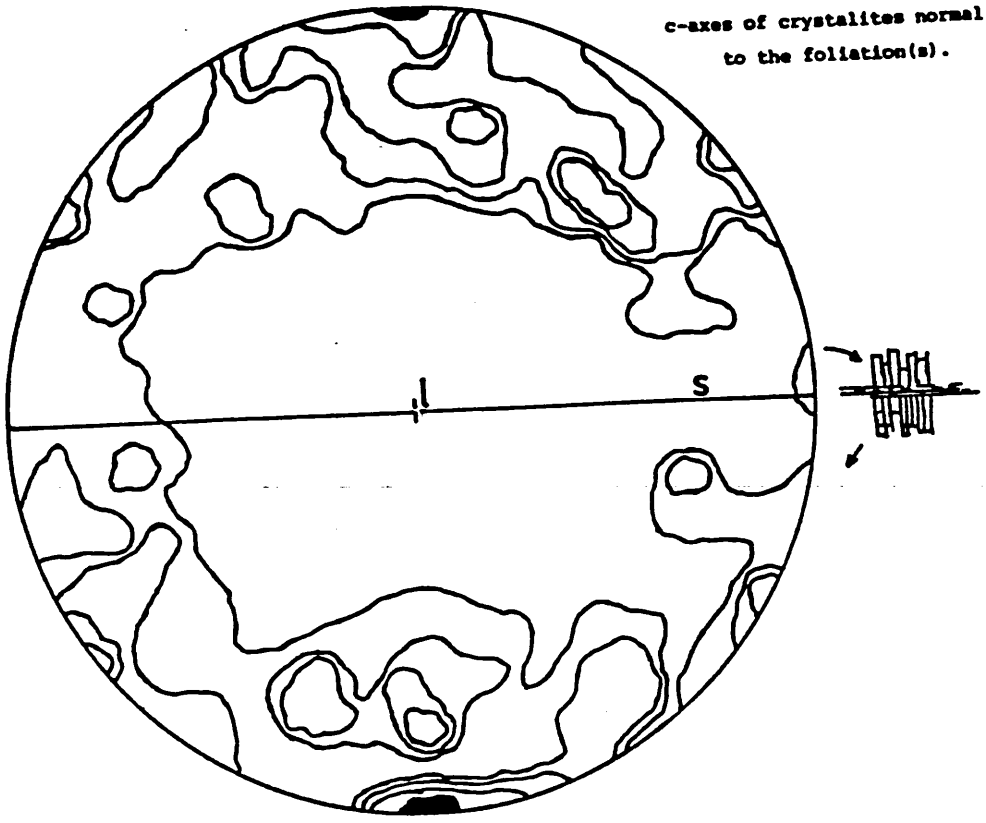

b

Er-19 Dol (150)

c-axes of crystalites growing normal to the foliation(s).

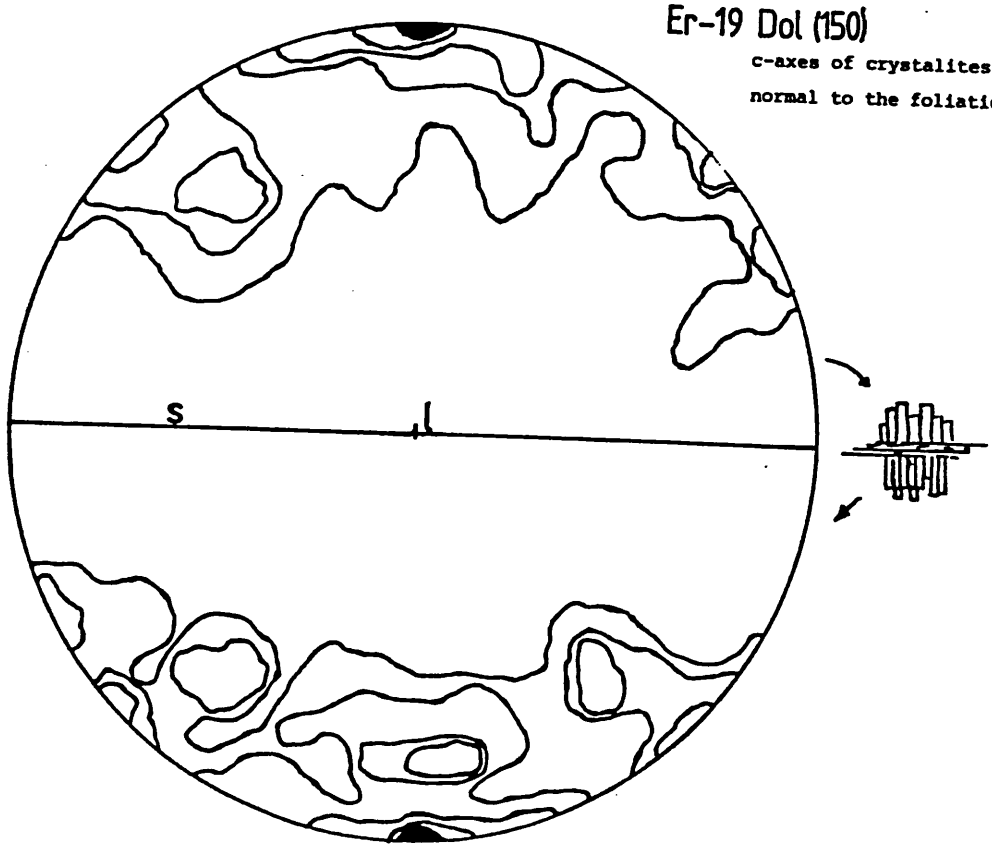

c

Er-15 Dol (200)

c-axes of crystalites growing normal to the foliation(s).

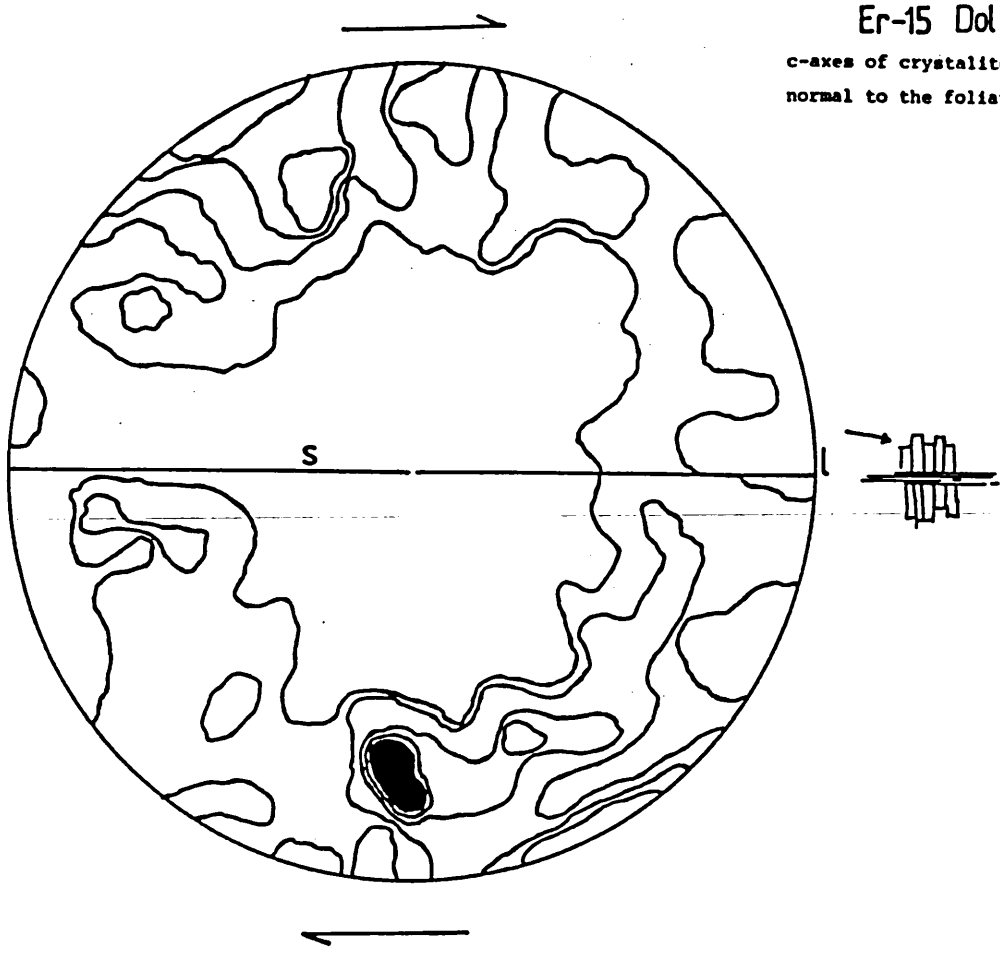

d

Er-15 Dol (150)

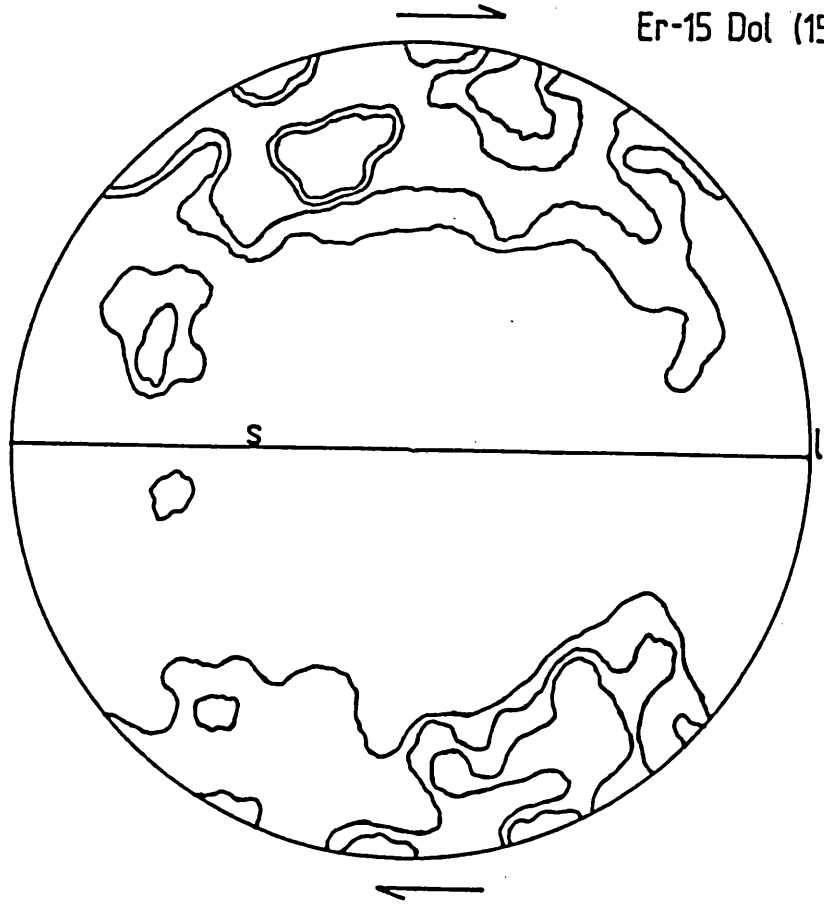

6.6.5.2 Growth c-axis crystallographic fabrics of Dolomite

As shown in Figure 6.7, the fibrous dolomite microstructure described in section 6.4 has a fairly strongly developed c-axis preferred orientation. This seems to vary a little from sample to sample, but there is a tendency for the maximum concentration areas (> 10% per 1% area) to lie at a high angle ($\sim 90^{\circ}$) to the foliation (e.g. Er - 9 and Er - 19). In Figure 6.7c and d, the fabric of dolomite due to growth (c) is compared to that due to strain (d). Both (c) and (d) were obtained from the same rock sample (Er - 15), and although the mechanisms that produced the respective fabrics were different, the resulting fabrics bear some resemblance, at least in skeletal outline. Once more the symmetry of the growth fabrics both in terms of skeletal outlines and detailed features is pseudo-orthorhombic (Er - 9 and Er - 19), with the foliation as one of the planes of symmetry.

6.6.5.3 Interpretation of Preferred Orientation of the Dolomite Fibres

Growth fabrics of quartz and calcite in veins have been studied by Durney and Ramsay (1973). Although their quartz c-axes showed random orientations, they noticed that calcite c-axes in the same rocks showed a slight fabric with respect to the pyrite face on which they grew. Earlier Pabst (1931) noticed that quartz fibres growing in the stretching direction (pressure shadows) in abutment to pyrite grains produced no definite and consistent patterns of preferred orientation. In both studies the temperature of the rock was not estimated, or taken into consideration. The work of Sander (1970, being a translation of his work of 1930), first showed the possibility of the development of a good preferred orientation under pure growth

conditions. He showed that under growth conditions (as opposed to strain and recrystallization) calcite and aragonite affixed to a single substratum, and calcite and quartz growing in veins could develop strong c-axis preferred orientations (see Sander, 1970 pp612 and 613). His fabrics showed calcite c-axes (fabrics 160 and 162) to tend to point maxima perpendicular to the wall or substratum from which growth took place, and on which the fibres stand at right angles (as in Fig. 6.7). These fabrics strongly resemble the c-axis fabrics of calcite produced in strain conditions (see Fabrics 61, 63 and 69 of pp596 -597). Also quartz growing in veins (Fabrics 165 and 166) was shown to develop quite strong c-axis preferred orientations normal to the vein walls, with some very weak orientations parallel to the wall (Fabric 165).

The dolomite fibres analysed in the present study have been shown to grow consistently foliation-normal (Plate 6.13), in tectonites that have undergone intense plastic deformation and the generation of a fine foliation. Any such crystal growth before and during deformation would have produced curved or bent crystals as a result of the deformation process (Ramsay and Graham, 1970; Wickham and Elliott, 1970; Durney and Ramsay, 1973; White and Wilson, 1978; Spry, 1979). Hence the growth is very likely to be late phase or post-tectonic. The straight nature of the fibres means that the direction of opening of the foliation has remained constant. This combined with the inference in Chapter Five of fluid assistance in jacking up the foliation (see also Shearman et al. 1972), would indicate that fibre nucleation and growth was by combinations of secretion and displacement. The rate of growth of new dolomite crystals depended on the orientation relation between the new grains and the deformed host dolomite crystals (Spry, 1979; p223). As figure

6.7 shows, the most favoured orientation was such that established or preserved optical continuity between host and new dolomite crystals. Once the optical continuity relationship was established, given the dimensional anisotropy of dolomite (longest dimension parallel to the c-axis), the dimensional fabric was also fixed. Hence growth was fastest parallel to the c-axis.

6.6.5.4 Relationship of the Fibres to Mylonitization in the Durness Carbonates

In subsection 6.4.1, the very fine grained nature of the carbonates below the Moines at Eriboll, the fine or very close schistose banding they exhibit and the presence of high strains which resulted in twinning and ribbon textures of the carbonate grains were all presented as evidence to support the application of the term "mylonite" to this part of the Durness Formation. The reduction in grain size during the mylonitization and recrystallization processes not only increased grain boundary area per unit rock volume, but also the grain boundary porosity, due to the development of voids at grain boundaries (White, 1976b; White and Wilson, 1978; White and White, 1980). The presence of a fine mylonitic foliation created multiple channels for fluid passage into and out of the rock, making possible the dissolution and transportation or growth of materials out of solution. Also the presence of very high strains in the rocks (resulting from dislocation glide and twinning) made the rocks more susceptible to dissolution and diffusive mass transfer (strain solution, see Bosworth, 1981 and Engelder, 1982). The combination of these factors effectively changed the deformation mechanism in the carbonate rocks from a dominantly crystal plastic process to one in which material dissolution, diffusive mass transfer and grain growth were more stable processes. Such

a change in deformation mechanism as a function of grain size in quartz was predicted by White (1976a), and used by White and Wilson (1978) to explain the presence of quartz pressure fringes in mylonites of Mount Isa (Australia).

6.7 CONCLUSION

Microstructural development in the Durnesss Formation of the Moine Thrust Zone can be traced from the foreland with dominantly bedding-parallel styldites and pressure solution seams to intermediate strain zones with crenulation cleavage and evolution of new minerals in some places. The high strain areas very close to the thrust may be subdivided into a northern area (Eriboll), characterized by mylonitization in the bulk rock, slip, twinning and recrystallization of dolomite and late stage solution, diffusive mass transfer and crystal growth from solution. The southern area was dominated by cataclastic deformation which produced a wide range of fracture sizes.

The stress/grain size relationship for deformed dolomite grains has been estimated, using the Twiss (1977) format, as $\sigma = 5.795\ D^{-0.68}$, where σ is the differential stress in MPa and D is the grain size in (mm). Estimates of stresses associated with the deformation of the carbonate rocks in the Moine Thrust Zone produced values ranging from 44.26 MPa to 76.48 MPa. These estimates using calcite and dolomite equilibrium grain sizes are comparable to those made by earlier workers in the MTZ using other minerals and different microstructural parameters.

Dolomite c-axis fabric showed a fairly complex pattern in Assynt, becoming more organised into a pattern at a high angle to foliation characteristic of dolomites towards Eriboll. The fabrics of dolomite, like those of host grain quartz below

the Moine Thrust plane tend to be highly symmetric with respect to the foliation and lineation characteristic of plane strain. Those of recrystallized calcite and quartz are asymmetric with respect to the foliation and lineation, typical of non-coaxial deformation at a later stage.

The c-axis fabrics of fibrous dolomite are thought to be host grain controlled, while the grain growth itself was a late stage, post tectonic process fastest parallel to the c-axis. This change in microstructure is presented as evidence of a change in deformation mechanism from dominantly crystal plastic to dissolution, diffusive mass transfer and grain growth processes, i.e. grain boundary dominated processes.

CHAPTER SEVEN

GENERAL CONCLUSION AND INFERENCES

In this chapter the main conclusions arrived at in the thesis are presented. An attempt is made to draw inferences based on these conclusions and the chapter ends with a presentation of suggestions for further research.

7.1 CONCLUSIONS

1. Macroscopic deformation of the Durness Formation at the level of present exposure below the Moine Thrust plane, varies from cataclasis at Knockan to crystal plasticity at Eriboll, which has induced the mylonitization there.

2. Mylonitization and lineations in the carbonates were not found outside the Moine Thrust contact, although folds of varying orientations exist as far from the thrust as the westernmost boundary of the Caledonian deformation. In the south of the Assynt region at least, there is no apparent relationship between the timing of mylonitization events in Moine rocks and in Durness carbonates. Also in this region, movement along the Moine Thrust plane is likely to have outlived that on the Assynt Thrust as well as the intrusions of Loch Ailsh and Borolan.

3. Prograde metamorphism of the Durness Formation accompanied and was closely associated with Moine thrusting. The highest grade of metamorphism of the carbonates presently exposed is greenschist, with temperatures reaching approximately 390^{o}C.

4. A temperature difference of approximately 80°C exists between Knockan and Eriboll in the carbonate rocks, while that between Knockan and Cnoc a' Chaoruinn could be 19°C.

5. The energy for prograde metamorphism of Durness carbonates was mostly derived from the overthrust Moine nappe and partly from warm fluids associated with the thrusting.

6. Earlier observations that the FeO/MgO ratio of chlorites may be an increasing function of grade of metamorphism are confirmed by this study. The relationship of temperature to the FeO/MgO ratio, thus: $T(^{o}C) = 278.0 + 456.0\ FeO/MgO$, in chlorites applies to clinochlore and to mean temperatures only. It may not apply when the error band associated with the temperatures is taken into consideration.

7. The last phase of Moine thrusting might have been aided by fluids of minimum pressure up to 143 MPa and possibly as high as 186 MPa. Fluid pressure difference between Knockan and Eriboll is in the range of 40 MPa, the maximum being at Eriboll. This difference may have contributed to the change in style of deformation and resultant microstructure in the carbonates of the two areas.

8. The confining pressure during the last phase of thrusting in the Moine Thrust Zone might have ranged from 133 MPa to 176 MPa, the upper limit believed to have prevailed at Eriboll.

9. On a microscopic scale, the deformation of the Durness carbonates in the high strain zone close to the Moine thrust plane is characterized by slip, twinning, recrystallization and late stage diffusive mass transfer and growth of dolomite in the northern area (Eriboll) and extensive fracturing in the south (Knockan), with some of the fractures being of grain size level.

10. The stress/grain size relationship for deformed dolomite has been calculated as $\sigma = 5.795d^{-0.68}$, where σ is the differential stress and d is the grain size. The power (0.68) was determined by Twiss (1977). Estimates of deviatoric stresses associated with the deformation of the carbonate rocks during Moine thrusting produced values ranging from about 44.0 MPa to about 76.0 MPa.

11. The c-axis crystallographic fabrics of dolomite showed a transition from a complex orthorhombic pattern in Assynt, towards a foliation-normal pattern at Eriboll. These highly symmetric fabrics are characteristic of plane strain tectonites.

7.2 INFERENCE

The main inference arising from this work relates to the noted temperature difference between the south of the Moine Thrust Zone (Assynt) and the north (Eriboll). Such a temperature difference in the carbonate rocks below the Moine nappe could mean that the Eriboll area was under a thicker cover of rocks than the south (see Oxburgh and Turcote, 1974). The same inference was arrived at by Coward (1982), who explained it with the suggestion of a steeper ramp climb in the north relative to the south.

7.3 SUGGESTIONS FOR FURTHER RESEARCH

The following problems were encountered in the course of or resulted from this research and would provide interesting areas for further research.

1. The effect of strain, if any, on the calcite/dolomite geothermometer.

2. The effect of pressure and/or differential stress on the newly derived geothermometer (relating FeO/MgO in chlorite to temperature) expressed in equation 5.2.

3. To continue the investigation for the temperature dependence of FeO/MgO in chlorite below 278°C and above 400°C.

4. The actual mechanism for the conversion of a 10Å phase to a 14Å phase phyllosilicate in a thrust plane and the effect of water in the process.

5. The actual relationship between the deviatoric stress and twinned calcite/dolomite grain size, at the inception of twinning and its paleopiezometric significance.

REFERENCES

Albee, A., 1962, Relationships between mineral association, chemical composition and physical properties of the chlorite series. Am. Mineralogist, 47: 851-870.

Ashby, M.F., 1972. A first report on deformation mechanism maps. Acta metallurgica, 20: 887-897.

Bailey, S.W., 1980. Structures of layer silicates. In: Crystal structures of clay minerals and their x-ray identification. G.W. Brindley and G. Brown (eds.) Mineral. Soc. London, PP1 - 123.

Bailey, J.E. & Hirsch, P.B. 1960. The dislocation distribution, flow stress, and stored energy in coldworked polycrystalline silver. Philos. Mag. 5, 485-497.

Baker, P.A. Kastner, M. Byerlee, J.D. Lockner, D.A., 1980. Pressure solution and hydrothermal recrystallization of carbonate sediments - An experimental study. Marine Geol. 38, 185 - 203.

Baker, P.A. Lockner, D.A., Byerlee, J.D., Kastner, M, 1979. Experimental pressure solution of carbonate sediments. Geol. Soc. Amer. Abstr. Programs 11 (7), 382.

Barber, A.J., 1965. The history of the Moine Thrust Zone, Lochcarron and Lockalsh, Scotland. Proc. Geol. Assoc. 76, 215 - 242.

Barber D.J., 1977. Defect microstructures in deformed and recovered dolomite. Tectonophysics 39, 193-213.

Barber, D.J., Heard, H.C., Wenk, H.R., 1981. Deformation of dolomite single crystals from 20 - 800°c. Phys. Chem. Minerals 7(6), 271 - 286.

Barber, D.J. & Wenk , H.R., 1979a. On geological aspects of calcite microstructure. Tectonophysics 54, 45 - 60.

Barber D.K. & Wenk , H.R., 1979b. Deformation twinning in calcite, dolomite, and other rhombohedral carbonates. Phys. Chem. Minerals 5, 141 - 165.

Bayliss, P.A., Lockner, D.A., Byerlee J.D., Kastner, M. 1979. Experimental pressure solution of carbonate sediments. Geol. Soc. Amer. Abstr. Programs 11 (7). 382.

Bayliss, P., 1975. Nomenclature of the trioctahedral chlorites. Can. Mineralogist 13, 178-180.

Beach A., 1977. Vein arrays, hydraulic fractures and pressure solution structures in a deformed flysch sequence, S.W. England: Tectonophysics, 40 (3-4). 201-225.

Bickle, M.J., Hawkesworth, C.J., England, P.C. & Athey, D.R., 1975. A preliminary thermal model for regional metamorphism in the Eastern Alps: Earth and Planetry Sci. Letters. 26, 13-28.

Bickle , M.J. & Powell, R., 1977. Calcite-dolomite geothermometry for iron-bearing carbonates. Contrib. Mineral. Petrol. 59; 281-292.

Birch, F., 1966. Compressibility, Elastic constants. In: Handbook of physical constants (Clark, S.P. ed.) Geol. Soc. Amer. Mem. 97, 97-173.

Borggard, O.K., Lindgreen, H.B. & Morup, S., 1982. Oxidation and reduction of structural iron in chlorite at 480^{o}c Clays and clay minerals, 30(5); 353 - 364.

Bosworth, W., 1981. Strain-induced preferential dissolution of halite. Tectonophysics, 78; 509 - 525.

Brasier, M.D., 1977. An early cambrian chert biota and its implications: Nature, 268(6522): 719 - 720.

Brewer, M.S. Brook, M. & Powell, D., 1979. Dating of the tectonometamorphic history of the S.W. Moine, Scotland. In: Harris, A.L., Holland, C.H. & Leake, B.E. (eds) the caledonides of the British Isles, Scott. Academic Press, 129 - 137.

Brewer J. & Smythe, D.K., 1984. Moist and the continuity of crustal reflector geometry along the Caledonian-Appalachian Orogen, J. Geol. Soc. Lond. 141, 105 - 120.

Brook, M., Brewer, M.S. & Powell, D., 1977. Grenville events in the Moine rocks of the Northern Highlands, Scotland. J. Geol. Soc. Lond. 133, 489 - 496.

Brook, M., Powell, D. & Brewer, M.S., 1976. Grenville age for rocks in the Moine of N.W. Scotland. Nature, Lond. 260, 515 - 517.

Busenberg, E. & Plummer, L.N., 1982. The kinetics of dissolution of dolomite in CO_2 - H_2O systems at 1.5 to 65^{o}c and O to 1 atm. P_{co2}. Am. J. Sci., 282, 45 - 76.

Carpenter, A.B., 1980. The chemistry of dolomite formation; the stability of dolomite. In: Concepts and models of dolomitization, (Zenger, D.H., editor et. al.) Spec. Publ. Soc. Econ. Paleon. Mineral. 28, 111 - 121.

Chaye, S.F., 1955. Potash feldspar as a by-product of the biotite-chlorite transformation. J. Geol. 63(1), 75 - 82.

Christie, J.M., 1958. Dynamic interpretation of the fabric of a dolomite from the Moine Thrust Zone in N.W. Scotland. Am. J. Sci. 256, 159 - 170.

Christie, J.M., 1963. The Moine Thrust Zone in the Assynt region - N.W. Scotland. Univ. Calif. Publs. Geol. Sci. 40, 345 - 439.

Christie, J.M., 1965. Moine Thrust: A reply. J. Geol., 73, 677 - 681.

Christie, J.M. & Ord, A., 1980. Flow stress from microstructures of mylonites; example and current assessment: In: Magnitude of deviatoric stresses in the earth's crust and uppermost mantle (Hanks, T.C., Convener; et. al.) J. Geophys. Res. B, 85(11), 6253 - 6262.

Clarebrough, L.M., Hargreaves, M.E. & West, G.W., 1955. The release of energy during annealing of deformed metals. Proc. R. Soc. Lond. A, 232, 252 - 270.

Cosgrove, J.W., 1976. The formation of crenulation cleavage. J. Geol. Soc. Lond. 132, 155 - 178.

Coward, M.P., 1980. The caledonian thrust and shear zones of N.W. Scotland, J. Struct. Geol. 2,11 - 17.

Coward, M.P., 1983. The strain and textural history of thin-skinned tectonic zones: Examples principally from the Moine Thrust. Int. Confer. Planar and Linear Fabrics of deformed rocks (abstracts) ETH Zurich.

Coward, M.P., 1982. Surge zones in the Moine Thrust Zones of N.W. Scotland. J. Struct. Geol. 4, 247 - 256.

Coward, M.P., Kim, J.H. & Parke, J., 1980. A correlation of Lewisian structures across the lower thrusts of the Moine Thrust Zone, N.W. Scotland, Proc. Geol. Assoc. Lond. 91, 327 - 37

Craig, J., Fitches, W.R. & Maltman, A.J., 1982. Chlorite- mica stacks in low-strain rocks from central Wales. Geol. Mag. 119(3), 243 - 256.

Dana, E.S., 1892. The system of mineralogy, 6th ed: New York, John Wiley and Son. P. 649, 652, 657.

Danielsson, A., 1950. Das Calcit-Wollastonitgleichgewicht. Geochim. et Cosmochim. Acta, 1, 55 -

Deer, W.A., Howie, R.A. & Zussman, J., 1962. Rock-forming minerals. Vol. 5 Non-silicates, pp371. Longmans.

Deffeyes, K.S., Lucia, F.J., Weyl, P.K. (1965): Dolomitisation of recent sediments. In: Pray, L.C., Murray, R.C. (eds.), Dolomitisation and Lmstone diagenesis, Soc. Econ. Paleont. Mineral. Spec. Publ. 13, 71 - 88.

Downie, C., 1981. Lower cambrian acritarchs from Scotland, Norway, Greenland and Canada. Trans. Roy. Soc. Edinburgh. Earth Sciences, 72, 275 - 285.

Dunoyer de Segonzac, G., 1969. Les mineraux argileux dans la diagenese. Passage au metamorphisme (Thesis Univ. Strasbourg.) Mem. Serv. Carte Geol. Alsace Lorraine, 29: 320pp.

Dunoyer de Segonzac, G., 1970. The transformation of clay minerals during diagenesis and low-grade metamorphism: A review. Sedimentology, 15, 281 - 346.

Durney, D.W. & Ramsay, J.G., 1973. Incremental strains measured by syntectonic crystal growths. In: Gravity and tectonics (eds. De Jong, K.A. & Scholten, R.) Wiley, New York, 67 - 96.

Edward, G.H., Etheridge, M.A. & Hobbs, B.E., 1982. On the stress dependence of subgrain size. Textures and microstructures 5, 127 - 152.

Elliott, D. & Johnson, M.R.W., 1980. Structural evolution in the northern part of the Moine Thrust belt, N.W. Scotland. Trans. R. Soc. Edinb. Earth Sci. 71, 69 - 96.

Engelder, T., 1982. A natural example of the simultaneous operation of free-face dissolution and pressure solution. Geochim. Cosmochin. Acta 46, 69 - 74.

Etheridge, M.A. & Wilkie, J.C., 1981. An assessment of dynamically recrystallized grain size as a paleopiezometer in quartz-bearing mylonite zones. Tectonophys. 78, 475 - 509.

Evans, D.J. & White, S.H., 1984. Microstructural and fabric studies from the rocks of the Moine Nappe, Eriboll, N.W. Scotland. J. Struct. Geol. 6(4), 369 - 389.

Fairbairn, H.W., 1942. Structural petrology of deformed rocks, Addison-Wesley Press, Inc. 143p.

Fairbairn, H.W. & Hawkes, H.E., Jr., 1941. Dolomite orientation in deformed rocks: Am. Jour. Sci. 239, 617 - 632.

Fawcett, J.J. & Yoder, H.S. Jr., 1966. Phase relationships of chlorites in the system MgO - Al_2O_3 - SiO_2 - H_2O. Amer. Mineral. 51, 353 - 380.

Fischbeck, A.I., 1979. Synthesis of protodolomite, high-magnesian calcite, hydromagnesite, and nesquehonite from calcium-magnesium bicarbonate solutions by freeze drying. Am. Ass. Pet. Geol. Bull 63(3) 450.

Folk, R.L., 1959. Practical petrographic classification of limestones. Am. Assoc. Petrol. Geol. Bull. 43, 1 - 38.

Friedman, G.M., 1979. Dolomite is evaporite mineral; evidence from rock record and from sea-marginal pools of Red Sea (abstr.): Am. Ass. Pet. Geol. Bull 63(3), 453 - 454.

Friedman, M. & Higgs, N.G., 1981. Calcite fabrics in experimental shear zones. In: Mechanical behaviour of crustal rocks - The handin volume. (Carter, N.L., Friedman, M., Logan, J.M. & Stearns, D.W., eds.) Amer. Geophys. Union. Geophysical Monograph 24, 11 - 27.

Foster, M.D., 1962. Interpretation of the composition and classification of the chlorites. Prof. Pap. U.S. Geol. Surv. 414 - A, 1 - 33.

Foster, M.D., 1964. Water content of micas and chlorites. Prof. Paper U.S. Geol. Surv. 474-F, 1 - 15.

Gaines, A.M., 1979. Dolomitization; recent experimental approaches (abstr.) Am. Ass. Pet. Geol. Bull, 63(3), 455.

Geikie, A., 1889. Recent researches into the origin and age of the Highlands of Scotland and the west of Ireland. Lecture to the Royal Institution of Great Britain, 7th June.

Giletti, B., Moorbath, S & Lambert R. St. J. 1961. A geochronological study of the metamorphic complexes of the Scottish Highlands. Jl. Geol. Soc. Lond. 117, 233 - 264.

Girou, A., Esclamadon, J., Humbert, L., Jacquin, C., Poulet M., $ Roques, H., 1982. Dissolution experimentale d'un rhomboedre de calcite soumis a une contrainte. Bull. Mineral. 105 (3), 301 - 306.

Gobbett, D.J., & Wilson, C.B., 1960. The Oslobreen Series, Upper Hecla Hoek of Ny Friesland, Spitsbergen: Geol. mag., 97, 441 - 460.

Goetze, C., of Kohlstedt, D.L., 1977. The dislocation structures of experimentally deformed marble. Contrib. Mineral. Petrol., 59, 293 - 306.

Goldschmidt, V.M., 1912. Die Gesetze der Gesteinsmetamorphose mit beispielen aus der Geologie des sudlichen Norwegens. Vidensk. Skr. I, Mat - Naturv. KL., no. 22

Goldsmith, J.R., 1980. Thermal stability of dolomite at high temperatures and pressures. J. Geophys. Res. 85(12) 6949 - 6980.

Goldsmith J.R., & Newton, R.C., 1969. P - T - X relations in the system $CaCO_3$ - $MgCO_3$ at high temperatures and pressures. Amer. J. Sci. Schairer vol. 267-A, 160 - 190.

Graff, D.L., & Goldsmith, J.R., 1955. Dolomite magnesian-calcite relations at elevated temperatures and CO_2 pressures: Geochim. et Cosmochim. Acta, 7, 109 - 128.

Gray, D.R., 1977b. Some parameters which affect the morphology of crenulation cleavages: J. Geol. 85, 763 - 780.

Gray, D.R., 1979. Microstructure of crenulation cleavages: An indication of cleavage origin. Amer. J. Sci. 279, 97 - 128.

Griggs, D.T., Turner, F.J., & Heard, H.C., 1960. Deformation of rocks at 500°c to 800°c. In: Rock deformation (Griggs, D., & Handin, J. eds.) Geol. Soc. Am. Memoir, 79.

Gross, K.A., 1965. X-ray line broadening and stored energy in deformed and annealed calcite. Phil. Mag. 12, 801 - 813.

Gunderson & Wenk, H.R., 1981. Heterogeneous microstructures in oolitic carbonates. Amer. Mineral. 66, 789.

Hallam, A. & Swett, K., 1966. Trace fossils from the lower Cambrian pipe rock of the N.W. Highlands. Scott. J. Geology., 2, 101 - 106.

Handin, J.W., 1966. Strength and ductility, In: Clarke, S.P. Jr., ed., Handbook of physical constants: Geol. Soc. Amer. Memoir 97, 223 - 290.

Handin, J.W. & Fairbairn, H.W., 1953. Experimental deformation of Hasmark dolomite. Geol. Soc. Am. Bull, 64, 1429 - 1430.

Handin, J.W. & Fairbairn, H.W., 1955. Experimental deformation of Hasmark dolomite. Geol. Soc. Am. Bull 66, 1257 - 1274.

Harker, R.I. & Tuttle, O.F., 1955a. Studies in the system CaO - MgO - CO_2 (Part 1). The thermal dissociation of calcite, dolomite and magnesite. Amer. J. Sci. 253, 209 - 224.

Harker, R.I., & Tuttle, O.F., 1955b. Studies in the system CaO - MgO - CO_2 (Part 2). Limits of solid solution along the binary join $CaCO_3$ - $MgCO_3$. Amer. J. Sci. 253, 274 - 282.

Harris, A.L., Johnson, M.R.W., & Powell, D., 1978. The orthotectonic caledonides (Moines and Dalradians) of Scotland. Pap. Geol. Surv. Can. 78, 79 - 85.

Heard, H.C. & Raleigh, C.B., 1972. Steady-state flow in marble at 500 - 800°c. Geol. Soc. Am. Bull. 83, 935 - 956.

Helgeson, H.C., Delanyi, J.M., Nesbitt, H.W., & Bird, D.K., 1978. Summary and critique of the thermodynamic properties of rock-forming minerals. Am. J. Sci., 278-A, pp 229.

Higgins, A.G., 1967. The age of the Durine Member of the Durness limestone formation at Durness, Scott. J. Geol. 3, 382 - 8.

Higgs, D.V. & Handin, J., 1959. Experimental deformation of dolomite single crystals. Geol. Soc. Am. Bull, 70, 245 - 227

Hobbs, B.E., Means, W.D. & Williams, P.F., 1976. An outline of structural geology. pp 571. John Wiley & Sons N.Y.

Holzner, J., 1938. Occurence, optical properties, and chemical relations of several iron chlorites from the Lahn region, Germany. Neues Jb, Beil. - Bd. 73, Abt. A. H. 3, p389 - 418.

Hutcheon, I. & Moore, J.M. 1973. The tremolite isograd near marble lake, Ontario, Can. J. Earth sciences 10, 936 - 947.

Iwasaki, M., 1963. Metamorphic rocks of the Kotu-Bizan area, eastern Shikoku. J. Fac. Sci. Univ. Tokyo, Sect. 2, 15: 1 - 90.

Jamison, W.R. & Spang, J.H., 1976. Use of calcite twin lamella to infer differential stress. Bull. Geol. Soc. Am. 87, 868 - 872.

Johnson, M.R.W., 1957. The structural geology of the Moine Thrust Zone in Coulin Forest, Wester Ross. Q. Jl. Geol. Soc. Lond. 113, 241 - 270.

Johnson, M.R.W., 1960. The structural history of the Moine Thrust Zone at Loch Carron, Wester Ross. Trans. R. Soc. Edinb., 64, 139 - 168.

Johnson, M.R.W., 1975. Morarian Orogeny and Grenville belt in Britain. Nature, Lond. 257, 301 - 302.

Johnson, M.R.W., Sanderson, D.J., & Soper, N.J., 1979. Deformation in the caledonides of England, Ireland and Scotland. In: The Caledonides of the British Isles - reviews (edited by Harris, A.L., Holland, C.H. & Leake, B.E.) Spec. Publs. Geol. Soc. Lond., 8, 165 - 185.

Johnson, K.S., & Pyktowiczs, R.M., 1978. Chloride ion pairs in seawater (abstr): EOS (Am. Geophys. Union, Trans), 59(4) 307.

Johnstone, G.S., 1975. The Moine succession. In: Harris A.L. et al. (eds.) A correlation of the Precambrian rocks in the British Isles. 30 - 42. Spec. Rep. Geol. Soc. Lond. 6.

Johnstone, G.S., Plant. J., & Watson, J.V., 1979. Regional geochemistry of the Norther Highlands of Scotland. In: The Caledonides of the British Isles - reviewed., Harris, A.L., et al. (eds). Geol. Soc. Lond. Spec. Publ. 8, 117 - 128.

Katz, A., & Mathews, A., 1977. The dolomitization of $CaCO_3$: An experimental study at 259 - 295°c. Geochim. Cosmochim. Acta. 41, 297 - 303.

Kennedy, W.Q., 1949. Zones of progressive regional metamorphism in the Moine Schists of the Western Highlands of Scotland. Geol. Mag. 86, 43 - 56.

Kennedy G.C., & Holser, W.T., 1966. Pressure-volume-temperature and phase relations of water and carbon dioxide, in handbook of physical constants. Geol. Soc. Am. Mem., 97, 371 - 383.

Kern, H. & Wenk, H.R., 1983. Calcite texture development in experimentally induced ductile shear zones. Contrib. Mineral. Petrol. 83, 231 - 236.

Kittrick, J.A., 1982. Solubility of two high-Mg and two high-Fe chlorites using multiple equilibria. Clays and clay minerals. 30(3), 167 - 179.

Knipe, R.J., 1981. The interaction of deformation and metamorphism in slates. Tectonophys. 78, 249 - 272.

Kohlstedt, D.L., & Weathers, M.S., 1980. Deformation-induced microstructures, paleopiezometers, and differential stresses in deeply eroded fault zones. J. Geophys. Res. 85(B11), 6269 - 6285.

Lachenbruch, A.H., 1980. Frictional heating, fluid pressures, and the resistance to fault motion. J. Geophys. Res., 85(11), 6097 - 6112.

Lapworth, C., 1885. The Highland controversy in British geology; its causes, course and consequence. Nature, Lond. 32, 558 - 559.

Law, R.D., Knipe, R.J., & Dayan, H., 1984. Strain path partitioning within thrust sheets: microstructural and petrofabric evidence from the Moine Thrust Zone at Loch Eriboll, N.W. Scotland, J. Struct. Geol. 6(5), 477 - 497.

Lipmann, F., 1973. Sedimentary carbonate minerals. New York, Springer - Verlag, 229p.

Lister, G.S., 1978. Texture transition in plastically deformed calcite rocks. In: Gottstein, G. & Lucke, K., (eds.), Proc. 5th Int. Conf. on texture of materials, Aachen. 2, 199 - 210., Springer Verlag.

Lister, G.S. & Williams, P.F., 1979. Fabric development in shear zones: theoretical controls and observed phenomena. J. Sturct. Geol. 1, 283 - 297.

Long, L.E., 1964. Rb - Sr chronology of the Carn Chuinneag intrusion, Rosshire, Scotland, J. Geophys. Res. 69, 1589 - 1597.

Long, L.E. & Lambert, R. St. J., 1963. Rb - Sr isotopic ages from the Moine Series. In: British Caledonides (Johnson, M.R.W. & Stewart F.H. eds.) Oliver & Boyd, Edinburgh, 217 - 248.

Margara, K., 1974. Aquathermal fluid migration: Am. Assoc. Petrol. Geologists Bull. 58, 2513 - 2521.

McClay, K.R. & Coward, M.P., 1981. The Moine Thrust Zone: an overview. In: Thrust and nappe tectonics (McClay, K.R. & Price, N.J., eds.) Spec. Publ. Geol. Soc. Lond. 9, 241 - 260.

McQueen, H.J., & Jonas, J.J., 1975. Recovery and recrystallization during high temperature deformation. In: Treatise on material science and technology, (Arsenault, R.J., ed.) Academic, New York. 6, 393 - 493.

McIntyre D.B., 1950. Note on lineation, boudinage, and recumbent-folds in the struan flags (Moine), near Dolnacardoch, Perthshire (Scotland). Geol. Mag. 87(6) 427 - 432.

McIntyre, D.B., 1951. Note on the tectonic style of the Ord Ban Quartzites, Mid-strathspey. Geol. Mag. 88(1) 50 - 54.

McLeish, A.J., 1971. Strain analysis of deformed pipe rock in the Moine Thrust Zone, N.W. Scotland. Tectonophys. 12, 469 - 503.

Mendum, J.R., 1979. Caledonian thrusting in N.W. Scotland. In: The Caledonides of the British Isles - reviewed (edited by Harris, A.L., Holland, C.H. & Leake, B.E.). Spec. Publs. Geol. Soc. Lond. 8, 291 - 297

Mercier, J.C., Anderson, D.A., & Carter, N.L., 1977. Stress in the lithosphere: Inferences from steady-state flow of rocks. Pure and applied geophys. 115, 199 - 226.

Merrill, R.H., 1964. In situ determination of stress by relief techniques. In: State of stress in the earth's crust (Judd, W.R., ed.) American Elsevier Publishing Company, Inc., New York, pp 343 - 378).

Metz, P., 1966. Untersuchung eines heterogenen bivarianten Gleichgewichts mit CO_2 und H_2O als fluider phase bei hohen Drucken. Ber. Bunsenges. Phys. Chem. 70, 1043 - 1045.

Metz, P., 1967. Experimentelle Bildung von Forsterit und calcit aus tremolit und dolomit. Geochim. et Cosmochim. Acta 31, 1517 - 1532.

Metz, P. & Puhan, D., 1970. Experimentelle Untersuchung der metamorphose von kieselig dolomitishen sedimenten. Contr. Mineral. and Petrol. 26, 302 - 314.

Metz, P. Puhan, D. & Winkler, H.G.F., 1968. Equilibrium reactions on the formation of talc and tremolite by metamorphism of siliceous dolomite. Naturwissenschaften 55, 225 - 226.

Metz, P. & Trommsdorff, V., 1968. On phase equilibria in metamorphosed siliceous dolomites. Contr. Mineral. and Petrol. 18, 305 - 309.

Metz, P. & Winkler, H.G.F., 1963. Die bildung von talc aus Kieseligem, Dolomit. Geochim. et Cosmochim. Acta 27, 431 - 457.

Metz, P. & Winkler, H.G.F., 1964. Experimentelle untersuchung det dispsidbildung aus tremolit calcit und quartz. Naturwissenschaften 51, 460.

Milne, K.P., 1978. Folding and thrusting in the upper Glen Oykel area, Assynt, Scott. J. Geol. 14,(2), 141 - 146.

Moorbath, S., 1969. Evidence for the age of deposition of the Torridonian sediments of N.W. Scotland. Scott. J. Geol. 5,389 - 412.

Moore, J.N., & Kerrick, D.M., 1976. Equilibria in siliceous dolomites of the Alta aureole, Utah. Amer. J. Sci. 276, 502 - 524.

Morey, G.W., 1962. The action of water on calcite, magnesite and dolomite. Amer. Mineral, 47, 1456 - 1460.

Nelson, B.W., & Roy, R., (1958). Synthesis of the chlorites and their structural and chemical constitution. Amer. Mineral. 43, 707 - 725.

Neumann, E.R., 1969. Experimental recrystallization of dolomite and comparisons of preferred orientations of calcite and dolomite in deformed rocks. J. Geol. 77, 426 - 438.

Nicolas, A., & Poirier, J.P., 1976. Crystalline plasticity and solid state flow in metamorphic rocks. John Wiley & Sons - Lond. pp444.

Norris, R.J., & Henley, R.W., 1976. Dewatering of a metamorphic pile. Geology. 4, 333 - 336.

Ord, A., & Christie, J.M., 1984. Flow stresses from microstructures in mylonitic quartzites of the Moine Thrust Zone, Assynt area, Scotland. J. Struct. Geol. 6(6) 639 - 654.

Oxburgh, E.R., & Turcote, D.L., 1970. The thermal structure of island arcs. Geol. Soc. Amer. Bull., 81, 1665 - 1681.

Oxburgh, E.R., & Turcote, D.L., 1974. Thermal gradients and regional metamorphism in overthrust terraines with special reference to the Eastern Alps. Schweizerische Mineral. Petrol. Mitt. 54 (2/3), 641 - 662.

Pabst, A., 1931. Pressure shadows and the measurement of the orientation of minerals in rocks. Amer. Mineral. 16, 55 - 70.

Palmer, T.J., McKerrow, W.S., & Cowie, J.W., 1980. Sedimentological evidence for a stratigraphical break in the Durness Group. Nature, 287(5784), 720 - 722.

Pankhurst, R.J., 1970. The geochronology of the 'younger' basic complexes of N.E. Scotland, Scott. J. Geol. 6, 83 - 107.

Pankhurst, R.J., 1974. Rb - Sr whole rock chronology of Caledonian events in North East Scotland. Geol. Soc. Am. Bull, 85, 345 - 350.

Paterson, M.S., 1973. Non-hydrostatic thermodynamics and its geologic applications. Rev. Geophys. Space Phys. 11, 355 - 389.

Paterson, M.S., 1976. Deformation mechanisms in carbonate crystals. Proc. 25th Int. Geol. Congr. Sect. 14, 10th meeting of Int. Mineral. Assoc., Abstr. 2: 590 - 591.

Paterson, M.S., 1979. Deformation mechanisms in carbonate crystals. In: Physics of materials (Borland, D.W., Clarebrough, L.M., Moore, A.J.W., eds.) Univ. Melbourne, pp199 - 208.

Paterson, M.S. & Weiss, L.E., 1961. Symmetry concepts in the structural analysis of deformed rocks. Geol. Soc. Am. Bull., 72, 841 - 882.

Pauling, L., 1930. The structure of micas and related minerals. (.U.S.). Natl. Acad. Sci-Proc. 16, 123 - 129.

Peach, B.N., & Horne, J., 1930. Chapters on the geology of Scotland. Oxford Univ. Press.

Peach, B.N., Horne, J., Gunn, W., Clough, C.T., & Hinxman, L.W., 1907. The geological structure of the North-West highlands of Scotland. Mem. Geol. Surv. U.K. 668p.

Phillips, F.C., 1937. A fabric study of some Moine Schists and associated rocks. Geol. Soc. Lond. Quart. J., 93, 581 - 616.

Phillips, F.C., 1949. Lineations in Moine and Lewisian rocks. Geol. Mag. 86, 279 - 287.

Phillips, F.C., 1951. Apparent coincidences in the life-history of the Moine schists. Geol. Mag. 88(4), 225 - 235.

Phillips, W.J., 1972. Hydraulic fracturing and mineralisation. Geol. Soc. Lond. Jour. 128, 337 - 355.

Piasecki, M.A., 1980. New light on the Moine rocks of the Central Highlands of Scotland. J. Geol. Soc. Lond. 137, 41 - 59.

Piasecki, M.A.J., & Van Breemen, O., 1979b. A Morarian age for the "younger Moines", of central and western Scotland. Nature, 278, 734 - 736.

Poirier, J.P., & Nicolas, A., 1975. Deformation induced recrystallization by progressive misorientation of subgrain-boundaries, with special reference to mantle peridotites. J. Geol. 83, 707 - 720.

Potts, E.J., 1964. The in-situ measurement of rock stress based on deformation measurements. In: State of stress in the earth's crust, (Judd, W.R. ed.). American Elsevier Publishing Company, Inc. New York, 397 - 407.

Powell, D., 1983. Pers. Comm.

Powell, D., 1974. Stratigraphy and structure of the western Moine and the problem of Moine orogenesis. J. Geol. Soc. Lond. 130, 575 - 593.

Powell, D., Brook, M. & Baird, A.W., 1983. Structural dating of a PreCambrian pegmatite in Moine rocks of N. Scotland and its bearing on the status of the "Morarian Orogeny". J. Geol. Soc. Lond. 140, 813 - 823.

Powell, R., 1978. Equilibrium thermodynamics in petrology-An introduction. Harper & Row-Lond. pp 284.

Powers, M.C., 1957. Adjustment of land derived clays to the marine environment. J. Sedim. Petrol. 27, 355 - 372.

Price, N.J., 1966. Fault and joint development in brittle and semi-brittle rock. Pergamon Press. pp176.

Price, N.J., 1975. Fluids in the crust of the Earth: Sci. Progress, 62, 59 - 88.

Price, N.J. & Hancock, P.L., 1972. Development of fracture cleavage and kindred structures. Int. Geol Congr. 24th Montreal Sec. 3, 584 - 592.

Ragan, D.M., 1973. Structural Geology - An introduction to geometrical techniques. 2nd edition. John Wiley & Sons, pp208.

Raleigh, B., & Evernden, J., 1981. Case for low deviatoric stress in the lithosphere. In: Mechanical behaviour of crustal rocks, the Hand in volume, (Carter, N.L., Friedman, M., Logan, J.M., & Stearns, D.W. eds.) Geophysical Monograph 24, Amer. Geophys. Union. Washington.

Raleigh, C.B., & Kirby, S.H., 1970. Creep in the upper mantle. Mineral. Soc. Amer. Spec. Pap. 3, 183 - 190.

Raleigh, C.B., & Talbot, J.L., 1967. Mechanical twinning in naturally and experimentally deformed diopside - Amer. J. Sci. 265(2), 151 - 165.

Ramez, M.R.H., & Murrell, S.A.F., 1964. A petrofabric analysis of Carrara marble. Int. J. Rock. Mech. Mining, 1, 217 - 229.

Ramsay, J.G., 1963. Structure and metamorphism of the Moine and Lewisian rocks of the N.W. Caledonides. In: The British Caledonides, Oliver & Boyd Ltd. Edinburgh and London pp143 - 175.

Ramsay, J.G., & Graham, R.H., 1970. Strain variation in shear belts. Can. J. Earth Sci. 7, 786 - 813.

Read, H.H., 1934. Age problems of the Moine Series of Scotland. Geol. Mag. 71, 302 - 317.

Reeder, R.J., 1980. Phase transformations in dolomite. Ph. D. Thesis. Univ. Calif., Berkeley, P159.

Rice, J.M., 1970. Contact metamorphism of impure dolomitic Limestone in the Boulder Aureole, Montana. Contrib. Mineral. Petrol. 59, 237 - 259.

Roberts, J.L., 1972. The mechanics of overthrust faulting: A critical review: In: Tectonics - section 3, Int. Geol. Congr. Proc. - Programme, No. 24, 593 - 598.

Roberts, W. & Ahlblom, B., 1978. A nucleation criterion for dynamic recrystallization during hot working. Acta metallurgica 26, 801 - 813.

Robie, R.A., Hemingway, B.S., Schafer, C.M., et al. 1978. Heat capacity equations for minerals at high temperatures: U.S. Geol. Surv. Open-file Rep. No. 78-934, pp18.

Rose, A.W., Hawkes, H.E., & Webb, J.S., 1979. Geochemistry in mineral exploration. Academic Press - Lond.

Rosenberg, P.E., & Holland, H.D., 1964. Calcite-dolomite-magnesite stability relations in solutions at elevated temperatures. Science, 145, 700 - 702.

Rutter, E.H., 1974. The influence of temperature strain rate and interstitial water in the experimental deformation of calcite rocks. Tectonophys. 22, 311 - 334.

Rutter, E.H., 1976. The kinetics of rock deformation by pressure/solution. Phil. Trans. R. Soc. Lond. A. 283, 203 - 219.

Rutter, E.H., & Rusbridge, M., 1977. The effect of non-coaxial strain paths on crystallographic preferred orientation development in the experimental deformation of a marble. Tectonophys. 39(1 - 3), 73 - 86.

Sander, B., 1930. Gefugekunde der Gesteine. Springer, Berlin.

Sander, B., 1970. An introduction to the fabric study of geological bodies (Phillips, F.C., & Windsor, G. translators). Pergamon Press, Oxford.

Schmid, S.M., 1976. Rheological evidence for changes in the deformation mechanism of solnhofen limestone towards low stresses. Tectonophys. 31: T21 - T28.

Schmid, S.M., Boland, J.N., & Paterson, M.S., 1977. Super plastic flow in finegrained limestone. Tectonophys. 43(1/2), 257 - 291.

Schmid, S.M., Paterson, M.S., & Boland, T.N., 1980. High temperature flow and dynamic recrystallization in Carrara marble.. Tectonophys. 65, 245 - 280.

Segnit, E.R., Holland, H.D., & Biscardi, C.J., 1962. The solubility of calcite in water between 75° and 200°c. at CO_2 pressures up to 60 atm. Geochim. et Cosmochim. Acta, 26, 1301 - 1331.

Scholz, C.H., Beavan, J., & Hanks, T.C., 1979. Frictional metamorphism, argon depletion, heat flow and stress on the Alpine fault, New Zealand. J. Geophys. Res. 84, 6770 - 6782.

Scholz, C.H., 1980. Shear heating and the state of stress on faults. J. Geophys. Res. 85(B11), 6174 - 6184.

Shearman, D.J., Mossop, G., Dunsmore, H., & Martin, M., 1972. Origin of gypsum veins by hydraulic fracture. Trans. Inst. Min. Metall. B81(789), 149 - 155.

Sheppard, S.M.F., & Schwarcz, H.P., 1970. Fractionation of carbon and oxygen isotopes and dolomite. Contrib. Mineral, Petrol. 26, 161 - 198.

Shirozu, H., (1960). Ionic substitution in iron-magnesium chlorites. Mem. Fac. Sci. Kyushu Univ. D, 9, 183 - 186.

Sibson, R.H., 1975. Generation of pseudotachylite by ancient seismic faulting. Geophys. J. Roy. Astron. Soc., 43, 775 - 794.

Sibson, R.H., 1979. Fault rocks and fault mechanisms. J. Geol. Soc. Lond. 133, 191 - 214.

Skinner, B.J., 1966. Thermal expansion. In Clark, S.P., Jnr. ed. Handbook of physical constants: Geol. Soc. Am. Mem. 97, 75 - 96.

Soper, N.J., 1971. The earliest Caledonian structures in the Moine Thrust belt. Scott. J. Geol. 7, 241 - 247.

Soper, N.J., & Barber, A.J., 1979. Proterozoic folds on the northwest Caledonian Foreland. Scot. J. Geol. 15, 1 - 11.

Soper, N.J. & Barber, A.J., 1982. A model for the deep structure of the Moine Thrust Zone. J. Geol. Soc. Lond. 139, 127 - 138.

Soper, N.J., & Brown, P.E., 1971. Relationship between metamorphism and migmatization in the northern part of the Moine nappe. Scott. J. Geol. 7, 305 - 325.

Soper, N.J., & Wilkinson, P., 1975. The Moine thrust and Moine nappe at Loch Eriboll, Sutherland, Scott. J. Geol. 11, 339 - 359.

Spiers, C., 1982. The development of deformation textures in calcite rocks. Ph. D. Thesis (unpublished). Univ. Lond.

Spiers, C.J., & Wenk, H.R., 1980. Evidence for slip on r and f in the +ve sense in deformed single crystals. EOS, Trans. Am. Geophys. U. 61, 1128.

Spry, A., 1979. Metamorphic textures, Pergamon Press, Oxford. pp350.

Staplin, F.L., 1977. Interpretation of thermal history from colour of particulate organic matter - A review. Palynology 1, 9 - 18.

Stephens, M.B., Glasson, M.J., & Keays, R.R., 1979. Structural and chemical aspects of metamorphic layering development in metasediments from Clunes, Australia, Am. J., Sci. 279, 129 - 160.

Swett, K., 1965b. Dolomitization, silicification and calcitization patterns in Cambro-Ordovician oolites from N.W. Scotland. J. Sed. Petrol. 35, 928 - 938.

Swett, K., 1966a. Diagenetic mottling in dolomitic limestones, dolostones and cherts., N.W. Scotland (abstr). Geol. Soc. Am. Spec. Paper 87, 171 - 172.

Swett, K., 1969. Interpretation of depositional and diagenetic history of Cambrian-Ordovician succession of N.W. Scotland, A.A.P.G. Mem. 12, Pap. 45, 630 - 646.

Swett, K., 1981. Geol. Mag. 118(3), 225 - 250.

Takeuchi, S., & Argon, A.S., 1976. Steady state creep of single phase crystalline matter at high temperature. J. Mater, Sci. 11, 1542 - 1566.

Thomas, J.M., & Renshaw, G.D., 1967. Influence of dislocations on the thermal decomposition of calcium carbonate. J. Chem. Soc. Lond., A - 2058 - 2061.

Trommsdorff, V., & Wenk, H.R., 1965. Die Regelung des dolomites von crevola simplongruppe. Schweiz, Mineralogische U. Petrographische Mitteilungen. 45, 551 - 568.

Tullis, T.E., 1980. The use of mechanical twinning in minerals as a measure of shear stress magnitudes. J. Geophys. Res. 85(B11) 6263 - 6268.

Tullis, T.E. & Yund, R.A., 1982. Grain growth kinetics of quartz and calcite aggregates. J. Geol. 90, 301 - 318.

Turcote, D.L., 1983. Mechanisms of crustal deformation J. Geol. Soc. Lond. 140, 701 - 724.

Turner, F.J., 1968. Metamorphic Petrology. New York: McGraw-Hill 403p.

Turner, F.J., Griggs, D.T., & Heard H., 1954a. Experimental deformation of calcite crystals. Bull. Geol. Soc. Am. 65, 883 - 934.

Turner, F.J., Griggs, D.T., Heard, H., & Weiss, L.E., 1954b. Plastic deformation of dolomite rock at 380^{o}c. Amer. J. Sci. 252, 477 - 488.

Turner, F.J., Griggs, D.T., Clark, R.H. & Dixon, 1956. Deformation of Yule marble: Part VII - Development of oriented fabrics at 300^{o} - 500^{o}c. Geol. Soc. Am. Bull, 67, 1259 - 1294.

Turnock, A.C., 1960. The stability of iron chlorites. Carnegie Institution of Washington, Yearbock 59, 98 - 103.

Twiss, R.J., 1977. Theory and applicability of re-

crystallized grain size paleopiezometer. Pure Appl. Geophys. 11, 227 - 244.

Twiss, R.J., 1980. Static theory of size variation with stress for subgrain and dynamically recrystallized grains, magnitude of deviatoric stresses in the earth's crust and upper mantle. Open file Report. 80. 625, 665 - 683, U.S. Geol. Surv. Menlo Park, Calif.

Van Breeman, O., Afralion, M., & Allaart, J.H., 1974. Isotopic and geochronologic studies on granites from the Ketilidian mobile belt of south Greenland. Geol. Soc. Am. Bull, 85(3) 403 - 412.

Van Breeman, O., Pidgeon, R.T., & Johnson, M.R.W., 1974. Precambrian and Palaeozoic pegmatites in the Moines of northern Scotland. Q. Jl. Geol. Soc. Lond. 130, 493 - 507.

Velde, B., 1983. Diagenetic reactions in clays. In: Sediment diagenesis, (Parker, A., & Sellwood, B.W. eds.) D. Reidel Publishing Company, P215 - 268.

Velde, B., & Rumble, D., 1977. Alumina content of chlorite in muscovite-bearing assemblages. Carnegie Inst. Washington Yearbook, 76, 421 - 423.

Wagner, F., Wenk, H.R., Kerr, H., Van Houtte, P., & Esling, C., 1982. Development of preferred orientation in plane strain deformed limestone: Experiment and theory. Contrib. Mineral. Petrol. 80(2), 132 - 139.

Watson, J., 1975. The Lewisian Complex. In: Harris et al. (eds.) A correlation of the PreCambrian rocks in the British Isles. Geol. Soc. Lond. Spec. Rep. 6, 15 - 29.

Watson, J., & Dunning, F.W., 1979. Basement-cover relations in the British Caledonides. In: The Caledonides of the British Isles - reviewed (Harris, A.L., Holland, C.H., & Leake, B.E., eds.) Spec. Publs. Geol. Soc. Lond. 8, 67 - 91.

Weathers, M.S., Bird, J.M., Cooper, R.F., & Kohlstedt, D.L., 1979. Differential stress determined from deformation-induced microstructures of the Moine Thrust Zone. J. Geophys. Res. 84, 7496 - 7509.

Weaver, C.E., 1960. Possible uses of clay minerals in search for oil. Bull. Am. Assoc. Petrol. Geologists, 44: 1505 - 1518.

Weber, K., 1976. Fabric studies on transversally foliated rocks of the eastern Rheinisches Schiefergebirge. Geol. Jahrb. Reihe D. 151, 3 - 98.

Weber, K., 1981. Kinematic and metamorphic aspects of cleavage formation in very low-grade metamorphic slates. Tectonophys. 78, 291 -

Weertman, J., 1975. High-temperature creep produced by dislocation motion. In: J.C.M.Li & A.K. Mukherjee (eds.) Rate Processes in plastic deformation of materials. ASM, Metals Park. Ohio P315 - 336.

Weiss, L.E., & Turner F.J., 1972. Some observations on translation gliding and kinking in experimentally deformed calcite and dolomite. Geophys. Monogr. Serial 16. Flow and fracture of rocks. Am. Geophys. Union, (H.C. Heard, et al. eds.) 95 - 107.

Wenk, H.R., & Shore, J., 1975. Preferred orientation in experimentally deformed dolomite. Contrib. Mineral. Petrol. 52, 115 - 126.

Wenk, H.R., Trommsdorff V & Baker, D.W., 1968. Inverse pole-figures of two carbonate fabrics. Schweiz, Mineral. Petrograph. Mitteilungen 48, 467 - 470.

Wenk, H.W., Venkitsubramanyan, C.S., & Baker, D.W., 1973. Preferred orientation in experimentally deformed limestone. Contrib. Mineral. Petrol. 38, 81 - 114.

White, S.H., 1976a. Estimation of deformation parameters from dislocation substructures in naturally deformed quartz. In: Venables, J.A. (ed.), Developments in electron microscopy and analysis. Academic Press, London, pp505 - 509.

White, S.H., 1976b. The effects of strain on the microstructures, fabrics and deformation mechanisms in quartzites. Philos. Trans. R. Soc. London. Ser. A, 283, 69 - 86.

White, S.H., 1979b. Grain and sub-grain variations across a mylonite zone. Contrib. Mineral. Petrol. 70, 193 - 202.

White, S.H., 1979a. Difficulties associated with paleostress estimates. Bulletin Mineralogie, 102, 210 - 215.

White, S.H., 1979c. Paleo-stress estimates in the Moine Thrust Zone, Eriboll, Scotland. Nature 280 (5719), 222 - 223.

White, J.C., & White, S.H., 1980. High-voltage transmission electron microscopy of naturally deformed polycrystalline dolomite. Tectonophys. 66, 35 - 54.

White, J.C., & White, S.H., 1983. Semi-brittle deformation within the Alpine fault zone, New Zealand. J. Struct. Geol. 5(6), 579 - 589.

White, S.H., & Wilson, C.J.L., 1978. Microstructure of some quartz pressure fringes. N. Jb. Miner. Abh. 134, 33 - 51.

Wickham, J.S., & Elliott, D.E., 1970. Rotation and strain history in folded carbonates, Front Royal area, N. Virginia. Trans. Am. Geophys. Union. 51(4), 422 -

Wilson, G., 1953. Mullion and rodding structures in the Moine Series of Scotland. Proc. Geol. Ass. 64, 118 - 151.

Winchell, A.N., 1926. Chlorite as a polycomponent system. Am. J. Sci. 5th Ser., 11, 283 - 300.

Winkler, H.G.F., 1979. Petrogenesis of metamorphic rocks. Berlin-Heidelberg - New York, Springer.

Yoder, H. S., 1952. The MgO - Al_2 - SiO_2 - H_2O system and the related metamorphic facies. Am. Jour. Sci. Bowen Vol. 569 - 627.

APPENDIX 1 METHOD OF CALCULATING MOLES % $MgCO_3$, $MnCO_3$ or $CaCO_3$ FROM THE RESULT OF AN EDS ANALYSIS OF CALCITE.

ELMT	%ELMT	%OXIDE	FORMULA	
Mg	0.536	0.889	0.006	Atomic weight of Mg = 24.32 g/mole
Ca	39.211	54.864	0.262	Atomic weight of Ca = 40.08 g/mole
Mn	0.217	0.280	0.001	Atomic weight of Mn = 54.94 g/mole

100g of calcite contain 0.536g Mg = $\frac{0.536g\ Mg}{24.3g/mol.}$ = 0.022 moles Mg.

100g of calcite contain 0.217g Mn = 0.0039 moles Mn.

100g of calcite contain 39.211 gla = $\frac{0.978 \text{ moles Ca}}{}$
= 1.004 moles metal carbonate.

Therefore for 1 mole of calcite, there is:-

$\frac{0.022}{1} \times \frac{100}{1}$ = 2.2 mole % $MgCO_3$,

$\frac{0.978}{1} \times \frac{100}{1}$ = 97.8 mole % $CaCO_3$, and

$\frac{0.004}{1} \times \frac{100}{1}$ = 0.4 mole % $MaCO_3$

APPENDIX 2 National Grid References of all Sample Locations correct to 10m.

SUB-AREA A

A6 - NC 25492272
A11 - NC 27571710
A21 - NC 24602251
A23 - NC 26172230
A40 - NC 24032413
A48 - NC 23622415
A50 - NC 23812397
A97 - NC 26062100
A98 - NC 26142063
A99 - NC 26272063
A102 - NC 24921986
A117 - NC 24941984

SUB-AREA B

B4 - NC 32481221
B5 - NC 33101225
B6 - NC 33141224
B12 - NC 29441321
B13 - NC 29401330
B15 - NC 29091379
B43 - NC 32401163
B45 - NC 32221161

SUB-AREA C

C13 - NC 31940900
C39 - NC 30110825
C40 - NC 30110831
C43 - NC 29780837
C50 - NC 29880839
C76 - NC 30110898
C83 - NC 30510895
C84 - NC 30600898
C88 - NC 31560908
C89 - NC 31960920
C91 - NC 32000925
C105 - NC 29920847
C106 - NC 29920834

SUB-AREA D

D1 - NC 19090945
D2 - NC 19060944
D3 - NC 19060944
D6 - NC 19140940
D24 - NC 19910939
D23 - NC 19880933
D60 - NC 19880916
D61 - NC 19810893
D62 - NC 19790845
D63 - NC 19980815
D31 - D31A-D31B-D1C-D31D-D32-NC 19110948
D46 - NC 20451032
D48 - NC 20851030
D64 - NC 20440935
D65 - NC 20600933

SUB-AREA ST

ST1, ST2 - NC 30602562
ST3 - NC 30602564
ST4, ST5 - NC 30732562
ST6 - NC 31002610
ST7 - NC 31002605
ST8 - NC 31102615
ST9 - NC 31322623
ST10 - NC 31542638
ST11, ST12 - NC 30732578

ERIBOLL

Eriboll Marble - NC 44005640
OY1, OY2 - NC 44325654
OY3, OY4 - NC 44345654
K1 - NC 44305812
K2, K3 - NC 44325809
K4 - NC 44705810
K5 - NC 44755812